Effects of Thermal and Seepage Actions on Seismic Response of Roller Compacted Concrete Dams

A thesis by

Parveen Khanzaei

Doctor of Philosophy

March 2017

Western Sydney University

Centre For Infrastructure Engineering (CIE)

School of Computing, Engineering and Mathematics

Kingswood Campus

Penrith NSW Australia

DEDICATION

To the Loving Memory of My Father…

ABSTRACT

Roller compacted concrete (RCC) dams have been developed for their rapid construction and low cost. However, some issues associated with the analysis and design of RCC dams are related to the seismically induced damages and possible failure of the dam, seepage due to the weakness of roller compacted layers and thermal stresses due to massive concreting. Large seismic events, in addition to the thermal and seepage effects, can cause the cracking and nonlinear behaviour where these cracks may expand further under the water pressure inside them to affect the stability of the structure. Therefore, developing a suitable constitutive material model and a reliable computational procedure for the safety evaluation and prediction of cracking risk of these structures has been a challenging and demanding task.

This research aims to present a new comprehensive numerical procedure to evaluate the seismically induced cracking of RCC dams under the effects of thermal and seepage actions. It takes into account the coupling effect of water pressure and the crack formation during an earthquake. In addition, more relevant features of the behaviour of concrete such as ageing, temperature, confining pressure and adiabatic temperature effects have been considered in the analysis.

A purposeful comprehensive numerical system consists of several individual features and in combination. The system includes a combination of field problems (thermal and seepage fields), continuum mechanics (stress analysis), seismic hazard assessment and safety evaluation. The combination uses finite elements to introduce compatible units capable of analysing infrastructure, such as RCC dams, to evaluate and predict level of safety in terms of crack pattern development. The method, which is based on a principle of birth and death process, is capable of simulating and assessing safety of RCC dams during the construction and the operation phase.

The constitutive material model for concrete is based on the combination of damage mechanics and plasticity. The mathematical models for mechanical behaviour of materials are given in the form of constitutive equations. The proposed constitutive

models have been reformulated and presented in convenient forms for RCC materials. Ageing, temperature and confining pressure effects were taken into account and implemented in the proposed constitutive models.

All the developments and analyses are performed using coded subprograms written in FORTRAN and developed in finite element program ABAQUS. Then, the validity of the proposed computational procedures and models has been confirmed by analysing and comparing the results obtained based on available experimental and analytical evidences. After the verification process, the material nonlinearity and proposed models are applied to analyse and evaluate the related dam safety against the cracking of an existing full-size dam. Finally, conclusions are drawn and recommendations are made based on the present research.

Based on the conclusions, it is revealed that the numerical procedure developed in this study for the seismic evaluation of RCC gravity dams under thermal and seepage actions provides a general framework for the analysis and design of these critical structures. The results of the evaluation indicate that different response patterns result when considering and neglecting THM (thermos-hydro-mechnical) model in seismic analysis, suggesting the significance of incorporating the thermal and seepage fields into the seismic assessment and design of concrete gravity dams.

ACKNOWLEDGMENTS

My foremost and sincere gratitude goes to Professor Bijan Samali, my academic supervisor, for his guidance, dedication, and support in the course of my graduate studies at Western Sydney University. He embodies the definition of a researcher as well as a mentor. I am deeply impressed by his enthusiasm, inspiration, knowledge, wisdom, and keen insight. He has invested enormous efforts and provided tremendous help in every aspect throughout all phases of this journey, making the completion of this treatise possible.

I would also like to express my appreciation to my co-supervisor Dr Chunwei Zhang for his valuable support, recommendations and encouragement.

Moreover, I am grateful to the financial support and research scholarship provided by Western Sydney University.

My gratitude also goes to the staff at the Centre for Infrastructure Engineering (CIE) and the administrative team for their generous and continued support. Furthermore, many thanks are extended to my colleagues and friends for their assistance in many different ways during my stay at CIE.

Finally, I am most indebted to my family for their indescribable sacrifice, unconditional love, continuous encouragement, and unfailing support over the years, without which I would have never been able to achieve this milestone.

TABLE OF CONTENTS

LIST OF TABLES

LIST OF FIGURES

LIST OF NOTATIONS /ABBREVIATIONS

Latin Upper Case

A	Area
$A(y)$	amplitude of annual variation of water temperature
$[B]$	strain-displacement matrix
$[C]$	capacitance matrix
$[D]$	global elastic rigidity matrix
E	elastic Modulus
$\{F_e\}$	equilibrated forces
$\{F\}$	vector of nodal force
G	shear modulus
H	distribution function of water head
$[J]$	Jacobian matrix
$[K]$	element stiffness matrix
K_x	hydraulic conductivity in x direction
K_y	hydraulic conductivity y direction
K_{nn}	normal stiffness
K_{ss}	shear stiffness
L	coupling matrix between mechanical and flow
$[M]$	mass matrices of the structure,
N_i	shape function at node i
Q	heat transfer rate per unit area
$\dot{Q}$	heat transfer rate per unit volume

$\dot{Q}$	heat of hydration rate per unit volume
$\{R\}$	unbalanced (residual) nodal load vector
S_s	storage capacity
T	temperature
T_{ad}	adiabatic temperature rise
T_{max}	maximum adiabatic temperature rise
T_s	the temperature of the solid surface
T_f	the temperature of the fluid surface
$\{T\}^e$	vector of element nodal temperatures
$\{\dot{T}\}^e$	vector of element nodal temperatures variation with time
V	wind speed

Latin Lower Case

c	specific heat coefficient
c'	effective cohesion
dV	elemental volume
e	void ratio
$f`_c$	compression strength
$f`_t$	tensile strength
h	convection heat transfer coefficient
h_c	concrete convection heat transfer coefficient
h_f	wind convection heat transfer coefficient
k_0	permeability of the media
κ_t	unixial tensile damage variable
κ_c	unixial compressive damage variable

k_x	thermal conductivity coefficients in x direction
k_y	thermal conductivity coefficients in y direction
k_z	thermal conductivity coefficients in z direction
n	porosity
$\bar{p}$	hydrostatic effective stress
q	heat flux
q_c	convection heat transfer rate
q_r	radiation heat transfer rate
t	time
u_w	pore water pressure
$\{\ddot{u}_g\}$	ground acceleration
u,v	tangential and normal displacements respectively
x,y,z	cartesian coordinate system
z_w^0	height of the phreatic surface

Greek Upper Case

$\{\Delta F\}$	incremental load vector
$\{\Delta\delta\}$	incremental nodal displacements vector
$\{\Delta\varepsilon\}$	incremental strains vector
$\{\Delta\sigma\}$	incremental stress vector

Greek Lower Case

α	hydration heat rate parameter
β	shear modulus reduction factor
$\{\delta\}$	vector of displacement
δ_{ij}	Kronecker delta

∇^2	Laplace operator
ε	coefficient of the surface emissivity
ε^e	elastic strain
ε^p	plastic strain
ε_v	volumetric strain
$\{\varepsilon\}$	vector of strain
ϕ'	effective friction angle
θ	transformation angle
μ	friction coefficient in joint interface.
ν	Poisson's ratio
ξ,η	natural coordinate system
ρ	material density
ρ_w	density of water
σ , ε	instantaneous values of the stress and the strain respectively
σ_i	principal stress in direction i
σ'	effective stress
σ_n	normal stress
σ_o , ε_o	the ultimate stress (peak) and the corresponding strain respectively
$\sigma_{t'}$	tensile bond strength of interface
$\{\sigma\}$	vector of stress
γ_w	specific weight of the pore fluid
γ'	buoyant unit weight
μ	viscosity of the water
τ_o	shear strength at $\sigma_n = 0$

τ_s	shear stress
τ_u	shear strength
$\|\psi\|$	displacement norm

ABBREVIATIONS

CMC	Conventional Mass Concrete
ECD	Enlarged Cotter Dam
FE	Finite Element
FV	Field Variable
NISA	Nonlinear Incremental Thermal Stress-Strain Analysis
RCC	Roller Compacted Concrete
SDV	Solution Dependent Variable
SSI	Soil–Structure Interaction

LIST OF PUBLICATIONS

❖ **Published**

1. ***Khanzaei, P***., Abdulrazeg, A. A., Samali, B., & Ghaedi, K. (2015). Thermal and Structural Response of RCC Dams During Their Service Life. Journal of Thermal Stresses, 38(6), 591-609.

2. Ghaedi, K., Jameel, M., Ibrahim, Z., & ***Khanzaei, P***. (2015). Seismic analysis of roller compacted concrete (RCC) dams considering effect of sizes and shapes of galleries. KSCE Journal of Civil Engineering, 1-12.

3. ***Khanzaei, P***., Samali, B., & Zhang, Ch. (2016). Coupled and Uncoupled Seepage-Stress Analysis of Roller Compacted Concrete Dams. ISH Journal of Hydraulic Engineering. Taylor & Francis.

4. Ghaedi, K., ***Khanzaei, P***. Vaghei, R., Fateh, A., Javanmardi , A. (2016). Reservoir hydrostatic pressure effect on roller compacted concrete (rcc) dams. Malaysian Construction Research Journal, 19 (2).

❖ **Accepted**

5. ***Khanzaei, P***., Samali, B., & Zhang, Ch. (2016). Thermal Cracking Evaluation of RCC Dams Considering the Effect of Placement Schedule. European Journal of Environmental and Civil Engineering.

6. Abdulrazeg, J. Noorzaei, ***P. Khanehzaei***, M. S. Jaafar, T. A. Mohammed. Methods of Thermal, Structural and Cracking Analysis of RCC Dam in Hot Climatic Region, Journal of Applied Thermal Engineering, (2016).

❖ **Under Review**

7. Ghaedi, K., ***Khanzaei, P***. Hejazi, F. (2016). Flexible Foundation Effect on Seismic Analysis of Roller Compacted Concrete (RCC) Dam. KSCE Journal of Civil Engineering.

CHAPTER 1

INTRODUCTION

1.1 General

Dams have been constituted, from the beginning of human civilization, as an essential element for conquest and adaptation by humankind of his environment, and to improve his quality of life. They are an integral component of the society's infrastructure system. Dams have been constructed to create reservoirs to store water for drinking water supply, agricultural irrigation, flood control, river navigation, and more recently for electric power generation and industrial use (Berga 2003).

Dam engineering has always paid a very special attention to the issues related to the safety, economy and speed in the construction of dams from the beginning of the 1960s. As part of this effort, Roller Compacted Concrete (RCC) has been introduced as an alternative in dam construction. Since the 1980s, the RCC method in construction of concrete gravity dams has been successfully applied in many important projects (Dunstan 2003). Roller-compacted concrete (RCC) continues to gain recognition as a competitive material for construction of new gravity dams and for rehabilitation of existing dams. During the past three decades, many design details and construction methods have been implemented to improve this relatively new dam construction method with the goal of enhancing the product while maintaining the RCC's competitive edge associated mainly with speed of construction (Abdo, 2008).

The RCC dams consist of concrete placed at a lower ratio of water to cement as compared to conventional concrete with the aid of compaction equipment and methodologies normally employed for earth-fill placement. It involves building a concrete gravity dam by methods usually associated with earth dam construction (Hansen, 1996). This construction method permits a considerable reduction in costs and construction time of dams.

The roller compacted concrete (RCC) dams, due to their sound structural behaviour, earthquake performance and from the economical point of view are attractive to dam consultants around the world. Furthermore, RCC dams have the obvious advantage of being built quickly, unlike conventional concrete, which needs only 3-5 days to set; RCC can be built up non-stop in 300 mm layers. This economical method of construction has sufficiently proven that very large dams can now be designed. Techniques have been developed for the design of the mixture proportions of an RCC to have sufficient cohesion and tensile strength to withstand the required static, thermal and seismic loading on these large dams (Dunstan 1992).

However, because the RCC dams are still a newly developed technology, there are several problems to be overcome. Due to the speed of construction, different RCC placing temperatures and the weakening interface between compaction layers, the possibility of the thermally induced cracking, water seepage and infiltration from the reservoir in this type of dam is higher than in conventional concrete dams. Furthermore, one important area of consideration in designing RCC dams is the safety evaluation of these structures under the effects of earthquake-induced ground motion by the fracture and stability analysis. Therefore, studies on the parameters including strengths and the stress-strain relationship of RCC, the seismically induced cracking and safety evaluation of RCC dams under the effects of thermal and seepage loading are imperative.

1.2 Application of RCC Dams

From the first experiences of Roller Compacted Concrete (RCC) dams begining in 1978, there has been a fast development of RCC technology applied in dam construction throughout the world due to obvious advantages of being more economical and more efficient. At the end of 1996 there were 157 completed RCC dams in 20 countries, and then by the end of 2002 there were 251 completed RCC dams in the world. RCC dams are showing a continuously increasing trend in popularity, as at the end of 2014 there were 533 RCC dams throughout the world. Figure 1.1 shows a breakdown of the dams built in various countries. The country with maximum number of RCC dams is China, having 165 dams (Dunstan, 2014).

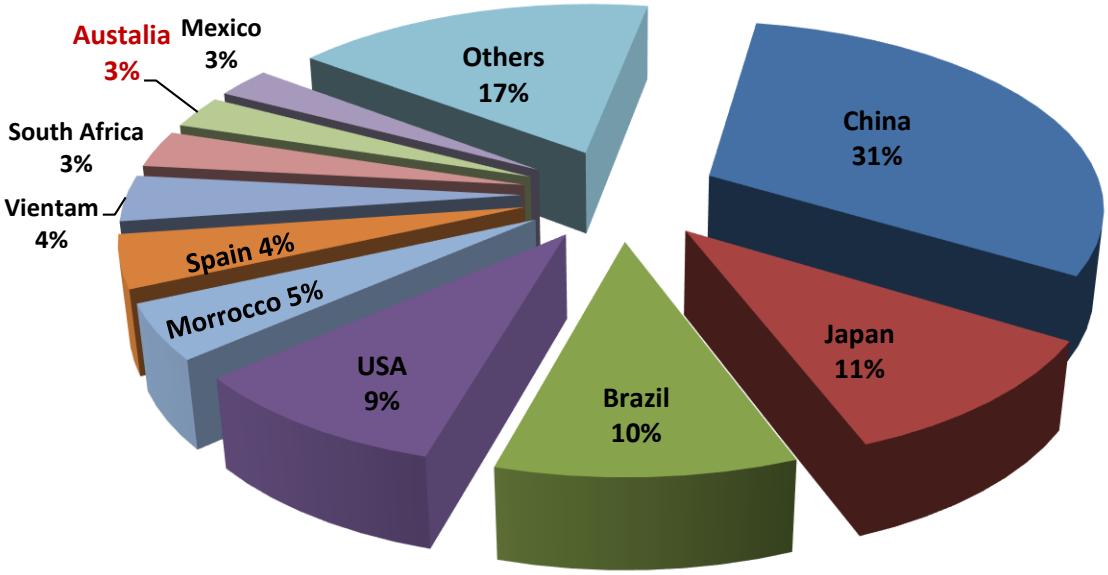

Figure 1.1 Distribution of RCC Dams throughout the World at the End of 2014 (Dunstan, 2014)

Australia has a long history of dam building, albeit with considerable variation in intensity. RCC has been commonly used in a number of dam projects since the mid 1980's in Australia. In this application, it is gaining status as a preferred technology for modern dam construction, requiring a smaller embankment volume than earth filled, but a quicker construction time than formed structural concrete. There are a total number of 15 RCC dams in Australia until now as tabulated in Table 1.1 (Dunstan 2015).

Kidston RCC dam known as Copperfield dam in Queensland was built to provide water to the Kidston Goldmine in 1984 on the Copperfield River. The dam was the first dam built in Australia using the Roller Compacted Concrete technique. Later on, the largest dam of Roller Compacted Concrete built in Australia up to 2011 was the New Victoria RCC (fifth RCC dam in Australia) dam near Perth. The dam has an overall length of 285 m and is built to a height of 52 m. After this successful experience, the South Eastern Australia suffered a major drought from 1998 to 2010, which severely impacted on the water supply of urban communities in the region. Canberra, the capital city of Australia, reacted to this situation by initiating a number of water supply projects to reduce the long term risk of significant impacts of future droughts. One of these projects was the Enlarged Cotter Dam (ECD), constructed in

2014, Consisting of an 87 m high RCC dam on the Cotter River and two auxiliary saddle dams on the right bank to the south west of the main dam spanning neighbouring low lying valleys (Peter Buchanan,2012).

The enlargement of the Cotter Dam has secured the water supply for the Australian Capital Territory (ACT) and surrounding regions for the future by expanding the storage capacity by 35%. The new 87 m high dam is constructed of roller compacted concrete and is the highest dam of its type in Australia.

Table 1.1 List of RCC Dams in Australia (Dunstan 2015)

	Name	Location	Height (m)	Completion Date
1	Copperfield (Kidston)	Hughenden, QLD	40	1984
2	Craigbourne	Colebrook ,TAS	25	1986
3	Wright's Basin	Canberra, ACT	18	1989
4	New Victoria	Perth, WA	52	1991
5	Kroombit	Biloela, QLD	26	1992
6	Burton Gorge	Mackay, QLD	26	1992
7	Lower Molonglo Bypass Storage	Canberra, ACT	32	1994
8	Loyalty Road Flood Retarding Basin	Sydney, NSW	30	1996
9	Cadiangullong	Cadia, NSW	43	1998
10	Paradise	Burnett, QLD	50	2005
11	Meander	Northern Tasmania	47	2007
12	North Para	Barossa Valley, SA	33	2007
13	Wyaralong	South East Queensland	48	2011
14	Enlarged Cotter	Canberra, ACT	82	2013
15	Connors River	Lotus Creek, QLD	45	2014

1.3 Availability of the Code of Practice

Several reports and standard practice regarding the RCC material are available in the literature. However, the purpose of these works is to provide information and guidance on the use of roller compacted concrete (RCC) in dams and design considerations. These works do not cover design specifications for RCC dams. In addition, there are no specific formulations for RCC material properties, and most of these works were based on conventional concrete properties. Elements discussed

include investigation and selection of materials, mixture proportion, design and construction consideration, construction equipment and techniques, inspection and performance. Stress or dynamic analysis have not been discussed. Despite the differences in the construction method and material properties, the same technique of analysis and design which are used in conventional gravity dams are implemented in RCC dams. Some of these reports and standard practice are tabulated in Table 1.2.

Table 1.2 Standard Practices of RCC Dams

	Reference	Objective
1	ACI 207.5R-99 of Roller Compacted Mass Concrete.	Provides guidance in planning, designing, executing and inspecting construction.
2	USACE. 1995. Gravity Dam Design, Engineering Manual 1110-2-2200. U.S. Army Corps of Engineers.	Provides technical criteria and guidance for the planning and design of concrete gravity dams. Specific areas covered include load conditions, methods of stress analysis, seismic analysis guidance.
3	USACE. 1997. Thermal Studies of Mass Concrete Structures, Engineering Manual 1110-2-542. U.S. Army Corps of Engineers.	Reviews the methods for predicting creep, shrinkage and temperature effects in concrete structures.
4	USACE. 1997. Roller Compacted Mass Concrete, Engineering Manual EM 1110-2-2006.	Provides information and guidance on the use of roller compacted concrete (RCC) in dams and other civil work structures.

1.4 Research Problem

The problems associated with the analysis, design and construction of RCC dams may be related to the structural modelling of the dam, material nonlinearity, seismically induced damage and failure of the dam, seepage due to the weakness of roller compacted layers and thermal stresses due to massive concreting.

The safety assessment of dams to earthquake hazards requires particular attention because they are “long structures,” such as pipelines, tunnels and bridges, which extend over long distances parallel to the ground, and, hence, large and varying seismic ground motions may occur over their base dimensions and cause large damage and failure of such structures (Zerva 2009). Moreover, the idea that the seismic action on dams could almost be neglected for structures located in areas of low seismic activity is no longer valid, and according to USACE (1995) this action is

the most important to be considered in safety studies involving failure issues and scenarios.

Furthermore, there are still a number of issues that have not been extensively examined and/or fully addressed in the modelling of the RCC dams, as;

i. The nonlinear mechanical behaviour of the water, RCC, and the rock;
ii. The interaction between the dam body, reservoir, sediment and the foundation; and
iii. The seismic stability evaluation of RCC dam under seepage flows and thermal actions.

Most researchers have ignored the effect of dam body-reservoir-sediment-foundation interactions in analysing RCC dams. The interaction between the dam-foundation systems is an important element to simulate the actual interaction between the dam and the foundation system (Calayir, 2005). Water pressure is considered as important actions acting on the upstream face of the dam under static and seismic analysis. Thus, dam-reservoir interaction should be considered in the analysis. In addition, the previous studies on hydraulic structures have been focusing on the dynamic stability and strength. In general, seismic response considering seepage and thermal stresses are not considered in design, so seismic analysis of gravity dams based on coupled seepage-stress and thermal-stress analysis is an important factor that should be considered.

The big volume RCC dam is built with many thin layers, therefore, the main problem is the integration of roller compacted layers. The engineering practice has proven that the roller compacted layer is often the weak part of the dam, and is also the main channel for seepage through the body of the dam. Thus, the seepage problem of the RCC dam is greatly different from that of the earth dam and the ordinary concrete dam (Junrui, 2005).

It has been well recognized in geotechnical engineering practice (dams, slopes, landslides, underground spaces, etc.) that seepage flow has a great influence on the deformation, stress field and stability of hydraulic structures (Chen, 2010). Therefore, it is of great importance to evaluate the safety of gravity dams under the

coupled seepage-stress interactive system whose behaviour is controlled by the mechanical and hydraulic properties of concrete materials and rock foundation.

On the other hand, high temperatures arising in a RCC dam due to the hydration of concrete, environmental boundary conditions and quick construction process can induce a high thermal gradient in interior mass and exterior surfaces of the dam (Noorzaei et al 2006). This thermal gradient can induce significant thermal tensile stresses; if these thermal stresses in addition to the tensile stresses resulting from the other loads exceed the tensile strength of RCC, cracks will develop in the dam's body. Thus, thermal analysis of large volume concrete structures constructed in thin layers is important, especially, because these structures are normally unreinforced, which makes tensile stresses a critical part, and are subjected to loads and constraints that can lead to cracking. Thermal cracks have frequently been linked to the damage of concrete dams. Cracks on the upstream and downstream faces of dam are generally of small dimensions, but their occurrence can lead to further deterioration and other structural pathologies (Berga, 2006)

Despite the fact that there are several publications by researchers to predict the heat exchange (interaction) between the dam body and the impounding water, still the variation of the water temperature with seasonal changes of the air temperature or with depth of the reservoir is usually neglected or approximated by an assigned fixed temperature. Therefore, in order to obtain a realistic isothermal profile of the dam body, it is necessary to predict the accurate initial temperature of the reservoir water for thermal analysis.

Considering the importance of thermal and seepage loading on obtaining a reliable estimation of the final stress fields in RCC dams, the ground motion effect in these structures should be considered together with their effects in the analysis.

Large seismic events, in addition to the thermal and seepage effects, can cause the cracking and nonlinear behaviour where these cracks may expand further under the water pressure inside them and affect the stability of the structure. Therefore, the assumption of linear behaviour may not be appropriate in the analysis because tensile cracks will form and propagate in the concrete, affecting the fracture response of concrete gravity dams. Moreover, although the importance of water pressure in

cracks of concrete gravity dams has long been recognized, its effect during earthquakes remains a major source of uncertainty in design and safety assessment of concrete dams (Javanmardi, 2005).

This research aims to present a new comprehensive numerical procedure to evaluate the seismically induced cracking of RCC dams under the effects of thermal and seepage actions. In addition, more relevant features of the behaviour of concrete such as ageing, temperature, confining pressure and adiabatic temperature effects have been considered in the analysis.

1.5 Study Objectives

This study aims at achieving the following objectives:

1. To develop a new comprehensive system to evaluate the safety and seismically induced cracking of RCC dams under the effects of thermal and seepage actions.
2. To propose suitable, constitutive material and mechanical models of RCC that include the ageing, temperature and confining pressure effects.
3. To develop a numerical model to simulate the RCC dam –foundation- reservoir interaction (DFRI) system to carry out the seismic response of RCC dams under thermo-hydro-mechanical loading.

1.6 Scope and Limitations of the Study

Several activities have been performed to cover the numerical model requirements developed in this study. In order to achieve the study objectives, the following tasks have been carried out in this study:

1. Simulating the sequence of construction stages of RCC dams using birth-and-death element technique for all types of analysis.

2. To propose rigorous constitutive material and mechanical models to capture RCC dams performance incorporating the ageing, temperature and confining pressure effects.

3. Introducing a special type of boundary and initial conditions (reservoir water interaction, drainage boundary and initial stresses), also carrying out the procedure for the calculation of phreatic surface in the dam body.

4. Modifying the concrete constitutive crack models for simulating and investigating the crack process in concrete dam structures.

5. Modifying the latest RCC elastic models to account for temperature effect using maturity concept.

6. Simulation of the heat exchange between the RCC dam body and the impounding reservoir water taking into account the variation of reservoir temperature with depth.

7. Evaluation of the safety and seismic response of RCC dams during the construction and their lifetime under combination of gravity, temperature, seepage, hydro-dynamic and hydrostatic loads.

Limitations of the present work:

i. Time dependent behaviour such as creep and shrinkage is not included in the present work.
ii. No experimental studies have been conducted in this study.

1.7 Layout of the Thesis

The thesis has been divided into nine chapters and brief description of each chapter is described below:

The introduction and the definition of the problems for the present investigation have been highlighted in **Chapter 1** along with the objectives and scope of the study.

A comprehensive survey of literature associated with the numerical models of RCC gravity dams and mechanical properties of roller compacted concrete are presented in **Chapter 2** in order to establish the state-of-the-art of knowledge in this field.

Chapter 3 deals with the methodology and mathematical description of fluid flow problems, temperature and stress development in RCC dams and seismic fracture analysis procedures of these structures. Moreover, finite element method for continuum mechanics and mathematical description for mechanical responses have been presented in this chapter.

In **Chapter 4** the numerical and computational strategies of three different types of analysis including, coupled seepage-stress, coupled temperature-stress and seismic fracture analysis have been presented. The development of finite element code for each type of analysis has been discussed.

The validation of the developed FE code and proposed mathematical solution for each analysis are presented in **Chapter 5.** Experimental and analytical evidences have been used for the purpose of verification.

Chapters 6 to **8** are devoted to the analysis and results of field problems (thermal and seepage fields), continuum mechanics (stress analysis), seismic hazard assessment and safety evaluation of large-scaled RCC gravity dams. The structural response of the RCC dams subjected to the seismic excitation including thermal and seepage fields are discussed and presented in terms of acceleration, displacement, stresses and cracking patterns according to failure mechanics.

Chapter 9 deals with the conclusions of the current reseach and recommendations for further research, followed by bibliography and appendices.

CHAPTER 2

LITERATURE REVIEW

2.1 Introduction

The roller compacted concrete has gained worldwide acceptance as an alternative to conventional concrete in the field of dam engineering due to the construction advantages and good performance during the operation. The increasing number of roller compacted concrete dams being built around the world demands accurate methodologies and systems for reliable short and long-term evaluations of the risk of damage and cracking in these constructions, which has led to considerable number of publications reported in literature regarding this type of structures.

Generally, the body of research literature on the RCC dams mainly focus on three distinct fields, as shown in Figure 2.1, which are; (i) Construction method, (ii) Material technology, and (iii) Numerical simulation. The major focus of the present investigation is on numerical simulation of RCC dams.

The simulation of RCC dam behaviour and especially simulation of its deformation and crack sensitivity has become an important field in structural analysis. Numerical simulations of the stress development may be evaluated in the design phase in order to predict the cracking development. To obtain a reliable and economical design of RCC dams, such simulations require simulating the construction processes and appropriate boundary conditions. All aspects that influence the structural behaviour with time have to be included. In addition, for the material and mechanical properties such as heat of hydration, hydraulic conductivity and modulus of elasticity, the time dependent properties of concrete must be considered.

Numerical simulation tools have been used extensively by researchers and practising engineers in the field of dam engineering. This is attributed to the drawbacks of the experimental work in this field such as limitations of lab testing, difficulty of constructing a large enough scale dam and economic considerations.

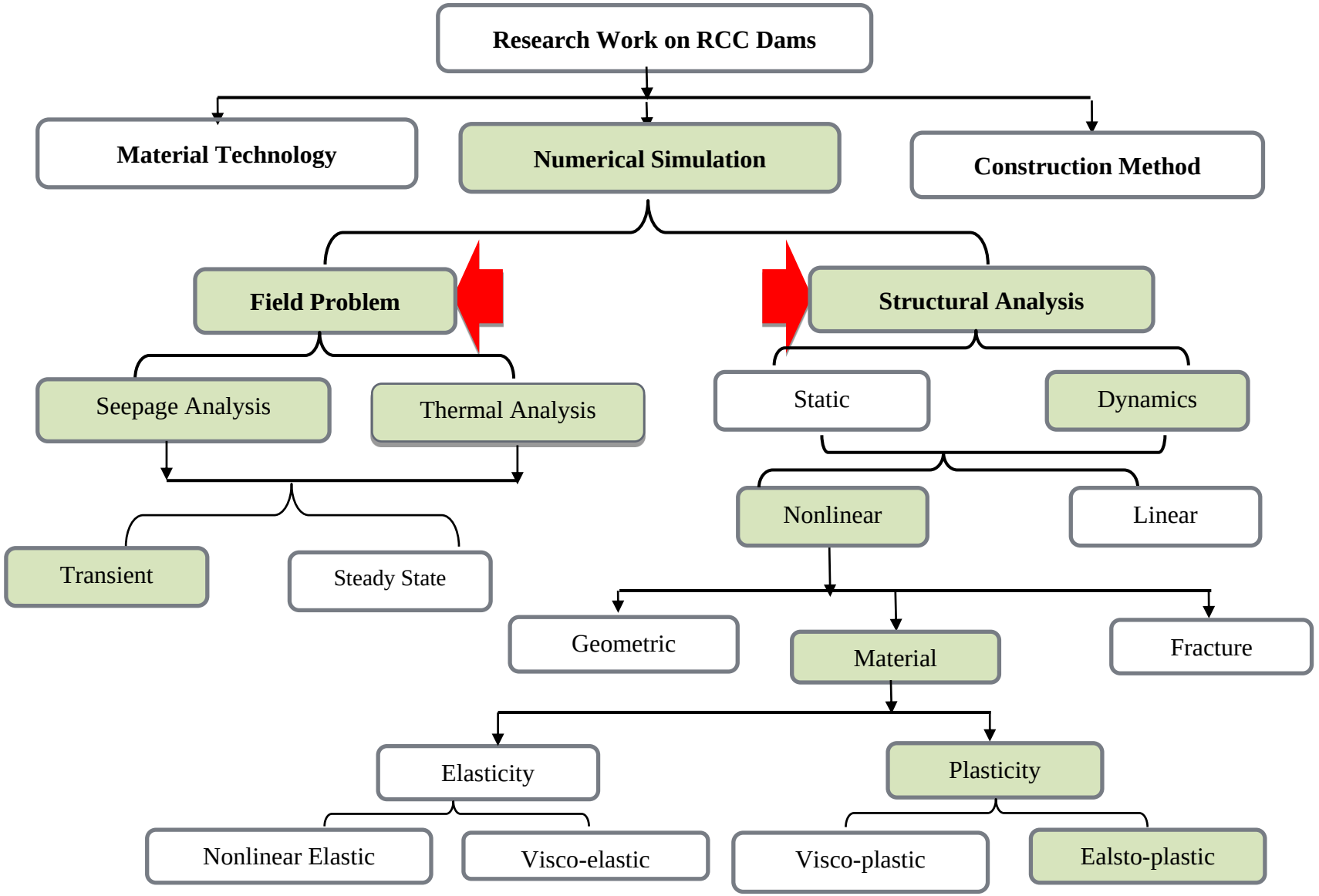

Figure 2.1 Flow Chart of the Research Activities on the RCC

In the last three decades, numerous analytical and numerical methods have been proposed to study the significant mechanical actions and the resulting induced stresses in RCC dams during and after the construction phases. The proposed methods range from crude approximate methods to highly sophisticated ones using complicated constitutive relationships to present the material behaviour. In this chapter, a review of literature including the research on numerical simulation of the temperature, seepage and stress fields of RCC gravity dams along with their seismic behaviour are conducted for identifying the gaps in the literature. In addition, some examples of RCC dam failure are presented in this chapter in order to highlight the significance of the present study.

2.2 Examples of Gravity Dam Failure

Dams are deceptively simple structures in appearance. Despite outward appearance, there is always the possibility that a dam might experience either partial or total failure causing damage downstream. This could result in flooding leading to loss of life, injury to people or livestock, damage to houses, buildings and roads or interruption to public utility services (eg. electricity) as well as environmental damage. If a dam fails, the additional losses resulting from lack of water could result in major economic and social consequences.

Failure of a dam does not necessarily mean the same as ‘collapse’ of the dam. More generally, it may mean failure to meet its design objectives. Hence, any damage to a dam (such as development of cracks due to temperature changes and earthquake excitation) or any failure to retain water as designed (such as excessive leakage through, under or around the dam) or inability to pass incoming flood waters via the spillway, may be regarded as a failure of the dam, though some failures may be more serious than others.

Dams are massive structures that are usually subject to risk of ground motions. Since concrete has weak tensile behaviour, therefore, with increasing the earthquake intensity, the concrete dam may go through the softening stage and finally result in cracks to appear in the body of the dam. Crack patterns and their size can normally show weakness of gravity dams.

Satisfactory performance of concrete gravity dams during a seismic event is necessary because the release of the impounded water can cause considerable amount of devastation in the populated downstream areas. Therefore, the fact that there has not been a complete failure of a concrete dam during an earthquake should not lead to an underestimation of the importance of thorough seismic analysis of this type of structures.

The safety of dams under earthquake loading is very important due to the possibility of large damage and consequences resulting from the failure of dams located in seismically prone regions. On average Australia experiences two earthquakes over magnitude 5 per year (Leonard, 2008) and a magnitude 6 every five years (Wilson et al., 2008). This corresponds to a higher level of seismic activity than other active, intra-plate regions around the world. Earthquake events such as the M6.8 Meckering earthquake in 1968, M5.4 Adelaide earthquake in 1954 and three M>6 earthquakes occurring within a twelve hour period at Tennant Creek in 1988 clearly demonstrate that moderate to large size earthquakes can occur and have the potential to tragically affect Australian communities. This has led to earthquake loading to be part of the general design for structures in all areas of Australia (Wilson et al., 2008). It is, therefore, imperative to understand the seismic performance of the Australian hydraulic structures such as dams under different levels of earthquake loading.

Moreover, the assumption that the seismic action on dams could almost be neglected for structures located in areas of low seismic activity is no longer valid, and according to USACE (1995) earthquake action is the most important to be considered in safety studies involving failure scenarios.

The risks posed by earthquakes on concrete gravity dams have been demonstrated by the damage of such dams throughout the world, as, e.g. the Koyna Dam in India (Chopra et al. 1972, Wieland 2003) and the Shih-Kang Dam in Taiwan (Sugimura, 2001). The Koyna Earthquake in 1967, with the magnitude of about 6.5 on the Richter scale, resulted in a considerable amount of damage to the Koyna Dam, including the development of cracks in the dam, water leakage on the downstream

face of the dam, and spalling of concrete along the vertical joints between monoliths. The Shih-Kang Dam was also severely damaged by fault movements and ground shaking during the 1999 Chi-Chi earthquake in Taiwan. Figures 2.2 and 2.3 show the damaged Shi-Gang Dam caused by the 7.3 magnitude Chi-Chi Earthquake and damage to the Koyna dam parts, respectively.

Figure 2.2 Shih-Kang Spillway Weir Destroyed Spillway Units (Sugimura, 2001)

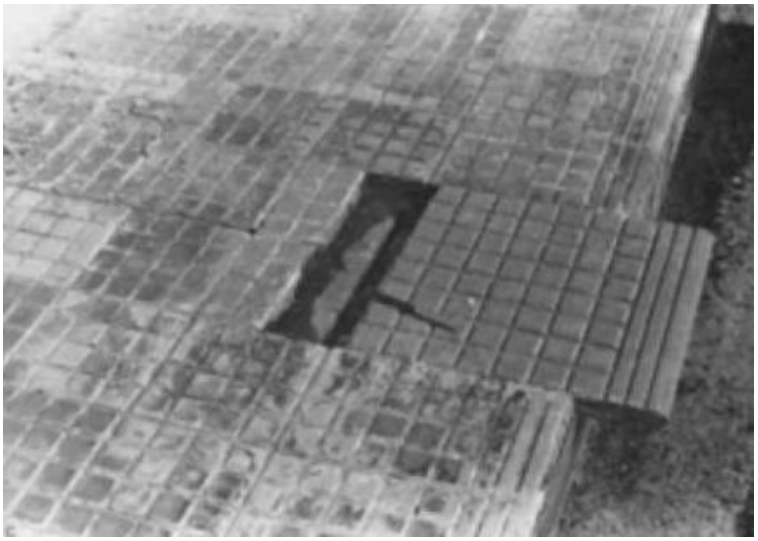

Figure 2.3 Movement of the unfixed tiles on the span of the Koyna Dam (Gupta 1992)

When RCC dams started to be used in dam construction, for a time it was thought that there was no problem in the temperature control of RCC because the amount of cement in RCC is much less than that in conventional concrete. However, research has revealed that RCC dams have problems with thermal stress and temperature

control (Bofang 2013). This could be attributed to low conductivity of concrete and the quick construction process, which can induce a high thermal gradient in the interior mass and exterior surface of the dam (Noorzaei et al 2006). Temperature variation, shrinkage and expansion due to hydration of cement and applied static and dynamic loadings are both considered as damages, i.e., the internal and external effective damages.

The Upper Stillwater Dam in Utah experienced thermal induced cracks at maximum stress points throughout the dam. Since the time of initial construction, a series of cracks have developed from the upstream face to the downstream face and vertically from the crest to the underlying bedrock foundation. The crack widths on the face of the dam range from hairline to approximately 0.5 inches as shown in Figure 2.4.

Figure 2.4 Cracks of Upper Stillwater RCC Dam (Smoak 1991)

Moreover, seepage erosion of material from rock joints, movement along faults or shear zones and water leakage within the cracks in dam body, known as internal damage, can also contribute to failure. Excessive concrete cracking may cause excessive seepage with the resulting damaging effects on durability and even structural stability of dam. Experience shows that thermal cracking is a major concern for RCC dams and a reliable assessment of this phenomenon beforehand is mandatory. The first generation of RCC gravity dams, those built in the 1980s, experienced seepage through lift joints and at shrinkage cracks (Abdo 2008).

First in line was Willow Creek Dam in Oregon, USA. The dam was completed in 1982, had no joints, and used a lean dry RCC mixture. Equipment operated on and off the RCC lifts, tracking soil and other contaminants onto the lift joints. Although the dam was deemed structurally sound, excessive water seepage at lift joints took place during first filling of the dam (Abdo 2008).

A few years later, between 1985 and 1987, USBOR's Upper Stillwater Dam was constructed. USBOR's approach to building Upper Stillwater was quite different from USACE's approach to Willow Creek. The Bureau elected to use a richer RCC mixture (higher cementitious content) with a wetter consistency. The upstream vertical face and the downstream stepped face of the central spillway section were formed using conventional concrete. In addition, the richer mix and the upstream conventional concrete facing provided better seals and prevented seepage at lift joints. The dam did not include contraction joints. However, vertical thermal cracks developed at an average spacing of approximately 190 ft. (58 m). The cracks were not structurally significant; however, one crack produced excessive water leakage and required major waterproofing repairs using polyurethane resin. Figures 2.5 and 2.6 show a seepage path of Willow Creek and Upper Stillwater dam (Smoak, 1991).

Figure 2.5 Willow Creek Dam deformed face with seepage (Smoak, 1991)

Figure 2.6 Cracks at Upper Stillwater dam (Smoak, 1991)

2.3 Seepage and Stress Fields of Gravity Dams

It has been well known in geotechnical engineering practice (dams, slopes, landslides, etc.) that seepage flow has a great influence on the deformation, stress field and stability of hydraulic structures (Chen, 2010). Conversely, at the same time, the variation of the dam stress field will change its permeability and in turn the seepage rate. Clearly, an interaction exists between seepage and stress fields (Gu

2013). This interaction between the seepage and the stress fields is called hydro-mechanical coupling.

The term ‘coupled processes’ indicates that, each process affects the initiation and progress of the others. Therefore, the response of rock foundations and the structure above them cannot be predicted with confidence by considering each process independently (uncoupled analysis). For the coupled seepage-stress model, it is essential to investigate the two-way interactions among seepage and stress fields (Lanru 2003).

A large number of researchers have paid more attention to the interaction between the fractures and that of structures experiencing the flow of water. The behaviour was recorded in terms of pore pressures, displacements, stresses and stability of the structures. Several case studies have been undertaken by various researchers to check the stability of various hydraulic structures, such as dams, under the effect of seepage and stress conditions.

Junrui et al. (2004) analysed the interaction between the seepage and stress fields in the rock mass around the Xiaowan arch dam of 292 m high located in China. Numerical solution of this coupled model was analysed by means of the multi-level fracture network model and the finite element method. In this study, the coupled analysis was carried out only for rock mass and the body of the dam was neglected.

A year later, a coupled model of seepage and stress fields for roller compacted concrete (RCC) dam was presented by Chong-Shi et al. (2005). A 3-D Finite Element program was developed in this study to reflect the effect of the construction interfaces more adequately. Moreover, the interaction of seepage and stress fields of RCC dam and the influence of interfaces was simulated by including the influence of thickness and the physical mechanical parameters of interfaces. The proposed method was validated by analysing a typical RCC dam with the height of 87m. However, in this study, a foundation block was not included in the FE model and the distribution of total head was not shown in the analysis.

Zhu et al. (2006) analysed in detail optimal design schemes for the control of seepage of RCC dams. The analysis was based on a wide and in-depth study on the property and characteristics of permeability and seepage control techniques for RCC dams. The contours of hydraulic head distributions for Guangzhao RCC dam located in China are obtained in the study. However, the structural field and crack prevention has not been addressed in the study.

Later on, Ouria et al. (2007) investigated the effect of the coupled and uncoupled seepage-stress analysis through a dam foundation. A two dimensional transient seepage analysis was carried out using the finite element formulation based on Galerkin approach. Comparing the results of coupled and uncoupled models showed that the time required to reach steady-state condition in coupled model is considerably shorter than the uncoupled model. Coupled analyses show that the effective stress due to seepage forces were smaller than ones calculated by the uncoupled method**.** In this study only a 2D linear analysis was carried out and also body of the dam was not considered in the analysis.

Lai et al. (2008) proposed a coupled creep and seepage model for hybrid media composed of joints and the equivalent continuum. This coupled problem relations were established based on the fundamental mechanism of creep effects on the permeability of the rock mass, together with the empirical equations for hydraulic conductivity, coupled creep and seepage equations for filled joints and equivalent continuum. A simplified numerical solution was also proposed to solve the coupled creep and seepage model and to simulate the seepage, deformation, and stress field. However, in this study, the linear visco-elastic stress-strain relation was used, but the variation of hydraulic conductivity with stress and temperature was not taken into account.

Later on, Li et al. (2009) carried out the seepage analysis of an 81 m high concrete dam located in China to study the seepage control mechanism. In the calculation of seepage field, the effect of the parameters of concrete, cut-off wall, drainage hole and grout curtains were considered. The research indicated that the reinforcement measures of the parameters of concrete, cut-off wall, drainage hole and grout curtains

all have influences on the spill point altitude of the wet surface, cut-off wall has the most significant effect among all reinforcement measures. However, the permeability coefficient was considered constant in the analysis.

In the same year, Deng and Wu (2009) studied a hybrid analysis model for the coupled problem of seepage and stress fields in the rock mass of equivalent continuum by linking the seepage coefficient, porosity and stress. The FEM numerical method was used to analyse an example when the seepage field is unsteady. The computation results have shown that the coupled seepage-stress action makes the stress components in rock mass to increase by different degrees. However, in this study (Deng and Wu 2009), the analysis was performed for foundation only and the body of the dam was neglected. Moreover, the pore pressure distribution contours were not provided in this research work.

A mathematical model of moving water under concrete dam in porous media was presented by Shamsai et al. (2010). Finite volume method of the governing equations in porous media was selected in this study. The results of seepage was discharged by using three powerful seepage codes (Seep/w, Mseep and Plaxis) that are based on finite element method and were compared with results of FV seep model which was based on finite volume method. However, the body of dam has been neglected in this study.

Gu et al. (2011) studied a new safety and seepage monitoring model of roller compacted concrete (RCC) dam, based on the comprehensive analysis method of the information entropy theory and the fuzzy matter-element analysis theory. Constructing the corresponding evaluation factor sets and review sets, the entropy-based fuzzy element analysis model of the RCC dam seepage monitoring has been put forward and verified by an example. This model has provided another way to analyse the RCC dam seepage behaviour. However, the pore pressure distribution analysis has not been carried out in this study.

Liu et al. (2011) presented a coupled hydro-mechanical mathematical model to describe the uplift process of the rock mass and gravity dam. A 3D numerical model was used to evaluate the representative elementary volume (REV) and to identify the

parameters related to the mechanical and hydraulic properties of the rock mass. The Tongjiezi dam which is a composite type, consisting of a concrete gravity dam in the river bed and rock-filled dams on both sides has been taken as a case study. In addition, the time-dependent deformation was also studied in the laboratory and numerically. The D–P (Drucker–Prager) plastic yield criterion and the visco-elasto-plastic model was used in the coupled seepage-stress analysis to describe the time-dependent deformation of the dam foundation rock. However, the stress effect on the failure criteria parameters has not been taken into consideration in the study.

Sun and Bagale (2012) studied the slope stability of the concrete dam under the interaction of fluid-solid coupling in the conditions of water level rising and rainfall intensity increasing using the method of strength reduction. Three cases were analysed in this study. It was concluded that the water level has a great influence on the slope stability of the dam. The higher water level causes stronger seepage effect, the larger the deformation of the dam skeleton, the larger the stress and the strain in the dam. However, the effect of temperature of reservoir water on the seepage response of the dam body was not taken into account in this study.

A constitutive model of endochronic damage was established by Chong-Shi et al. (2013) based on the endochronic theory and damage mechanics. The suggested model abandons the traditional concept of elastic-plastic yield surface for roller compacted concrete and basic equations were proposed for the fluid−solid coupling analysis. Then, the method was applied to an actual project, and the obtained results show that the fluid-solid interaction impacts on the dam deformation and dam abutment stability, which is consistent with practice.

Gan et al. (2014) applied Comsol Multiphysics analysis platform to couple seepage and stress fields of high arch dam. The coupled seepage-stress field was compared with uncoupled condition under normal storage level. The seepage, stress and displacement fields of the dam were analysed for discussing the coupled effect. It was concluded that coupled effects of seepage cannot be ignored under high water pressure. Later on, a three-dimensional simulation of flow through concrete dam foundation was performed by Shahrbanozadeh et al. (2015) using finite element

(Seep3D model) and artificial neural network (ANN) models. The suitable prediction in time and space of the seepage path through the foundation dam by the models indicates that these models can be employed to verify the piezometer readings to detect the unusual in the pore water and seepage fields.

2.4 Temperature and Stress Fields of RCC Dams

The temperature development in RCC dam is determined by the balance between the developments of heat due to hydration and the exchange of heat with surrounding environment. The most important factors for temperature development in RCC dams are (i) construction process and (ii) boundary conditions. The accuracy of any numerical model depends on how accurate these factors will be implemented in the proposed model. According to that, a large number of mathematical models for RCC materials have been presented for reliable prediction of temperature distribution and stress fields in RCC dam during the construction and operation phases. For instance,

Ishikawa (1991) analysed the thermal stress distribution for the gravity concrete dam using the ADINA computer program. In the presented study, the thermal stress analysis was executed considering two conditions; variation of the elastic modulus with time and the sequence of construction. The latter condition was applied using birth and death technique which was provided in the used software ADINA. However, the first condition was applied by modifying the used software to include the variation of the elastic modulus with time. The finite element results were compared with observation data, and good agreement was obtained. However, the analysis was carried out during the construction phase and for the thermal analysis only.

Later on, Tatro and Schrader (1992) introduced a practical discussion of the relevant issues influencing the thermal cracking. In the presented study, a step-by-step guide for computing the crack location using manual and desktop computational methods was presented. However, this simplified method did not consider the variation of the mechanical properties of concrete with time.

Saetta et al. (1995) proposed a finite-element procedure for the stress-strain analysis in concrete structures exposed to time-variant environmental conditions. The heat generation phenomenon in massive concrete structures and the seasonal and daily variation of temperature were taken into account in the presented work. The stress-strain-thermal analyses of 87 m height RCC Sa- Stria dam located in Italy was carried out for the purpose of analysis. However, linear elastic structural analysis was carried out where the variation of the elastic modulus with time was not taken into account. In addition, time-dependent effects were neglected.

Nehrin and Fujii (2001) presented a numerical procedure to evaluate the distribution of thermally induced stresses for Hinata RCC dam located in Japan during the construction phase. The analysis was carried out using a three-dimensional finite-element modelling and included consideration of heat generation due to hydration, conduction, solar radiation, as influenced by environmental factors such as ambient temperature and elastic effects. The commercially available software ANSYS was used to perform the analysis. However, in this study, a foundation block was not included in the FE model. In addition, the variation of the elastic modulus was not taken into consideration.

Thermal analysis of 188 m high RCC Mile dam has been carried out by Lopez et al. (2003) to evaluate the stresses and strains generated by the increasing temperature inside the body of the dam, as well as with its later cooling. The finite element program called Therm, developed at the University of Berkeley, California, was used in the analysis. In this work, one-dimensional and two-dimensional models of the heat transfer were analysed with the purpose of implementation of different boundary conditions of the dam body. The results obtained from thermal analysis were used as input data for the structural analysis. In the study, the two dimensional thermal analysis and linear stress - strain relationship were used.

Malkawi et al. (2004) analysed the thermal stress distribution of 60 m high RCC Al-Mujib dam located in Jordan using two and three dimensional finite element methods. The analysis was carried out using two different approaches. The first approach was a conventional approach in which the dam construction was simulated

by placing continuous RCC layers of 3 m thick every 10 days. The second approach, named the actual approach, considers the actual placement schedule of RCC layers which were 30 cm thick. The finite element software ANSYS was used in the analysis. A fixed value for the air temperature was assumed in the thermal analysis for both approaches. In addition, a simplified approach was used in order to check crack width and the required number of contraction joints.

Zhiqi et al. (2007) simulated the temperature and stress fields of the Longtan RCC dam during the construction and operation phases based on the actual construction parameters. The finite element results have been compared with the observation data from the prototype dam. The results have shown that, the results derived from the computation were in full agreement with observed data. The safety of the dam against the cracking potential was not provided in the presented study.

Jaafar et al. (2007) dealt with the development of a finite element based computer code for the determination of temperatures within the dam body. A thermal analysis was carried out using a two-dimensional finite-element method to simulate the construction process of RCC dams. An engineering application of this program was presented by simulating the construction of a real RCC dam called Roodbar in Iran. However, an approximated formula was used to calculate the ambient temperature.

A distribution of temperature and stress of Xiaowan gravity dam in China was simulated by Lingfei and Li (2008). Several factors affecting the dam temperature and stress fields, such as thermal and mechanical properties, construction process, and temperature variation of environment were taken into account in the numerical simulation. However, the effect of placement schedule was ignored. Later on, a three- dimensional finite element relocating mesh method was developed by Zhang et al (2009) to simulate the construction process of the RCC dams. In this work, thermal adiabatic rise of temperature with age, the process of placement by layer and the change of air temperature were considered. However, no study on the possibility of cracking development due to the thermal loads was carried out in this research.

Fujun et al. (2012) studied the cracking reasons for concrete overflow dam of Hadashan Hydro Project by developing a finite element method to simulate the

temperature distribution and thermal stress analysis during the construction phase. Results have shown that the cracks of the concrete overflow dam are temperature cracks due to combined actions of the internal thermal gradient and the external restraints. The analysis was carried out during the construction phase only.

A year later, a 3D numerical model to analyse unsteady thermal-stress in RCC dams has been developed by Kuzmanovic ei al. (2013). The temperature field was computed first, providing a derivation for the unsteady, nonlinear, viscoelastic, stress-strain analysis. This model was devised with actual initial and boundary conditions, appropriate material properties, and the observed concrete placement schedule.

2.5 Seismic Response of Gravity Dams

The safety of dams under earthquake is very important due to the possibility of large damage and consequences resulting from the failure of dams located in the seismological affected regions. Several attempts were made to study the seismic response of RCC dams for their safety evaluation. Seismic safety evaluation of concrete dams relies heavily on the results of numerical procedures and finite element analysis.

A boundary-element technique developed by Dominguez et al. (1997) for the dynamic analysis of continuous systems consisting of water and viscoelastic and poro-elastic zones of arbitrary shape was applied to a dam-reservoir-sediment-foundation system subjected to ground motion. This model was used to evaluate the effects of fully and partially saturated sediments on the seismic response of gravity dams. As for the influence of the degree of saturation and the thickness of bottom sediment it was concluded that, the changes in the thickness of the sediment layer produce significant changes in the dam response.

Sasaki et al. (1998) studied the stress field of the concrete gravity dams and their safety using seismic data from Kobe Earthquake. They introduced the characteristics of ground acceleration observed at dam sites during the earthquake and discussed the effect of the vertical and horizontal seismic motion and the safety of the concrete gravity dams. The response spectrum method with the finite element model of the

concrete gravity dam was used in the analysis of the dynamic stresses in the dam. The dam was constructed on the rock foundation and the effect of reservoir water was accounted for as the added mass in the mass matrix during the modal analysis.

Later on, Guanglun et al. (2000) analysed the seismic fracture of concrete gravity dams using non-linear fracture mechanics. Theory of non-linear crack band was used to inspect the two dimensional seismic fracture analyses of concrete gravity dams. The size of the finite element meshing adopted was close to the attributes size of the crack band of the concrete material, therefore, the strain softening effect for concrete could be taken in account. The procedures were validated with the test outcomes of a cloven beam and then applied to non-linear fracture analysis of the Koyna dam. Moreover, several properties of the analysis and the expected process of the fracture of concrete were also investigated.

Chuhan et al. (2002) considered the experimental tests of rolled compacted concrete and nonlinear failure analysis of RCC dams. Strain controlled uniaxial tension and compression tests of roller compacted concrete (RCC) were carried out to establish the constitutive relationship of RCC. To satisfy the test requirements for getting the material strain-softening behaviour, the fixity conditions on sample parameters and machine rigidity were presented based on the meaning of the strain localization. By employing test results of RCC, Longtan RCC Dam of 200 m high, was analysed for earthquake resistance using the process of nonlinear failure mechanics and the compression-shear fracture mechanism for concrete. A safety evaluation of the dam's capability to withstand the design earthquake under various reservoir elevations was performed.

Seismic safety evaluation of concrete dam relies heavily on mathematical models that adequately capture dynamic characteristics of the dam-water-foundation system. US Army Corps of Engineers (2003) presented a systematic performance evaluation criterion to assess the dam response in the damage control range. The linear time history analysis was used to formulate a systematic and rational methodology for assessment of performance and qualitative estimate of probable level of damage.

This criterion depends on the stress demand capacity ratios, cumulative overstress duration and spatial extent of overstressed regions.

Lotfi (2004) proposed the parametric observations of nonlinear smeared crack models and damage mechanics to analyse concrete dams. In this research the results of these two analyses showed that the simultaneous increment of tension strength and Young's modulus cause to create an interaction for prediction of dam behaviour. Eventually, the results of this study have confirmed that damage mechanics model has less failure than the propagated crack model at the body of the dam and therefore, damage mechanics model has more stability.

Javanmardi et al. (2005) investigated the seismic structural stability of concrete gravity dams using transient uplift pressure in crack. A theoretical model was developed by transient fluid pressure differences alongside a tensile crack of seismic concrete named crack wall. Moreover, an empirical test was implemented to verify the projected model. Numerical and empirical results showed that water can go through new seismic cracks.

Ayothiraman et al. (2006) investigated the dam-reservoir-foundation interaction to predict seismic behaviour of concrete gravity dam, through a case study using Bichom dam located in North-Eastern India. The significance of the dam foundation flexibility to dynamic response was studied by comparing the results with rigid foundation. The hydrodynamic effects of reservoir water was modelled as an added mass by Chopra method. The results demonstrated that the dam was safe except for some miner cracks at the heel of non-overflow monolith for rigid foundation. The response of the dam bedding on flexible foundation showed that the dam suffers moderate damage when the reservoir was empty and full. However, a linear elastic behaviour was used in this study.

A foundation flexibility and nonlinearity in the seismic response of gravity dams has been considered by Burman et al. (2008). SAP 2000 was used to obtain the results for Koyna dam under El-Centro excitation in 1940. Material nonlinearity of the foundation material was modelled by combination an advanced plasticity-based soil model called Boscawen elasto-plastic model. Both the linear and nonlinear analyses

were done to compare their responses in the soil-structure interaction analysis. The results were illustrated clearly the significance of nonlinear analysis of the coupled dam-foundation system.

Seismic responses of 160 m high concrete gravity dam with and without reinforcement under earthquake excitation have been studied by Long et al. (2009). The numerical analysis considered many different non-linearities, such as, recovery of stiffness, concrete cracking and bond-slip effects. As a result, the bond-slide effects illustrated that recovery of stiffness effect has an important influence on the dynamic behaviour of the dam such as cracking patterns, horizontal displacement and residual deformations. The results showed that the presence of the reinforcement in the concrete was helpful to improve the seismic resistance ability of the concrete gravity dam.

Mazloumi et al. (2012) investigated the nonlinear seismic response of Roller Compacted Concrete (RCC) dam considering orthotropic behaviour of the layers. They considered a nonlinear smeared crack model to inspect an anisotropic behaviour of RCC dams in perpendicular and parallel directions for the layers interface. Koyna (India, 1967) earthquake was applied to the tallest monolith of Jahgin dam and Kobe (Japan, 1995) earthquake was applied to the reservoir. Results illustrated that the cracks were propagated from the slope changes of the upstream in horizontal direction. Another zone which suffered from cracking was related to the downstream face on the upper segment area.

In order to assess the nonlinear damage potential of strong aftershocks, Zhang et al. (2013), evaluated the effects of seismic sequences on the nonlinear seismic response and accumulated damage of concrete gravity dams. Both local and global damage indices were established to study the influence of strong aftershocks on the cumulative damage of concrete gravity dams. A Concrete Damaged Plasticity (CDP) model including the strain hardening or softening behaviour was selected for the concrete material. This model was used to evaluate the nonlinear dynamic response and the seismic damage process of Koyna dam during 1976 Koyna earthquake. Comparison of the results of the present nonlinear approach with the Koyna dam

prototype observation, model test, and those of available methods in the literature indicated that the CDP model selected for the concrete gravity dams can be used successfully in seismic accumulated damage analysis.

2.6 Discussion on the Literature Review

The literature on RCC dams, which can be divided into three parts, has been discussed extensively in this chapter. The first part addresses the coupled seepage-stress analysis of RCC dams. The second addresses the thermal modelling of RCC dams during construction and operation phase. And the last part deals with the seismic response of these types of structures.

2.6.1 Seepage and Stress Field of RCC Dams

It has been well recognized in geotechnical engineering practice (dams, slopes, landslides, underground spaces, etc.) that groundwater seepage (flow) has a great influence on the deformation and stability of soils, rocks and geotechnical structures. Seepage control is critical for maintaining the stability and safety of the engineering works (Jiahai 1986, Dunlu 1987, Zhang 2002, Chen 2007, Djehiche 2008). Understanding the physical mechanisms and their corresponding numerical modelling approaches of engineering measures for seepage control is obviously of paramount importance for safety assessment, optimization of design, and construction and operation of a seepage control system.

The problem becomes more complex when the existence of water is not uniform throughout the whole analysis region. One part of the region may be saturated while the other part may be dry. This situation is sometimes handled simply by assuming a ground water table. In most cases, however, a horizontal plane of the water table cannot properly represent the actual state, and thus it is necessary to evaluate a more accurate phreatic surface of the ground water flow through seepage analysis. This is the reason why the seepage analysis needs to be coupled with stress analysis in modelling soil mechanical problems (Li, 1983, Lai, 2008, Rice, 2009).

Previous researchers have formulated mathematical models for evaluating the

permeability of porous and fractured media, but omitted the effect of confining pressure and the associated deformation. More recently, a few publications have appeared which include the effect of confining and pore pressures on the effective permeability of fractured media (Walsh 1979, 2003).

Furthermore, at present, there have been many conventional concrete dam seepage monitoring models (Zhongru 2003, Chongshi, 2006, Huaizhi 2006) which mainly apply the methods for conventional concrete dam, while there are rare safety monitoring models for roller compacted concrete dams because of their complexity.

2.6.2 Thermal and Stress Fields of Gravity Dams

During the construction of RCC dams, a number of papers have been published that compare the predicted temperature in RCC dams with measurements on the applicable prototypes (Malkawi et al. 2003; Zhiqi 2007; Bayagoob 2010) and the technology of temperature prediction has been demonstrated through monitoring to be accurate.

During the operation phase, several publications reported by many researchers predicted the heat exchange (interaction) between the dam body and the impounding water (Zhu and Xu 1999; Zhang and Zhu 2003; Bayagoob 2010; Cervera et al. 2000), but the variation of the water temperature with the seasonal changes of air temperature or with depth of reservoir is usually neglected or approximated by an assigned fixed temperature. The accurate simulation of the heat exchange between the dam body and reservoir water will lead to realistic temperature distribution profiles through the dam body and determine the accurate structural response of dam.

Several research works have been carried out concerning the stress fields in RCC dams. Generally, the predicted temperature due to the thermal analysis is translated into thermal strain to be added to the other loads acting on the dam body during the construction or the service life of the dam. In greater part of these works the commercial packages were used to perform such analyses (Nehrin and Fujii 2001; Malkawi et al. 2004; Lopez et al. 2003). However, due to inadequate representation of the reference temperature, many commercial software such as ADINA failed to

simulate the stress history of maturing concrete with the temperature variation correctly (Ayotte et al.1997). In addition, many of these investigators used a simplified relation for stress-strain relationship (Seatta et al. 1995; Agullo and Aguado 1995; Kruger et al. 2003; Zhang and Zhu 2003), which will overestimate the stress of the dam (Crichton et al. 1999).

It is of particular significance to observe that most studies simply assumed that RCC behaves in the same manner as conventional concrete and various models developed for the conventional concrete were applied for RCC without any form of verification. Furthermore, the material laws for concrete were mainly based on the age of concrete and very limited studies considered the temperature effect on the mechanical properties of the materials (Luna and Wu 2000; Cervera et al. 2000).

Despite considerable number of works having been published and addressing the thermal and stress analysis of RCC dams, limited works have been published on the safety evaluation of the RCC dam (Cervera et al. 2000; Noorzaei et al. 2006).

2.6.3 Seismic Response of Gravity Dams

Dams are massive structures which are usually subject to risk of ground motions. Crack patterns and their size can normally show the weakness of gravity dams. Therefore, in recent years, study of crack patterns and seismic behaviour of concrete dams have been the subject of extensive research during the past decade concerning dam safety under earthquake excitations (Calayir and Karaton 2005; Ftima and Leger 2006; Wei 2008).

Seismic analyses and design of concrete gravity dams were studied in detail by Chopra and his colleagues, and later by others (Bougacha & Tassoulas, 1991; Cha´vez & Fenves, 1995; Chopra, 1972, 1978; Chopra & Zhang, 1991; Medina et. al. 1990; United States Army Corps of Engineers (USACE), 1995). However, in their studies, the seismic stability of RCC dams has not been evaluated under seepage flows and thermal actions.

On the other hand, seismic design of dams still remains an important challenge in many countries worldwide where new dams are being built, such as China and Spain (Akpinar et. al. 2011; Dursun & Gokcol, 2011; Hong, Du, & Jiang, 2010).

Gravity dams are fluid-structure-soil interaction problems. It is obvious that the foundation soil and water reservoir affect the dynamic response of gravity dams during earthquakes. Many factors have effect on the dynamic response of concrete gravity dams against earthquake motion. Some of these factors include dam-reservoir-foundation interaction, sediments at the bottom of the reservoir and nonlinear behaviour of concrete gravity dams. Being a multi-physics problem, the seismic analysis of dam-reservoir-foundation interaction was generally treated as a two-dimensional problem for concrete gravity dams [Calayir and Karaton (2005), Akköse and Simsek (2010), Jiang and Du (2012), Mazloumi et al. (2012), Zhang et al. (2013), Paggi et al (2013)]. However, the effects of openings in dams have been neglected in the above studies.

In addition, the hydrodynamic pressure due to the impounded water and dam deformation under earthquake excitations interact with each other and the significance of hydrodynamic pressure effect on dam behaviour subjected to earthquake has been recognized. Thus, the effect of water level under earthquake response has to be considered in the nonlinear dynamic analysis (Akkose et al., 2008; Perumalswami and Kar, 1973). And more recently, the safety evaluation of existing dams appears to be a crucial issue in many countries (Chuhan et. al. 2002; Gogoi & Maity, 2005; Jiang, Du, & Liu, 2009; Le´ger & Javanmardi, 2006; Mills-Bria et. al. 2008; Tekie & Ellingwood, 2003).

2.7 Concluding Remarks

It is evident from the above literature review that continuous efforts should be made to arrive at a realistic numerical modelling of stress fields in RCC dams, in construction and operational phases. Based on the literature review in this chapter, the following major points could be drawn:

- The Mechanical properties of the conventional mass concrete were used to

model RCC material. However, the actual properties of RCC materials should be used in the analysis.

- In recent studies, the material laws for RCC were mainly based on the age of concrete. However, in reality, the temperature and confining pressure also influence the material's mechanical properties.

- In the prediction of cracking tendency in RCC dams, the properties of RCC materials such as development of mechanical properties (strengths, E-modulus) and temperature effect have not been taken into consideration in any developed mathematical crack models.

- The effect of the reservoir water on the thermal and seepage response of the RCC dams was neglected or approximated in all presented models. Only few models have approximated this action by assigning a constant value of temperature at the upstream face of the dam or using linear variation of reservoir water temperature along the depth which was based on earlier long time observations.

- It is essential to evaluate the seismic stability of RCC dams under seepage flows and thermal actions.

CHAPTER 3

METHODOLOGY AND GOVERNING EQUATIONS

3.1 General

Numerical simulation enables engineers to develop large, economical and reliable structures by providing them with practical feedback when designing the infrastructures such as dams. This allows the designer to determine correctness and efficiency of a design before the dam is actually constructed. Consequently, the finite element methods have become one of the most powerful methods in engineering analysis and design. The development has been associated with rapid improvements, associated with availability of efficient computational facilities. The use of finite element methods is also to overcome difficulties associated with physical testing of large enough dam models to obtain meaningful results.

Based on the gaps and the suggestions in the literature review presented in Chapter 2, and the research problems in Chapter 1, and in order to achieve the study objectives, it is necessary to propose a comprehensive numerical technique and system to simulate the construction process and service life of RCC dams. The system also has to be capable of evaluating the seismically induced cracking of RCC dams under the effects of thermal and seepage actions. In addition, more relevant features of the behaviour of concrete such as ageing, temperature effect, confining pressure and adiabatic temperature have been considered in the analysis.

A purposeful comprehensive numerical system consists of several individual features and in combination. The system includes a combination of field problems (thermal and seepage fields), continuum mechanics (stress analysis), seismic hazard assessment and safety evaluation. The combination uses finite elements to introduce compatible units capable of analysing infrastructure, such as RCC dams, to evaluate and predict levels of safety in terms of crack pattern development. The method, which is based on principle of birth and death process, is capable of simulating and assessing safety of

RCC dams during the construction and the operation phase. Figure 3.1 illustrates the present system process.

The constitutive material model for concrete in this study is based on the combination of damage mechanics and plasticity. It uses concepts of isotropic damaged elasticity in combination with isotropic tensile and compressive plasticity to represent the inelastic behaviour of concrete. The mathematical models for mechanical behaviour of material are given in the form of constitutive equations. The proposed constitutive models have been reformulated and presented in convenient forms for RCC materials. Ageing, temperature and confining pressure effects were taken into account and implemented in the proposed constitutive models. Appropriate boundary conditions are used for the water interaction at the upstream face of the dam, taking into account the variation of temperature of the reservoir water with depth.

All the developments and analyses are performed using coded subprograms written in FORTRAN and developed in finite element program ABAQUS. Then, the validity of the proposed computational procedures and models has been confirmed by analysing and comparing the results obtained based on experimental and analytical evidences. After the verification process, the material nonlinearity and proposed models are applied to analyse and evaluate the related dam safety against the cracking of an existing full-size dam. Finally, conclusions are drawn and recommendations are made based on the present research.

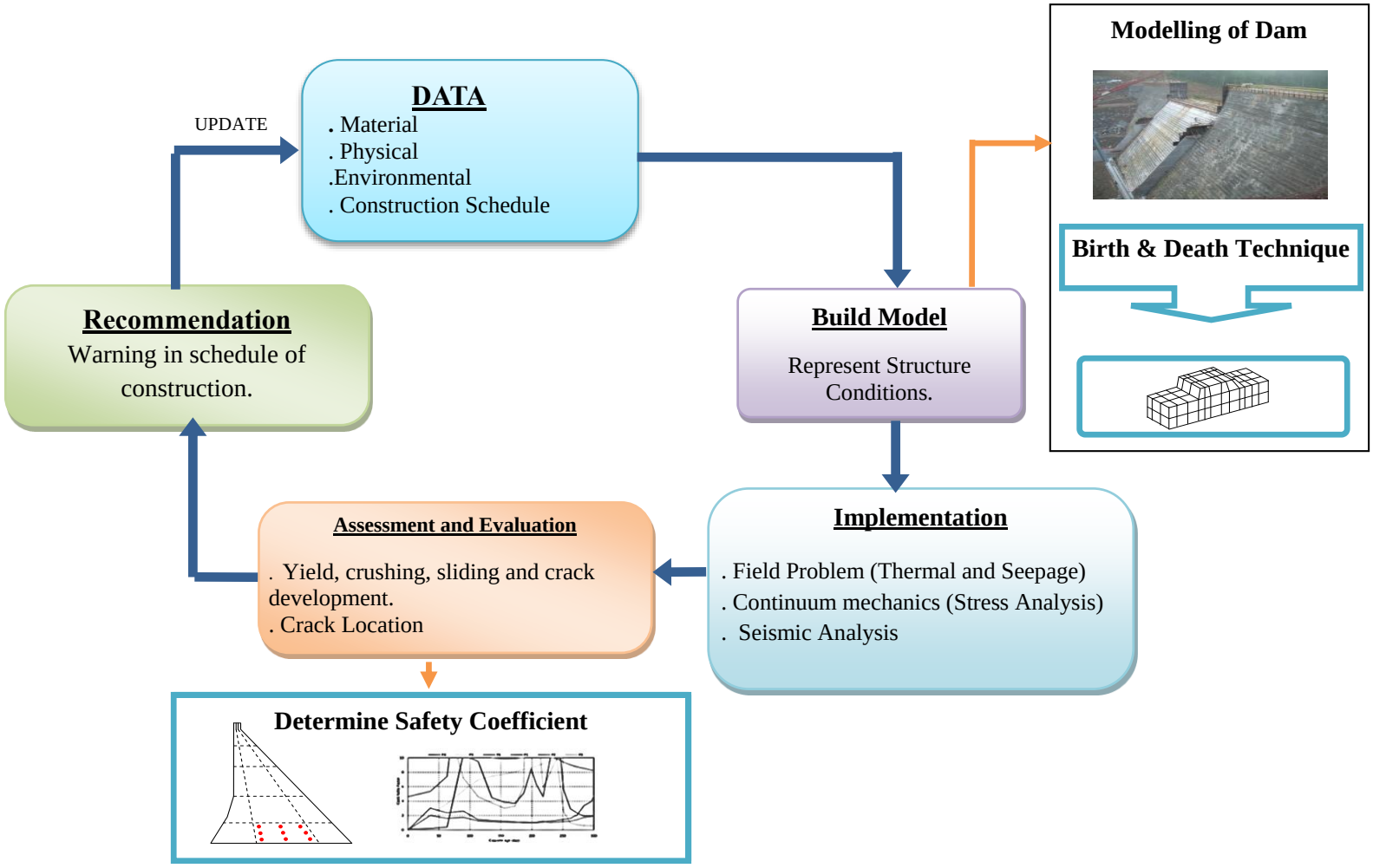

Figure 3.1 System Process Flow Diagram

3.2 Mathematical Equations on Fluid Flow and Stress Field Coupling

The porous medium theory used in ABAQUS (Ahola 1994) is based on the conventional effective stress principle, with compressibility of the solid and fluid phases allowed in the continuity equation. The governing equations for pore fluid flow/deformation are the equilibrium equation as well as the continuity equation for the wetting liquid phase in a porous medium.

3.2.1 Seepage Field Model

The internal seepage of RCC layer, by assuming that the temperature of water remains unchanged, meets the Darcy's Law. The basic two-dimensional continuity equation of the seepage field can be expressed as Eq. (3.1) based on the law of mass conservation (Zee et. al. 2011);

$$\frac{\partial}{\partial x}(K_x \frac{\partial H}{\partial x}) + \frac{\partial}{\partial y}(K_y \frac{\partial H}{\partial y}) + Q = S_s \frac{\partial H}{\partial t} \tag{3.1}$$

where K_x and K_y are the hydraulic conductivity in the x and y directions, respectively, Q is the applied boundary flux, H is the distribution function of water head in seepage area and S_s is the storage capacity. The relationship between H and pore water pressure u_w is given by;

$$H = u_w/(\rho_w g) + Z \tag{3.2}$$

where ρ_w denotes the density of water, g is the gravity acceleration and Z is the height.

3.2.2 Stress Field Model

In order to describe the deformation of porous media in two-dimensional consolidation, the equilibrium equation which takes into account the stress-strain relation needs to be considered. The fundamental relation of the interaction between the solid deformation and the fluid flow can be explained by the Terzaghi's effective stress principle as (Terzaghi, 1943):

$$\sigma = \sigma' + u_w \tag{3.3}$$

where σ' and σ are the effective and total stress and u_w is the pore water pressure. The stress-strain relations based on generalized Hook's law for plane strain condition can be written as follows (Timoshenko, 1970):

$$\sigma_{ij}' = 2G\varepsilon_{ij} + \left(K - \frac{2G}{3} \right) \delta_{ij} \varepsilon_v \tag{3.4}$$

where δ_{ij} is the Kronecker delta (δ_{ij}=1 when $i = j$ and δ_{ij}=0 when $i \neq j$), K and G are bulk and shear modulus, ε_v is the volumetric strain and ε_{ij} is the strain tensor field, respectively, and are calculated as following:

$$G = \frac{E}{2(1+\nu)} \tag{3.5-a}$$

$$\varepsilon_{ij} = \frac{1}{2}(u_{ij} + u_{ji}) \tag{3.6-b}$$

$$\varepsilon_v = \varepsilon_{11} + \varepsilon_{22} + \varepsilon_{33} \tag{3.7-c}$$

where E is elastic modulus, ν is Poission's ratio and u_{ij} are displacement components.

If the dam and its base rock are affected only by gravity and seepage forces, which are considered as body forces, and denoting that the tensile stress is positive, the balance differential equations can be given as Eq. (3.5):

$$\frac{\partial \sigma_{ij}}{\partial x_j} + F_i = 0 \qquad i, j = 1,2,3 \tag{3.8}$$

where F_i is the body force per unit volume.

The coupled governing equations of the RCC layer stress field and the seepage field are composed of equation (3.1) and (3.5) simultaneously. Whereas, in the uncoupled approach, the continuity equation for the water phase and the equilibrium equations are solved independently.

3.2.3 Stress Equilibrium and Fluid Continuity Finite Equations

The standard finite element matrices are formed using the principle of superposition. After space and time discretization, the coupled problem can be written in matrix notation (Lewis and Schrefler, 1998):

$$K\Delta u + L\Delta p = F \tag{3.6}$$

$$L^T\Delta u + E\Delta p = R \tag{3.7}$$

where K is the stiffness matrix, u is the solids displacement vector, L is the coupling matrix between mechanical and flow unknowns (i.e., displacement and pore pressure), F is the vector of force boundary conditions, E is the flow matrix, p is the pore pressure, and R is the source term for the flow drive.

Combining equations (3.6) and (3.7) results in the incremental form of the discretized fully-coupled Biot's equations:

$$\begin{bmatrix} K & L \\ L^T & E \end{bmatrix} \begin{Bmatrix} \Delta u \\ \Delta p \end{Bmatrix} = \begin{Bmatrix} F \\ R \end{Bmatrix} \tag{3.8}$$

3.2.4 Evaluation of Initial conditions

In fully or partially saturated flow problems, the initial void ratio, as well as the initial pore pressure and the initial effective stress, must be defined. In these problems (coupled deformation/flow analysis), it is important to establish initial stress equilibrium as well as steady state flow conditions. The initial conditions discussion that follows is based on the total pore pressure formulation (the magnitude and direction of the gravitational loading are defined by using the GRAV *DLOAD option in ABAQUS Software).

- **Initial void Ratio**

The void ratio (e) is the ratio of the volume of voids to the volume of solids, i.e.

$$e = \frac{V_v}{V_s} \tag{3.9}$$

The porosity (n) is the ratio of the volume of voids to the total volume of the media;

$$n = \frac{V_v}{V} \tag{3.10}$$

So, the void ratio and the porosity are inter-related as follows:

$$e = \frac{n}{1-n} \tag{3.11}$$

- **Initial Pore Pressure**

The initial pore pressures in seepage analysis can be defined as a linear function of elevation in the model or as a constant value. The initial pore water pressure (u_0) depends primarily on the depth of the point in the model and on the placement water content of the fill. In the geostatic state, the pore fluid is in hydrostatic equilibrium, so that

$$\frac{du_w}{dz} = -\gamma_w \tag{3.12}$$

where γ_w is the specific weight of the pore fluid. In the case, where γ_w is independent of z (which is usually the case, since fluid is almost incompressible), this equation can be integrated:

$$u_w = \gamma_w(z_w^0 - z) \tag{3.13}$$

where z_w^0 is the height of the phreatic surface, at which $u = 0$ and above which $u < 0$ and the pore fluid is only partially saturated (ABAQUS Manual, 2003).

- **Initial Effective Vertical Stresses**

In most geotechnical problems, a nonzero state of stress exists in the medium. This typically consists of a vertical stress increasing linearly with depth, equilibrated by the weight of the material, and horizontal stresses caused by tectonic effects. The active loading is applied on this initial stress state. Active loading could be the load on a foundation or the removal of material during an excavation. It is clear that, except for purely linear analysis, with a different initial stress state, the response of the system would be different (ABAQUS Manual, 2003).

The total vertical stress (i.e. the total normal stress on a horizontal plane) at depth z is equal to the weight of all materials (solids + water) per unit area above that depth, i.e. (Craig, 2004)

$$\sigma_v = \gamma_{sat} z \tag{3.14}$$

The pore water pressure at any depth will be hydrostatic since the void space between the solid particles is continuous, so at depth *z*;

$$u_w = \gamma_w z \tag{3.15}$$

Hence, from the Terzaghi principle($\sigma = \sigma' + u_w$), the effective vertical stress at depth z will be;

$$\sigma'_v = \sigma_v - u_w$$
$$= (\gamma_{sat} - \gamma_w)z = \gamma' z \tag{3.16}$$

where γ' is the buoyant unit weight and computed as follows (Craig, 2004);

$$\gamma' = \frac{G_s - 1}{1 + e}\gamma_w \tag{3.17}$$

and (G_s) is the specific gravity of the soil or rock particles and is given by;

$$G_s = \frac{\rho_s}{\rho_w} \tag{3.18}$$

where ρ_s is the particle (rock) density.

ABAQUS provides the *GEOSTATIC procedure to allow the user to establish the initial stress state. The user will normally specify the initial effective stresses using *INITIAL CONDITIONS, TYPE=STRESS, GEOSTATIC and in the first step of analysis, apply the body (gravity) loads corresponding to the weight of the material. Ideally, the loads and initial stresses should exactly equilibrate and produce zero deformations.

3.2.5 Simulation of Boundary Conditions

Seepage analysis problems associated with dam will involve four possible types of boundaries (Harr 1962) as shown in Figure 3.2.

- **Entrances and Exits (Reservoir Boundary)**

- The lines defining the area where water enters or leaves the pervious media mass are known as entrances or exits (upstream and downstream).
- Flow is perpendicular to an entrance or exit.

The upstream face of the dam (surface S_1), in Figure 3.2, is exposed to water in the reservoir behind the dam. Since ABAQUS uses a total pore pressure formulation, the pore pressure on this face must be prescribed to be $u_w = (H_1 - z)\rho_w g$, where H_1 is

the elevation of the water surface, z is height, g is the gravitational acceleration, and ρ_w is the mass density of the water. Likewise, on the downstream face of the dam (surface S_2), $u_w = (H_2 - z)g\rho_w$.

- **Surface of Seepage (Seepage face)**

- The saturated pervious media may have a boundary exposed to the atmosphere and allow water to escape along this boundary.
- Pressure along this surface is atmospheric.

A special boundary condition is needed if the phreatic surface reaches an open, freely draining surface, as indicated on surface S_5. In such a case, the pore fluid can drain freely down the face of the dam, so that $u_w = 0$ at all points on this surface and below its intersection with the phreatic surface. Above this point $u_w < 0$, with its particular value depending on the solution.

- **Impervious Boundaries**

- Interface between saturated, pervious mass and adjacent material such as; very low permeability soil or concrete.
- No flow takes place across this interface (q=0)

The bottom of the dam (surface S_3) is assumed to rest on an impermeable foundation. Since the natural boundary condition in the pore fluid flow formulation provides no flow of fluid across a surface of the model, no further specification is needed on this surface.

- **Phreatic Surface Boundary (Free Surface)**

Phreatic or seepage surface is defined as the line within a dam body, which separates the saturated region of flow from dry or unsaturated zone of the media (Sharma et al, 2008). However, in the case of seepage through the dam body, below this line, the media is submerged and the hydrostatic pressures are positives (Punmia, 2005). The hydrostatic pressure on the line itself is atmospheric or zero and above the line, the media is dry (moist) and there is a zone of saturation due to capillary action which is neglected (S_4 boundary in Fig.3.2).

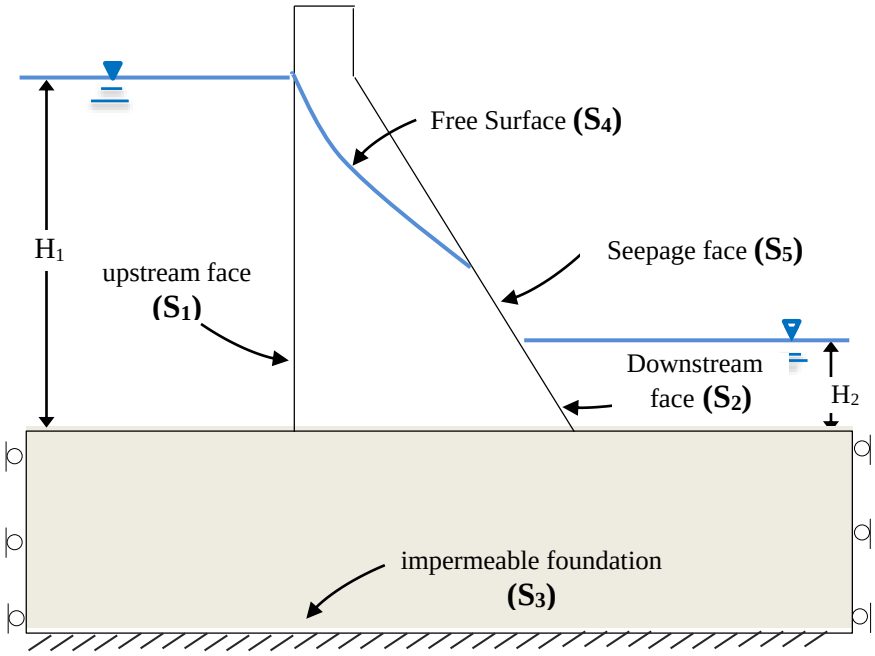

Figure 3.2 Illustration of the Boundary Conditions

The determination of phreatic surface location in the dam is necessary to assess the media properties while testing the stability of the dam. The calculation procedure of phreatic face is as follows;

- **Calculation of Phreatic Surface**

Complex variable theory can be used to obtain a solution to the dam problem. Let the complex number $w = \phi + i\,\psi$ be an analytic function of $r = x + iz$. Consider the function:

$$r = Cw^2 \tag{3.19}$$

where C is a constant. Thus,

$$x + iz = C(\phi + i\psi)^2$$

$$= C(\phi^2 + 2i\phi\psi - \psi^2) \tag{3.20}$$

Equating real and imaginary parts:

$$x = C(\phi^2 - \psi^2)$$

$$z = 2C\phi\psi$$

Equations (3.19) and (3.20) govern the transformation of points between the r and w planes (Figure 3.3). The equation of the phreatic line can be derived by substituting the conditions;

$$\psi = q$$

$$\phi = -kz$$

Thus;

$$z = -2Ckzq$$

$$\therefore C = -\frac{1}{2kq} \tag{3.21}$$

Hence;

$$x = -\frac{1}{2kq}(k^2z^2 - q^2)$$

$$x = \frac{1}{2}\left(\frac{q}{k} - \frac{k}{q}z^2\right) \tag{3.22}$$

The curve represented by Eqn.3.22 is referred to as Kozeny's basic parabola and is shown in Figure 3.3 (b), the origin and focus both being at A.

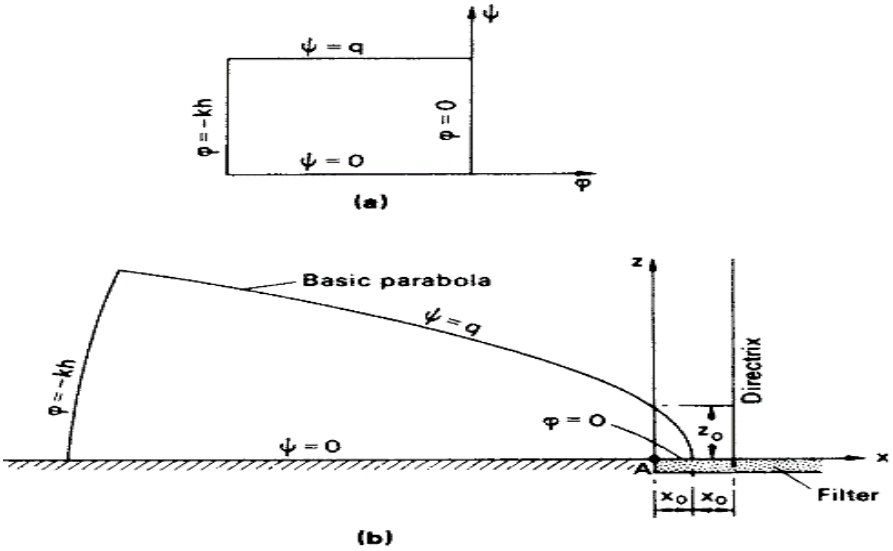

Figure 3.3 Transformation for embankment dam section, *w* and *r* plane (Craig, 2004)

When $z = 0$ the value of x is given by

$$x_0 = \frac{q}{2k}$$

$$\therefore q = 2kx_0 \tag{3.23}$$

where $2x_0$ is the directrix distance of the basic parabola. When $x = 0$ the value of z is given by;

$$z_0 = \frac{q}{k} = 2x_0 \tag{3.24}$$

Substituting Eqn.3.24 into Eqn.3.22 yields;

$$x = x_0 - \frac{z^2}{4x_0} \tag{3.25}$$

The basic parabola can be drawn using Eqn.3.25, provided the coordinates of one point on the parabola are known initially. Based on an extensive study of the problem, Casagrande recommended that the initial point of the basic parabola should be taken at G (Figure 3.4), where $GC = 0.3HC$. The coordinates of point G, substituted into Eqn.3.25, enable the value of x_0 to be determined; the basic parabola can then be plotted. The top flow line must intersect the upstream slope at right angles; a correction CJ must ,therefore, be made (using personal judgment) to the basic parabola. The flow net can then be completed as shown in Figure 3.4. (Craig, 2004).

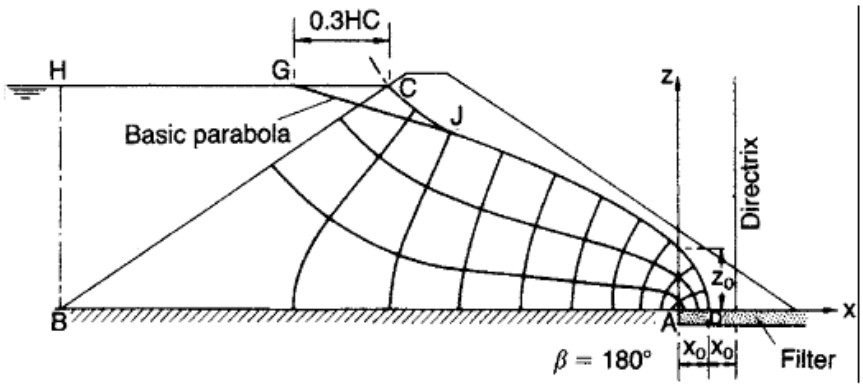

Figure 3.4 Flow net for embankment dam section (Craig, 2004)

3.2.6 Hydraulic Conductivity of Concrete

The hydraulic conductivity of the concrete dam body is not only a function of the concrete media properties, but also a function of the properties of the fluid flowing through the dam body. The hydraulic conductivity of the concrete dam body is inversely proportional to the viscosity of the water, i.e.

$$K = \frac{k_0 \gamma}{\mu} \tag{3.26}$$

where K is the hydraulic conductivity ($m/\sec$), k_0 is the permeability of the media (m^2), γ and μ are the specific weight and viscosity of the water (kg/m.s)(Junrui, 2002).

The behaviour of permeability of concrete (k_0) is closely related to its durability. By conducting laboratory experiments, it was shown that a relation exists between the permeability of the concrete and the confined pressure exerted. From the results, it could be concluded that the permeability of the concrete will decrease with the confined pressure increasing, which may be described as an exponential equation (Wang, 2011);

$$k_0 = a_0 + a_1 \exp(-\sigma/b) \tag{3.27}$$

where,

k_0 = Permeability (μm^2)

a_o,a_1,b = constant values (obtained from Table 3.1)

σ = confining pressure (MPa)

Table 3.1 The Constant Value for Permeability of Concrete Specimens (Wang, 2011)

	Constant Value			Correlation Coefficient
	a_o	a_1	b	r
Loading	0	382.5651	0.7808	0.9802
Unloading	0.0909	1855.284	0.4294	0.9934

Furthermore, the viscosity of the fluid is a function of the fluid temperature. For example, the viscosity of water can be obtained by the following empirical equation ((Junrui, 2002);

$$\mu = \frac{(0.01775)}{(1+0.033T+0.000221T^2)} \tag{3.28}$$

in which T is the temperature of water (°C); μ is the viscosity of water (kg/m.s). It can be shown from this equation that water temperature has a great impact on the viscosity of water.

The variation of the water temperature with the seasonal changes of the air temperature as well as the depth of the reservoir is usually neglected or approximated by assigned fixed temperature. These simplified approaches are usually based on long term observations of similar reservoirs. However, it is practically hard to generalize the conditions of these reservoirs with respect to the reservoir under consideration. Reservoir temperature varies with depth and follows a cyclical seasonal variation as shown in Figure 3.5. Based on the observed data for many years at different reservoirs, the water temperature at different water depths can be expressed as follows (Bofang, 1997);

$$T(y,t) = T_m(y) + A(y)\cos\omega\,(t - t_0 - \varepsilon) \tag{3.29}$$

where t is time in months, y is the depth of water, $T_m(y)$ is the annual mean temperature of water, ε is the phase difference between the maximum temperature of water and air, ω is the circular frequency of temperature variation. $A(y)$ is the amplitude of annual variation of water temperature . These parameters are computed as follows (Bofang, 1997 and Yu 2011);

$$T_m = c + (c - b)e^{-\alpha y} \tag{3.29-a}$$

$$A(y) = A_0 e^{-\beta y} \tag{3.29-b}$$

$$\varepsilon = d - f e^{-\gamma y} \tag{3.29-c}$$

$$\omega = 2\pi/P \tag{3.29-d}$$

in which $c = \frac{T_b - bg}{1-g}$, $g = e^{-\alpha H}$, where H is the depth of the reservoir, T_b is the water temperature at the bottom, b is the annual mean temperature at the surface of the reservoir and P=12 months is the period of variation. Data used in this study was reported in the literature for reservoirs with similar climatic conditions (Bofang, 1997) which are;

$A_0 = 9.55$, $\alpha = 0.04$, $\beta = 0.018$, $c = 11.62$, $b = 6.54$, $d = 2.15$, $f = 1.3$ and $\gamma = 0.085$.

The facility of user defined solution-dependent field variable (SDFV) available in ABAQUS is used to implement these modifications.

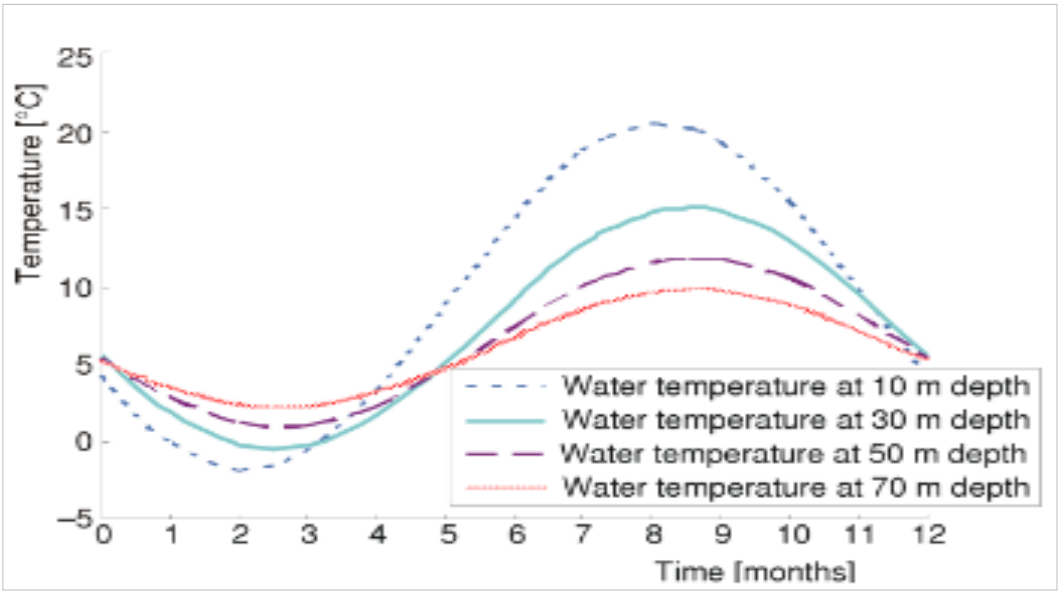

Figure 3.5 Water Temperature versus Different Months of the Year for Different Depths of Water (Zhu, 1997)

3.2.7 Constitutive Model

A linear elastic model is used for the rock foundation material and the Mohr-Coulomb behaviour with a non-associated flow rule which is widely used in the elasto plastic analysis of concrete dams (Azmi and Paultre 2002) is employed for the dam body materials.

- **Mohr-Coulomb Criterion**

In the Mohr-Coulomb yield surface for fluid flow analysis, the media is assumed to behave as a linear elastic perfectly plastic material; thus, no hardening/softening rules are required. The failure criterion for the model is shown in Figure 3.6 and can be expressed as (Helwany 2007):

$$\tau_f = c' + \sigma' \tan \phi' \tag{3.30}$$

where τ_f and σ' are the shear and the normal effective stresses on the failure plane, using the effective cohesion c' and the effective friction angle ϕ', respectively. The

Mohr-Coulomb yield function f , is formulated in term of effective principal stress which is given by;

$$f = \frac{1}{2}\left(\sigma_1' - \sigma_3'\right) + \frac{1}{2}\left(\sigma_1' + \sigma_3'\right)\sin\phi' - c'\cos\phi' \tag{3.31}$$

where, σ_1' and σ_3' are the major and minor effective principal stresses, respectively.

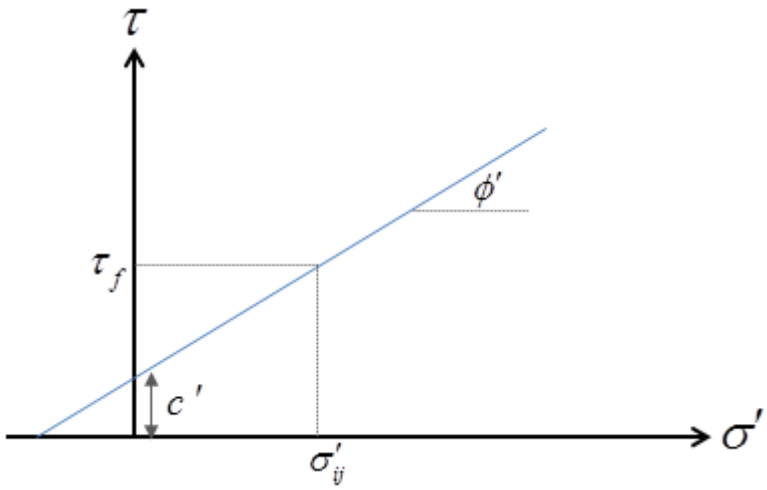

Figure 3.6 Mohr-Coulomb Failure Criterion

3.3 Computational Strategies for Thermal-Stress Analysis

3.3.1 Heat Transfer Analysis

- **Mathematical Model**

The basis for thermal analysis is the heat balance equation or governing heat transfer equation, which is based on the principle of energy conservation. The spatial and temporal varying temperature field in a solid medium can be evaluated from the well-known Fourier's differential equation as (Incropera and DeWitt 2002; Roland et al. 2004)

$$\frac{\partial}{\partial x}(K_x \frac{\partial T}{\partial x}) + \frac{\partial}{\partial y}(K_y \frac{\partial T}{\partial y}) + \dot{Q} = \rho c \frac{\partial T}{\partial t} \tag{3.32}$$

where T is the concrete temperature (℃); K_x and K_y are the concrete conductivity coefficients in x and y directions, respectively $(W/m\,℃)$; $\dot{Q}$ is the rate of heat introduced per volume (W/m^3); ρ is the material density (kg/m^3); and c is the

concrete specific heat(J/kg ℃).

Two main types of boundary conditions are Drichlet and Cauchy boundaries, which can be written, respectively as (Sergerlind, 1987):

$$T = T_p \quad (3.33)$$

$$k_x \frac{\partial T}{\partial x} l_x + k_y \frac{\partial T}{\partial y} l_y + q + h\left(T_s - T_f\right) = 0$$

where $\boldsymbol{T_P}$ is the known value of the nodal temperatures on the boundaries; q is flowing heat from surface; h is the film coefficient; T_s is unknown temperatures at the boundary nodal points; T_f is the ambient temperature; l_x and l_y are the direction cosines of the outward normal to the surface under consideration (Noorzaei, 2006).

- **Numerical Model**

The numerical solution scheme used in this study is based on the Taylor-Galerkin approach. Upon applying this approach, the following system of differential equations is obtained (Jaafar et al. 2007):

$$[C]^e \left\{\frac{\partial T}{\partial t}\right\}^{(e)} + [K_t]^{(e)} \{T\}^{(e)} - \{F_t\}^{(e)} = 0 \quad (3.34)$$

where $[C]^e$ is the capacitance matrix; $[K_t]^{(e)}$ is the heat stiffness (conduction and convection) matrix; and $\{F\}^{(e)}$ is the total load heat vector due to hydration and convection actions.

3.3.2 Computation of Stress Field

After thermal analysis is performed for every stage of construction, the structural analysis of the RCC dam is performed immediately (Noorzaei et al. 2006). The thermal strain due to temperature changes are converted into equivalent nodal forces and added to the dam self-weight and other external loads acting on the dam body. The incremental-iterative procedure has been adopted for the nonlinear finite element elasto-plastic analysis of RCC dams.

3.3.3 Constitutive Modelling

The Mohr-Coulomb model in ABAQUS (2007) is an extension of the classical Mohr-Coulomb failure criterion, which incorporates isotropic cohesion hardening/softening but utilizes a flow potential of a hyperbolic shape in the meridional stress plane and a smooth elliptic function in the deviatoric stress plane.

- **Strain Decomposition**

The Mohr-Coulomb model decomposes the total strain ε into two components:

$$\varepsilon = \varepsilon^e + \varepsilon^p \tag{3.35}$$

where ε^e is the elastic strain and ε^p is the plastic strain.

- **Yield Behaviour**

The Mohr-Coulomb yield surface can be expressed as:

$$F = R_{mc} q - p \tan\phi - c = 0 \tag{3.36}$$

where c and ϕ are the cohesion and friction angle of the material respectively; p is the hydrostatic stress, q is the von Mises equivalent stress and R_{mc} is the Mohr-Coulomb deviatoric stress measure defined as:

$$R_{mc}(\Theta,\phi) = \frac{1}{\sqrt{3}\cos\phi}\sin\left(\Theta + \frac{\pi}{3}\right) + \frac{1}{3}\cos\left(\Theta + \frac{\pi}{3}\right)\tan\phi \tag{3.37}$$

in which Θ is the deviatoric polar angle (Chen and Han 1988) defined as:

$$\cos(3\Theta) = \left(\frac{J_3}{q}\right)^3 \tag{3.38}$$

where J_3 is the third invariant of the deviatoric stress tensor.

- **Flow Rule**

The Mohr-Coulomb plasticity model assumes the following form of potential flow:

$$d\varepsilon^p = \frac{d\bar{\varepsilon}^p}{g}\frac{\partial G}{\partial \sigma} \tag{3.39}$$

where g is given by (ABAQUS 2007);

$$g = \frac{1}{c}\sigma : \frac{\partial G}{\partial \sigma} \tag{3.40}$$

and G is the flow potential function defined as:

$$G = \sqrt{(\alpha c_0 \tan\varphi)^2 + (R_{mw} q)^2} - p\tan\varphi \tag{3.41}$$

Where φ is the dilation angle measured in the $p - R_{mw}\ q$ plane at high confining pressure; c_0 is the initial cohesion yield stress; and α is an eccentricity parameter that defines the rate at which the function approaches the asymptote; and R_{mw} is the deviatoric elliptic function.

3.3.4 Material and Mechanical Properties of RCC

The accuracy of constitutive model of strain and restraint stress development in concrete structures depends primarily on how accurately the required material and mechanical properties are described. The main material and mechanical properties are heat of hydration, modulus of elasticity and strength properties (tensile and compressive).

These properties inevitably have to be considered as time and temperature dependent to reveal a clear picture of the thermal stress behaviour of the RCC dam, also in a preliminary thermal stress analysis. The variation in the RCC properties with time and temperature has been taken into account in this study using recent experimental models.

- **Heat of Hydration**

The generation of thermal stresses depends on both the rate and the total heat generated during the hydration process. Heat generated by the hydration of cement in RCC dams rises the internal temperature which can cause considerable temperature gradient and related mechanical stresses (USACE, 1997). The adiabatic model is a well-established model used for the simulation of the heat of hydration in massive structures. The adiabatic temperature rise of concrete is given by Ishikawa (1991) and JCI (1986):

$$T_{ad} = T_{Max}(1 - e^{-\alpha t}) \tag{3.42}$$

where T_{Max} is the maximum temperature of concrete under adiabatic conditions, α is a parameter that represents the heat generation rate, and *t* is the time (hrs). The cumulative heat generated due to hydration up to time *t* is given by:

$$Q = \rho c T_{ad} \tag{3.43}$$

where c is the specific heat. Using Equations (3.42) and (3.43), the expression for the rate of heat of hydration to be used can be written as:

$$\dot{Q} = \rho c T_{Max} \alpha e^{-\alpha t} \tag{3.44}$$

This equation is used to calculate the rate of heat of hydration in the present study. The heat generation of concrete and material models used in the heat transfer analysis are implemented in ABAQUS through user subroutines written in FORTRAN. User subroutine DFLUX passes heat generation rates to ABAQUS for each integration point per element. When used in an incremental construction application, DFLUX must be programmed to keep track of heat generation rates versus elapsed time relative to the placement time for each lift. Heat generation of concrete is normally determined by an adiabatic temperature rise test. At the outset of this project, the user was required to convert the adiabatic temperature rise versus age data to heat generation rate versus age data for elapsed times corresponding to calculation times. DFLUX is modified to calculate heat generation rates from user-entered adiabatic temperature rise data, density, and specific heat for the concrete mixture, and to interpolate between data points when data was not supplied at exact elapsed times corresponding to the calculation time step.

- **Modulus of Elasticity of RCC**

In the past, the material laws to simulate concrete were mainly based on the age of concrete. However, in reality the temperature also influences the material's mechanical properties. If the temperature increase, it will accelerate the initial elastic modulus of concrete, but the ultimate elastic modulus is not significantly affected (Bazant et al. 2004).

Effect of Time

Conrad et al. (2003) dealt with the evaluation of the elastic modulus resulting from the stress-strain-behaviour of one Roller Compacted Concrete mixture from the age of 6 hours to 365 days. A convincing regression of the measurement data is realized by an exponential type function expressed as

$$E(t) = E_c \exp(at^b) \tag{3.45}$$

where $E(t)$ is a time dependent modulus in MPa, E_c is the final modulus of elasticity, t is the concrete age in days, and a and b are the model parameters.

Effect of Temperature

Bazant et al. (2004) introduced the concept of the degree of hydration to include the temperature influence. Term of equivalent age (τ_e), represents the hydration period for which the same degree of hydration is reached at a current temperature as that reached during the actual time (t) at a reference temperature. The concrete equivalent age is expressed as

$$\tau_e = \int_0^{\tau} \beta_\tau(t)dt \tag{3.46}$$

where $\beta(t)$ is a function of current temperature and expressed as

$$\beta_\tau(t) = e^{\Pi_h(\frac{1}{T_r}+\frac{1}{T(t)})} \tag{3.47}$$

where $T(t)$ is current temperature, T_r = *20 K* and Π_h is function of hydration degree = 2700 K.

Using the introduced term of equivalent age τ_e, which represents the hydration period, the concrete age, τ will be replaced with this equivalent age τ_e in the elastic modulus developed by Conrad et al. (2003) (Eq. 3.45). So the modified model includes the ageing and temperature effects on the elastic modulus (Abdulrazeg et al. 2010] as;

$$E(\tau_e) = E_c e^{a\tau_e^{\,b}} \tag{3.48}$$

The time and temperature dependent variation in the modulus of elasticity in Eq. (3.48) is used to determine the equivalent nodal force due to initial strains caused by temperature and stiffness matrix for each element.

The modified modulus of elasticity has been implemented in ABAQUS using the subroutine USDFLD, written in FORTRAN. The USDFLD subroutine allows the use of solution dependents material properties for each integration point of the model using field variables. For each integration point and for each step of the analysis, the USDFLD subroutine is evaluated and the modulus of elasticity is calculated.

3.3.5 Initial Conditions

The temperature distribution in the foundation, the roller compacted concrete placing temperature and reservoir water temperature are the main initial conditions that need to be considered in the analysis.

- **Evaluation of the foundation temperature**

Determination of the foundation initial temperature is usually performed by assigning the mean annual air temperature as initial temperatures for the ground rock. Then the thermal analysis of the foundation has to be performed for a period of two or three years prior to dam construction time (Bayagoob 2007; Ishikawa 1991).

- **RCC Placing Temperature**

In heat transfer analysis of RCC dam the placing temperature can be taken as the surrounding temperatures unless there is any restriction considered in the design. These restrictions, for example, are to decrease the RCC placing temperature to a certain limit by applying some control techniques such as adding ice cubes or cooling the ingredients. Thus, in this case, this limit will be used for all laid RCC lifts (Luna and Wu 2000).

- **Evaluation of the Reservoir Water initial Temperature**

The procedure for the calculation of reservoir temperature is the same as seepage analysis described in section 3.2.6 of the present chapter.

3.3.6 Heat Transfer Constitutive Law

The analysis progresses in time in a series of steps that begin with the addition of elements to represent the placement of a single RCC lift. The rate of internal heat generation for each lift is relative to its placement time. Heat loss from the dam to the atmosphere occurs at the surface of RCC that include the upstream and downstream faces of the dam and the top surface of the most recent lift. As each new lift is added, the parameters governing heat loss through the top of the previously placed lift must be deactivated since this surface no longer forms part of the RCC through which convective heat transfer occurs. The incremental lift placement is executed for a duration that is sufficient for all lifts to have achieved a steady state temperature distribution, subject to minor variation in temperature due to changes in atmospheric conditions.

The temperature variations of a dam are related to the thermal environmental actions (such as air and water temperatures, as well as the effects of solar radiation) and to internal heat generation of concrete during the construction process. Heat transfer can occur due to three distinct mechanisms: conduction, convection and radiation, as follows:

- **Thermal Conduction**

Conduction (or heat conduction) is a mode of transfer of energy within and between bodies of media due to a temperature gradient. Governing equation of thermal conduction in continuous environments can be achieved according to the conservation principle of thermal energy on constant arbitrary volume surrounded by closed surface as describes in Section 3.3.1.

- **Thermal Convection**

Heat transfer between a surface and a moving fluid with different temperature is called convection. The exchange of heat by convection as a result of temperature differences between the exposed surface and the ambient temperature is given by Newton's cooling law;

$$q_c = h_c(T - T_a) \tag{3.49}$$

where q_c is the convective flux (W/m^2), h_c is the convection coefficient $(W/m^2.K)$, T is the temperature of the dam surface in contact with the air (K); and T_a is the ambient temperature (K).

Heat transfer by convection is a complex phenomenon, and can be influenced by many variables in its numerical implementation such as: fluid velocity, speed and surface roughness. Some formulae have been proposed for the definition of the convection heat transfer coefficient, which can be used to determine, accurately, the amount of heat transferred by convection. The equation proposed by McAdams has been used in the present study (Duffie and Beckman, 2006);

$$h_c = 5.7 + 3.8V \tag{3.50}$$

where *V* is the wind speed (m/s).

- **Thermal Radiation**

Exchange of the heat by electromagnetic radiation is measured by the Stefan–Boltzman law;

$$q_r = eC_s(T^4 - T_a^4) \tag{3.51}$$

where q_r is the radiation flux (W/m^2), *e* is the emissivity of the surface, and C_s is the Stefan–Boltzman constant which is 5.669×10^{-8} (W/m^2). Equation (3.51) can be re-written in a linear form as follows:

$$q_r = h_r(T - T_a) \tag{3.52}$$

where h_r is a linearized radiation coefficient $(\boldsymbol{W/m^2})$, and is defined by the expression:

$$h_r = eC_s(T^2 + T_a^2)(T + T_a) \tag{3.53}$$

Figure 3.7 illustrates the heat transfer process for a concrete dam.

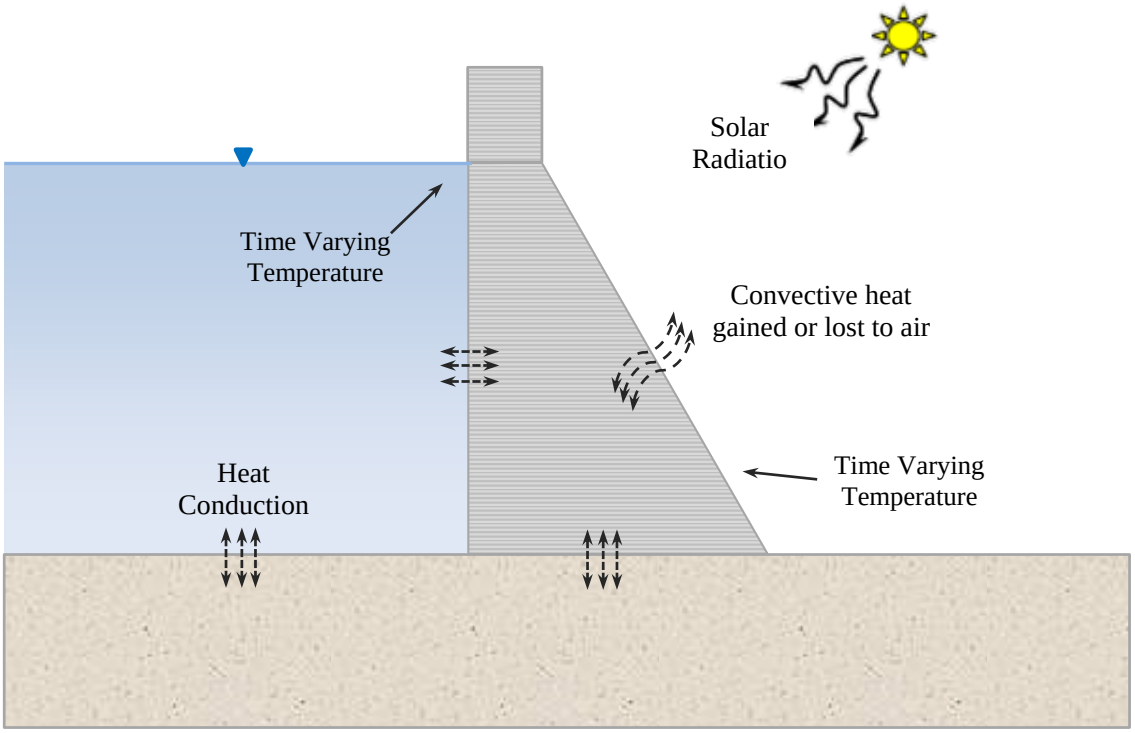

Figure 3.7 Heat Transfer Process for a Concrete Dam

3.4 Numerical Formulation of Seismic Fracture Analysis

3.4.1 Basic Description of the Dam-Reservoir- Foundation System

The dam-reservoir-foundation system can be categorized as a coupled field system in a way that these physical domains interact only at their interfaces. To model concrete gravity dam-reservoir-foundation problem using the finite element procedure, the discretised dynamic equations of the fluid and structure, including dam and its foundation, need to be considered simultaneously to obtain the coupled fluid–structure-foundation.

3.4.2 Modelling of the Fluid Domain and its Boundaries

Assuming that water is linearly compressible and neglecting its viscosity, the small amplitude irrotational motion of the water is governed by the two dimensional Helmoltz wave equation (Kucukarslan, 2004)

$$\nabla^2 p = \frac{1}{c^2}\frac{\partial^2 p}{\partial t^2} \tag{3.54}$$

where p is the acoustic hydrodynamic pressure, t is time, ∇^2 is the Laplace operator and c is the compressive wave velocity defined as:

$$c = \sqrt{\frac{K}{\rho}} \tag{3.55}$$

in which K is the bulk modulus of water and ρ is the density of fluid.

- **Reservoir Boundary Conditions**

The formulation of the boundary conditions associated with the reservoir boundaries is simply an expression of the physical situations in mathematical terms. It should be noted that in addition to the spatial (or geometric) boundary conditions, there are temporal boundary conditions which specify the state of the variable of interest at some points in time. This temporal condition is called an "initial condition". In the case of dam-reservoir interaction, there are four spatial boundary conditions namely, dam-reservoir, reservoir-foundation, free surface, and reservoir far-end boundary conditions. A typical dam-reservoir system is shown in Figure 3.8.

The following boundary conditions at the interfaces of the fluid domain are then defined:

- ***At the dam-reservoir interface (S_1)***

The compatibility condition between the fluid and solid domains leads to (e.g. Ihlenburg 1998; Rizos and Karabalis 2000; Tsai et al. 1990):

$$\frac{\partial p}{\partial n} = -\rho a_n \tag{3.56}$$

where n is a unit normal vector to the interface, p is the acoustic hydrodynamic pressure and a_n is the normal acceleration on the interface.

- ***At the foundation- reservoir interface (S_2)***

The reservoir bottom material is represented by the following impedance condition (Fenves and Chopra 1984):

$$\frac{\partial p}{\partial n} = -\rho a_n - \overline{q}\frac{\partial p}{\partial t} \tag{3.57}$$

where $\bar{q}$ is the damping coefficient characterizing the effects of absorption of hydrodynamic pressure waves at the reservoir boundary (Fenves and Chopra, 1983).

- ***At the free surface of the reservoir (S_3)***

At the free surface when the surface wave is neglected, the boundary condition is defined as:

$$p = 0 \tag{3.58}$$

- ***At the reservoir far-end (Truncated Boundary) (S_4)***

To determine the hydrodynamic pressure on the dam due to horizontal ground motion under the assumption of infinite reservoir, the reservoir must be truncated at a reasonable distance. The Sharan boundary condition (Sharan, 1987) at the far-end truncated boundary can be written as:

$$\frac{\partial p}{\partial n} = -\frac{\pi}{2h} p - \frac{1}{c}\frac{\partial p}{\partial t} \tag{3.59}$$

where h is the height of the reservoir.

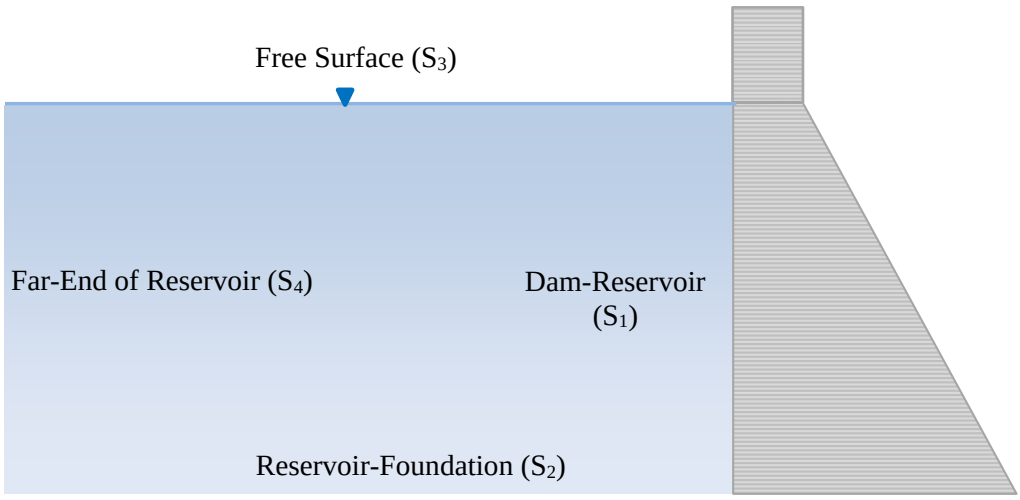

Figure 3.8 Boundaries of the Dam-Reservoir System

3.4.3 Equation of Interaction System of Dam-Foundation-Water

- **Dam-Reservoir Interaction:**

The dam–reservoir interaction is represented by two coupled differential equations of the second order. The equations of the structure and the reservoir can be written in the following form (Ghaemian & Ghobarah 1999):

$$[M]\{\ddot{u}\}+[C]\{\dot{u}\}+[K]\{u\}=\{f_1\}-[M]\{\ddot{u}_g\}+[Q]\{p\}=\{F_1\}+[Q]\{p\} \tag{3.60}$$

$$[G]\{\ddot{p}\}+[C']\{\dot{p}\}+[K']\{p\}=\{F_2\}-\rho[Q]^T\{\ddot{u}\} \tag{3.61}$$

where [*M*],[*C*] and [*K*] are mass, damping and stiffness matrices of the structure, and [*G*],[C'] and [K'] are matrices representing mass, damping and stiffness of the reservoir, respectively. [*Q*] is the coupling matrix and {f_1} is the vector of body force and hydrostatic force. {F_2} is the component of the force due to acceleration at the boundaries of the dam–reservoir and reservoir–foundation. {*p*} and {*u*} are the vectors of pressures and displacements. $\{\ddot{u}_g\}$ is the ground acceleration and ρ is the density of the fluid. The dot represents the time derivative.

- **Dam-Foundation Interaction:**

The most common soil–structure interaction (SSI) approach is based on the "added motion" formulation. This formulation is valid for free–field motions caused by earthquake waves generated from all sources. The method requires that the free–field motions at the base of the structure be calculated prior to the soil–structure interaction analysis (Wilson 2000):

Therefore, nonlinear dynamic analysis of concrete gravity dams including dam-reservoir-foundation interaction, Eqn. 3.60, must be replaced with Eqn.3.62 as following;

$$[M]\{\ddot{u}\}+[C]\{\dot{u}\}+[K]\{u\}=-[m_s]\{\ddot{u}_g\}+\{f_1\}+[Q]\{p\} \tag{3.62}$$

where [M] , [C] and [K] are the mass, damping and stiffness matrices, respectively, of the dam-foundation structure and [m_s] is only the mass matrix of the dam structure.

3.4.4 Concrete Damaged Plasticity Constitutive Modelling

- **Stress-Strain Relationship**

The concrete constitutive model implemented in this research is the damaged plasticity model (ABAQUS 2007), which is built on the models proposed by Lubliner et al. (1989, 1990) and by Lee and Fenves (1998a, 1998b). This model is primarily intended to provide a general capability for the analysis of concrete structures under cyclic and/or dynamic loading. Under low confining pressures concrete behaves in a brittle manner; the main failure mechanisms being (a) cracking in tension, and (b) crushing in compression. The brittle behaviour of concrete disappears when the confining pressure is sufficiently large to prevent crack propagation. In these circumstances the failure is driven by the consolidation and collapse of the concrete microporous microstructure. The constitutive theory of the model used aims to capture the effects of irreversible damage associated with the failure mechanisms that occur in concrete under fairly low confining pressures.

In the incremental theory of plasticity, a fundamental assumption is that the total strain is decomposed into an elastic part and a plastic part:

$$\varepsilon = \varepsilon^e + \varepsilon^p \tag{3.63}$$

$$\varepsilon^e = E^{-1}\sigma \tag{3.64}$$

where ε is the total strain tensor, the elastic stiffness E is a rank-four tensor, σ is the stress tensor, ε^e is the elastic strain tensor, and ε^p is the plastic strain tensor. Since the effective stress $\bar{\sigma}$ is defined with the undamaged elastic stiffness from Eqn. (3.64), it becomes

$$\bar{\sigma} = E_0(\varepsilon - \varepsilon^p) \tag{3.65}$$

where E_0 is the initial elastic stiffness tensor. Scalar degradation damage, such that $E = (1-d)E_0$, is assumed in many cases. Accordingly, the stress is factorized into stiffness degradation and effective stress parts as (Lee and Fenves 1998);

$$\sigma = (1-d)\bar{\sigma} = (1-d)E_0(\varepsilon - \varepsilon^p) \tag{3.66}$$

The plastic strain rate is evaluated by the flow rule, defined in terms of plastic potential function G. For a plastic potential in the effective stress space, the plastic strain is given by

$$\dot{\varepsilon}^p = \dot{\lambda} \frac{\partial G(\bar{\sigma})}{\partial \bar{\sigma}} \tag{3.67}$$

where $\dot{\varepsilon}^p$ is the plastic strain rate tensor, $\dot{\lambda}$ is a non-negative scalar function named plastic consistency parameter (Lee and Fenves 1998b).

- **Damage Evolution**

In line with Lubliner et al. (1989, 1990) and Lee and Fenves (1998a, 1998b), the index for damage is characterized by the damage variable κ, in ABAQUS (2007), termed as hardening variable.

In the uniaxial condition, the damage variable κ is represented by two independent variables:

$$\kappa = \begin{bmatrix} \kappa_t \\ \kappa_c \end{bmatrix} \tag{3.68}$$

where κ_t and κ_c are referred to as unixial tensile and compressive damage variable, respectively. The unixial tensile damage variable κ_t is defined as:

$$\kappa_t = \frac{\int_0^{\varepsilon^p} \sigma_t(\varepsilon^p) d\varepsilon^p}{\int_0^{\infty} \sigma_t(\varepsilon^p) d\varepsilon^p} \tag{3.69}$$

where σ_t and ε^p are the tensile stress and plastic strain, respectively. Analogously, the uniaxial compressive damage variable κ_c is defined as:

$$\kappa_c = \frac{\int_0^{\varepsilon^p} \sigma_c(\varepsilon^p) d\varepsilon^p}{\int_0^{\infty} \sigma_c(\varepsilon^p) d\varepsilon^p} \tag{3.70}$$

where σ_c and ε^p are the compressive stress and plastic strain respectively.

- **Stiffness Degradation**

Equation (3.66) indicates that the reduction of the elastic modulus is controlled by the stiffness degradation variable *d*. This variable is considered to be a function of the damage variable κ (Lee 1996), i.e.

$$d = d(\kappa) \tag{3.71}$$

For uniaxial monotonic loadings, the stiffness degradation variable *d* is characterized by its uniaxial version, i.e. the uniaxial tensile and compressive stiffness degradation variables denoted by d_t and d_c, respectively. In ABAQUS (2007), they are termed as uniaxial tension and compression damage variables instead. Graphical illustrations of the two variables are presented in Figures 3.9 Figure 3.10.

Applying Equation (3.66) to the uniaxial monotonic loading case results in the stress-strain relationship for tension:

$$\sigma_t = (1-d_t)\,\mathrm{D}_0(\varepsilon_t - \varepsilon_t^{\,p}) \tag{3.72}$$

and for compression:

$$\sigma_c = (1-d_c)\,\mathrm{D}_0(\varepsilon_c - \varepsilon_c^{\,p}) \tag{3.73}$$

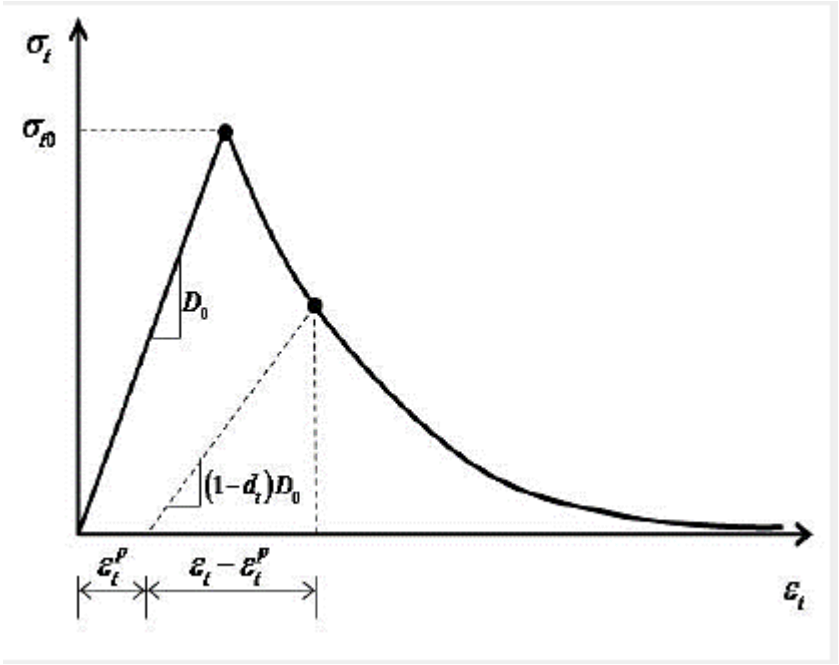

Figure 3.9 Illustration of the uniaxial tension damage variable d_t (modified from ABAQUS 2007)

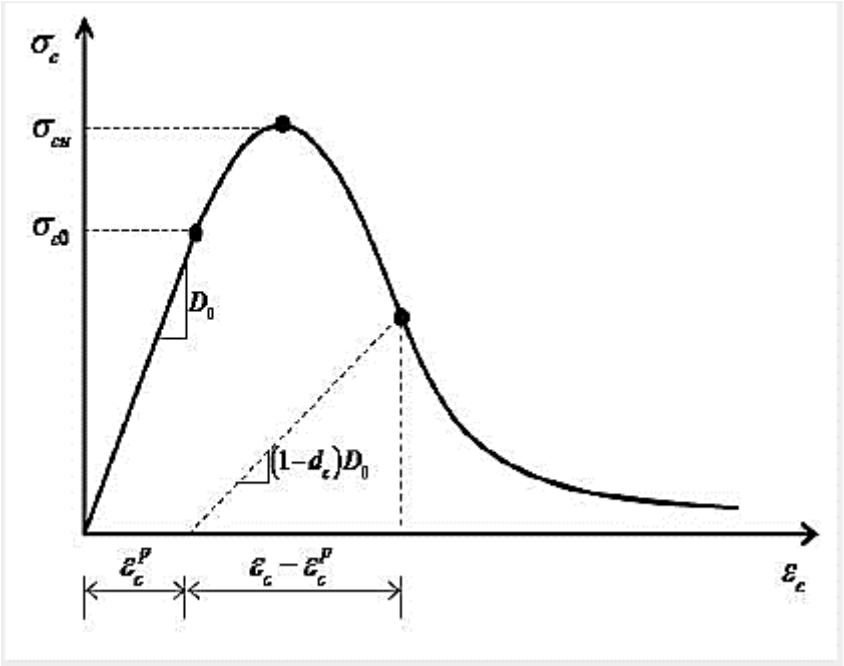

Figure 3.10 Illustration of the uniaxial compression damage variable d_c (modified from ABAQUS 2007)

- **Yield Condition**

The plastic-damage concrete model uses a yield condition based on the yield function proposed by Lubliner et al. (1989) and incorporates the modifications proposed by Lee and Fenves (1998) to account for different evolution of strength under tension and compression. The yielding criterion for the damaged plasticity model embedded in ABAQUS (2007) is described by:

$$F(\bar{\sigma},\kappa)=\frac{1}{1-\alpha}(\bar{q}-3\alpha\bar{p}+\beta(\kappa)(\hat{\bar{\sigma}}_{max})-\gamma(-\hat{\bar{\sigma}}_{max}))-c(\kappa) \qquad (3.74)$$

where $\bar{p}$ is the hydrostatic effective stress, defined as;

$$\bar{p}=-\frac{1}{3}\bar{\sigma}I \qquad (3.75)$$

in which $\bar{\sigma}$ is the effective stress tensor and I is the identity tensor, $\bar{q}$ is the von Mises equivalent effective stress, $\hat{\bar{\sigma}}_{max}$ is the algebraic maximum principal effective stress, $c(\kappa)$ is the cohesion, whose evolution is controlled by the damage variable κ; α, β and γ are dimensionless material constants.

3.4.5 Concluding Remarks

In this chapter, the methodology to achieve the objectives of this study has been presented including;

- The mathematical and finite element formulation of coupled seepage-stress problem, heat transfer and seismic fracture analyses.

- Development of proper boundary and initial conditions for the water interaction at the upstream face of the dam, taking into account the variation of temperature of the reservoir water with depth.

- Development of constitutive material and mechanical model of RCC such as hydraulic conductivity, heat of hydration and elasticity modulus of RCC that includes the ageing, temperature and confining pressure effects.

CHAPTER 4

COMPUTATIONAL AND PROGRAMING PROCEDURES

4.1 Introduction

In the present chapter, computational strategies implemented in order to achieve the objectives of the current research work are presented. At first, the methods of simulation of sequence of construction of RCC gravity dam using ABAQUS software are proposed, then, the implementation of the initial condition in software via MACRO environment is introduced. After that, the computational strategies and development of the finite element code for coupled seepage-stress, heat transfer and seismic analysis will be followed. These strategies are fully described and illustrated in the accompanying flowcharts.

Furthermore, this chapter presents the development of a safety system evaluation of RCC dam. This system is one of the primary objectives of the present work, which is a computational system to determine the level of safety of RCC dams either in short or long term.

4.2 Simulation of Sequence of Construction

4.2.1 Construction Stages

Usually RCC dams are constructed by laying the RCC lifts sequentially. The dam is divided into a number of blocks along its length and each block is placed in lifts ranging from a minimum thickness of 150 mm (compacted thickness) to well over 1 m (U.S. Army Corps of Eng. EM 1110-2-2006). Therefore, to simulate the RCC gravity dam each block is analysed separately and different blocks could be taken along the dam length.

RCC dams are special structures, because they are constructed in layers (Figure 4.1), the gravity load is changing with construction process, in addition, stresses will increase with time as volume of placed concrete is increased (Bouyge, 2007). Moreover, each layer has different age and consequently different mechanical and hydraulic properties. Therefore, it is necessary to simulate the construction process of RCC dams according to the casting schedule of concrete.

Figure 4.1 Construction Sequence of Boussiaba RCC Dam, Algeria (Abdulrazeg 2010)

The birth and death element technique is used in the analyses to simulate the process of construction of the RCC dam (Bayagoob 2007; Ishikawa 1991). This technique is shown in Fig. 4.2. Finite element mesh of the dam body and foundation of the RCC dam is generated as shown in Fig. 4.2. First, rock ground elements are made active and are considered for the purpose of analysis as depicted in Fig. 4.2(b). Next, a first layer of the RCC dam body is made active and added to a previous stage as shown in Fig. 4.2(c). Similarly, sequence of construction of the RCC dam is modelled as shown in Figure 4.2 (d).

ABAQUS uses *Model Change option in Interaction module to simulate the sequence of construction.

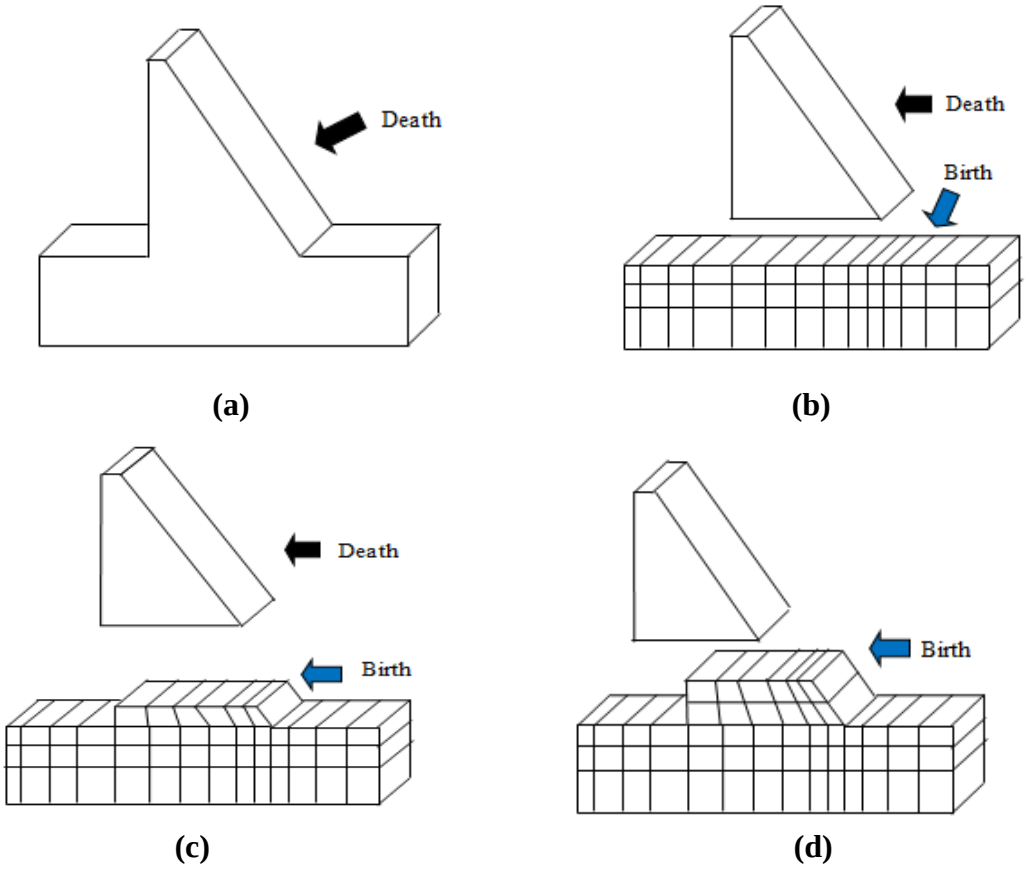

Figure 4.2 Birth and Death Element Technique

4.2.2 Operation Phase

The finite element model used to simulate the heat exchange between the impounding water and dam body at the upstream side is developed as follows;

i) The water finite elements are added in layers according to the reservoir filling schedule (filling rate).

ii) The thickness of each water layer is kept equal to the corresponding opposite RCC lift in order to maintain the finite element continuities.

iii) The time of activation and deactivation of each water layer is set according to the planned reservoir filling and operation as shown in Fig. 4.3.

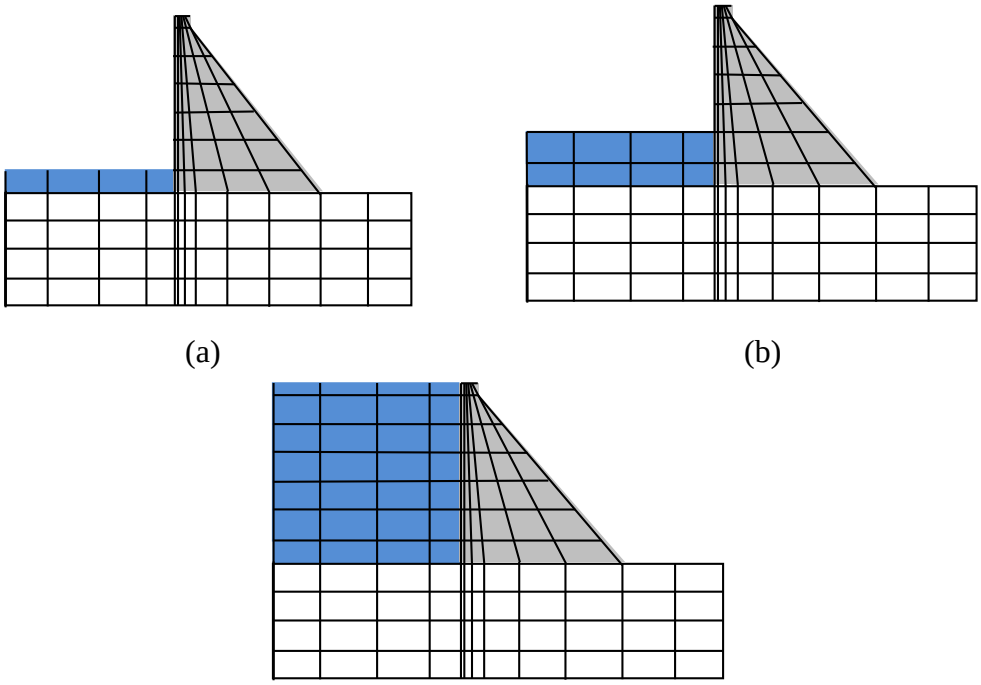

Figure 4.3 Simulation of Operation Phase

4.3 Computational Strategies for Coupled Seepage-Stress Analysis

There are two common approaches for solving coupled equations. One approach is to solve two sets of equations first and then use the results to solve the last equation. These results, in turn, are fed back into the first two set of equations to see what changes occur in the solution. This process continues until succeeding iteration produces negligible changes in the solution obtained. This is so called staggered approach to the solution of coupled systems of equations. The second approach, used in the present study, is to solve the coupled system directly. This direct approach has rapid convergence even in highly non-linear cases.

ABAQUS has the ability to conduct the analysis of porous media in two stages:

- Geostatic - for checking and modifying the initial conditions defined for the steady-state equilibrium of ground under geostatic loading: This stage is used to ensure that analysis begins from a state of equilibrium under geostatic loading.

- Consolidation - for transient response analysis of partially saturated media under transpiration: To avoid non-physical oscillation and also convergence problems caused by non-linearities; this stage includes a time dependent analysis using time intervals for the analysis period.

Initial conditions are calculated based on the formulation in Section 3 of Chapter 3 and entered as FEMGEN loads via the 'PROPERTY LOAD' or the 'PROPERTY INITIAL' command in MACRO environment of ABAQUS. The implementation of these initial conditions using some modifications in ABAQUS software is done through MACRO environment of the software as shown in Figure 4.4.

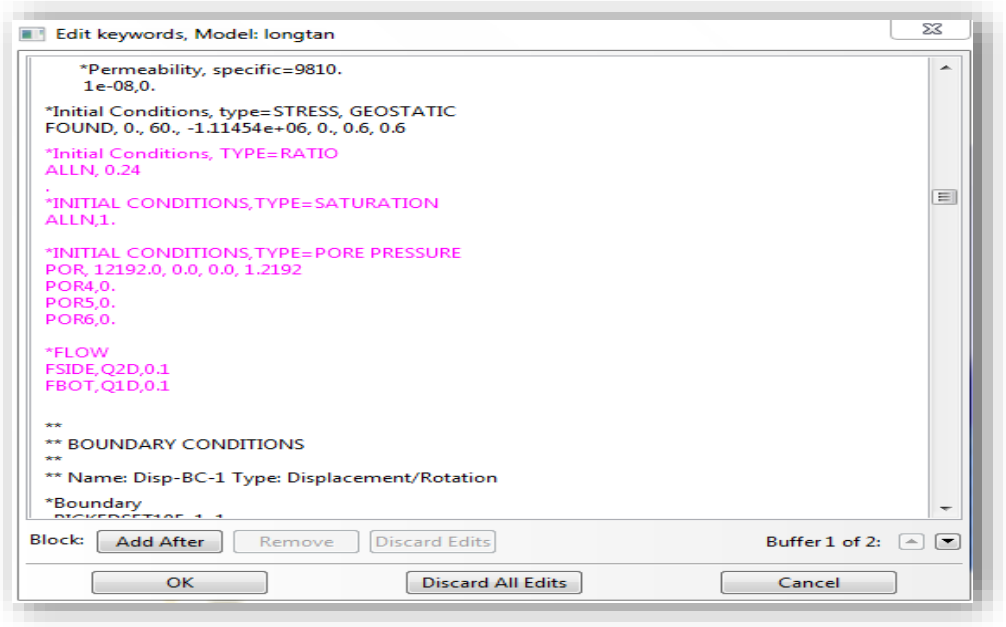

Figure 4.4 Implementation of Initial and Boundary Conditions

4.3.1 Development of Seepage Properties of Roller Compacted Concrete

ABAQUS allows the inclusion of modifications to its constitutive models, within their general theoretical frameworks. Modifications can be implemented using the Solution-Dependent Field Variable (SDFV) option with a user subroutine, as noted by Chen (2007).

In ABAQUS, the material properties (such as hydraulic conductivity) can be set to be dependent on the solution-dependent field variables (SDFV) using the user-defined subroutine USDFLD. A solution-dependent field variable is a field variable that varies throughout the solution process (such as the confining pressure and stresses).

This facility provides the possibility for the material models in ABAQUS to account for additional material characteristics.

In the present study, the option of SDFV was adopted to define the dependence of permeability of concrete on the confining pressure, water temperature, time and depth of the reservoir. By doing so, the variation of the material properties during the loading process can be appropriately captured. The flowchart for USDFLD subroutine is shown in Figure 4.5. Furthermore, Figure 4.6 shows the flowchart to solve the coupled flow-deformation governing equations used in this study considering the developed hydraulic conductivity model. In this study, the porous media is modelled by attaching the finite element mesh to solid phase and then fluid can flow through this mesh.

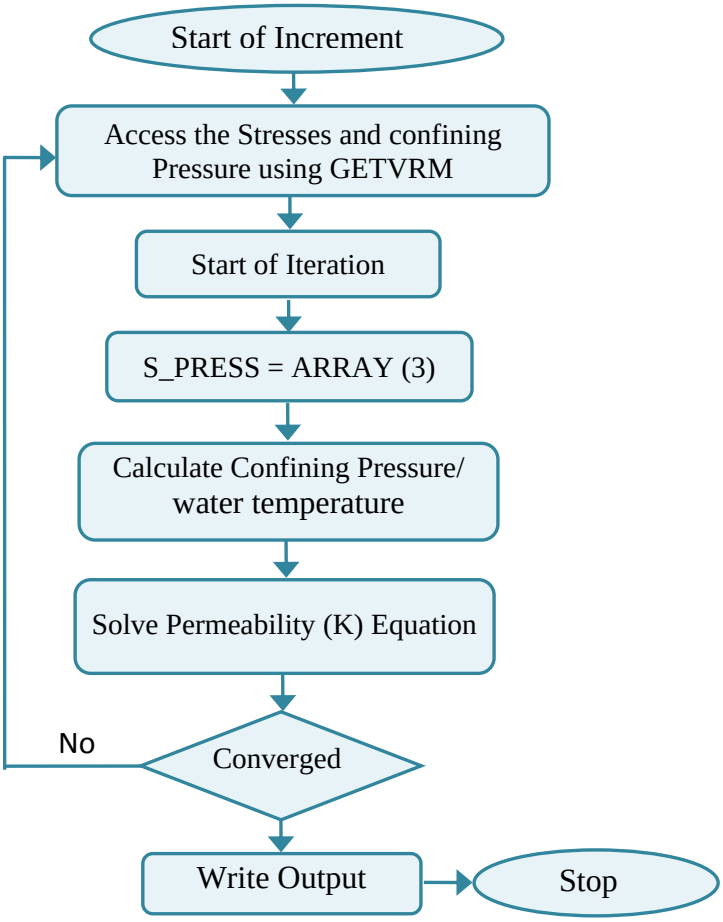

Figure 4.5 USDFLD Subroutine Flowchart

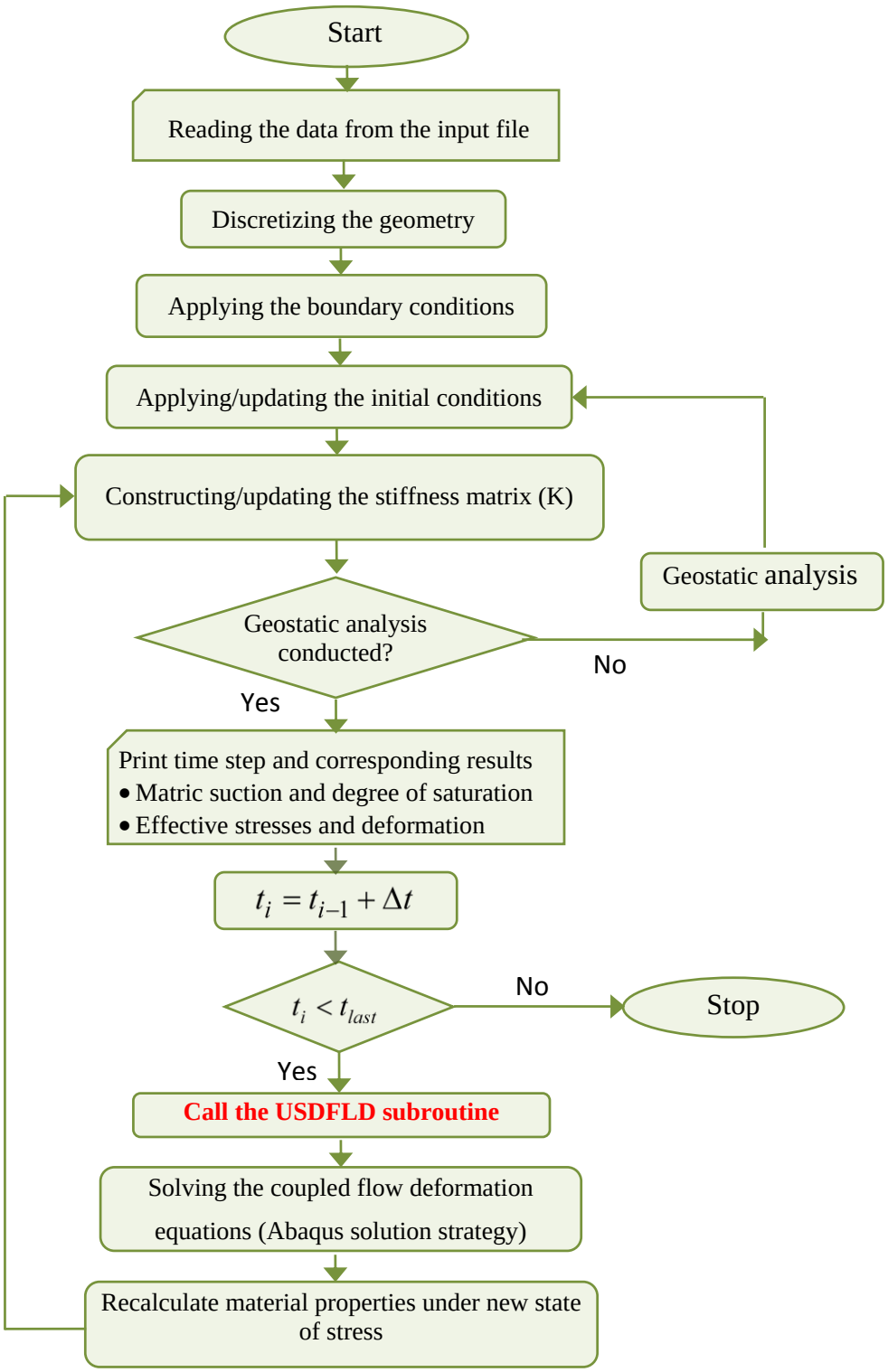

Figure 4.6 Flowchart of approximate solution of coupled flow-stress governing equation

4.4 Computational Procedure and Development of FE Code for Thermal-Stress Analysis

The purpose of the nonlinear incremental thermal stress-strain analysis (NISA) is to assess the magnitude of thermal stresses for the proposed RCC dam and the potential for cracking. An implicit assumption in the NISA procedure is that the thermal and stress problems are uncoupled, i.e., structural deformations do not affect the thermal component (USACE, 1994). Consequently, the thermal and stress analyses may be decoupled and run sequentially with the time dependent temperature distribution computed from the thermal analysis imposed as part of the mechanical loads and boundary conditions for the stress analysis. The initial thermal analysis and the subsequent stress analysis were conducted using ABAQUS (HKS, 2002). A description of these two types of analyses is provided in the following sections.

4.4.1 Incremental Thermal Analysis

The heat transfer analysis is performed to determine how the temperatures within the structure change with time. The first step is the basic step necessary for any FE analysis in which the structure and foundation are discretised into a group of elements defined by nodes. Once the nodes and elements have been defined, it is necessary to define node and element sets for items such as material properties, initial conditions, and film coefficients. The material properties must then be defined and should include the conductivity, density, and specific heat of any materials used in the analysis. This will require properties for both the concrete and foundation and possibly air. The initial temperature of the concrete must be defined and is typically assumed to be the placing temperature. A definition of the air and water temperatures should be made as described in Chapter 3. Finally, a definition of the time history must be made as shown in steps 6 and 7 of Figure 4.7. This includes defining the length of each step and its increment, changing the model as necessary, applying, removing, and changing film coefficients as required, applying the heat generation (DFLUX subroutine), and defining any required output. It is critical that a temperature output file be defined properly to ensure that temperatures needed for the stress analysis are computed properly. A flow chart defining the steps in a heat transfer analysis is presented in Figure 4.7

- **Heat Generation Subroutines (DFLUX)**

All required functionality of the thermal analysis is supported in the standard executable version of ABAQUS with variation in internal heat generation considered through user subroutines.

Heat generation of concrete in ABAQUS is input by the user subroutine DFLUX. DFLUX passes heat generation rates to ABAQUS for each integration point per element. When used in an incremental construction application, DFLUX must be programmed to keep track of heat generation rates versus elapsed time relative to the placement time for each lift. Heat generation of concrete is normally determined by an adiabatic temperature rise test. DFLUX was modified to calculate heat generation rates from user-entered adiabatic temperature rise data, density, and specific heat for the concrete mixture, and to interpolate between data points when data was not supplied at exact elapsed times corresponding to the calculation time step. Annotated description of the DFLUX subroutine is given in Appendix A.

4.4.2 Incremental Stress-Strain Analysis

The incremental stress-strain analysis of the dam is followed sequentially from the thermal analysis to determine the stress and strain state of the structure based on the changing temperatures resulting from heat transfer, gravity loads, changing material properties, and the boundary conditions.

The node and element data defined in the heat transfer analysis for the concrete are typically used in the stress analysis and these data can then be used to identify the needed node and element sets. A definition of the initial boundary conditions must be specified prior to beginning a time-history analysis. As in the heat transfer analysis, the final process in the stress analysis is to define the time-history analysis to take place as shown in steps 6 and 7 of Figure 4.8. This includes defining the time of the steps and their increments, defining changes in the model, application of mechanical loads, accessing the temperature data from the heat transfer analysis to define thermal loads, and definition of the output desired. A flow chart defining the steps in a stress analysis is presented in Figure 4.8.

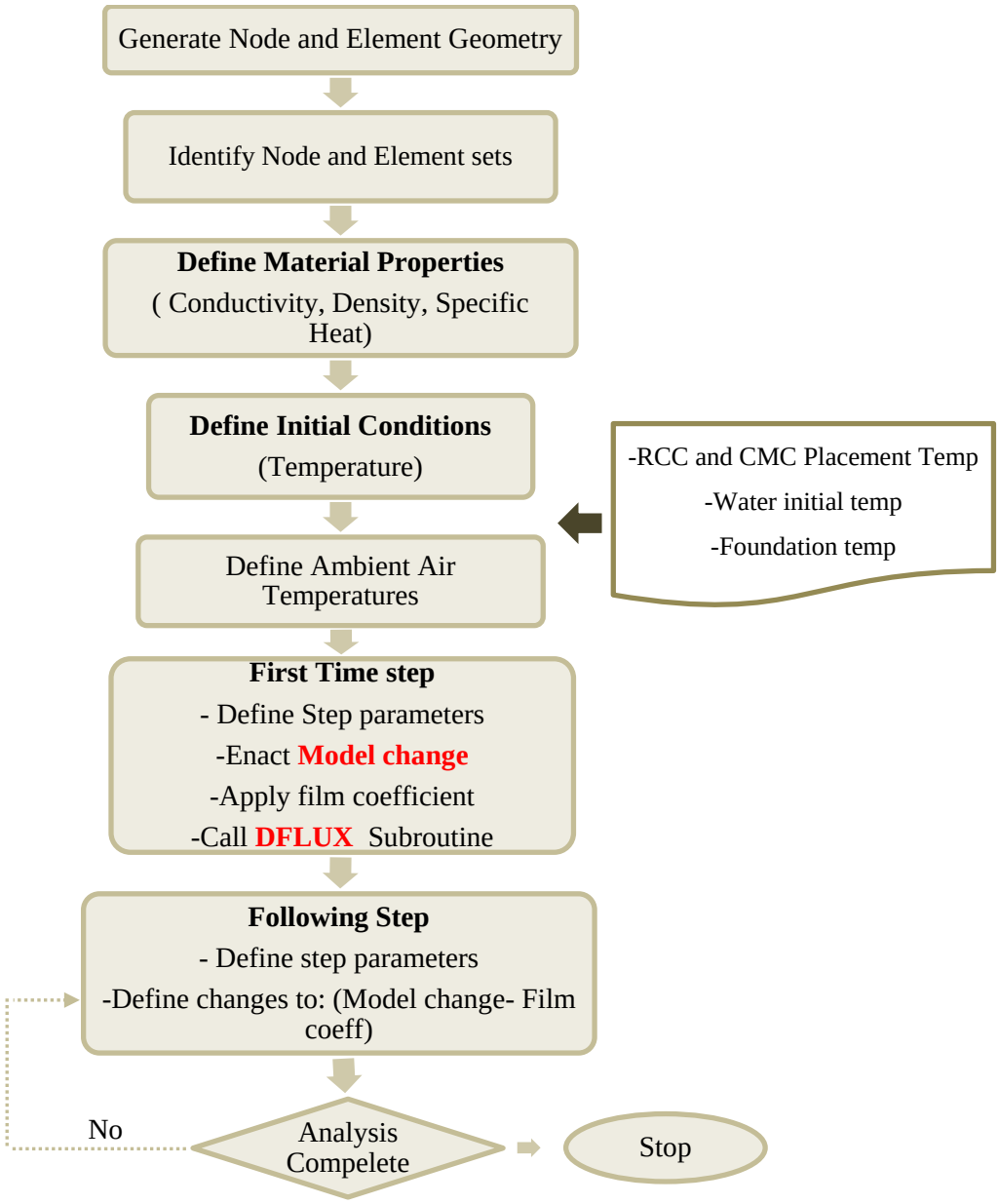

Figure 4.7 Thermal Analysis Flowchart

- **Development of Modulus of Elasticity**

In the past, the material laws to simulate concrete were mainly based on the age of concrete. However, in reality the temperature also influences the material's mechanical properties such as modulus of elasticity.

The modulus of elasticity is defined as the ratio of normal stress to corresponding strain below the proportional limit. For practical purposes, only the deformation which occurs during loading is considered to contribute to the strain in calculating

the modulus of elasticity. The modulus of elasticity is a function of the degree of hydration and, therefore, is time dependent. It is also temperature dependent (USACE, 1994) as described in section 3.3.3 of Chapter3.

The modified modulus of elasticity has been implemented in ABAQUS using the subroutine USDFLD, written in FORTRAN. The USDFLD subroutine allows the use of solution dependent material properties for each integration point of the model using field variables. For each integration point and for each step of the analysis, the USDFLD subroutine is evaluated and the modulus of elasticity is calculated. The procedure of implementation of USDFLD subroutine is illustrated in section 4.3 of this chapter.

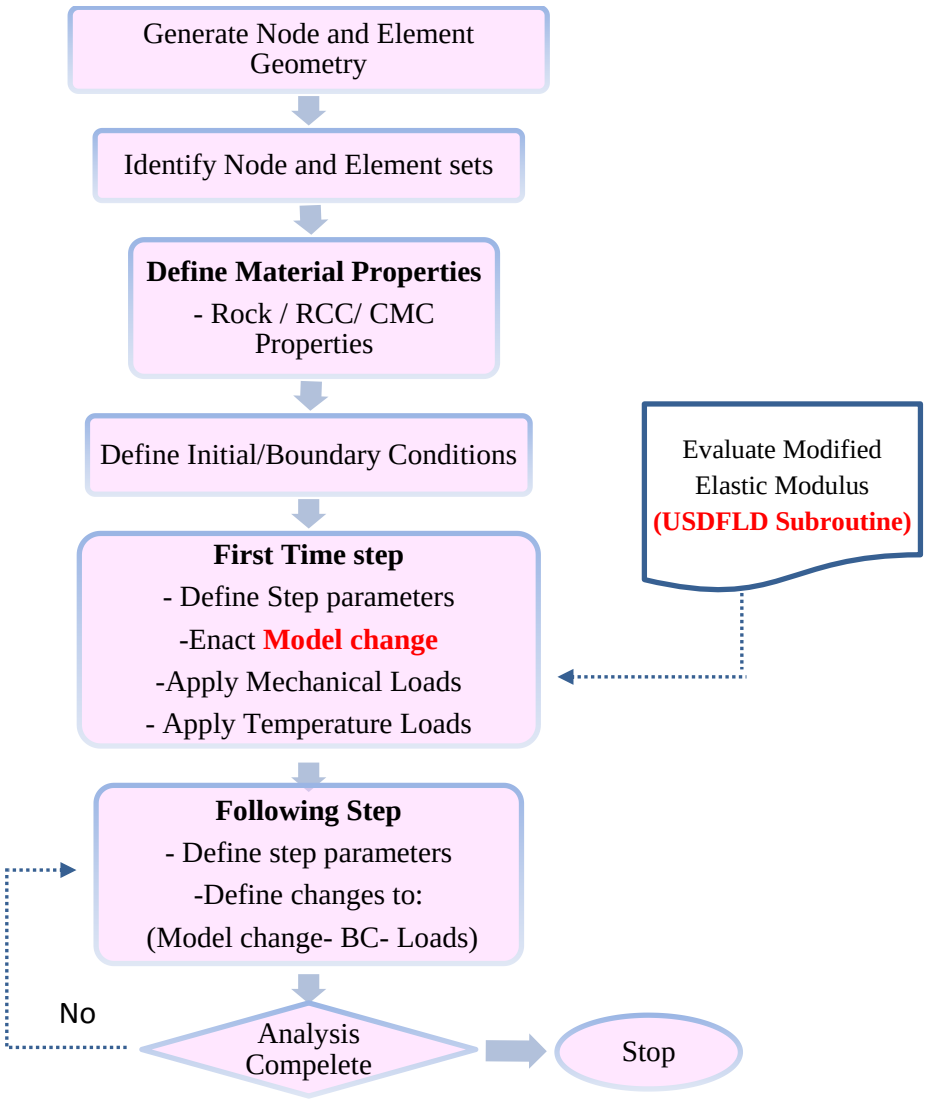

Figure 4.8 Structural Analysis Flowchart

4.5 Computational Strategies for Seismic Cracking Analysis

ABAQUS offers several methods for performing dynamic analysis of problems in which inertia effects are considered. Direct integration of the system equations must be used when nonlinear dynamic response is being studied. Implicit direct integration is provided in Abaqus/Standard.

Figure 4.9 illustrates a methodology for comprehensive seismic safety evaluation of concrete gravity dams. First, the finite element model is defined and all the nonlinearity sources (material, joints, geometry) as well as interactions (fluid-structure and soil-structure) are applied in the model. Then, the free vibration analysis is performed in the second step which includes the eigen frequencies and mode shapes. This information is useful for understanding the dynamic behaviour of the dam. Finally, nonlinear earthquake response analysis is carried out using time history method. A detailed description of these steps is provided in the following sections.

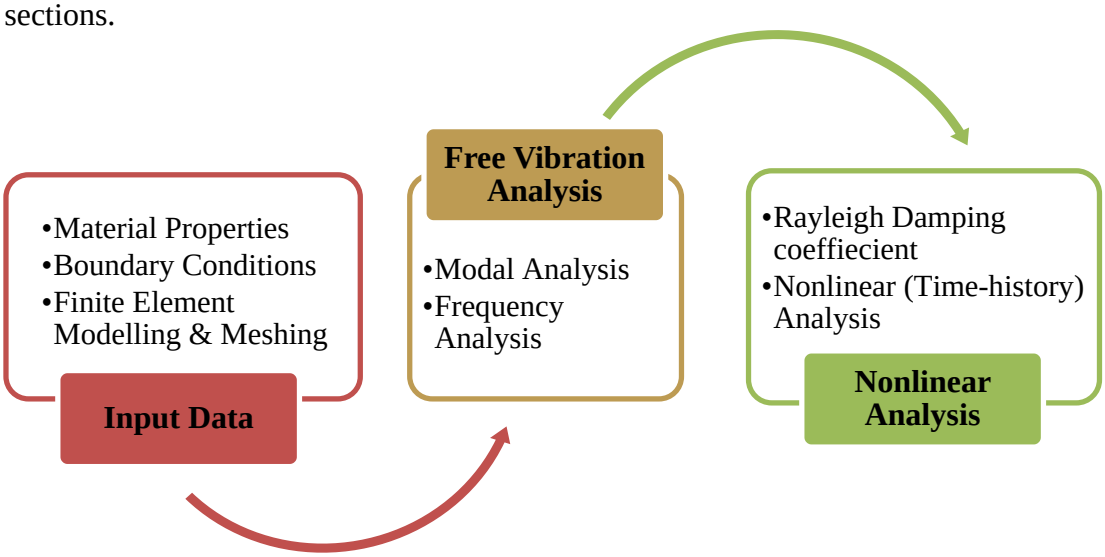

Figure 4.9 Flowchart of Nonlinear Dynamic Analysis for Gravity Dam

4.5.1 Input Data and Modelling Process

Prior to dynamic simulation of earthquake, the dam is subjected to gravity loading and hydrostatic pressure. In the Abaqus/Standard analysis these loads are specified in two consecutive static steps, using the *DLOAD option with the load type labels GRAV (for the gravity load) in the first step and HP (for the hydrostatic pressure) in the second step. For the dynamic analysis in the third step,

hydrodynamic pressures exceeding the hydrostatic pressure at upstream face of the dam, and the transverse and vertical components of the ground accelerations at the base of the dam are applied to all nodes in these areas as shown in Figure 4.10.

Since considerable nonlinearity is expected in the response, including the possibility of unstable regimes as the concrete cracks, the overall convergence of the solution in the Abaqus/Standard analysis is expected to be non-monotonic. In such cases the use of the *CONTROLS, ANALYSIS=DISCONTINUOUS option is generally recommended to prevent premature termination of the equilibrium iteration process because the solution may appear to be diverging. The unsymmetric matrix storage and solution scheme is activated by setting UNSYMM=YES on the *STEP option.

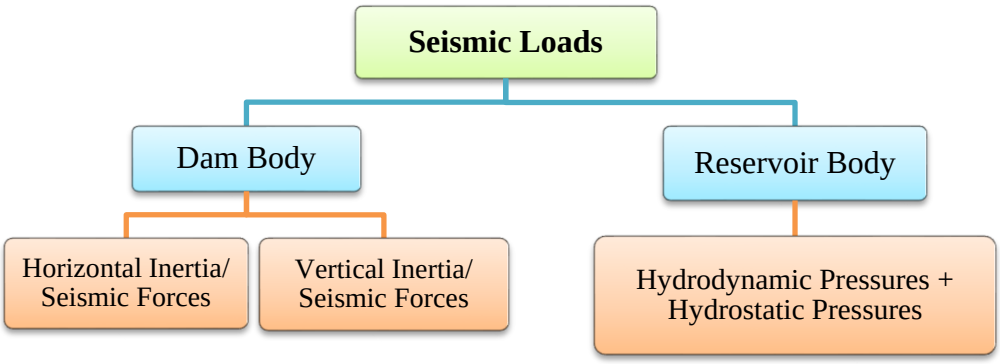

Figure 4.10 Gravity Dam Loads for the Dynamic analysis

- **Interfacial Modelling**

The dam- foundation- reservoir system is a multi-phase system. This section presents the approaches used for the modelling of the dam-foundation, the dam-reservoir, and the foundation-reservoir interactions.

- ***Dam-Foundation Interaction***

The modelling of the dam-foundation interaction herein follows the contact mechanics based approach. Computational modelling of dynamic contact problems is cumbersome because, usually, the problems are highly nonlinear and non-smooth (Belytschko et al. 2013; Wriggers 2002; Zhong 1993). The description herein follows ABAQUS (2007). To properly simulate the mechanical behaviour at the dam-foundation interface, a surface based contact pair is defined at the dam-foundation

interface. The contact interaction in the normal direction is modelled by the “hard” contact approach (ABAQUS 2007).

- ***Dam-Reservoir and Foundation-Reservoir Interactions***

The fluid medium could not be modelled to infinity in the upstream direction; therefore, a non-reflective planar acoustic impedance boundary, which means that the pressure is completely absorbed, was applied on the upstream end surface (Lysmer and Kuhlemeyer 1969).

ABAQUS provides two techniques for modelling interaction between acoustic and structural media. These include surface based interaction and acoustic interface elements. The surface based approach can be used to model interacting structural and acoustic meshes which constitute different node numbering and whose surface meshes may not be spatially coincidental (Simulia, 2010). Whereas, the special purpose acoustic interface elements are restricted to meshes whose node numbers coincide. Hence, the above comparison led to the surface based approach being picked as it is easier to use and computationally cost effective.

The surface-based approach allows for nonconforming node numberings and meshes at the fluid-structure interface. Herein, the acoustic fluid (reservoir) surface is selected as the slave surface and the solid (dam and foundation) surfaces are assigned as the master surface, as illustrated in Figure 4.11. As a result, the fluid-solid coupling conditions, i.e. Eqn. (3.57) and Eqn. (3.58), are imposed at the slave nodes. The values at each fluid node are constrained to be the average of the values at nearby master surface nodes.

- **Hydrodynamic Pressure on Dam**

During an earthquake the water in the reservoir is set in motion, resulting in hydrodynamic forces exerted on the upstream face of the dam. The dam–reservoir dynamic interactions resulting from the transverse component of ground motion can be simulated by modelling the reservoir using acoustic elements. The hydrodynamic pressures resulting from the vertical component of ground motion are assumed to be small and are neglected in all the simulations.

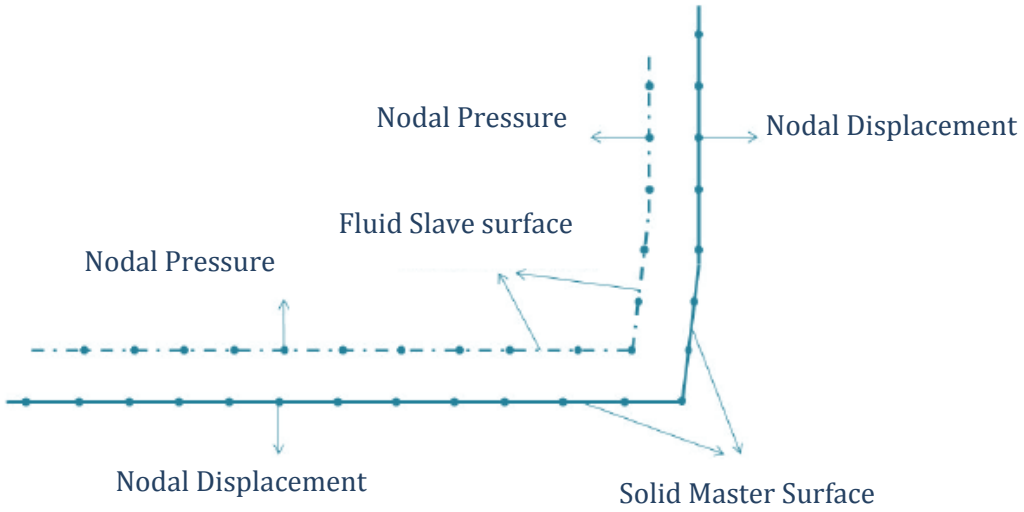

Figure 4.11 Graphical illustration of Fluid-Slave-Solid-Master Interface

- **Acoustic Elements**

Acoustic fluids or acoustic elements in finite element analyses are special purpose elements which describe the sound wave/pressure distribution over time in acoustic media like gases or water. Their only degree of freedom is pressure so no deformation can take place. The acoustic medium equation is a combination of Newton's law of motion (conservation of momentum) and the continuity equation (conservation of Mass). Commonly used in sound simulations, such elements also allow for simulating fluid-structure interaction problems if the following assumptions are valid:

- the fluid is compressible (density changes due to pressure variations),
- the fluid is inviscid (no viscous dissipation),
- the fluid is irrotational,
- there is no mean flow of the fluid (only small translations and small velocity $v \ll 1$),
- no body forces,
- homogeneous medium.

4.5.2 Free Vibration Analysis

The determination of the vibration eigen frequencies and eigen modes of the fluid-solid coupled system is conducted in this section through a natural frequency evaluation. Generally, each mode obtained by this procedure has contributions from both the fluid and the solid domain. Apparently, the coupling effect of the fluid-solid interaction depends on the characteristics of the solid and the fluid medium. For example, if the frequency values of the pure solid part are close to those of the pure fluid part, a strong coupling effect of the fluid and the solid may exist. But, on the other hand, if the frequencies are not in the same range, the coupling effect is less significant. Some of the modes may exhibit predominant participations from the structure, and are referred to as the modes dominated by the structure. For these modes, the presence of the fluid may have a comparatively minor effect on the structural response. Therefore, the modal characteristics of the dam, the reservoir, and the foundation are first examined separately, and then the coupled system is built. After gaining insight into the individual modal behaviour of the system's components, the analyses can then be extended to the dam reservoir system and eventually progressed to the dam-reservoir-foundation system.

4.5.3 Nonlinear Time History Analysis

The aim of the dynamic analysis is to determine the responses of the structure concentrating on the maximum tension and compression stresses and the displacements, based on the characteristics of the structure and the nature of the earthquake. Dynamic methods usually apply the modal technique which is based on some simplified assumptions i.e. the responses can be computed independently in each natural mode of vibration followed by a combination of these responses in order to obtain the total response (Chopra, 1987).

Two methods are recommended for the analysis of the stresses in gravity dams by using the finite element method: finite element response spectrum method and finite element acceleration time history method. Due to the ability of taking small time intervals of the earthquake record during the analysis, the finite element acceleration time history method is used in this study to determine the dynamic responses of the RCC dam in the attempt to produce more accurate information.

Time history method has the advantage of analysing time dependent characteristics of dynamic responses which in turn provide more information about the evaluation of the dam safety; information such as whether or not high stresses occur at the same time, short duration and repeated many times .The only drawbacks of this approach are its sophistication and the relative sensitivity of its outcome to the choice of input ground motions (FERC, 1999).

- **Structural Damping**

Damping in mechanical systems, especially in the equation of motion, is defined as a velocity dependent quantity (viscous damping), which describes the dissipation of energy during a dynamic oscillation. Damping factors are hard to define for even simple structures. In the case of civil engineering structures, where each structure is more or less a prototype, the damping is not known in the design phase. Due to the complexity of some structures and their interaction with the soil or water and the use of different materials it is almost impossible to account for all damping effects separately.

Consequently, one may use values measured at similar structures, which can be found in relevant literature. These values are mostly stated in terms of the fraction of the critical damping or modal damping factor ζi for specific materials, buildings or soils. In modal superposition the fraction of critical damping ζi can be applied directly on each natural mode separately if needed. On the contrary, in direct time integration methods, the damping matrix $\boldsymbol{C}$ has to be calculated, because the equation of motion is no longer uncoupled. Defining damping values for each degree of freedom (position in the matrix $\boldsymbol{C}$) is practically not possible, therefore, the so called Rayleigh damping, which is a well-established approach in finite element analyses is adopted. The method for determination of the Rayleigh constants by the classical Rayleigh damping is given by details in Appendix B.

4.6 Development of Safety Evaluation System for RCC Dams

Figure 4.12 illustrates a methodology for a comprehensive numerical system to evaluate the seismically induced cracking of RCC dams under the effects of thermal and seepage actions. The method includes a combination of field problems

(temperature and seepage fields), continuum mechanics (stress analysis), seismic hazard assessment and safety evaluation to achieve the most critical conditions. The combination uses finite elements to introduce compatible units capable of analysing infrastructure, such as RCC dams, to evaluate and predict levels of safety in terms of crack pattern development. The method, which is based on principle of birth and death process, is capable of simulating and assessing safety of RCC dams during the construction as well as the operation phase.

First, the finite element model is defined and all the nonlinearity sources (material, joints, geometry) as well as interactions (fluid-structure and soil-structure) are applied in the model. Then, Coupled or uncoupled thermo-mechanical and hydro-mechanical analyses are implemented to realize the performance of the dam at the pre-earthquake condition. Pre-earthquake safety assessment of the concrete dams may be conducted for a relatively long period of time (based on the seismicity condition of the site). In such a case, safety evaluation analysis should include the ageing constitutive models. Finally, seismic analysis is performed and the associated thermal and seepage stresses obtained from the previous steps are calculated and combined with other static loadings (self-weight and hydrostatic) and dynamic ones. For dynamic analysis, a coupled system of dam and reservoir is considered. Static stability analysis and seismic analysis are required to ensure the safety of the dam.

All the developments and analyses are performed using coded subprograms written in FORTRAN and developed in ABAQUS finite element program.

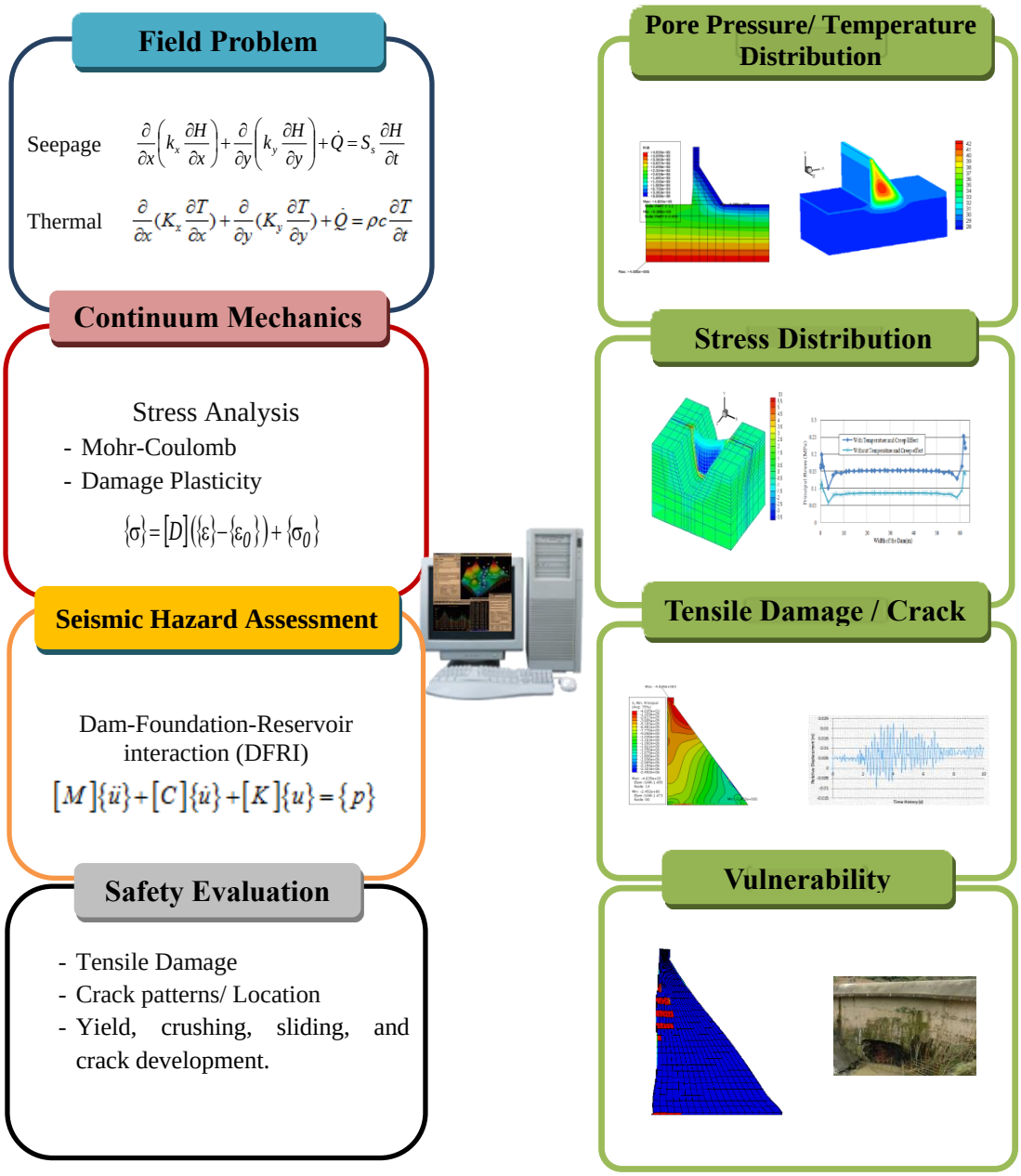

Figure 4.12 Methodology for Comprehensive Numerical System to Evaluate the Safety of a Dam

4.7 Concluding Remarks

In this chapter, computational strategies implemented in the present research work including, the computational procedures for thermal analysis, continuum mechanics, coupled seepage-stress problem and seismic cracking analysis have been presented. These strategies were fully discussed and illustrated in the accompanying flowcharts.

In addition, the development and modification of the ABAQUS finite element code for these analyses were discussed along with user subroutines written in FORTRAN. Finally, the development of a system of crack predication of RCC dam was presented in this chapter. This system is one of the primary objectives of the present work, which is a computational system to determine the safety level of RCC dams either in the short or the long term under critical loading conditions.

CHAPTER 5

VALIDATION OF THE DEVELOPED FE CODE AND PROPOSED MATHEMATICAL SOLUTION

5.1 Introduction

Due to the fact that the host finite element code has been extensively modified in view of addressing the objectives of the present study, the developed finite element code has been verified based on available experimental and analytical evidences, in order to check the code's accuracy and performance.

At first, the coupling effect of seepage and stress fields of RCC gravity dams is validated based on some numerical examples reported in the literature. Then, regarding the experimental verifications the developed codes are verified against the monitoring temperatures measured by insulating thermocouples in two full real scale tests of RCC dams for thermal analysis. The modified finite element programs are also used to solve some numerical examples reported in the literature.

Finally, in order to verify the seismic analysis of gravity dams via the developed code, a full scale dam reported in the literature has been selected and analysed. Both conditions of including and excluding the dam body-reservoir hydrodynamic interactions are taken into account in the analysis.

5.2 Validation of the Developed FE Code and Mathematical Solution for Coupled Seepage-Stress Analysis of RCC dam

The modified and developed code is used to solve some numerical examples reported in the literature for the purpose of validation of coupled seepage - stress analysis. At first, the procedure of calculation of phreatic surface is verified using a numerical example, then the implementation of the initial and boundary conditions in software via a MACRO environment is followed. Finally, all proposed modifications along with the simulation of the sequence of construction of RCC gravity dams using Birth and

Death of element technique in ABAQUS are validated through analysing the highest RCC dam located in China.

5.2.1 Phreatic Surface Calculation in a Dam (Seepage Analysis Only)

This example illustrates the use of ABAQUS to solve for the flow through a porous medium in which fluid flow is occurring in a gravity field and only part of the region is fully saturated, so the location of the phreatic surface is a part of the solution. The basic approach takes advantage of the ABAQUS capability to perform partially and fully saturated analysis: the phreatic surface is located at the boundary of the fully saturated part of the model and is calculated based on the materials presented in Section 3.2, of Chapter 3.

- **Problem Description and Material Properties**

The geometry of the particular earth dam considered is shown in Figure 5.1. This case is chosen because an analytical solution is available for comparison (Harr, 1962). The dam is filled to two-thirds of its height. Only a part of its base is impermeable (3.85 m from the bottom left corner). The material properties for the body of the dam are given in Table 5.1. This is not a very realistic model of physical absorption/exsorption behaviour, but this will not affect the results of the steady-state analysis significantly insofar as the location of the phreatic surface is concerned.

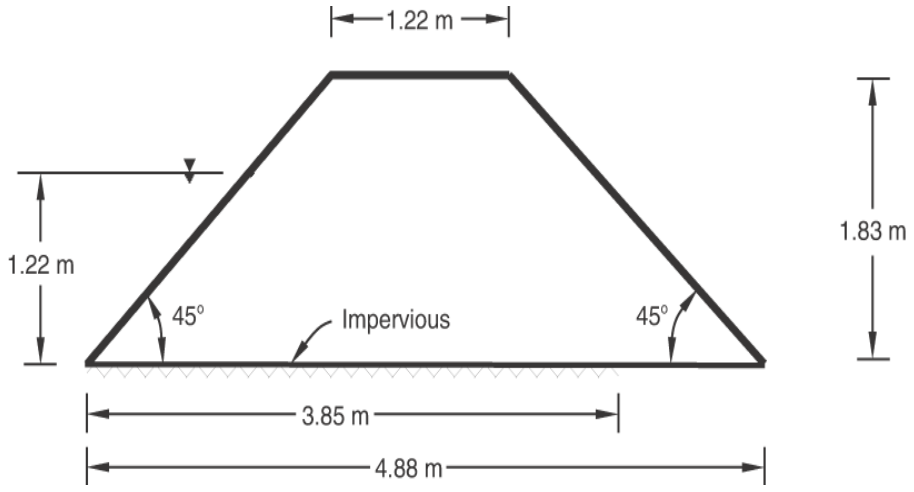

Figure 5.1 Typical Cross Section of the Dam

Table 5.1 Material Properties of an Earth Dam (Harr, 1962)

	Density *(kg/m^3)*	Hydraulic Conductivity *(m/s)*	Elastic Modulus *(kPa)*	Poisson's ratio
Dam Body	2000	0.2117E-3	1000	0

- **Finite Element Modelling and Boundary Conditions**

The two dimensional finite element mesh model of the dam is shown in Figure 5.2. Since the dam is assumed to be long, an 8-noded coupled pore pressure/displacement plane strain element (CPE8RP) is used in this example.

Figure 5.3 shows the finite element model of the element edges where the drainage-only boundary condition is applied. On these edges, the pore fluid pressure, is constrained by a penalty method to be less than or equal to zero, thus enforcing the proper drainage-only behaviour.

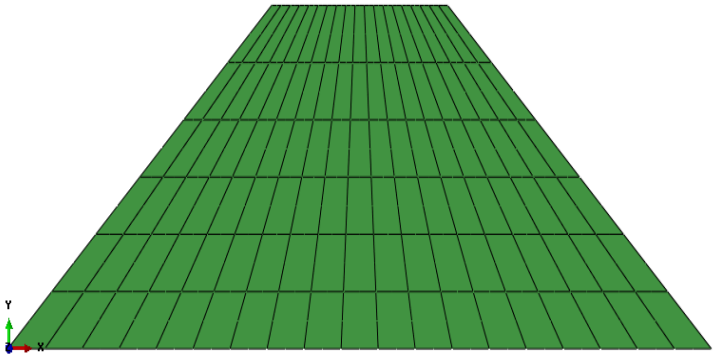

of les	No. of Elements
0	114

Figure 5.2 Finite Element Mesh of an Earth Dam

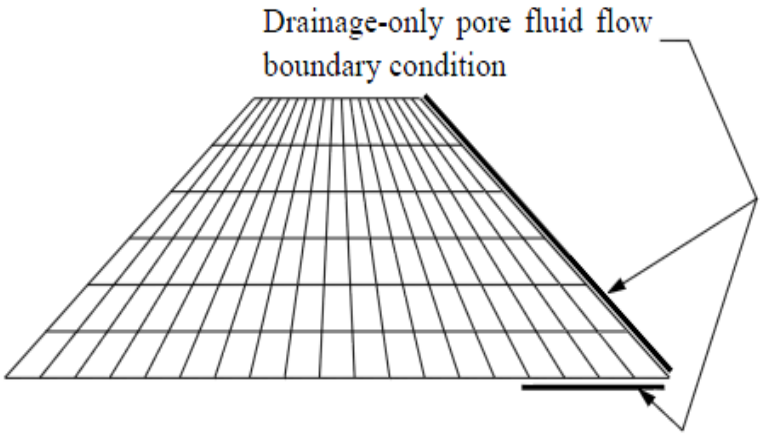

Figure 5.3 Drainage Boundaries of the Dam

- **Results and Discussion**

The steady-state contours of pore pressure (kPa) are shown in Figure 5.4 (note that Avg: 75% refer to the nodal averageing threshold defined in ABAQUS). The upper-right part of the dam shows negative pore pressures, indicating that it is partly saturated or dry.

The phreatic surface is best shown in Figure 5.5-a, where it has been chosen to draw the contours in the vicinity of zero pore pressure. This phreatic surface compares well with the analytical phreatic surface alculated by Harr (1962), shown in Figure 5.5-b.

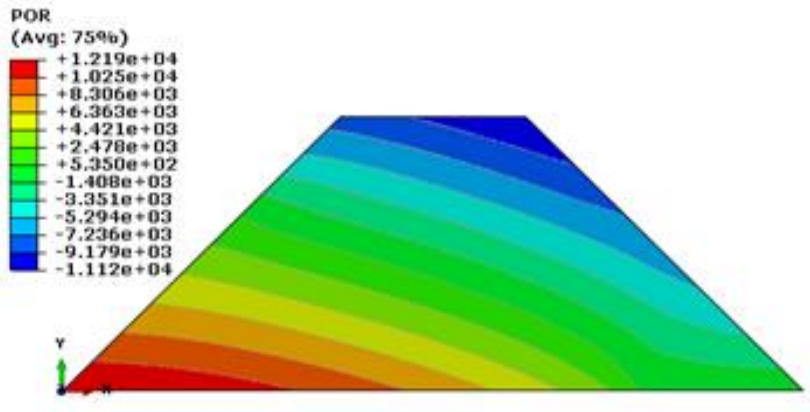

Figure 5.4 Pore Pressure Distributions (kPa)

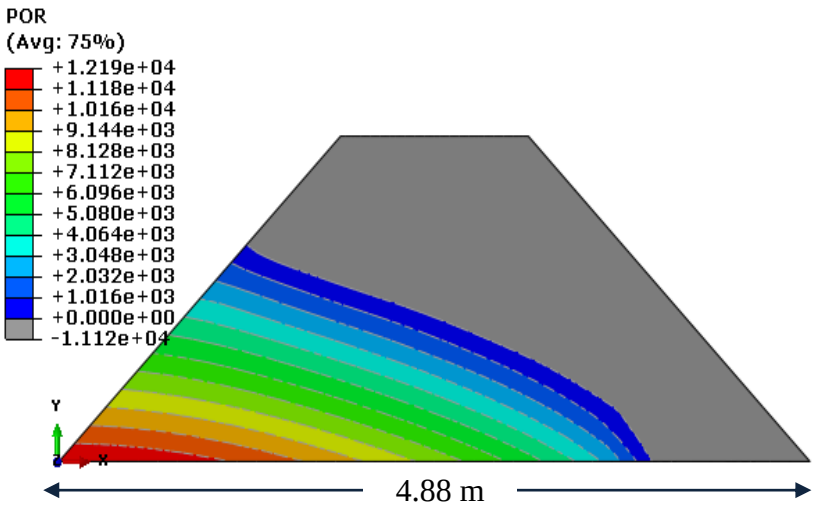

(a) Pore Pressure Contours showing Phreatic surface

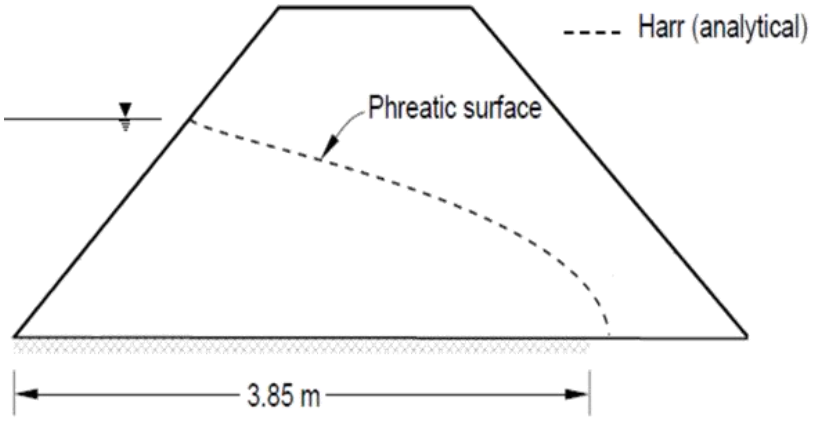

(b) Analytical Phreatic Surface (Harr, 1962)

Figure 5.5 Comparison of Predicted and Analytical Free Surface

5.2.2 Coupled Seepage-Stress Analysis of RCC Gravity Dam using Birth-and-Death Element Technique

The modified code and proposed procedure of calculation and implementation of initial and boundary conditions are verified based on analytical evidences. The Longtan RCC dam located in China, which is the highest RCC dam in the world with the height of 216.5 m, is considered as the numerical example.

- **Problem Description**

Longtan RCC dam with the height of 216.5 m is the main structure of Longtan hydropower plant with of the capacity of 5,400 MW. It is located in China. The construction of the project started in July 2001 and finished in 2006. Longtan dam is the highest roller compacted concrete dam in the world. Figure 5.6 shows a typical cross section of the dam (Junrui, 2005).

- **Material Properties and Site Conditions**

The material properties for the dam body and the rock foundation are given in Table 5.2. The hydraulic conductivity of dam body (RCC) was determined through experiments during a scientific research. The hydraulic conductivity of dam foundation (rock mass) is determined through field pressure water tests during geological investigation.

- **Initial and Boundary Conditions**

The seepage boundary conditions are determined mainly according to the project design shown in Table 5.3. The main initial conditions such as void ratio, pore pressures and initial stresses considered in the coupled analysis are based on the discussion in Section 3.2.4.

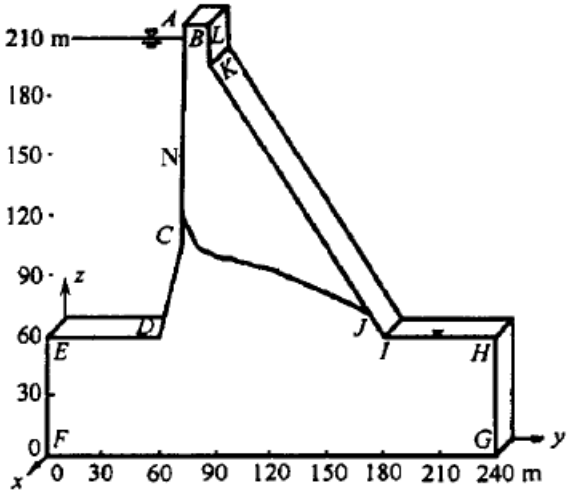

Figure 5.6 Typical Cross Section of Longtan RCC Dam

Table 5.2 Seepage and Structural Properties of Longtan Dam (Junrui, 2005)

	Specific Weights (N/ $m^{3)}$	Hydraulic Conductivity (m/s)	Elastic Modulus (GPa)	Poisson's ratio
Dam Body	23,520	10^{-10}	25.0	0.167
Anti-seepage plate	24,010	10^{-11}	28.0	0.167
Curtain grouting	26,559	10^{-9}	2.2	0.20
Foundation	26,460	10^{-8}	2.0	0.20

Table 5.3 Seepage Boundary Conditions (Junrui, 2005)

Seepage boundary conditions
$H\|_{BNCDE} = 150$ m, $H\|_{JIH} = 0$ m
$q\|_{CJ} = 0$, $H\|_{CJ} = z - 60$ m
$H\|_{JI} = z - 60$ m
$q\|_{FG} = q\|_{GH} = q\|_{EF} = 0$
$q\|_{x=0\ m} = q\|_{x=3\ m} = 0$

- **Two Dimensional Finite Element Model**

The two-dimensional finite element mesh model of the Non-overflow section of Longtan RCC dam is shown in Figure 5.7. A 4-noded plane strain reduced integration element (CPE4P) is used for the purpose of discretization of dam body and foundation. The two-dimensional finite element mesh model of the Non-overflow section of Longtan RCC dam is shown in Figure 4.12. A 4-noded plane strain reduced integration element (CPE4P) is used for the purpose of discretization of dam body and foundation.

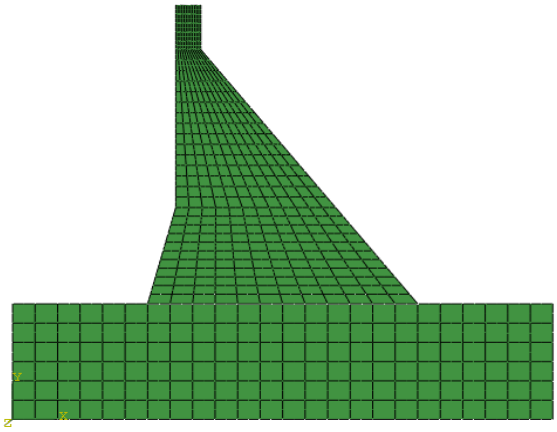

Figure 5.7 Finite Element Mesh of Longtan RCC Dam

- **Validation of the Proposed Mathematical Solution**

The proposed numerical procedure and modified code have been verified by comparing the predicted phreatic location, total head and stress distribution in the dam body with analytical results reported in the literature (Junrui, 2005).

Figure 5.8 shows a comparison between the predicted hydraulic heads and calculated free surface location, obtained from the code, and the analytical results for dam body and foundation. The comparisons show that the proposed modified model can accurately predict the total head distribution and phreatic face location of RCC gravity dams.

The comparison between predicted stresses from the code and analytical results, reported in the literature, are shown in Figures 5.9 and 5.10. It is clear from these plots that, the numerical solution agrees reasonably well with the analytical solution.

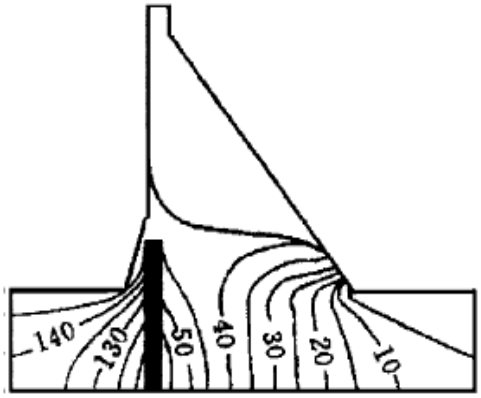

(a) Head Distribution (m) and Phreatic surface Location (Junrui 2005)

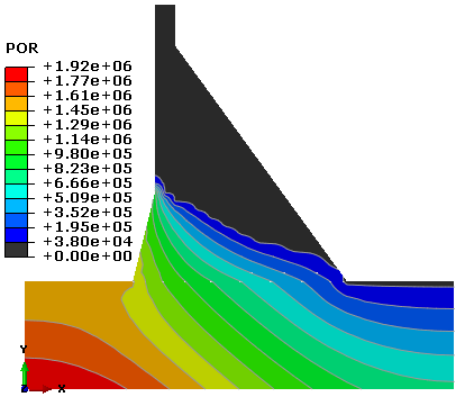

(b) Phreatic Surface Location (Code)

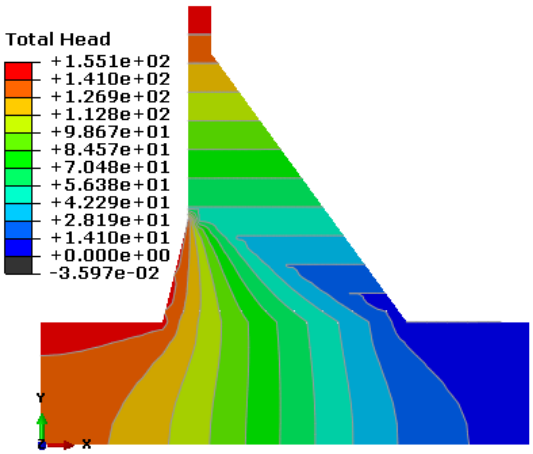

(c) Predicted Hydraulic Heads, m (Code)

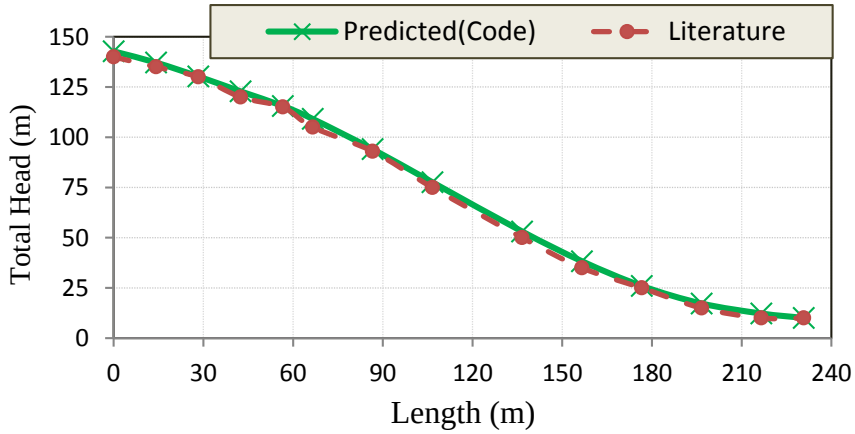

(d) Comparison of predicted and Analytical Hydraulic Heads

Figure 5.8 Contour of Hydraulic Heads and Phreatic Surface

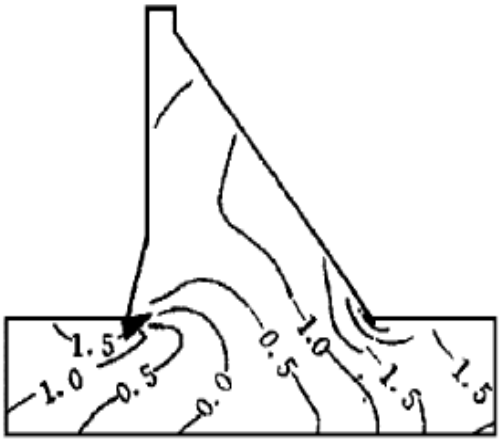

(a) Contour of (σ_y) Stress Distribution (MPa) (Junrui 2005)

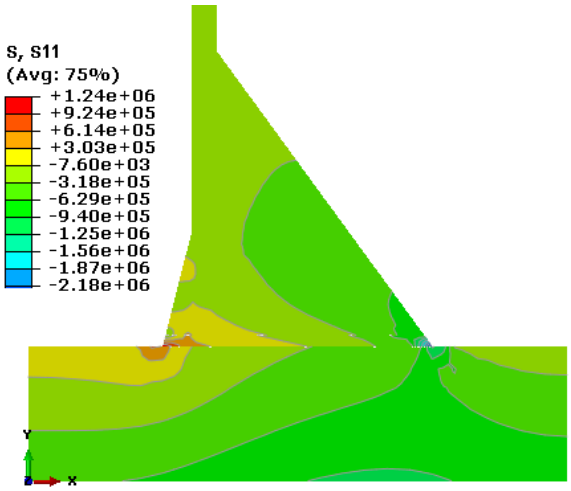

(b) Contour of Stress (σ_y) Distribution (Pa)(ABAQUS)

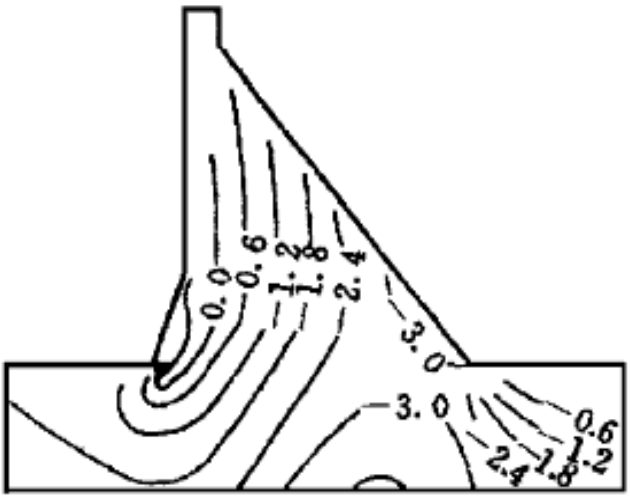

(c) Contour of (σ_z) Stress Distribution (MPa) (Junrui 2005)

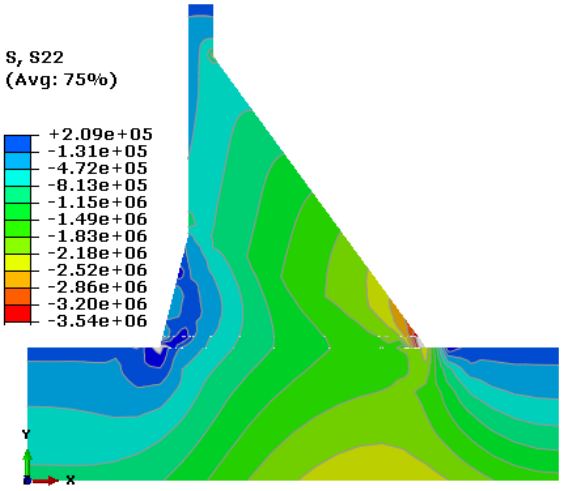

(d) Contour of Stress (σ_z) Distribution (Pa) (ABAQUS)

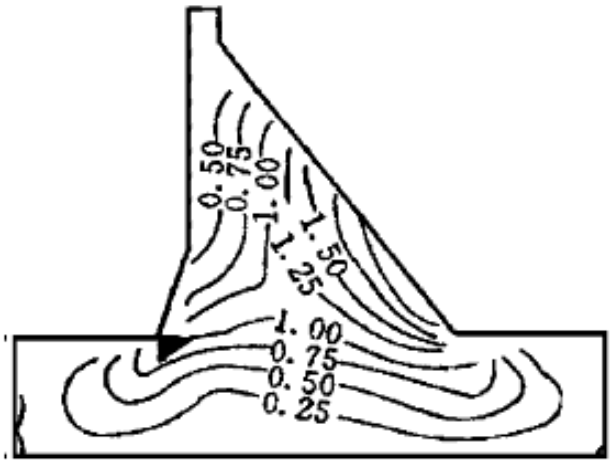

(e) Contour of (τ_{xy}) Stress Distribution (MPa) (Junrui 2005)

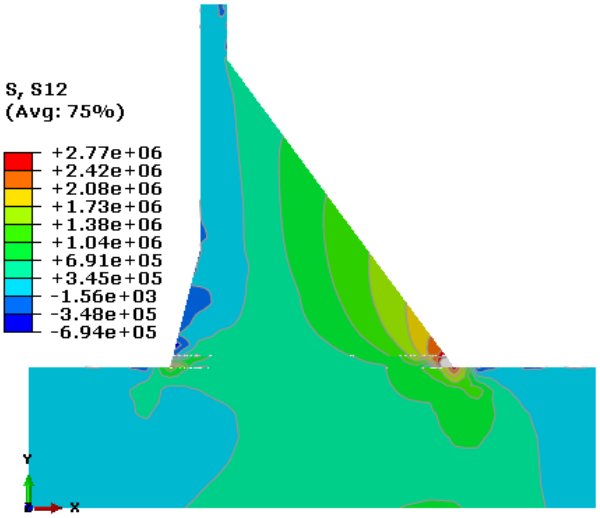

(f) Contour of Shear Stress Distribution (Pa) (ABAQUS)

Figure 5.9 Contour of Stress Distribution

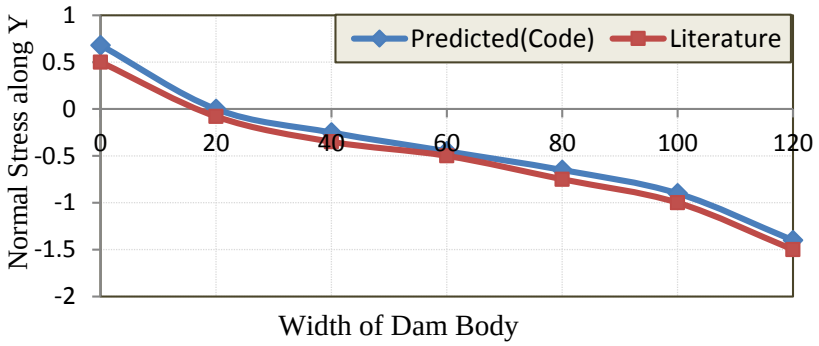

(a) Normal Stress Variation (σ_y)

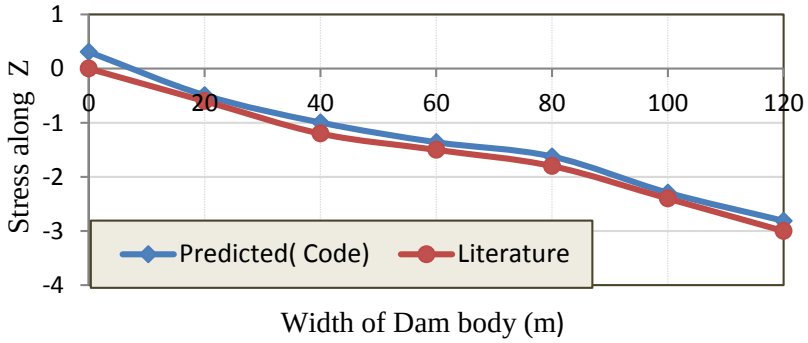

(b) Normal Stress Variation (σ_z)

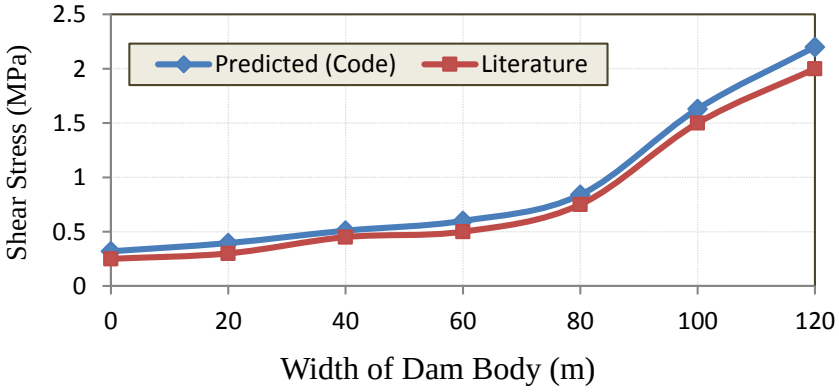

(c) Shear Stress Variation (τ_{xy})

Figure 5.10 Comparison of Predicted and Analytical Stresses (MPa)

5.2.3 Verification of the Developed FE Code with USDFLD subroutine for Coupled Seepage-Stress Analysis

The validation of the developed finite element code using USDFLD subroutine has been achieved using a Terzaghi consolidation problem reported in the literature. This one-dimensional problem has a well-known linear solution (Terzaghi and Peck, 1948) and, thus, provides a simple verification of the consolidation capability in ABAQUS. The analysis of saturated soils requires solution of coupled flow-stress equations. The coupling is approximated by the effective stress principle, which treats the saturated soil as a continuum, assuming that the total stress at each point is the sum of an "effective stress" carried by the soil skeleton and a pore pressure in the fluid permeating the soil. The Terzaghi problem is the simplest example of such a process.

The problem is shown in Figure 5.11. A body of soil with 2.54 m (100 inches) height is confined by impermeable, smooth, rigid walls on all surfaces except the top one. On that surface perfect drainage is possible, and a load is applied suddenly. Gravity is neglected. Because of the boundary conditions, the problem is one-dimensional, the only gradient being in the vertical direction. The purpose of the analysis is to predict the evolution of displacement, effective stress, and pore pressure throughout the soil mass for both conditions of with and without using USDFLD subroutine.

In user subroutine USDFLD, the field variable (FV) is assigned as permeability in this example, which is defined at a material point as functions of confining pressure or of any of the available material point quantities listed in the Output Variable Identifiers as a Solution Dependent Variable (SDV).

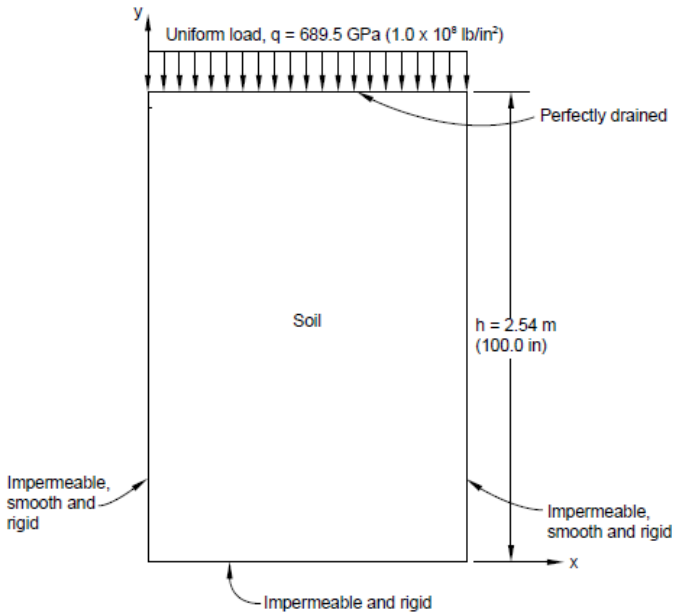

Figure 5.11 Geometry of Terzaghi Consolidation Problem

- **Numerical Modelling**

ABAQUS contains no one-dimensional elements for effective stress calculations. Therefore, a two-dimensional plane strain mesh, with one element only in the *x*-direction has been used and shown in Figure 5.12. An 8-noded plane strain reduced integration element (CPE8P) is chosen for the analysis. The material properties for the model are given in Table 5.4

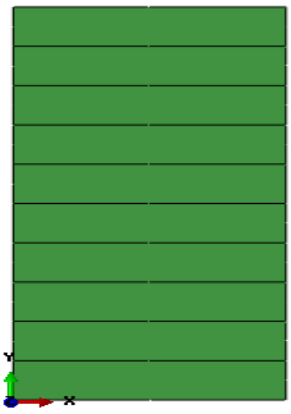

Figure 5.12 Finite Element Mesh

Table 5.4 Material Properties of Terzaghi Model (Terzaghi and Peck, 1948)

	Soil Body
Specific Weight (lb/ in^3)	1
Hydraulic Conductivity (in/min)	2E-4
Elastic Modulus (lb/in^2)	10E+08
Poisson's ratio	0.3

- **Results and Discussion**

The results of the analysis are summarized in Figures 5.13 and 5.14. Figure 5.13 shows the confining pressure, SDV and field variable (FV) profiles as a function of elevation. It is clear that the solution dependent variable has the same value as confining pressure. The predicted field variables are also in good agreement with hand calculated permeability as shown in Figures 5.13-c and 5.13-d**.** Furthermore, as expected, the value of hydraulic conductivity decreases as the confining pressure does increase as illustrated in Figure 5.13-d (Feng-bo, 2011)

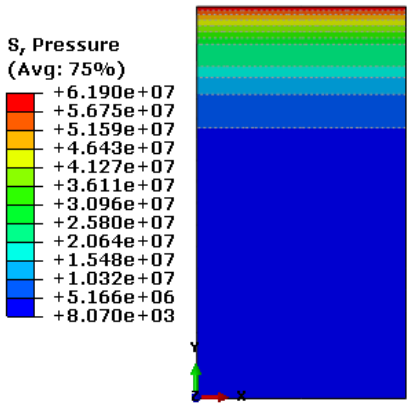

(a) Confining Pressure Pressure (lb/in2)

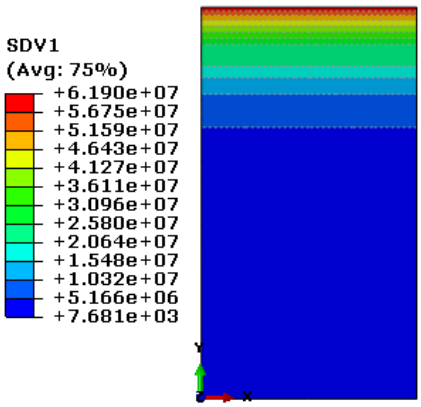

(b) Solution Dependent Variable (SDV)

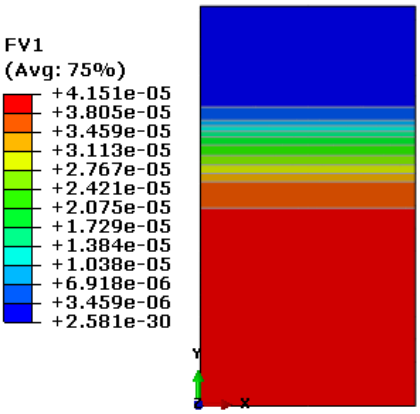

(c) Variation of Field Variable, in/Min (FV)

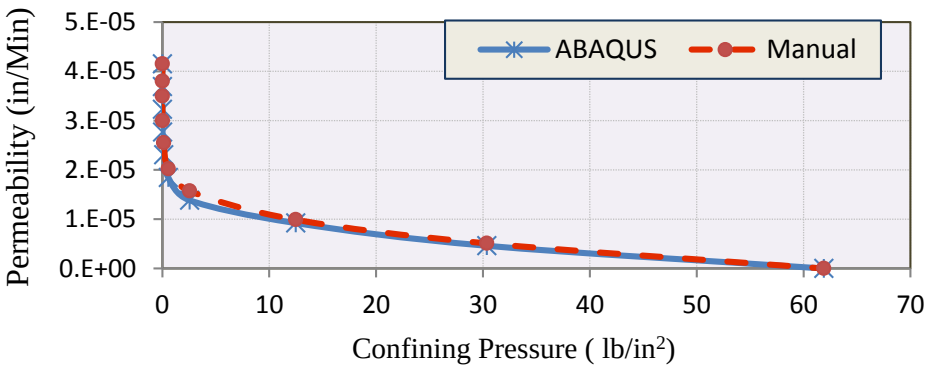

(d) Permeability VS field variable

Figure 5.13 Comparison of USDFLD and Manual Results

Contours of displacement variation in elevation for both cases of with and without using USDFLD subroutine are shown in Figure 5.14. As the former condition uses a constant value of permeability, in contrast to latter one where permeability is a SDV dependent value, there is a difference in displacement distribution within the body of the soil. The value of displacements considering USDFLD subroutine are less than those without using it, which is because of the decreasing rate of permeability with time (Figure 5.14-c).

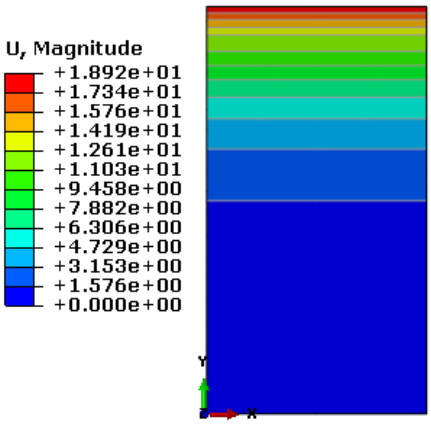

(a) Displacement without USDFLD (in)

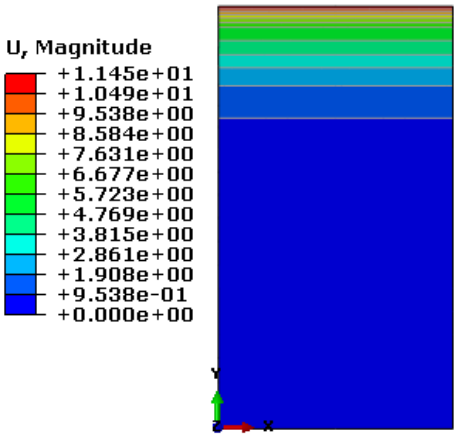

(b) Displacement with USDFLD (in)

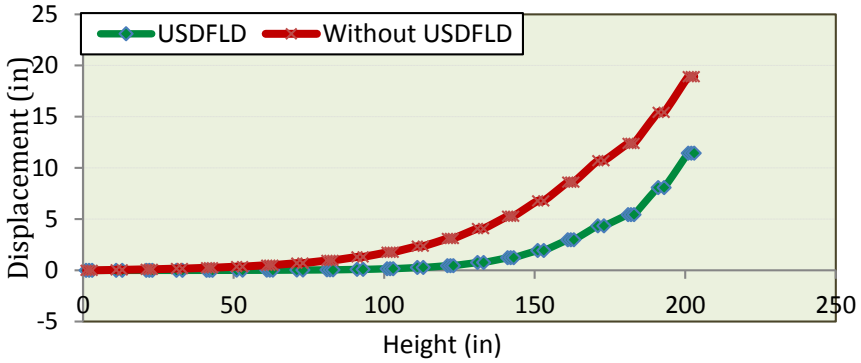

(c) Comparisons of Displacements

Figure 5.14 Contours of Displacement Variation in Elevation

The preceding comparisons show that the proposed developed and modified model can accurately predict the hydro-mechanical behaviour of RCC gravity dam.

5.3 Verification of the Developed FE Code for Heat Transfer Analysis

Before the application of code to the full-scale problem of real dam analysis, the developed code is verified against the monitoring temperatures measured by insulated thermocouples in two full scale tests of RCC dams. The two RCC dams have been selected in different regions. The first case is Kinta RCC dam located in Malaysia, which is a tropical region where the average temperature is $27\,^{o}C$. However, the second case is a relatively hot and dry climate condition such as Baluchistan state of Iran where the temperature ranges from 15 to $45\,^{o}C$, which has not been examined before.

5.3.1 An Experimental Validation of the Developed Code for Kinta RCC Dam

The analysis of this case of study is performed using the two dimensional model. Kinta dam is the first RCC gravity dam in Malaysia. Kinta dam project is a part of stage II development of the Ipoh Water Supply on the mainland of Malaysia located approximately 12 km east of Ipoh city, which in turn is located about 200 km north of Kuala Lumpur as shown in Figure 5.15. The maximum height of the dam is 78 m and the crest length is 700 m. Figure 5.16 shows a typical cross section of the dam

(SUNGAI Kinta dam RCC, 2002). The construction of the dam started in September 2004 and completed in April 2006 (Crichton et al. 2000). The progress of the dam construction with respect to time is shown in Figure 5.17.

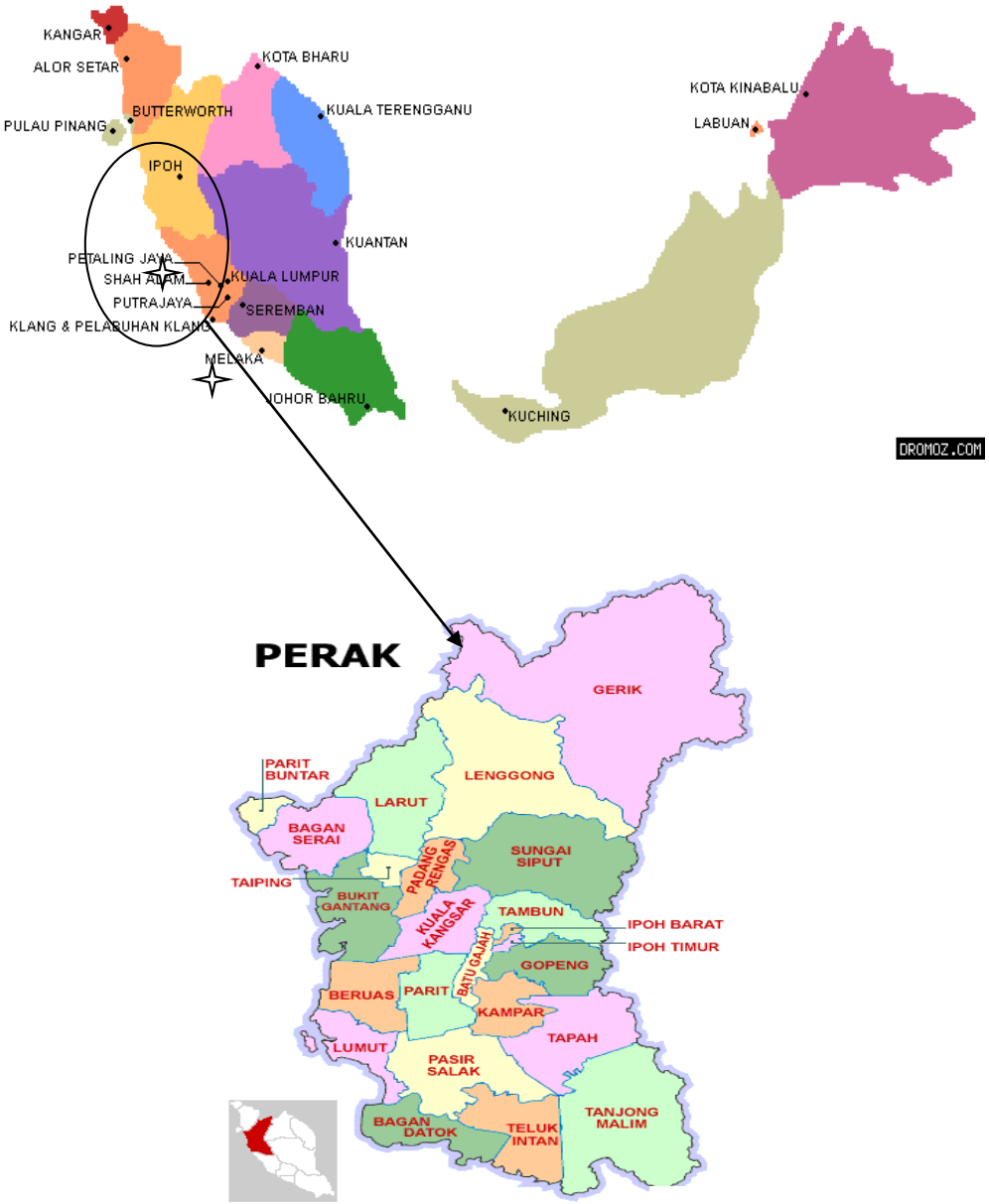

Figure 5.15 Location Map of Ipoh

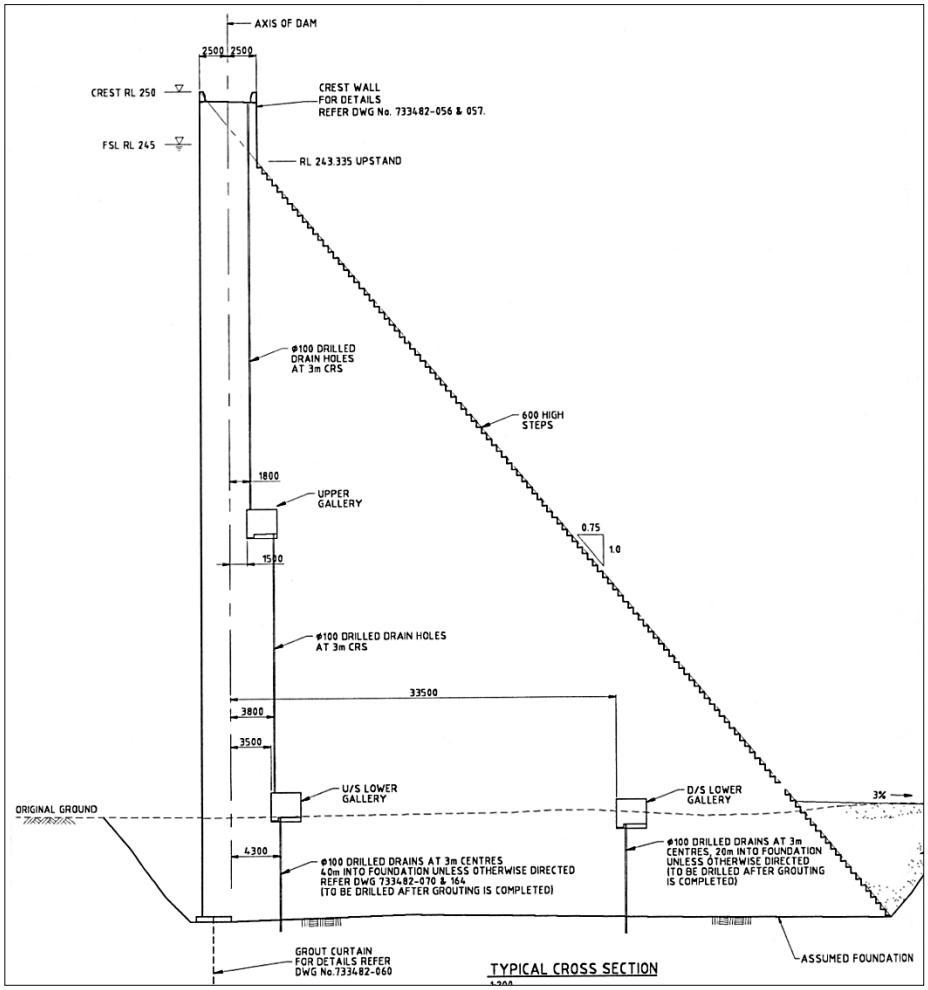

Figure 5.16 Typical Cross Section of the Dam (SUNGAI Kinta RCC dam 2002)

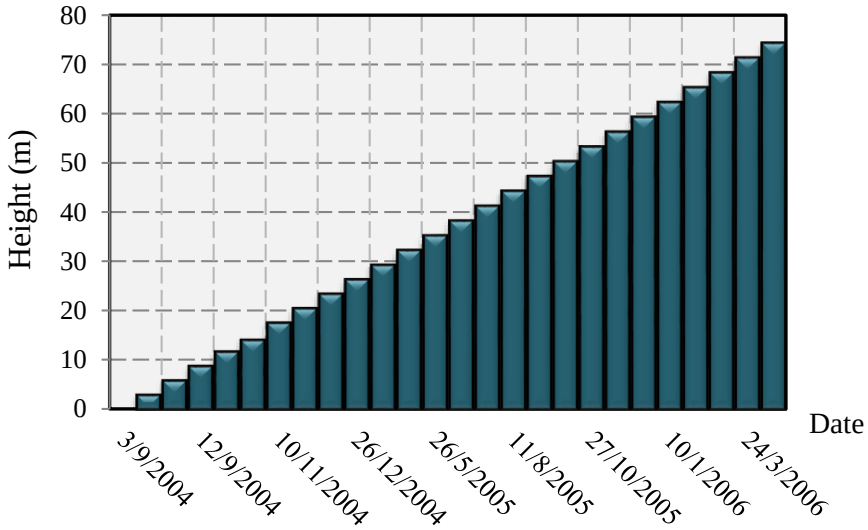

Figure 5.17 Kinta Dam Construction Progress

- **Material Properties and Site Conditions**

The material properties for the RCC, the conventional mass concrete (CMC), and the rock foundation, are given in Table.5.5 (SUNGAI Kinta dam RCC, 2002). These properties, which are the actual properties supplied by the consulting company, are used in the analysis as the input data. The recorded hourly environmental temperatures at the site, given in Figure 5.18, are used in the thermal analysis for the simulation of heat transfer by convention action. The cementitious content of the RCC mix used in the dam's construction are 100 kg/m^3 of Ordinary Portland Cement (lean RCC) and 100 kg/m^3 of Fly Ash.

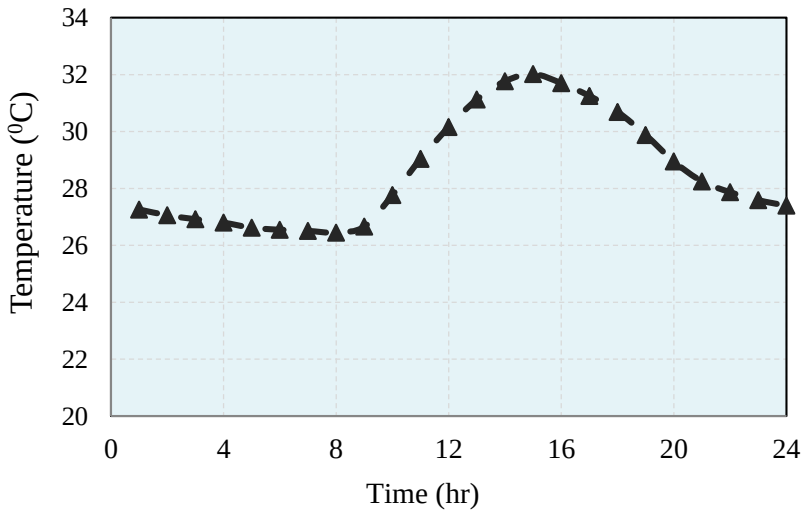

Figure 5.18 Average Recorded Daily Temperatures at Kinta Dam Site

Table 5.5 Relevant Thermal and Mechanical Properties

Property	Symbol	RCC	CMC	Rock
Thermal conductivity (W/mK)	K	2.7	2.7	2.97
Heat convection coefficient (W/m^2 K)	h	8.0	8.0	8.0
Specific heat (J/kgK)	$\boldsymbol{c}$	1150	1150	800
Density (kg/ m^3)	ρ	2325	2325	2650
Elasticity modulus (MPa)	E	18200	25700	24000
Poisson's ratio	ν	0.2	0.2	0.2

The main initial conditions considered in the thermal analysis are based on the discussion in Section 3.3.5. Thus; the rock foundation nodes are assigned an average initial temperature equal to the average annual temperatures at the site which is 28 °C. Then, the thermal analysis of the block foundation is performed for a period of two years prior to the dam construction time (Bayagoob 2007; Ishikawa 1991). The RCC placing temperature is taken as the environmental temperature at the casting time (Luna and Wu 2000).

- **Validation of the Developed Code for Two Dimensional Analysis**

The two-dimensional finite element code has been verified by comparing the predicted temperatures with actual temperatures recorded by thermocouples installed in the dam's body. The thermocouple locations, installed at some selected levels in the deepest block of the dam, are shown in Figure 5.19.

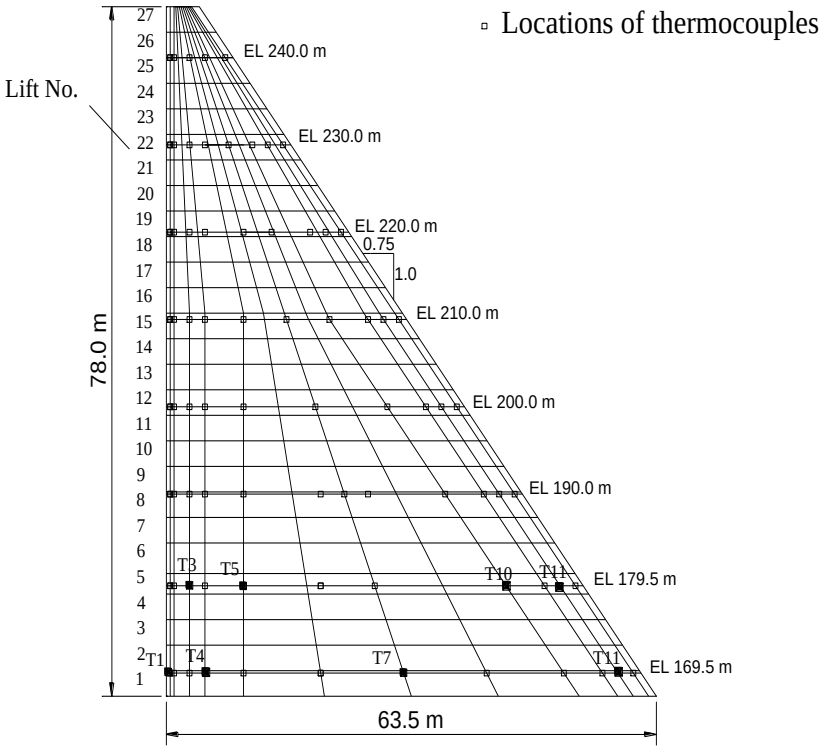

Figure 5.19 Thermocouples Locations of the Kinta dam deepest block (SUNGAI Kinta RCC dam 2002)

The two- dimensional finite element mesh model of Kinta RCC dam for the first 10 stages is shown in Figure 5.20. An eight nodded isoparametric element is used for the discretization of the dam body and foundation. The time step used in thermal analysis is 3 hr (Bayagoob 2007; Ishikawa 1991).

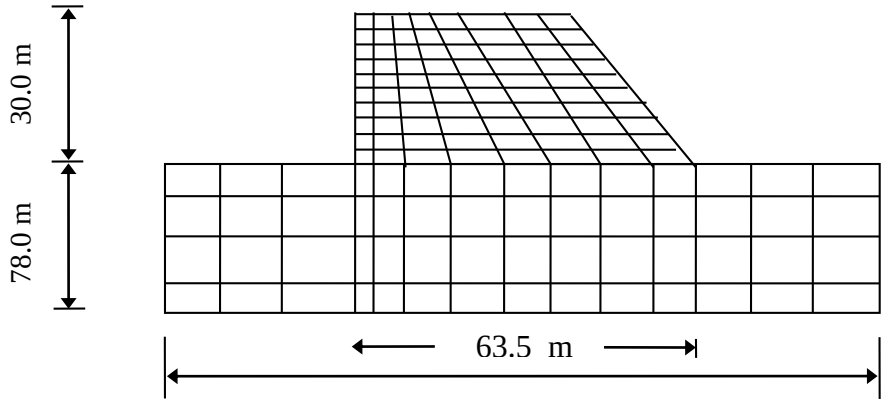

Figure 5.20 Two- Dimensional Finite Element Model for Stage No. 10

The comparison between the two dimensional finite element predicted temperatures and the monitored temperatures from the thermocouples installed at the elevations of 169 m and 179 m are shown in Figures 5.21-5.23, respectively.

It is clear that from these plots that; the predicted temperatures obtained from the developed code (2D analysis) are in good agreement with monitoring temperatures.

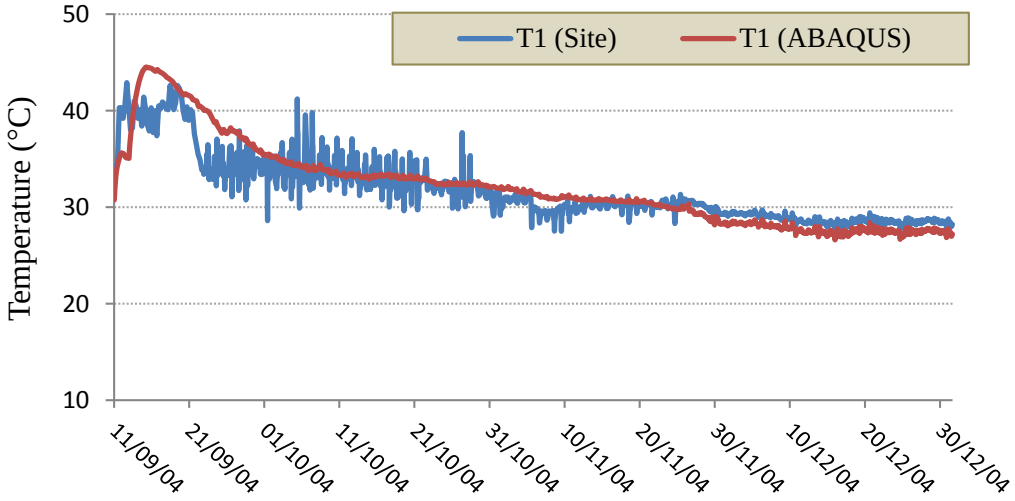

Figure 5.21 Comparison of Predicted and Monitored Temperatures at Level of 169.0 m (0.5 m from Upstream)

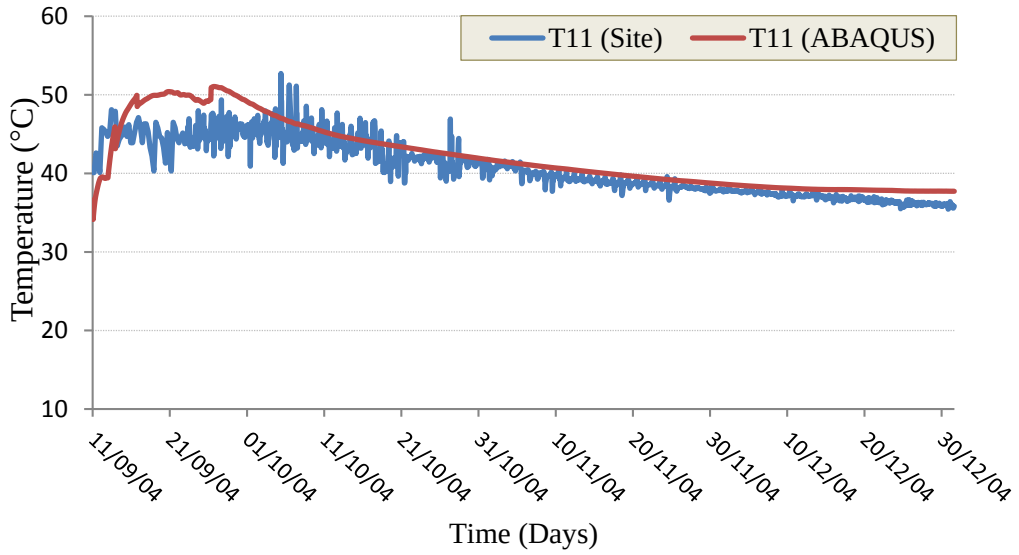

Figure 5.22 Comparison of Predicted and Monitoring Temperatures at Level of 169.0 m (3.0 m from Downstream)

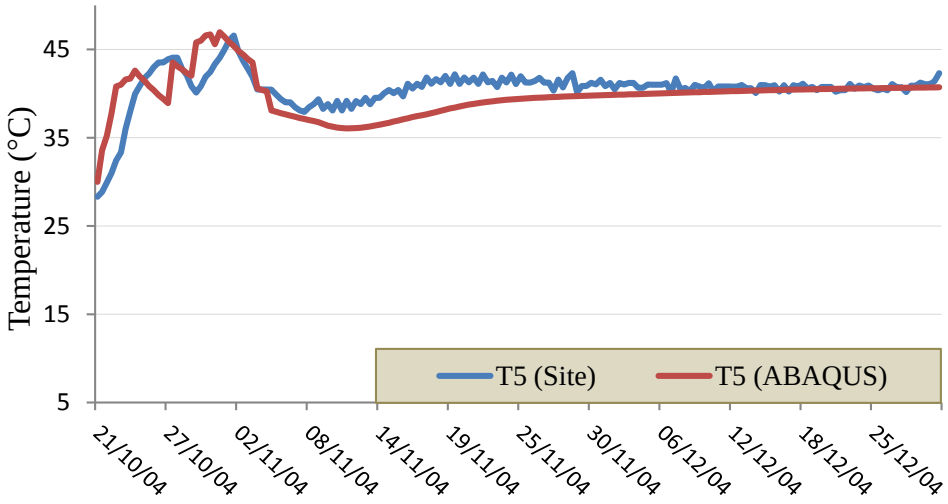

Figure 5.23 Comparison of Predicted and Monitoring Temperatures at Level of 179.0 m (10 m from Upstream)

5.3.2 An Experimental Case Study

Although the developed finite element code has been verified for Kinta RCC dam situated in Malaysia with approximately constant variation of environmental temperature, there was a need to test the performance of the developed code in the region with higher variability and also extreme hot temperatures. In this study, the

verification of the developed code for the heat transfer problem is presented by the analysis of a real trial as a case study. The analysis was performed as follows;

(a) Model verification against the field data available in a technical report supplied by the consulting company,
(b) Complete thermal analysis for the experimental phase according to the construction schedule.

The geometrical details of the trial study are shown in Figure 5.24. It is placed in 20 cm horizontal layers of Roller Compacted Concrete (RCC), with cohesion layer above rock of 5 cm thickness on the bottom that is made of conventional mass concrete (CMC). The construction of this segment was started in August 1999 and was completed in September 1999.

- **Material Properties and Site Conditions**

The material properties for the RCC, the conventional mass concrete (CMC), and the rock foundation, are given in Table 5.6 (Pazhouhab Consultant Engineers 1999). These properties, which are the actual properties supplied by the consulting engineers, are used in the analysis as the input data. In addition, the average monthly air temperature at the project site as shown in Figure 5.25, are used in the thermal analysis for the simulation of the heat transfer by the convention action.

Table 5.6 Thermal and Structural Properties of Trial Segment (Pazhouhab Consultant Engineers 1999)

Parameter	unit	Symbol	RCC	CMC	Rock
Heat conduction coefficient	W/m °C	K	2.8	2.8	2.7
Heat convection coefficient	$W/m^2°C$	h	15.25	15.25	15.25
Specific heat	J/kg°C	c	1256	1256	1256
Density	kg/m^3	ρ	2400	2400	2710
Elasticity modulus	GPa	E	1.67	2.25	0.6
Poisson's ratio	-	ν	0.18	0.18	0.3

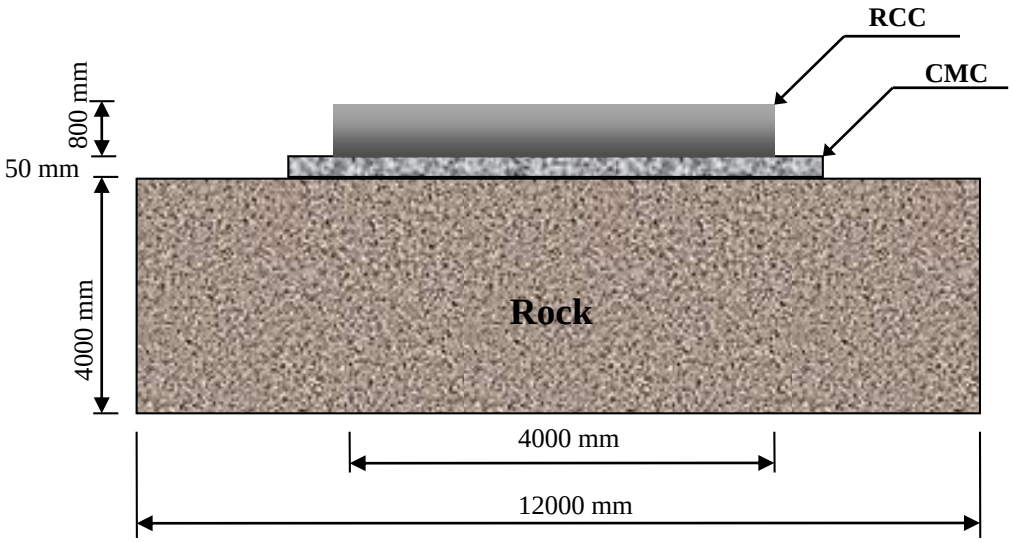

Figure 5.24 Typical Cross Section of Experimental Study

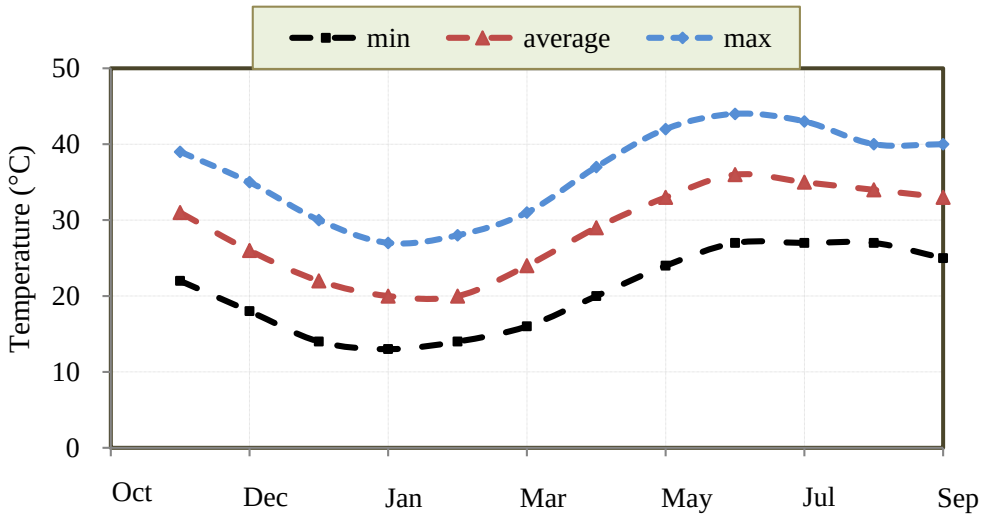

Figure 5.25 Monthly air Temperature at Project Site

- **Two Dimensional Analysis**

The 2D finite element mesh model for this segment is shown in Figure 5.26. The Eight-noded isoparametric elements are used in the 2D thermal analysis.

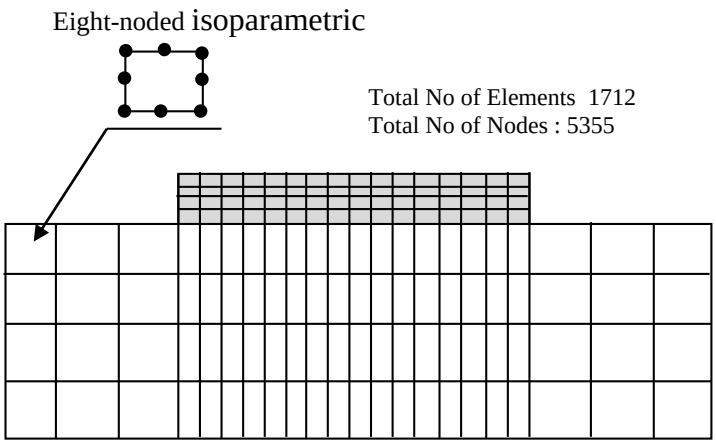

Figure 5.26 2D Finite Element Mesh of Experimental Segment

The developed F.E. code is verified by comparing the actual temperatures measured in the field using the thermocouples installed in the trial segment at some levels. Figure 5.27 shows the thermocouple locations.

The comparison between the two dimensional FE predicted temperatures and the monitored temperatures from the thermocouples at the selected points are shown in Figure 5.28. It is clear from these plots that the predicted temperatures obtained from developed code are in good agreement with monitored temperatures.

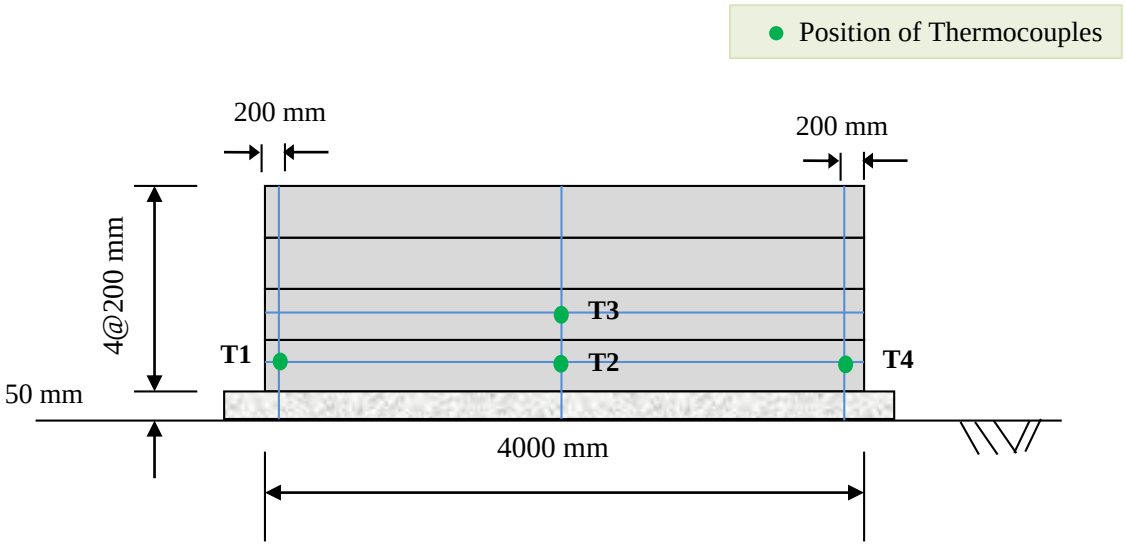

Figure 5.27 Thermocouple Locations of the Trial Segment

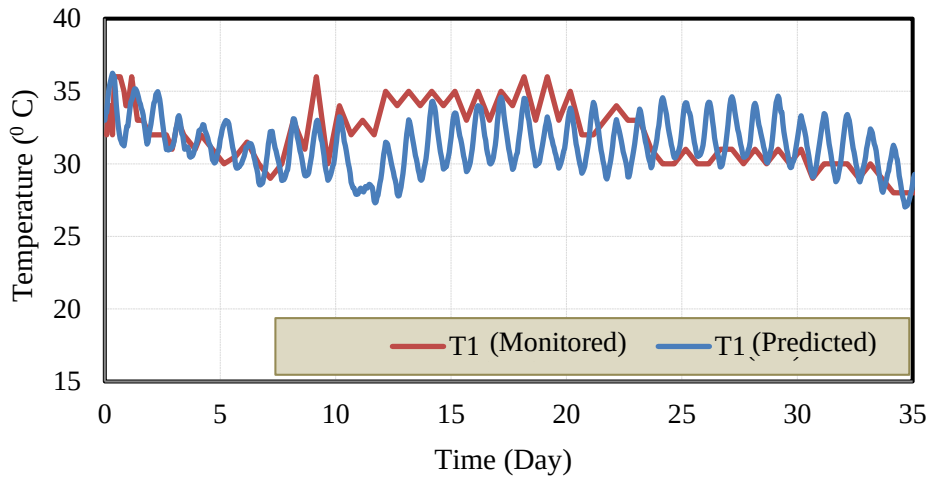

(a) Point No. 1

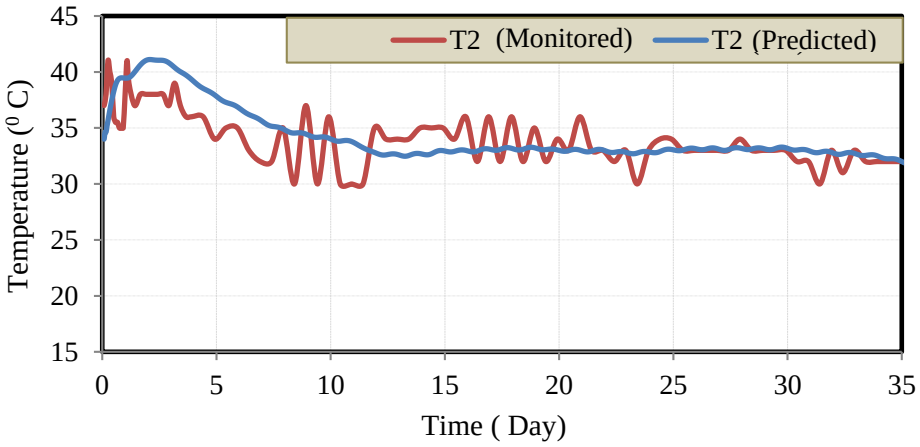

(b) Point No. 2

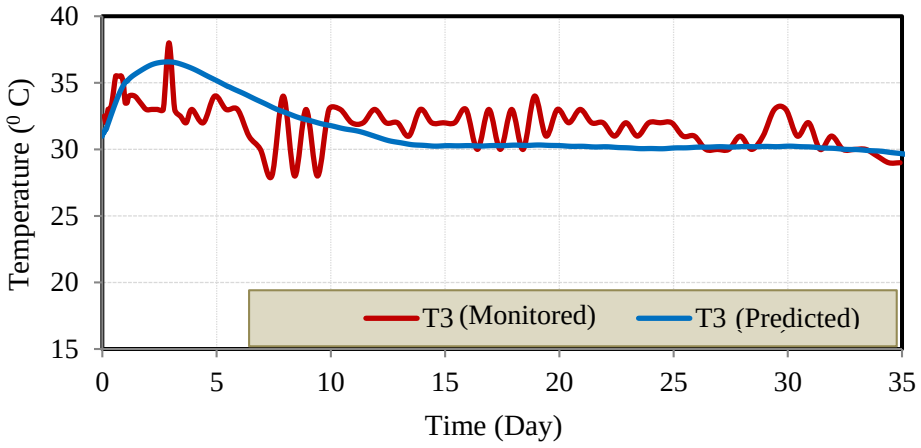

(c) Point No.3

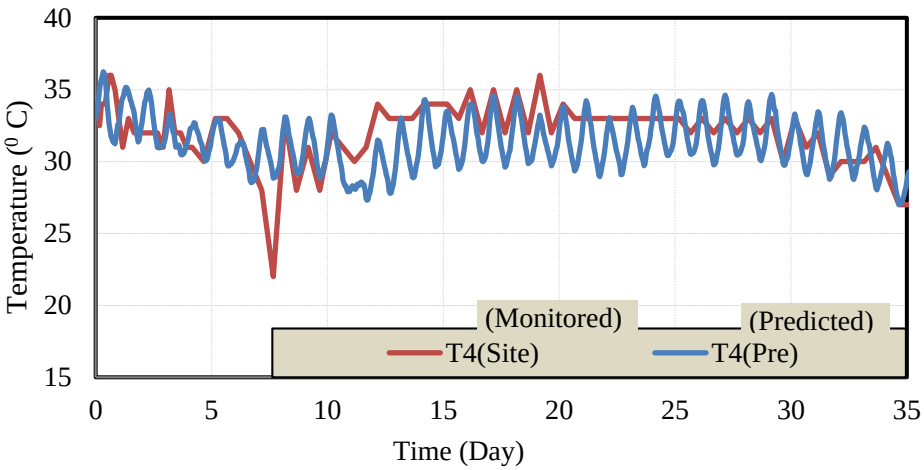

(d) Point No. 4

Figure 5.28 Comparison of Predicted and Monitored Temperatures

5.3.3 Analytical Verification of Developed FE Code for Thermal-Stress Analysis

In order to validate the proposed mathematical modelling, computational algorithm and developed finite element program, a concrete block (Wu and Luna, 2001) has been analysed. The block geometry is shown in Figure 5.29. The material properties are summarized in Table 5.7. The upper surface of the block is exposed to the air and the ambient temperature is 10 ^{o}C.

Table 5.7 Thermal and structural properties of concrete block (Wu and Luna 2001)

Parameter	Concrete
Heat conduction coefficient K (W/m °C)	2.16
Heat convection coefficient h (W/m^2 °C)	8.0
Specific heat c (J/kg °C)	1150
Density ρ (kg/ m^3)	2400
Elasticity modulus E (GPa)	25.5
Poisson's ratio ν	0.16

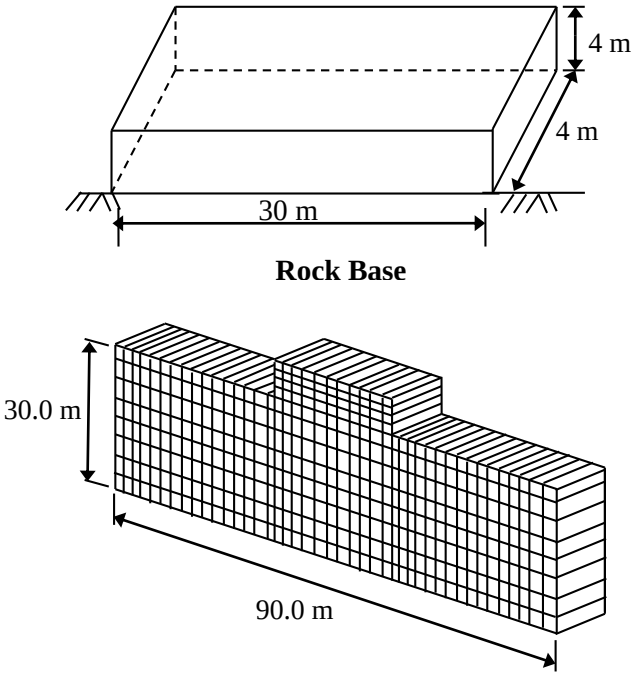

Figure 5.29 Concrete Block

Figure 5.30(a) shows the temperature at the central point of the concrete block. The temperature increases due to the heat produced by hydration, then reaches a maximum point at about 8 days after casting. Then the block starts to cool down due to the interaction with ambient temperature. Figure 5.30(b) shows the variation of the thermal stress at the same point of the block. The maximum compression stress also occurs about 8 days after the block is cast. Then the compression stress decreases which is expected because the block begins to cool down. Finally, the compression stress changes to tension stress and the tension stress becomes larger and larger because the block continues to cool down.

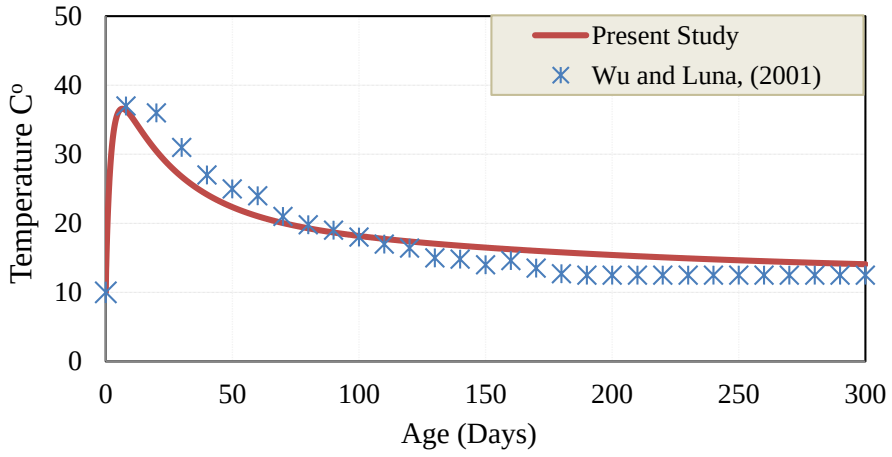

(a) Temperature Variation at the Central Point

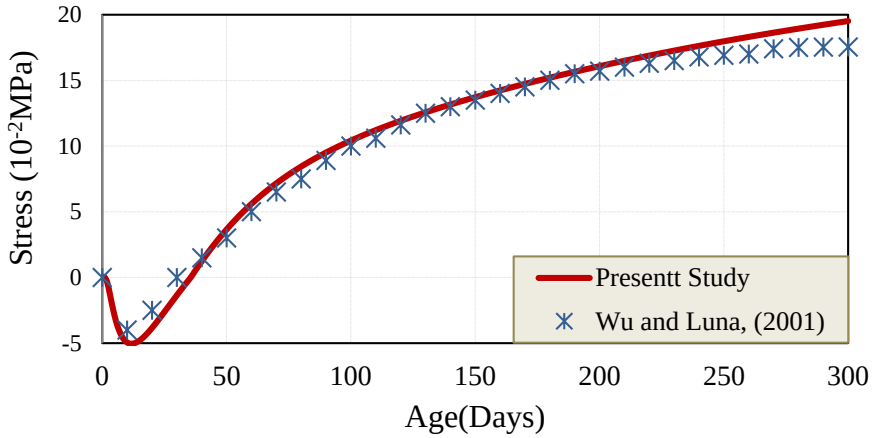

(b) Normal Stress Variation at the Central Point of the Block

Figure 5.30 Temperature and Stress Variation at the Central Point

5.4 Validation of Seismic Analysis of Gravity Dams Using ABAQUS

In order to verify the seismic analysis of gravity dams using the developed code, the Koyna dam reported in the literature has been selected and analysed. Both conditions of including and excluding the dam body-reservoir hydrodynamic interactions are taken into account in the analysis.

The example illustrates a typical application of the concrete damaged plasticity material model for the assessment of the structural stability and damage of concrete structures subjected to random loading. This problem is chosen as it has extensively been analysed by a number of investigators, including Chopra and Chakrabarti (1973), Bhattacharjee and Leger (1993), Ghrib and Tinawi (1995), Cervera et al. (1996), and Lee and Fenves (1998).

5.4.1 Problem Definition

Koyna dam is a concrete gravity dam and the largest dam in Maharashtra, India and constructed on Koyna River located in Koyna Negar, in Satara district, nestled in the Western Ghats on the state highway between Chiplun and Karad. Geometry of the non-overflow or deepest section and the geometrical details of the dam is shown in Figure 5.31. The monolith is 103 m high and 71 m wide at its base. The upstream wall of the monolith is assumed to be straight and vertical, which is slightly different from the real configuration. The depth of the reservoir at the time of the earthquake is 91.75

m. For the purpose of this example, the dam–foundation interactions was neglected by assuming that the foundation is rigid.

5.4.2 Material Properties

The material properties used for the simulations are given in Table 5.8 and Figure 5.32. These properties are assumed to be representative of the concrete material in the Koyna dam and are based on the properties used by previous investigators (Chopra, 1973; Bhattacharjee, 1993).

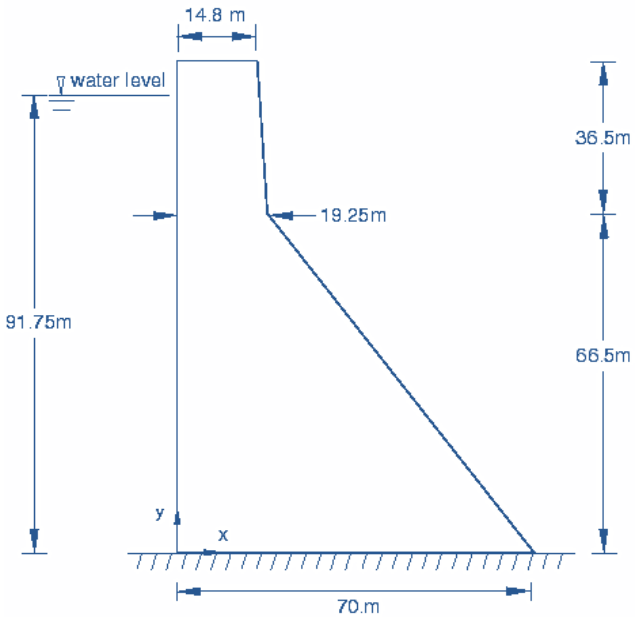

Figure 5.31 Geometrical Details of Deepest Section of Koyna RCC Dam (Sarkar *et al.*, 2007) and (Jiang and Du, 2012)

In obtaining some of these material properties, a number of assumptions are made. Of particular interest is the calibration of the concrete tensile behaviour. The tensile strength is estimated to be 10% of the ultimate compressive strength (σ_{cu} = 24.1 MPa), multiplied by a dynamic amplification factor of 1.2 to account for rate effects; thus, σ_{to} = 2.9 MPa.

To avoid unreasonable mesh-sensitive results due to lack of reinforcement in the structure, the tensile post failure behaviour is given in terms of a fracture energy cracking criterion by specifying a stress-displacement curve instead of a stress-strain curve, as shown in Figure 5.32-a. This is accomplished with the *CONCRETE TENSION STIFFENING, TYPE=DISPLACEMENT option. Similarly, tensile

damage, d_t is specified in tabular form as a function of cracking displacement by using the *CONCRETE TENSION DAMAGE, TYPE=DISPLACEMENT option. This curve is shown in Figure 5.32-b. The stiffness degradation damage caused by compressive failure (crushing) of the concrete, d_c is assumed to be zero. The mechanical behaviour of the concrete material is modelled using the concrete damaged plasticity constitutive model.

- **Damping**

It is generally accepted that dams have damping ratios of about 2–5%. In this example, the material damping properties are considered to provide approximately 3% of critical damping for the first mode of vibration of the dam. Assuming Rayleigh stiffness proportional damping, the factor β required to provide a fraction ξ_1 of critical damping for the first mode is given as $\beta=2\xi_1/\omega_1$.

Table 5.8 Material Properties for the Koyna Dam (Chopra, 1973)

Parameter		Value
Young's modulus	E	31027 MPa
Poisson's ratio	υ	0.15
Dilation angle	ψ	36.31°
Density	ρ	2643 kg/m^3
Tensile failure stress	σ_{to}	2.9 MPa
Compressive initial yield stress	σ_{co}	13.0 MPa
Compressive ultimate stress	σ_{cu}	24.1 MPa

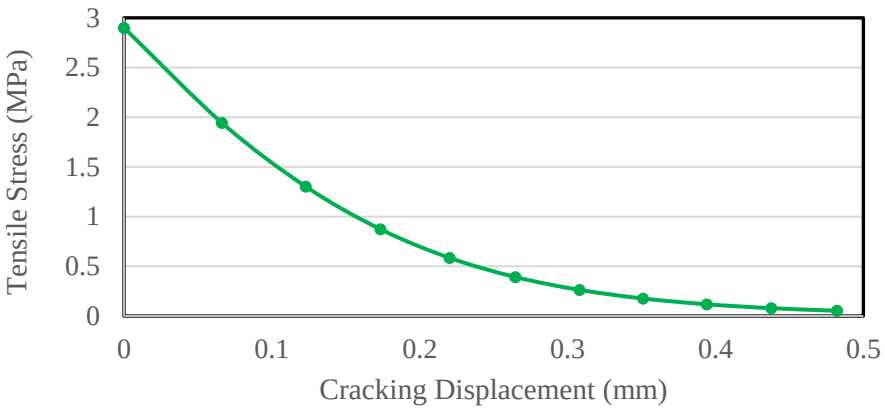

(a) Tension Stiffening

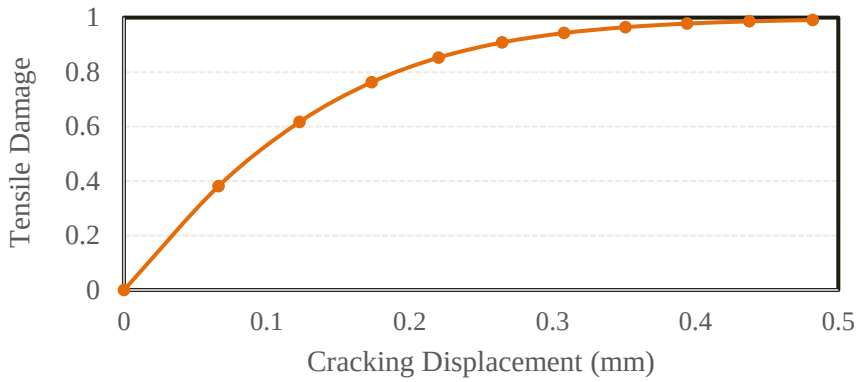

(b) Tension Damage

Figure 5.32 Concrete Tensile Properties (Chopra, 1973)

5.4.3 Loading Conditions

Loading conditions and solution controls for both cases of including and excluding dam body-reservoir in Abaqus/Implicit are discussed in the following for each analysis**.**

- **Without Hydrodynamic Interactions**

Prior to dynamic simulation of the earthquake, the dam is subjected to gravity loading and hydrostatic pressure. In the Abaqus/Standard analysis these loads are specified in two consecutive static steps, using the *DLOAD option with the load type labels GRAV (for the gravity load) in the first step and HP (for the hydrostatic pressure) in the second step. For the dynamic analysis in the third step, the transverse and vertical components of the ground accelerations recorded during the Koyna earthquake shown in Figure 5.33 (units of g = 9.81 m sec^{-2}) are applied to all nodes at the base of the dam.

- **With Hydrodynamic Interactions**

Loading conditions including self-weight of the dam, hydrostatic pressure, earthquake forces and hydrodynamic pressure are applied in the case when considering hydrodynamic interactions. The application of the first three loadings is the same as the previous case of excluding hydrodynamic conditions. However, the dam–reservoir dynamic interactions (hydrodynamic pressure) resulting from the transverse

component of ground motion can be modelled in a simple form of modelling reservoir using acoustic elements. The hydrodynamic pressures resulting from the vertical component of ground motion are assumed to be small and are neglected in all simulations.

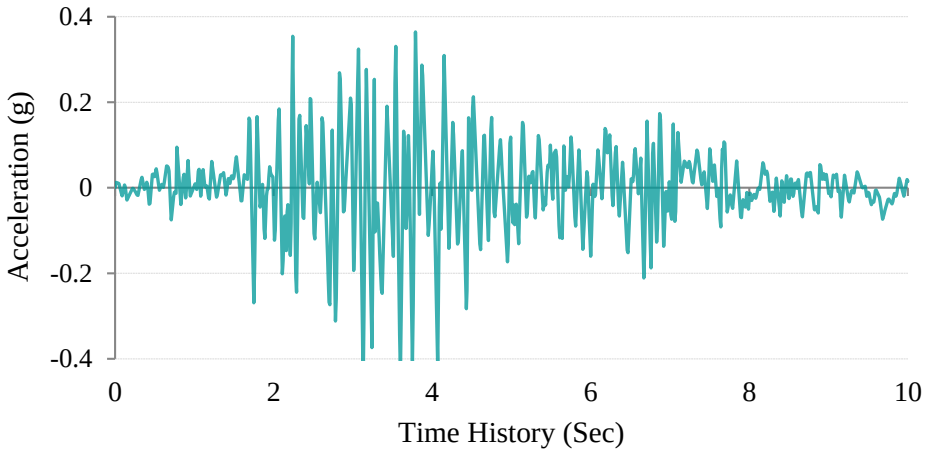

(a) Transverse Component

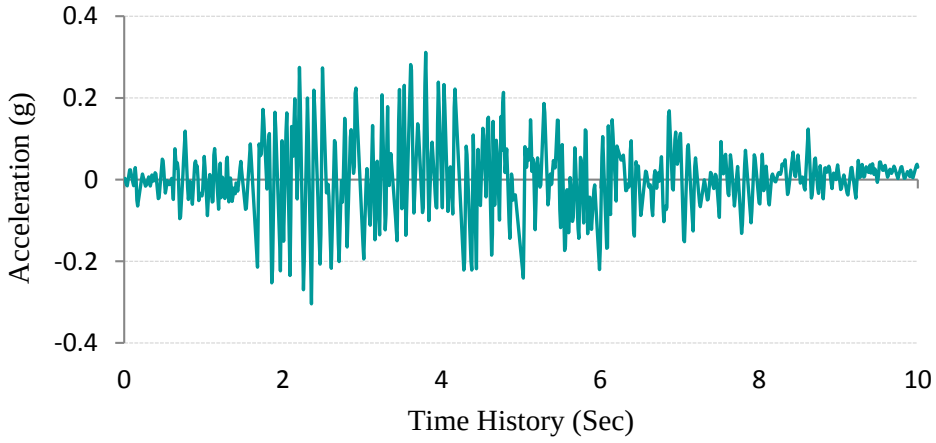

(b) Vertical Component

Figure 5.33 The Components of Koyna Ground Acceleration

5.4.4 Finite Element Idealization of the Koyna Dam

The 2-D finite element modelling of the Koyna dam was considered for the non-overflow deepest block assuming plane stress behaviours. Figure 5.34 shows the finite element mesh model utilized for the analysis. In this case the dam is modelled by 3,720 elements of CPS4R (4-noded bilinear plane stress quadrilateral, reduced integration, hourglass control) and 3,821 nodes.

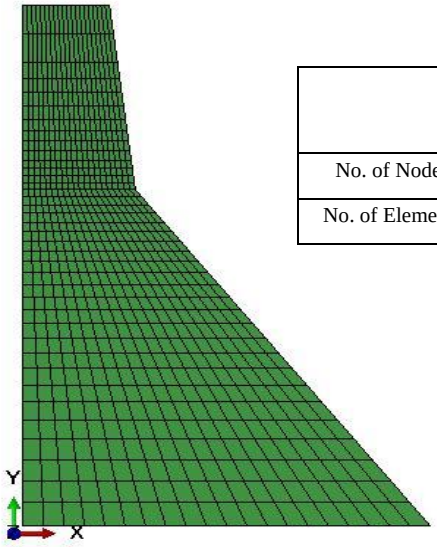

	Dam Body
No. of Nodes	3,821
No. of Elements	3,720

Figure 5.34 Finite Element Mesh of Koyna RCC Dam

5.4.5 Analysis and Results

Koyna dam has been analysed for both cases of including and exluding dam body-reservoir interactions. For the purpose of this example, a dam–foundation interaction is neglected by assuming that the foundation is rigid. The results obtained for each conditions are as follows;

- **Nonlinear seismic analysis of the Koyna dam without hydrodynamic interactions**

The results of crack zones in the case when not considering the reservoir hydrodynamic interaction are shown in Figure 5.35. Two major cracks develop during the earthquake, one at the base of the dam and the other at the downstream change of

slope. The orientation of cracks in this study closely matches the cracks trend reported by previous researchers (Figures 5.36 and 5.37) due to tensile damage at time of 10 seconds (Huang, 2011 ; Mansouri *et al*. 2011). Therefore, comparison of the results of the present analysis and aforesaid consequences indicate that the analysis of present study is capable of providing the crack response of the concrete gravity dam under ground motion excitation. The obtained results of the Koyna dam analysis without the reservoir interaction on the dam, pictures cracks in the heel regions of the dam and in the slope variations.

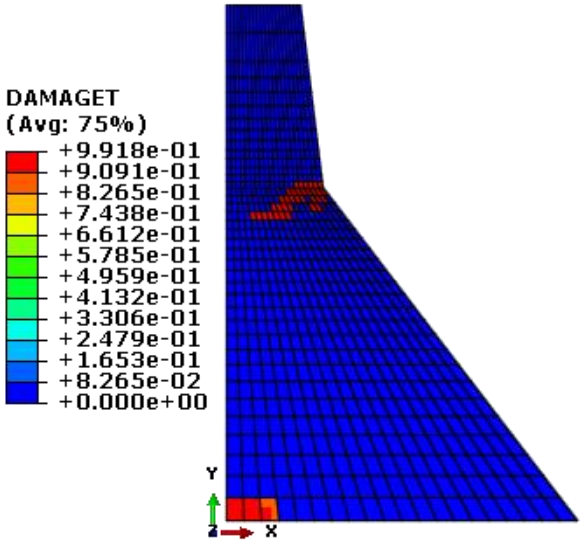

Figure 5.35 Crack Zones on the Koyna Dam with Medium Mesh in Present Study at 10 Sec

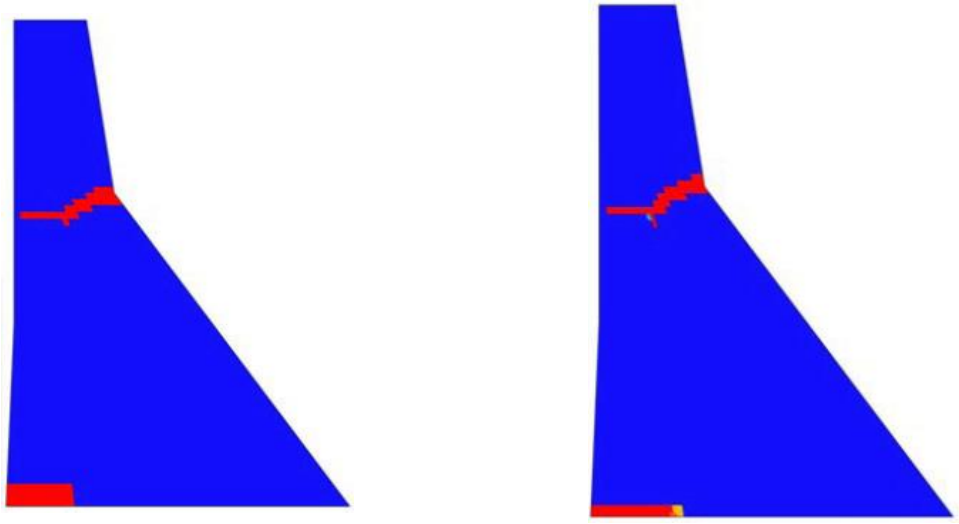

(a) medium mesh **(b) dense mesh**

Figure 5.36 Crack Zones on the Koyna Dam (Huang, 2011)

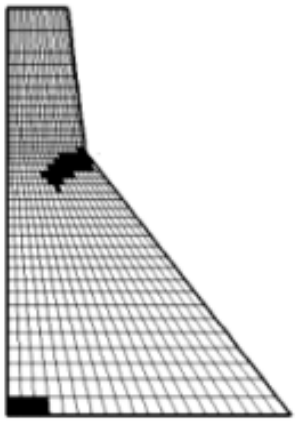

Figure 5.37 Crack Zones on the Koyna Dam (Mansouri et al., 2011)

- **Nonlinear seismic analysis of the Koyna dam with hydrodynamic interactions**

(a) Tensile Damage and Cracks

The results of crack zones and damage evolution in the Koyna concrete gravity dam of the present study during the earthquake excitation are illustrated in Figure 5.38 at four different times (3.5 sec, 4.0 sec, 4.5 sec and 10 sec) which are consistent with the results of previous works (Mansouri et al. 2011) during the mentioned time periods.

The concrete material remains elastic with no damage at the end of the second step, after the dam has been subjected to the gravity and hydrostatic pressure loads. Damage to the dam initiates during the seismic analysis in the third step. Times t_1 = 3.18 sec, t_2 = 3.89 sec, and t_3 = 4.32 sec correspond to the first three large excursions of the crest in the upstream and downstream directions, as shown in Figure 5.38. Time t_4 = 10 sec corresponds to the end of the earthquake where, damage has initiated at two locations: at the base of the dam on the upstream face and in the region near the stress concentration where the slope on the downstream face changes. This confirms that additional damage to the upstream wall occurs when the hydrodynamic interactions are taken into account.

Furthermore, in the case of body deformation of the dam when the reservoir is considerable, the dam displays different patterns of the body shape. It is clear that, the impulsive pressures of the earthquake excitation are the main points in relating to the body deformations of the dam.

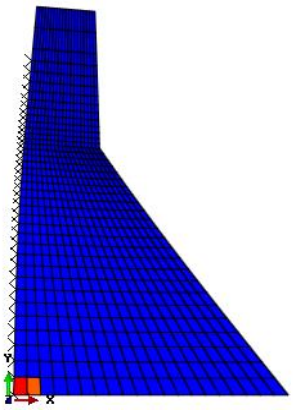

(a) Time step (t_1) = 3.18 sec

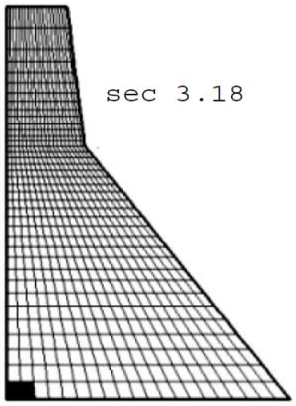

(b) Mansouri et al. 2011

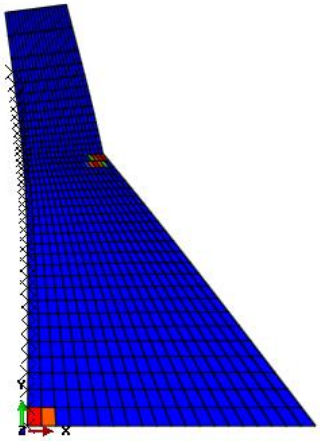

(c) Time step (t_2) = 3.89 sec

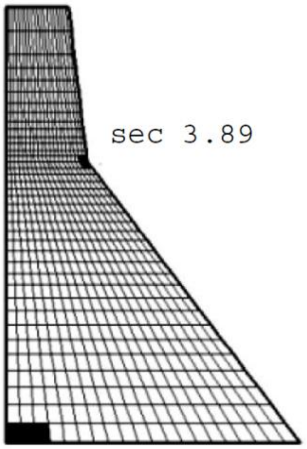

(d) Mansouri et al. 2011

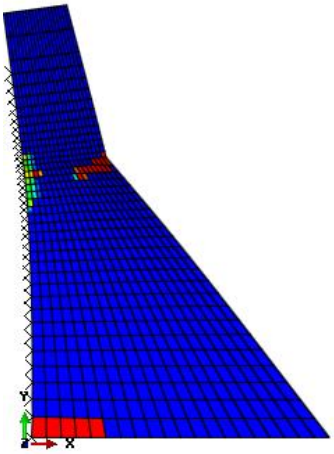

(e) Time step (t_3) = 4.32 sec

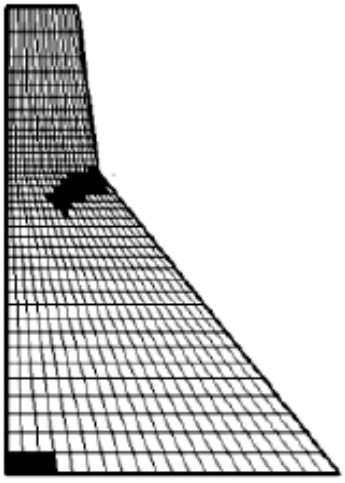

(f) Mansouri et al. 2011

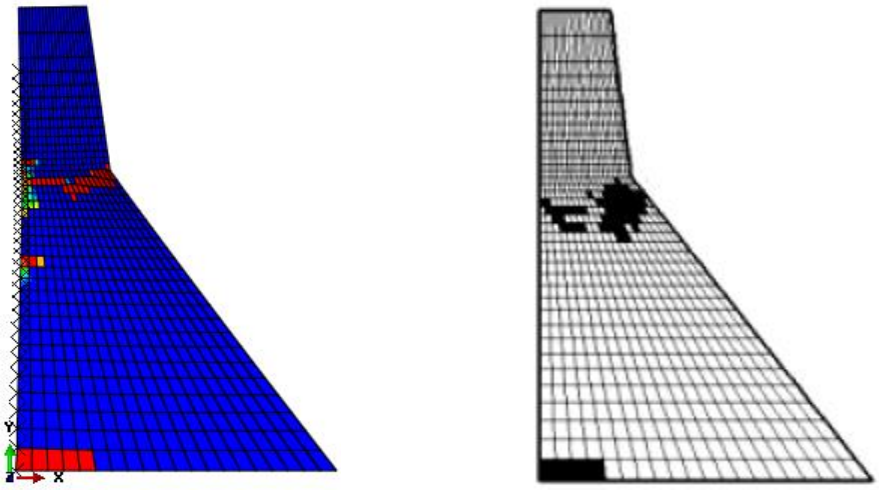

(g) Time step (t_4) = 10 sec **(h) Mansouri et al. 2011**

Figure 5.38 Selected Times to indicate the Crack Patterns of the Dam Due to Tensile Damage in the Present Study and (Mansouri et al. 2011)

(b) Displacement

In investigation of the dam-reservoir interaction, the variation of displacement is observed in this section. These displacements are considered at the upstream face in the topmost and lowest nodes as illustrated in Figure 5.39.

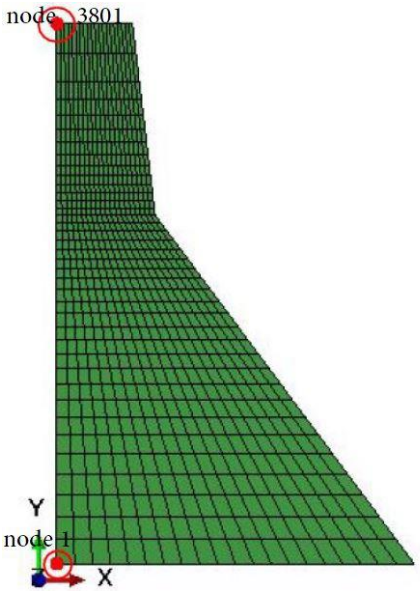

Figure 5.39 The Topmost and the Lowest Points of the Upstream

The horizontal displacement of the dam crest is indicated in Figure 5.40. These graphs represent the topmost and the lowest node of the Koyna dam (nodes 1 and 3801).

(a) Node 1

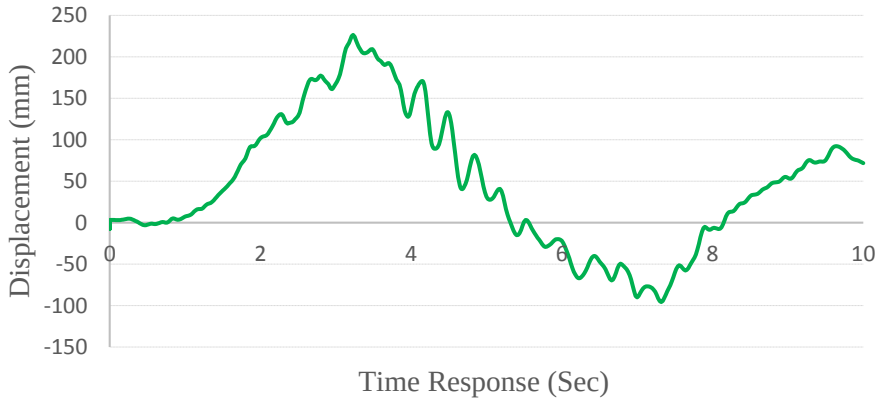

(b) Node 3801

Figure 5.40 Time History of Topmost and Lowest Points Displacements in Horizontal Direction

History of relative horizontal displacement of dam crest to the dam base is depicted in Figure 5.41. In this Figure, positive values represent displacement in the downstream direction. The crest displacement remains less than 30 mm during the first 4 seconds of the earthquake. After 4 seconds, the amplitude of the oscillations of the crest increases substantially. The present result is compared to the finite element modelling software ABAQUS user manual results (version 6.10) as previewed in Figure 5.41 (b) where the similarity of the horizontal crest displacement is quite clear in the present study and the scaled model.

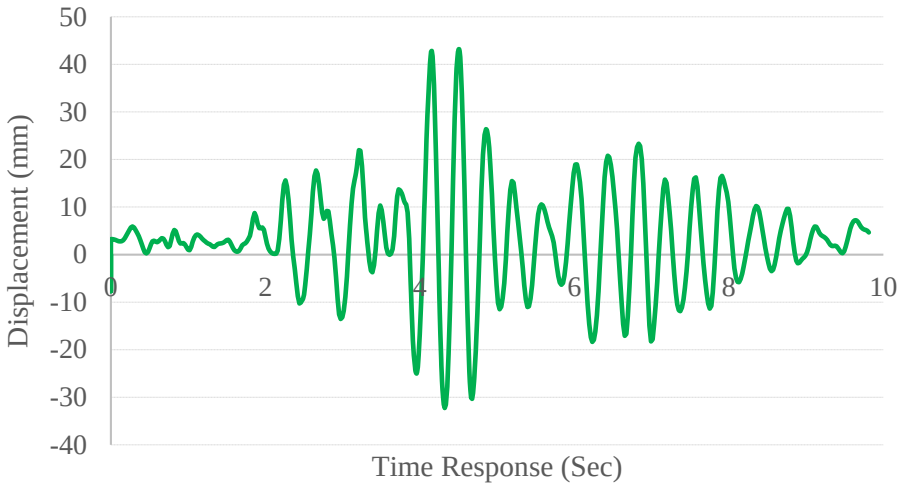

(a) Horizontal Crest Displacement in Nonlinear Analysis of the Koyna Dam in the Present Study ABAQUS (relative to ground displacement)

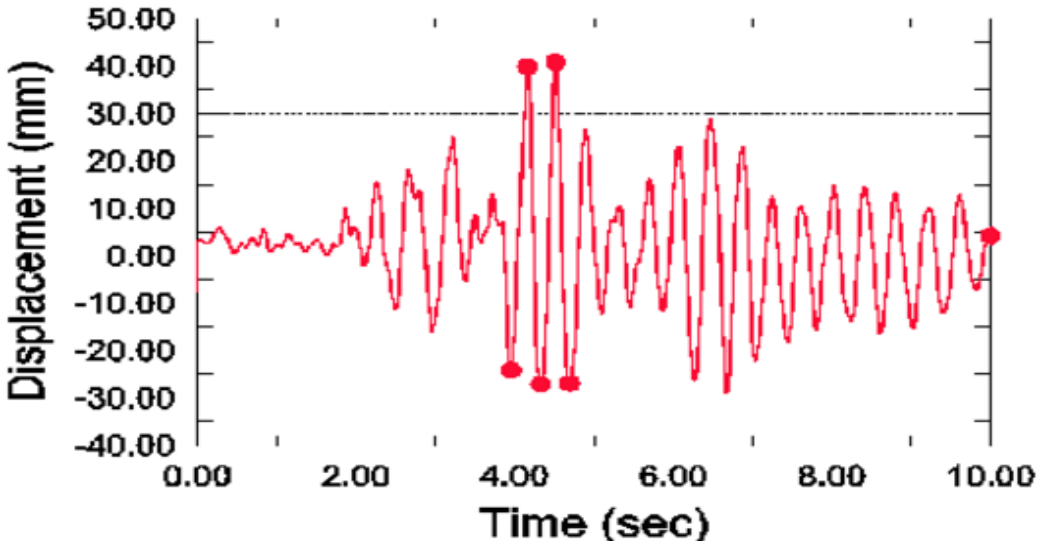

(b) Horizontal Crest Displacement In Nonlinear Analysis Of The Koyna Dam (ABAQUSE User Manual Version 6.10)

Figure 5.41 Verification of the Horizontal Crest Displacement in Nonlinear Seismic Analysis Considering Reservoir Interaction

5.5 Concluding Remarks

In this chapter, the developed finite element code has been verified based on previous experimental and analytical studies and the predicted results were consistent with the reported ones.

At first, the coupling effect of seepage and stress fields of RCC gravity dams was validated based on some numerical examples reported in literature. Then, based on the previous experimental studies, the developed codes were verified against the monitored temperatures measured by insulating thermocouples in two full scale RCC dams for thermal analysis. The modified finite element programs were also used to solve some numerical examples reported in literature.

Finally, in order to verify the seismic analysis of gravity dams via the developed code, a full scale dam reported in the literature has been selected and analysed. Both conditions of including and excluding the dam body-reservoir hydrodynamic interactions were taken into account in the analysis.

Results of the study, in terms of the seepage pattern and the effects of seepage on the mechanical properties of the RCC dam, have been illustrated in order to asses the capability of the developed code for coupled seepage - stress analysis. It was clear from the plots that, the numerical solution agreed reasonably well with the analytical solution.

In addition, in the case of thermal - stress analysis, the predicted temperatures obtained from the developed finite element code were found to be in good agreement with measured ones by thermocouples on site. Furthermore, according to available analytical results, the predicted results were consistent with the reported ones.

Finally, the overall results of the seismic analysis of Koyna dam by considering the dam-reservoir interaction highlight three significant weak points, namely, the dam heels, variable zones of slope of the neck and some regions in the upper section. The obtained results in the Koyna dam analysis, excluding the reservoir interaction on the dam, reveals cracks in the heel regions of the dam and in the slope variation region.

Consequently, horizontal relative displacement results are the most important output of the dynamic analysis to predict the stability of the dam under seismic excitations. On the other hand, prediction of the crack propagation in dams under ground motions is the other important aspect of the analysis related to the seismic behaviour of dams. As a result, the present study demonstrated the accurate prediction of cracking patterns and relevant displacements of the Koyna gravity dam under Koyna ground motions. And, the results of comparison of the results of this study with previous results presented by other researchers has shown that this study is capable of calculating and predicting the crack regions, its pattern and displacement of the nodes. Thus, it is important to pay especial attention to the hydrodynamic pressure on the concrete gravity dam.

CHAPTER 6

SEEPAGE- STRESS ANALYSIS OF RCC GRAVITY DAMS

6.1 Introduction

The seepage problem of roller compacted concrete (RCC) dams is more complex because of its construction features, involving compaction in its construction process in a series of layers. Considering the complex mechanical properties of the materials, these internal interfaces are responsible for weak links against seepage in a dam. After completion of reservoir storage, the distribution of dam seepage field will affect the stress field. At the same time, the change in the dam stress field will react on the dam's pores and cracks, reflecting the significance of seepage. Clearly, an interaction exists between seepage and stress fields. Therefore, it is of great importance and interest to evaluate the safety of gravity dams under the coupled seepage-stress interaction where the behaviour is controlled by the mechanical and hydraulic properties of concrete materials and rock foundation.

In this chapter, the interaction between seepage and stress fields of RCC dam is analysed based on coupled and uncoupled models. Numerical solution of coupled and uncoupled seepage and stress fields of Kinta RCC gravity dam (located in Malaysia) is analysed by means of finite element method in this study. The seepage, stress and displacement fields of the dam were analysed in order to highlight the coupling effect.

Recognizing the importance of the coupled hydro-mechanical effects on the performance of civil engineering structures involving fractured rocks, in this study, the stress-flow coupling mechanism of the dam-foundation system of Kinta RCC dam was simulated using ABAQUS Finite Element code, supported by elasto-plastic constitutive material models. Then, results of the coupling analysis are compared with uncoupled solution to demonstrate the time-dependent material behaviour of the dam concrete and the foundation rock.

In addition, in order to demonstrate the capability of the developed system, in this chapter a two dimensional finite element model is used to perform the coupled seepage-stress analysis of the actual evolutionary construction process and operation phase based on developed Seepage properties of roller compacted concrete using USDFLD subroutine. The permeability of a roller compacted concrete, which involves ageing, temperature and confining pressure effects, is proposed for the coupled analysis. Initially, the coupled analysis is performed for each time step and increment, then, the confining pressure is determined. After that, based on updated confining pressures and other variables, permeability is calculated.

Finally, the results of coupled flow-stress analysis for both cases of with and without modified seepage properties (using USDFLD subroutine) performed on a numerical model of the Kinta RCC Dam for the non-overflow section are presented. Transient construction process and impounding are taken into account in the analysis.

6.2 Coupled and Uncoupled Seepage-Stress Analysis of Kinta RCC Dam

The numerical analyses were carried out using ABAQUS finite element computer code on a plane strain idealization of the highest cross section of the Kinta RCC dam for the purpose of comparing the coupled and uncoupled flow-stress problems. The seepage pattern and the effect of seepage on the mechanical properties of dam body and rock mass below the dam have been investigated.

6.2.1 Problem Description

Kinta RCC dam is the first RCC gravity dam in Malaysia. The maximum height of the dam is 81.8 m. The construction of the dam started in September 2004 and completed in April 2006. The detailed technical information of Kinta RCC dam including geometrical section and schedule of construction are presented in Section 5.3.1.

In the actual construction of Kinta dam, the RCC layers are laid down with a grade of 1:30 from downstream towards the upstream and are 30 cm thick (Noorzaei et. al, 2006). However, in order to reduce the computational time, each lift is assumed to have a horizontal width of 3.0 m (Saetta et al., 1995). A finite element algorithm and the birth and death technique is used in this analysis to simulate the processes of

construction of the RCC dam (Ishikawa 1991, Jaafar 2007). To study the structural response of the Kinta RCC dam, non-overflow section of the dam, as shown in Figure 6.1, has been selected along the length of the dam.

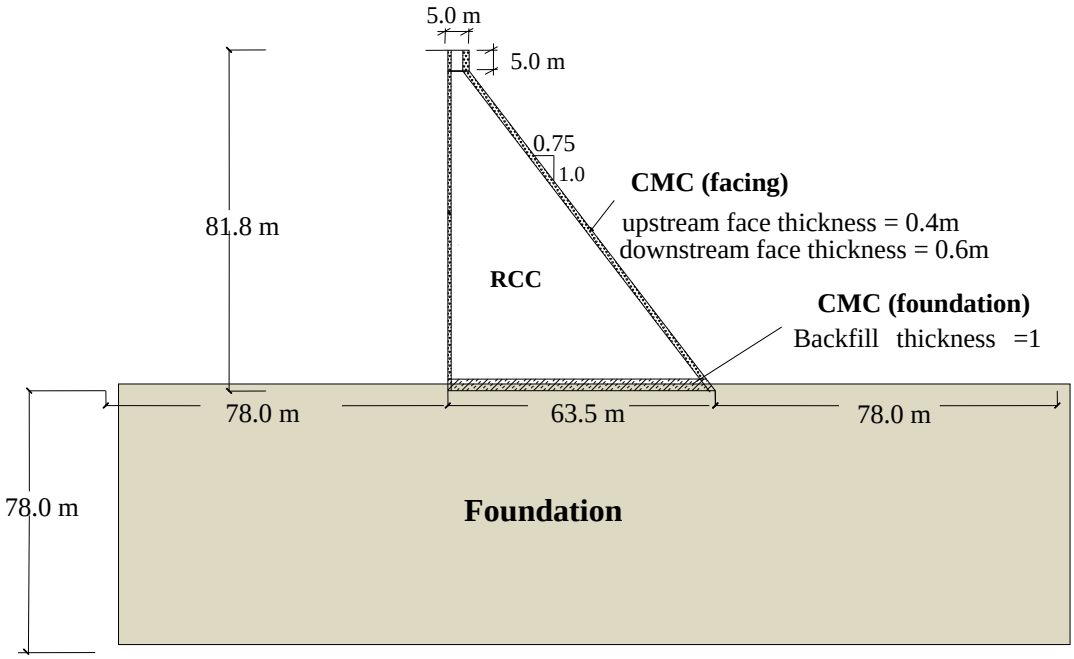

Figure 6.1 Non- overflow Standard Section of Kinta RCC Dam

The dam is modelled as a two-dimensional transient flow model using a birth and death procedure to simulate the real construction process of the dam according to the actual planned construction schedule (SUNGAI Kinta RCC dam 2002). A finite element mesh model of the Non- overflow section of the dam is shown in Figure 6.2. The mesh of the dam body is generated in such a way to simulate the construction process according to the placement schedule and thickness of the RCC layers. The dam is divided into 28 lifts; each lift has a thickness of 3 m. An 8-noded plane strain reduced integration element (CPE8P) is used for the purpose of discretization of dam body and foundation. Table 6.1 presents the material parameters used in the numerical analysis (SUNGAI Kinta dam RCC, 2002).

6.2.2 Loading Conditions

The governing equations and constitutive relations of fluid flow are coupled to stress-strain relations. With the appropriate boundary and initial conditions, these

equations are implemented as partial differential equations into customizable finite element software package ABAQUS.

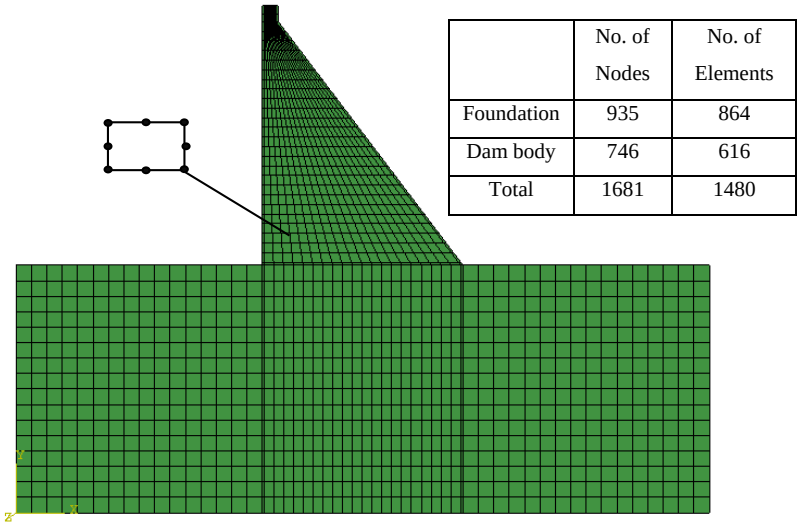

	No. of Nodes	No. of Elements
Foundation	935	864
Dam body	746	616
Total	1681	1480

Figure 6.2 Finite Element Mesh Model of the Kinta RCC Dam

Table 6.1 Seepage and Structural Properties of Kinta RCC dam (SUNGAI Kinta dam RCC, 2002)

	Density (kg/ m^3)	Elastic Modulus (MPa)	Poisson's ratio
Dam Body (RCC)	2325	18,200	0.2
Dam Body (CMC)	2325	25,700	0.2
Foundation	2650	24,000	0.2

Two types of loads have been considered for the stress analysis, namely, self-weight of the dam and the gravity load of rock foundation where, the construction loading was simulated by the stages involved in the dam construction. For coupled stress flow analysis, additional load comprises hydrostatic pressure on the upstream face of the dam under full reservoir condition.

6.2.3 Boundary Conditions

When coupling analysis is performed, two types of boundary conditions need to be specified: displacement boundary conditions and hydraulic boundary conditions. The seepage boundary condition for coupling computation is the same as single seepage field computation. Boundary conditions of the present study are defined as follows:

i. Stress analysis – A restrained condition has been imposed on the horizontal

bottom boundary, where no movement was allowed along the bottom of the layer, while nodes of the side boundaries have been restrained in the lateral direction and only vertical movement is allowed as shown in Figure 6.3.

ii. Seepage analysis – It involves two types of boundary conditions:

(a) Dirichlet boundary condition (water pressure/water head): A total head of 76.8 m has been applied on the upstream side of the dam body, while zero head has been applied on the downstream side as depicted in Figure 6.3. Moreover, a linear hydraulic head distribution was applied along the phreatic surface boundary.

(b) Neumann boundary condition (water flux): No flow has been permitted from the lower boundary and through the dam body.

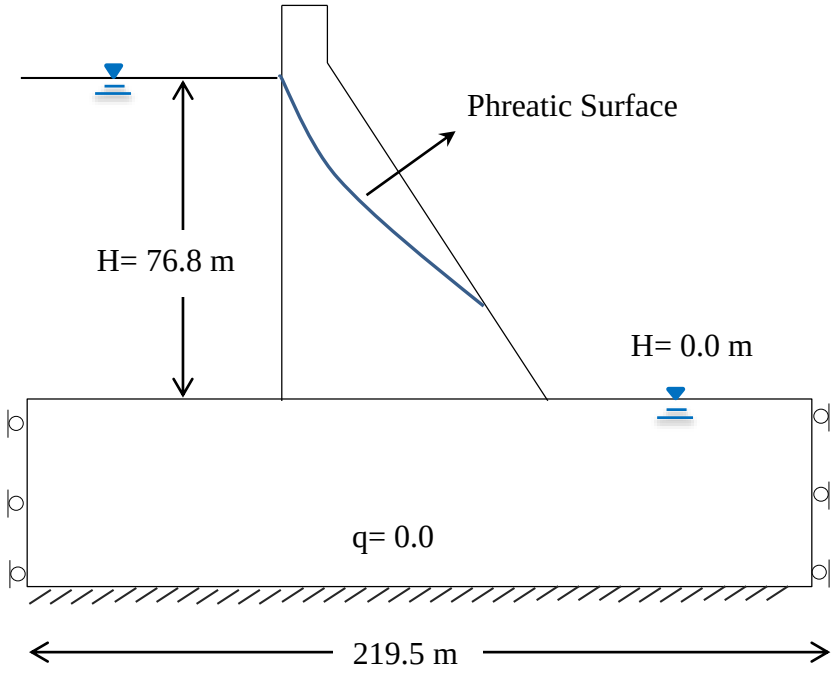

Figure 6.3 Illustation of the Boundary Conditions

6.2.4 Two– Dimensional Analysis Results and Comparison between Coupled and Uncoupled Solutions

Coupled seepage and stress fields are analysed by using the above data and FEM solution, which are also compared with the seepage and stress fields without the

consideration of coupled analysis. Results in terms of pore pressure, stress and displacement distribution contours for both types of analysis are displayed and compared to each other.

- **Stress Distribution**

From the two-dimensional analysis, plots of stress contour distribution of the Kinta RCC dam for the non-over flow section are presented in Figure 6.4 to Figure 6.6. The stress variations along the x and y axes and also in x-y plane (shear stress) for the dam body only and also including rock foundation below it are shown in these Figures. The results are then compared for both coupled and uncoupled solutions along the width of the dam body.

It is clear from the plots that the distribution pattern of different stresses is approximately the same for both cases of coupled and uncoupled situations; however, the values are different. The coupling effect causes the tensile stress along the x axis at upstream of the dam body to increase with the maximum increase of approximately 20%, and makes the stress concentration of σ_x near the dam heel more obvious as shown in Figure 6.4-a to Figure 6.4-c. This is mainly because of the drag force parallel with the layer and the hydrostatic seepage pressure vertical to the layer. Moreover, the Compressive stresses remain nearly unchanged for both coupled and uncoupled solutions.

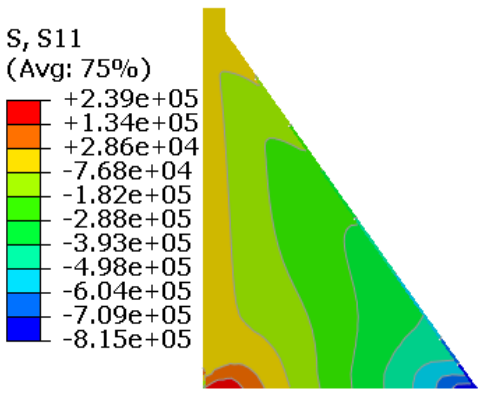

(a) Contour of Stress Distribution for Coupled Solution (Pa)

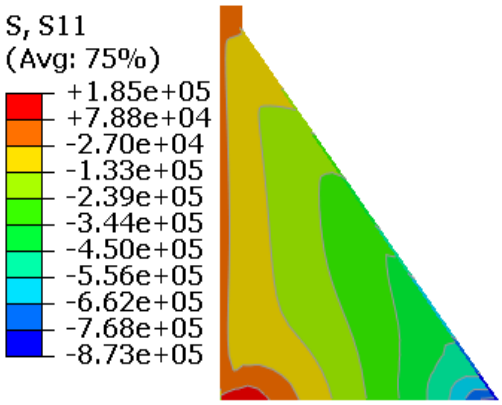

(b) Contour of Stress Distribution for Uncoupled Solution (Pa)

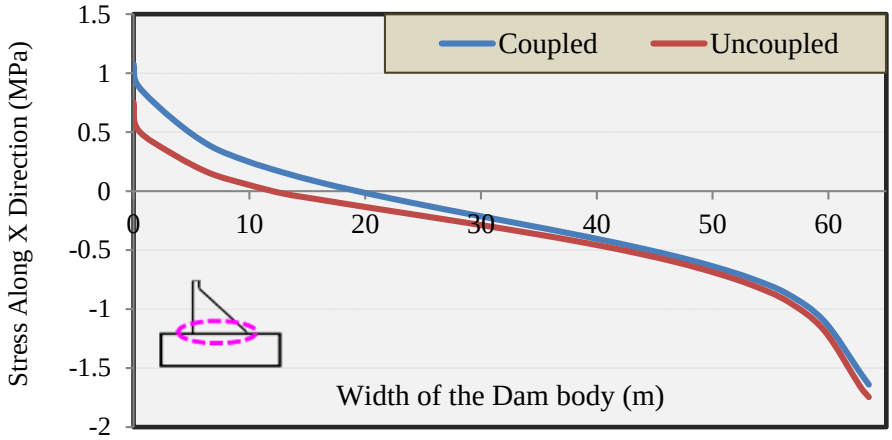

(c) Comparison of Stress Distribution between Coupled and Uncoupled Solution (MPa)

Figure 6.4 Stress Distribution along x Axis

Figure 6.5 shows the distribution of the stress field in y direction (vertical stress) obtained for both uncoupled and coupled seepage-stress analysis. It is clear from the plots that, the interaction between seepage and stress makes the tensile stress along y-axis at upstream side of the dam body to increase by 17%. The stress concentration of σ_y is more obvious near the dam heel resulting from the hydrostatic seepage pressure acting on the layers vertically.

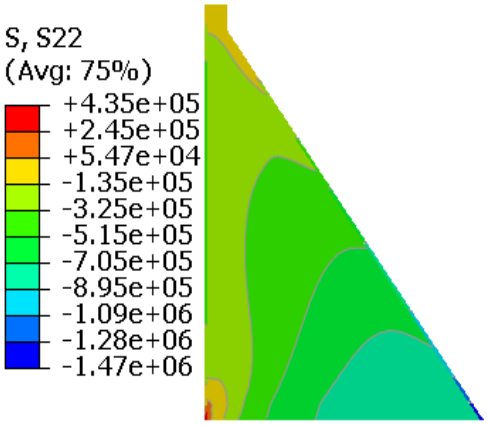

(a) Contour of Stress Distribution for Coupled Solution (Pa)

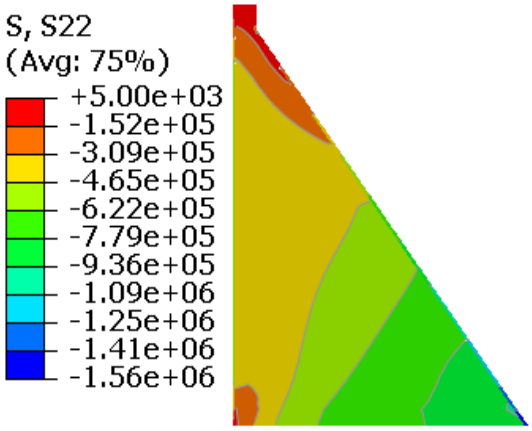

(b) Contour of Stress Distribution for Uncoupled Solution (Pa)

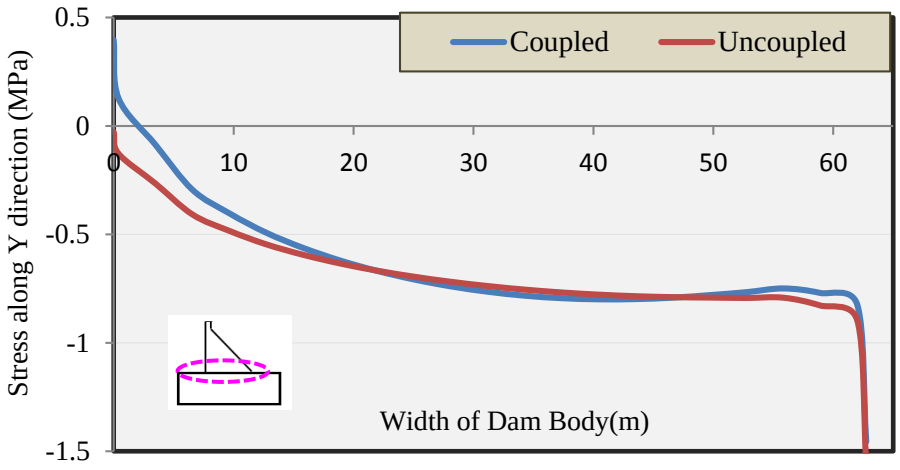

(c) Comparison of Stress Distribution between

Figure 6.5 Stress Distribution of Dam Body along *y* Axis

Another conclusion drawn from the comparison of the two types of analysis is that of the maximum stress distribution contours of the dam as depicted in Figure 6.6. According to this Figure, the maximum principal stresses are mainly tensile in the vicinity of upstream face, especially near the dam heel. Moreover, higher compressive stresses are obtained on the downstream side near the toe when coupling effect is considered.

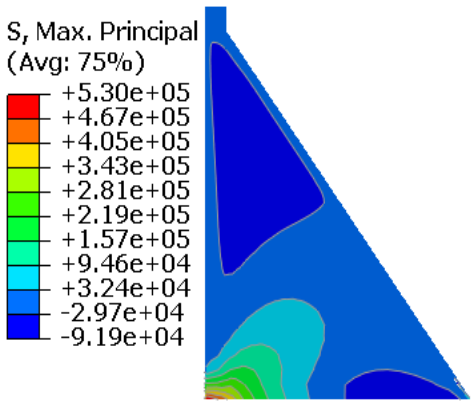

(a) Distribution of Max. Principal Stress for Coupled Analysis (Pa)

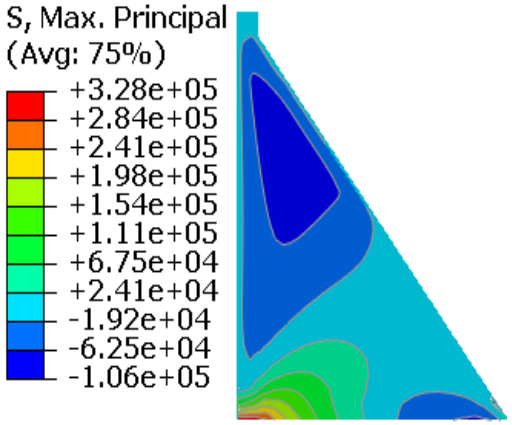

(b) Distribution of Max. Principal Stresses for Uncoupled Analysis (Pa)

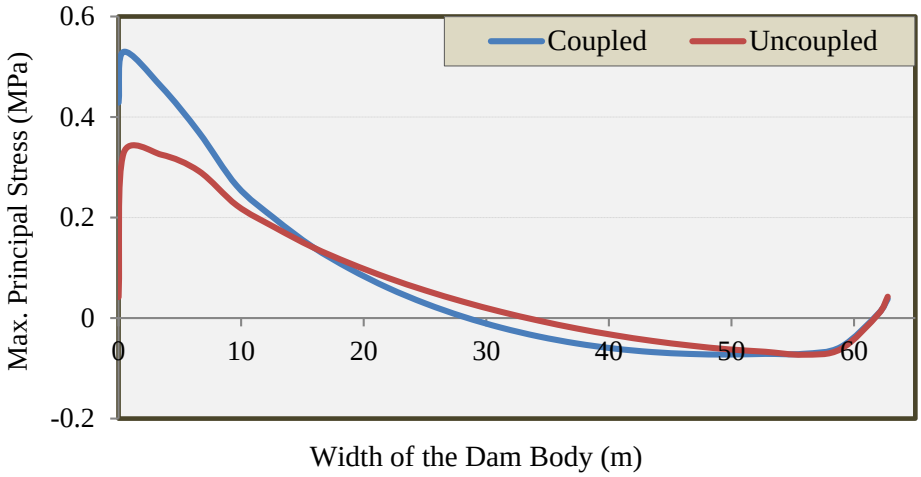

(c) Max. Principal Stress Distribution Comparison for Coupled and Uncoupled Analysis (MPa)

Figure 6.6 Maximum Stress Variation

The fact that maximum tensile and compressive stresses are increased due to seepage effects can be explained by considering seepage flows within the RCC lifts and water pressures applied on the upstream face of the dam. It is quite apparent that body forces induced by seepage flows and water pressures applied on the RCC layers at upstream side result in bending. These moments translate into tensile stresses on the upstream face and compressive stresses on the downstream face in those regions.

- **Pore Pressure Distribution**

In addition, an attempt has been made to show the pore pressure variation plots of the RCC dam for the seepage-stress analysis as shown in Figure 6.7. An increase in the pore water pressures of coupled analysis may be the effect of stress variation; however, due to the low permeability of the RCC material, seepage pressures within the structure do not show significant differences for both coupled and uncoupled results. The distribution of pore water pressures and the location of the phreatic surface for both cases are depicted in Figure 6.7.

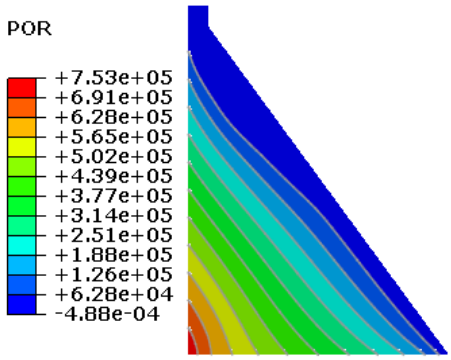

(a) Pore Pressure Distribution for Coupled Solution (Pa)

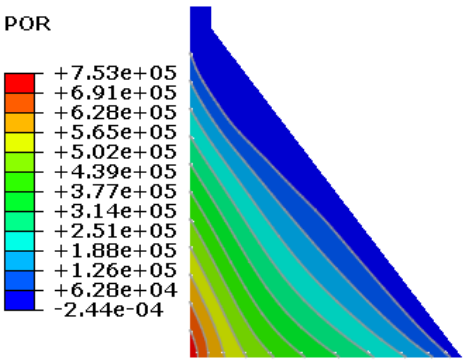

(b) Pore Pressure Distribution for Uncoupled Solution (Pa)

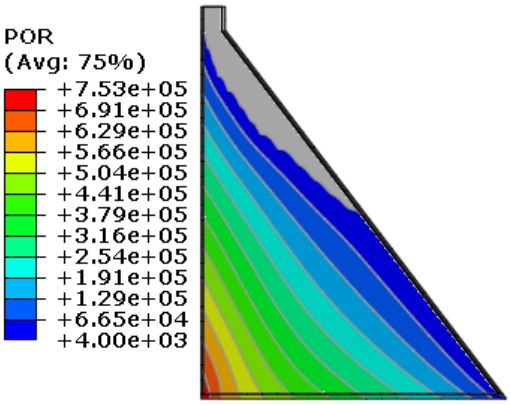

(c)Phreatic Surface Location

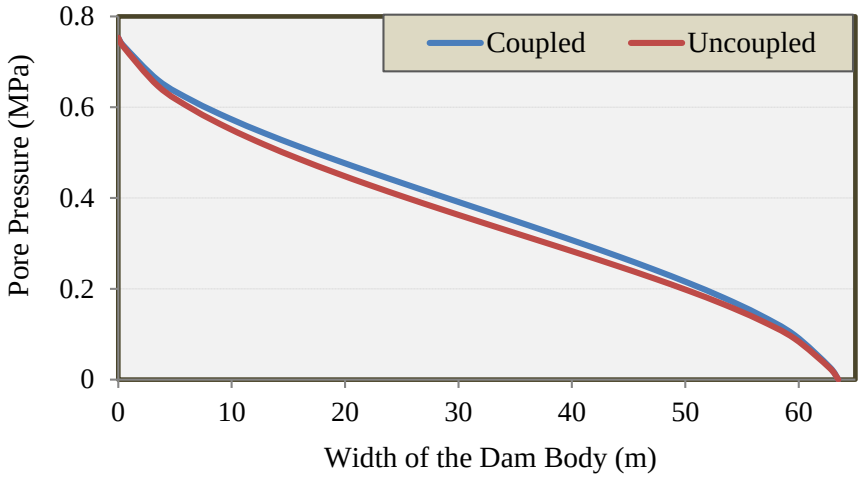

(d) Comparison of Pore Pressure Distribution for Coupled and Uncoupled Solutions (MPa)

Figure 6.7 Contours of Pore Water Pressure Distribution

- **Displacement Variation**

Figure 6.8 illustrates the total deformation of Kinta RCC dam. It is clear from the plots that, the displacement of the dam increases with the height for both coupled and uncoupled solutions. However, the coupling between seepage and stress increases the settlement of the dam significantly in contrast to uncoupled analysis that grows gradually as shown in Fig 6.8.c.

The maximum displacement occurs in the dam crest with a value of 8.52 mm for uncoupled condition (i.e. excluding seepage effects). Whereas, including the effects of seepage increases the maximum value of deformation even further to 16.5 mm which is approximately double.

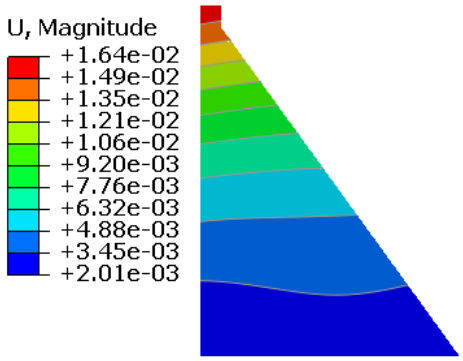

(a) Displacement Distribution for Coupled Solution (m)

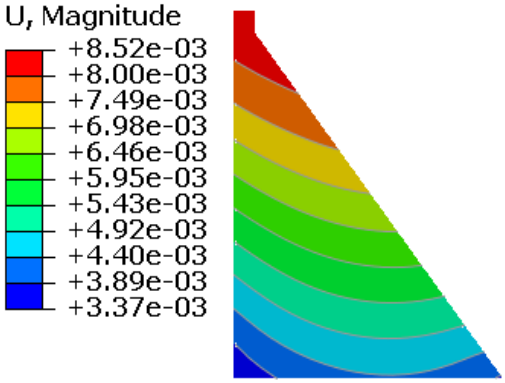

(b) Displacement Distribution for Uncoupled Solution (m)

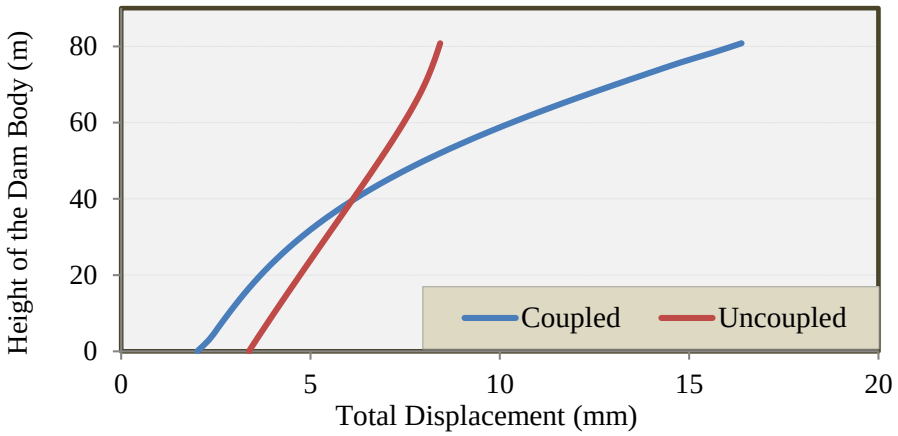

(c) Comparison of Displacement Distribution for Coupled and

Figure 6.8 Contours of Total Displacement Variations (mm)

6.3 Coupled Seepage - Stress Analysis via Developed Seepage Properties of Roller Compacted Concrete

In this section, results from the coupled flow-stress analysis for both cases of with and without modified seepage properties (using USDFLD subroutine) performed on a numerical model of the Kinta RCC Dam for the non-overflow section are presented. Transient construction process and impounding are taken into account in the analysis.

Based on the mathematical formulation described in Section 3.2.6, permeability of a roller compacted concrete, which involves ageing, temperature and confining pressure effects, is proposed for the coupled analysis. Initially the coupled analysis is performed for each time step and increment, then, the confining pressure is determined. Finally, based on updated confining pressures and other variables, permeability is calculated.

The main initial conditions such as void ratio, pore pressures and initial stresses considered in the coupled analysis are based on the discussion in Section 4.3. The seepage boundary conditions are also determined mainly according to the project design, where in this study, due to the lack of complete information, are calculated based on Section 3.2.5 in Chapter 3. Finally, the seepage pattern and the effect of seepage on the mechanical properties of dam body and rock mass below the dam have been investigated as follows;

- **Pore Pressure Distribution**

The plots of pore pressure distribution and also a calculated phreatic surface location for the whole structure and the dam body only are shown in Figure 6.9. A comparison of pore pressure values along the width of the dam body obtained for both cases of with and without USDFLD subroutine is shown in Figure 6.10. It is obvious from this plot that, there is a difference between the two curves, and the pore pressure values using the modified code are less than those of without using it.

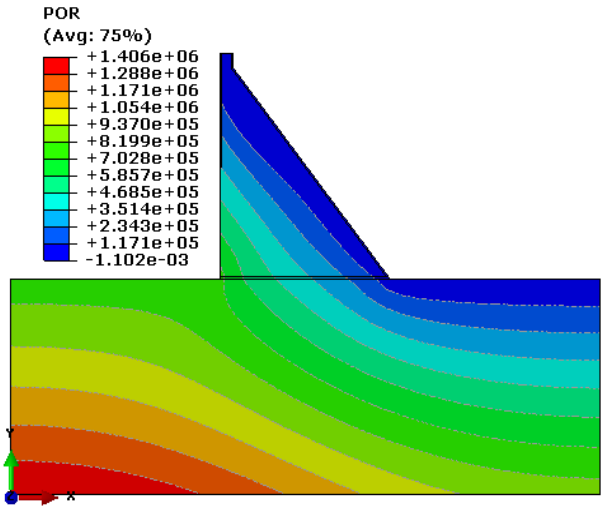

(a)Without USDFLD

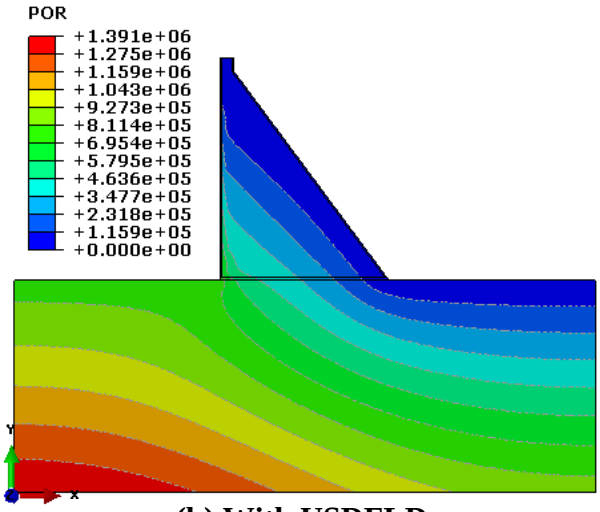

(b) With USDFLD

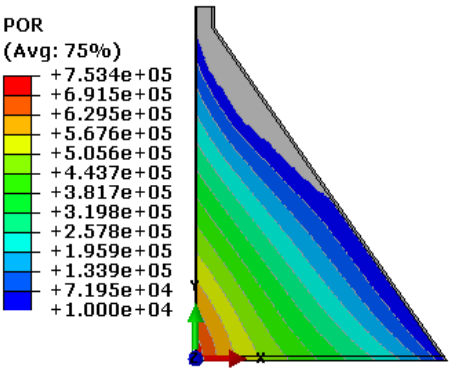

(c) Phreatic Surface (Without USDFLD)

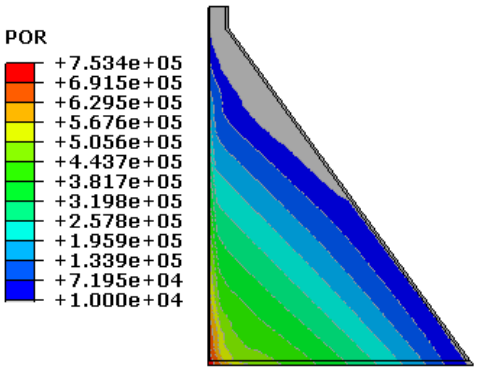

(d) Phreatic Surface (With USDFLD)

Figure 6.9 Pore Pressure Distribution (MPa) and Phreatic Surface Location in Kinta RCC Dam

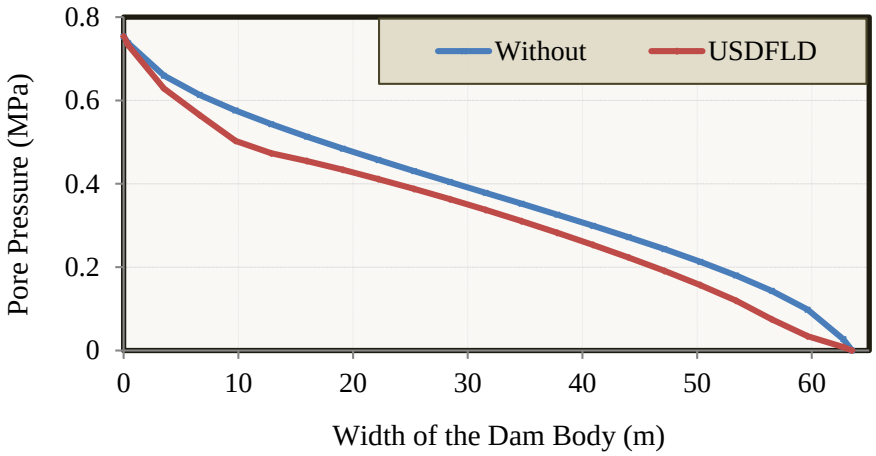

Figure 6.10 Comparison of Pore Pressure Distribution within the Dam Body (MPa)

- **Stresses Distribution**

In order to illustrate the effect of modified seepage properties on the stress development, the counters of maximum effective principal stresses and also effective shear stresses and their variations - from maximum value to minimum - have been drawn for the whole structure and dam body, respectively, as indicated in Figures 6.11- 6.13.

It is clear from the plots that, the effective stress variation using modified seepage properties are higher than those of without using them. The results completely follow the effective stress law of Terzaghi as discussed in Section 3.2 of Chapter 3; where decreasing pore pressure values makes the effective stresses to increase.

The results indicated that, the modified seepage properties make the maximum principal stresses to increase and makes the stress concentration near the dam heel more obvious, as shown in Figures 6.11 and 6.12. This is mainly a result of hydrostatic seepage pressure in upstream face of the dam.

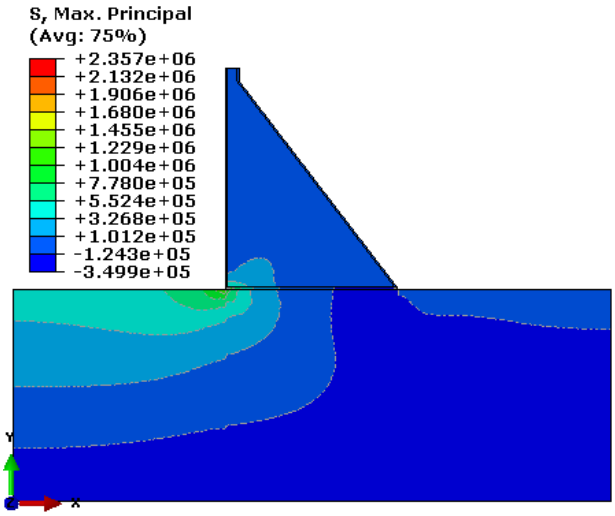

(a) Max.Principal Stress (Without USDFLD)

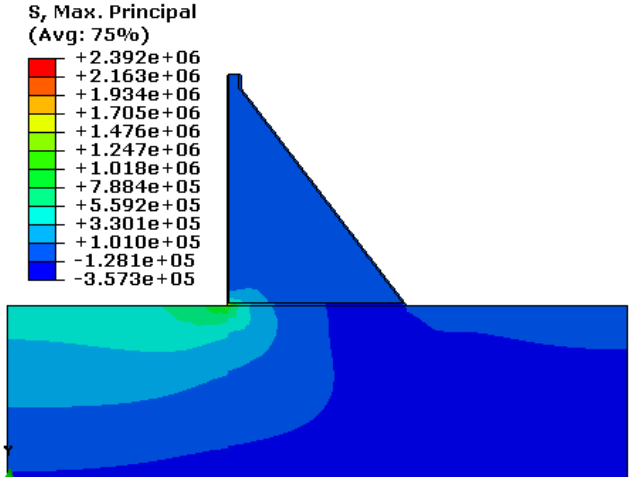

(b) Max.Principal Stress (With USDFLD)

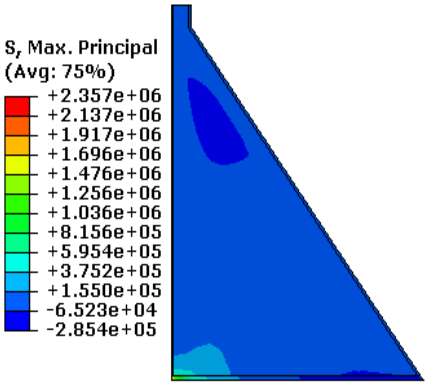

(c) Dam Body (Without USDFLD)

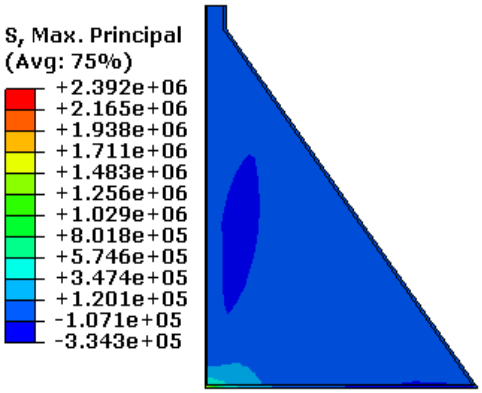

(d) Dam Body (With USDFLD)

Figure 6.11 Maximum Principal Stress Distributions (Pa)

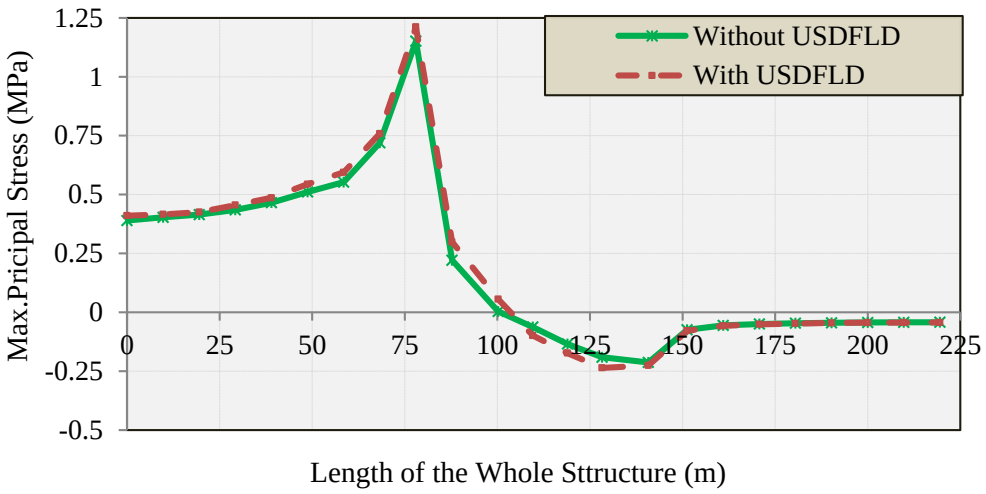

(a) Maximum Principal Stress Variation (MPa)

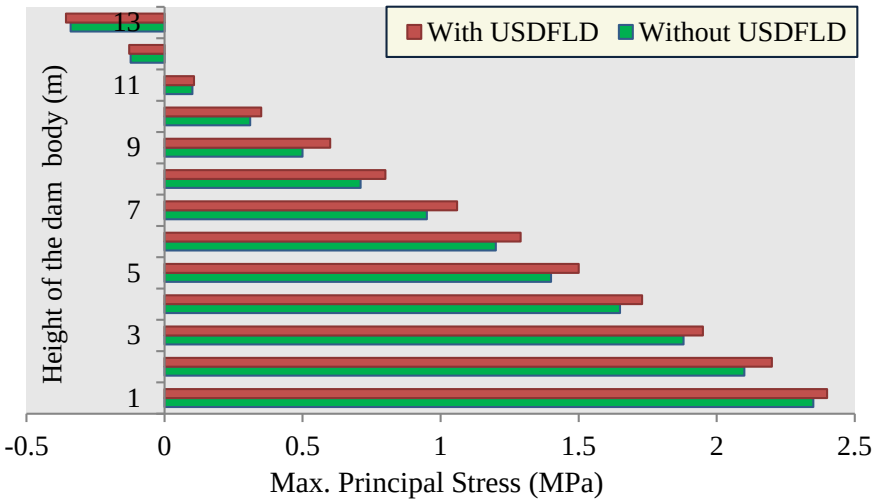

(b) Maximum Principal Stress Variation from Highest to Lowest (MPa)

Figure 6.12 Maximum Principal Stress with and without USDFLD (MPa)

The modified code also makes the shearing stresses increase at the downstream of the dam as illustrated in Figures 6.13 and 6.14. The stress concentration near the dam toe is more obvious.

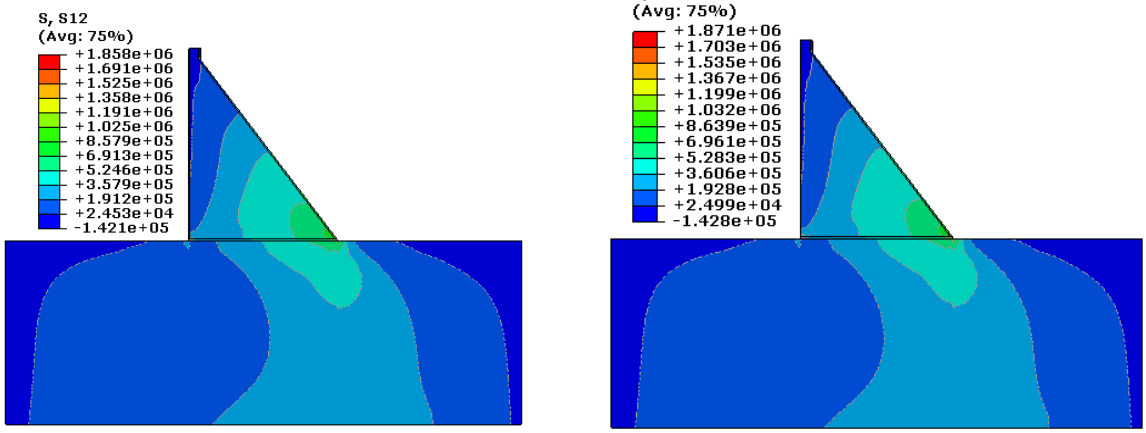

(a) Shear Stress (Without USDFLD) **(b) Shear Stress (With USDFLD)**

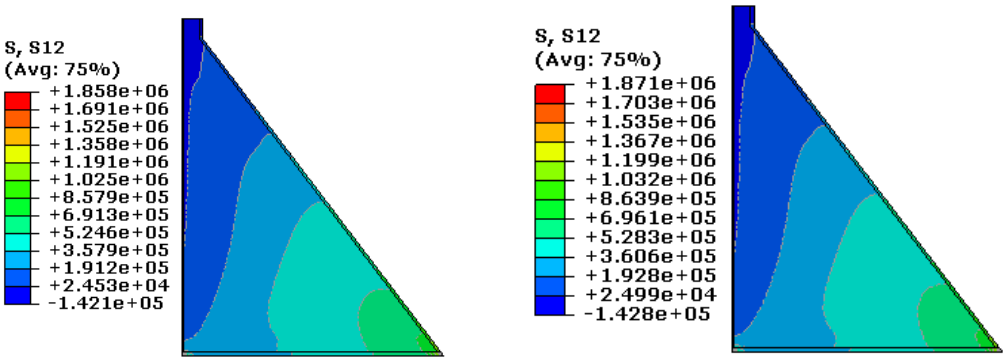

(c) Shear Stresses in Dam body (Without USDFLD) **(d) Shear Stresses in Dam body (With USDFLD)**

Figure 6.13 Shear Stress Distribution (MPa)

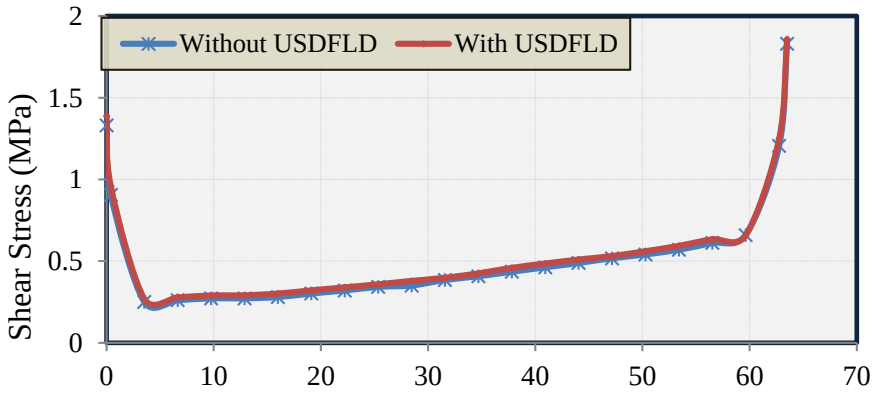

Figure 6.14 Shear Stress Variation along the Dam Body (MPa)

- **Displacement Variation**

In order to illustrate the effect of modified seepage properties, which is mainly based on confining pressure, on the displacement variation, contours of the confining pressure and displacements of the dam are shown in Figures 6.15 to 6.17.

It is evident from the plots that, the variation of confining pressures using USDFLD subroutine are more than those of without using it; where it results in decrease in displacement values based on literature (Feng 2011).

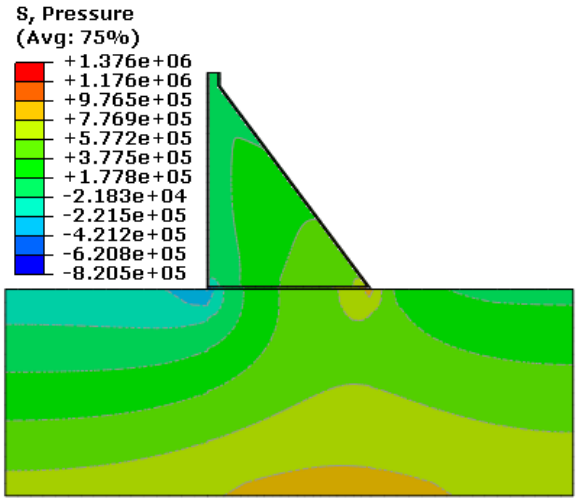

(a) Contours of Confining Pressures without USDFLD (MPa)

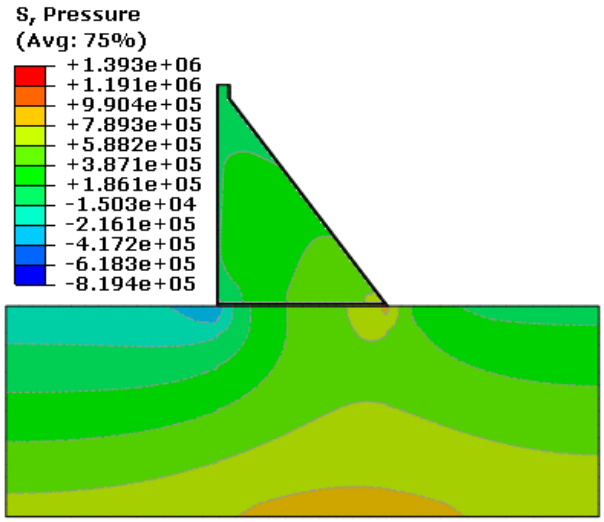

(b) Contours of Confining Pressures With USDFLD (MPa)

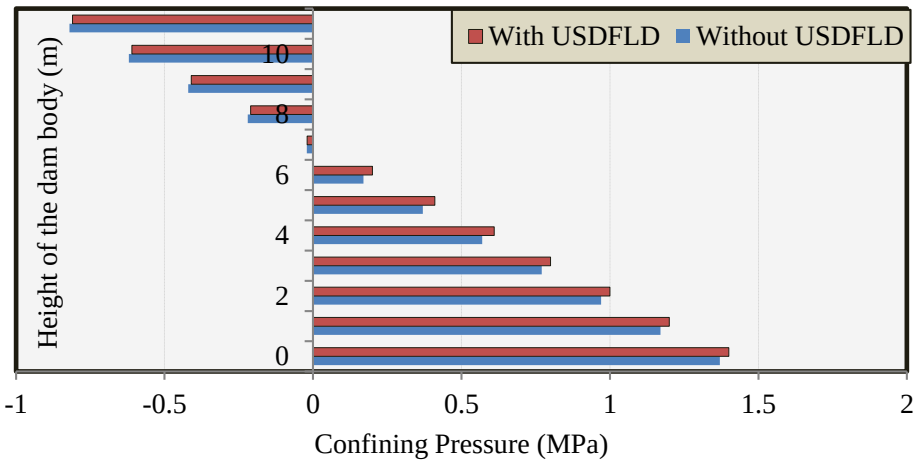

(c) Comparison of Confining Pressures (MPa)

Figure 6.15 Confining Pressures Profiles for Both conditions of with and without USDFLD (MPa)

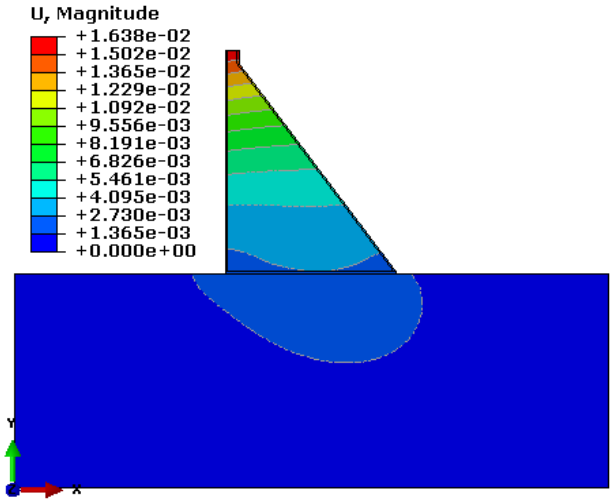

(a) Average Displacement without USDFLD (m)

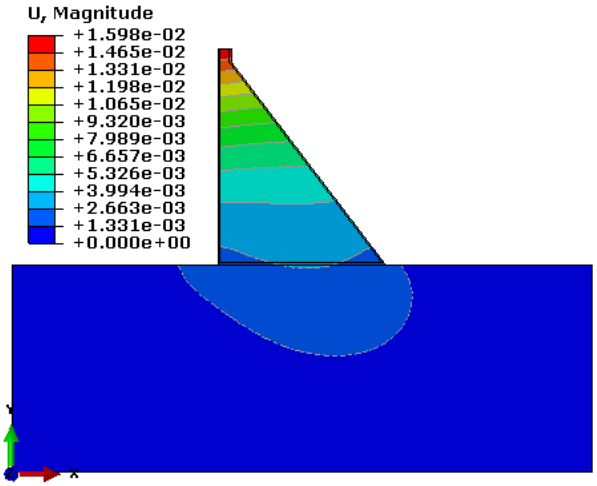

(b) Average Displacement with USDFLD (m)

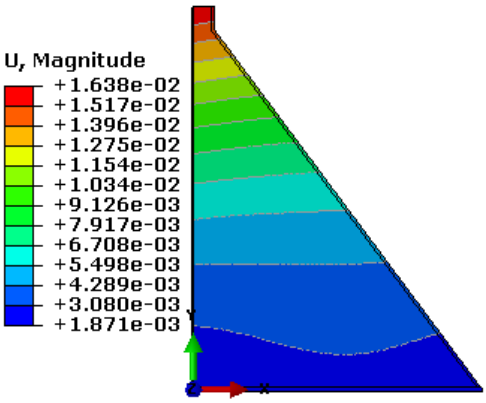

(c) Displacement in dam Body without USDFLD (m)

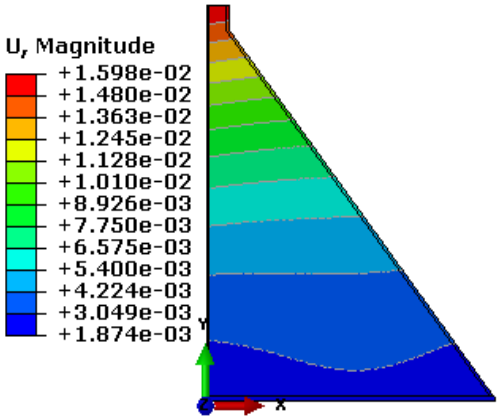

(d) Displacement in Dam Body with USDFLD (m)

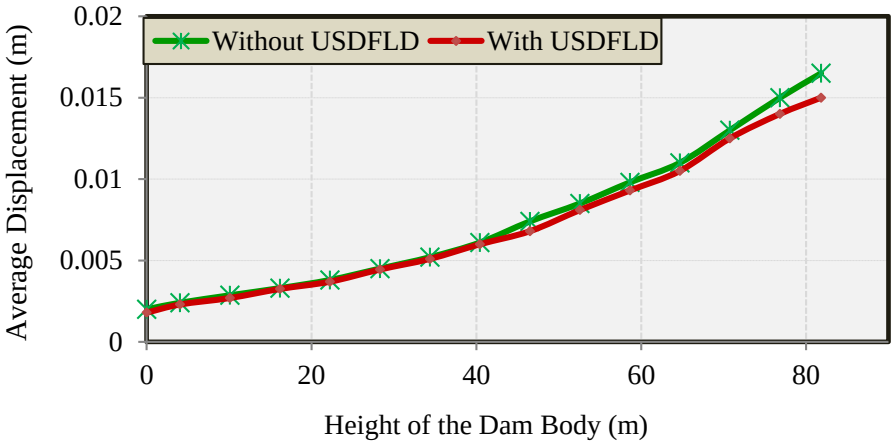

(e) Comparison of Displacement (m)

Figure 6.16 Contours of Average Displacement of the Dam with and Without USDFLD (m)

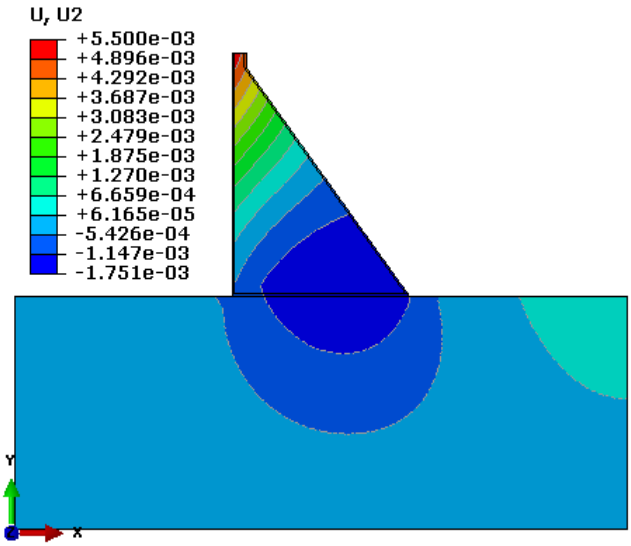

(a)Vertical Displacement without USDFLD (m)

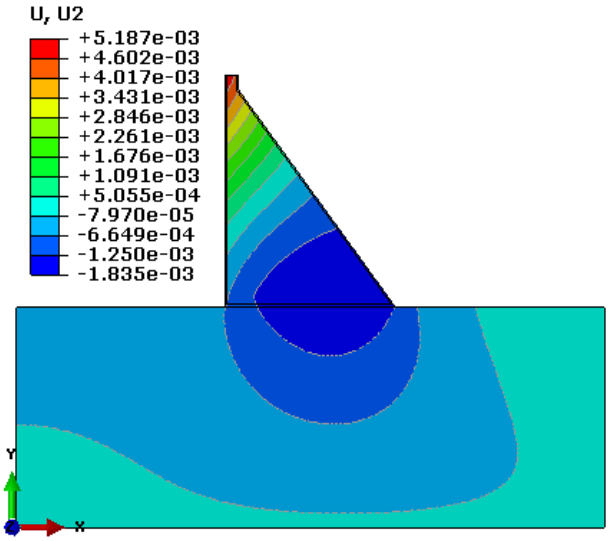

(b) Vertical Displacement with USDFLD (m)

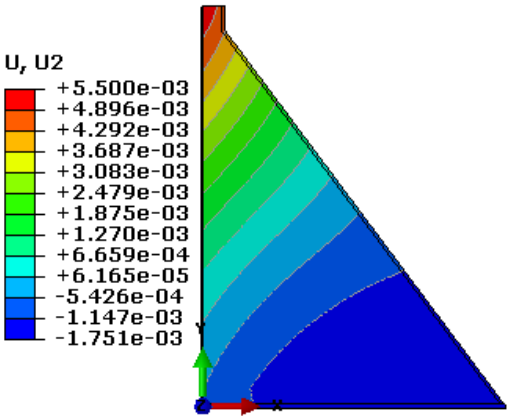

(c) Vertical Displacement in of the Dam Body without USDFLD (m)

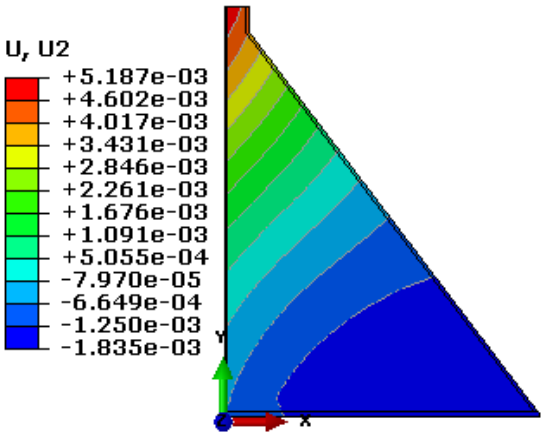

(d) Vertical Displacement of the Dam Body with USDFLD (m)

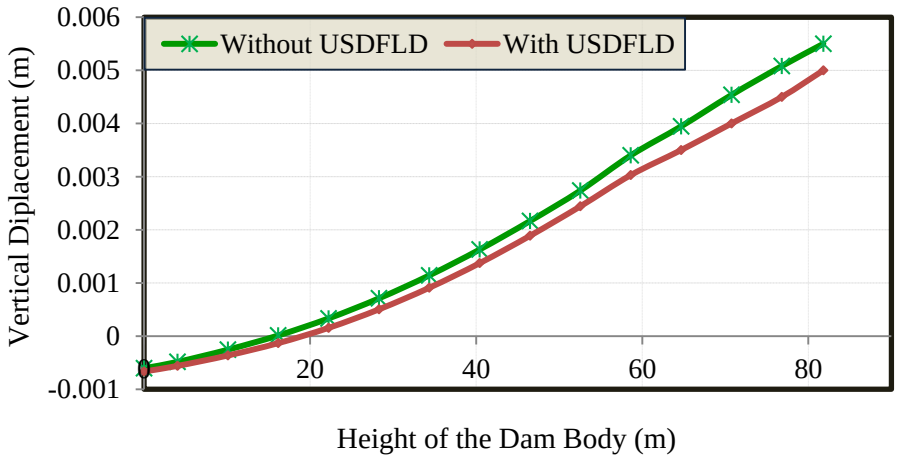

(e) Comparison of Vertical Displacements

Figure 6.17 Contours of Vertical Displacement of the Dam with and without USDFLD (m)

6.4 Discussion and Concluding Remarks

In the present Chapter, a two-dimensional finite element model has been used for the seepage, stress and coupled stress-flow analyses based on developed Seepage properties of roller compacted concrete. A linear elastic model was used for the rock foundation and the Mohr-Coulomb behaviour is employed for the dam body materials. Appropriate types of boundary conditions composed of water head condition, free boundary (phreatic surface) and flow boundary have been implemented in the analyses. Results of the study in terms of the seepage pattern and the effects of seepage on the mechanical properties of the RCC dam have been illustrated in order to compare the solutions. According to the results of the analyses, the following could be concluded:

(c) Although the distribution pattern of stress components with coupled solution is consistent with that of without coupled analysis, the increasing values of various stress components are different.

(d) The coupling effect makes the stress components increase in the RCC dam and the stress concentration near the dam heel more obvious. Therefore, the coupling effect should be taken into account in engineering design.

(e) High settlement has been observed at the upper elevations near the dam crest which gradually decreases by reducing the height of the dam.

(f) The coupling mechanism of seepage and stress field is absolutely essential in order to capture more reliable displacements and stress responses for realistic analysis of the RCC gravity dams.

(g)The modified seepage properties cause the stresses to increase and make the stress concentration near the dam heel more obvious which is mainly a result of hydrostatic seepage pressure in upstream face of the dam.

(h)The variation of confining pressures using USDFLD subroutine are more than those of without using it; and results in decrease in displacement values.

CHAPTER 7

THERMAL AND STRUCTURAL ANALYSIS OF RCC GRAVITY DAMS

7.1 Introduction

The computational procedures of unsteady temperature and stress simulation of RCC dams during the construction sequence and operational phases were discussed in Chapter 3. In order to further demonstrate the capability of the developed system, two real RCC gravity dams built in different environmental conditions are chosen to be analysed in this Chapter. The first RCC gravity dam is the Kinta RCC dam located in a tropical climate region in Malaysia and the second one is Zirdan RCC dam built in a hot - dry climate region located in south east part of Iran in neighbourhood of Pakistan.

In this chapter, two dimensional finite element model is used to perform the thermal analysis of the actual evolutionary construction process and operational phase taking into account the interaction between the reservoir water and the dam body of the above mentioned RCC dams. The stress analysis is performed for different load combinations, as well as some additional studies related to alternative construction schedules. Simultaneously, during the stress analysis, the safety evaluation of the dam against crack development will be discussed. The overall schematic mission adopted in the present chapter is depicted in Figure 7.1.

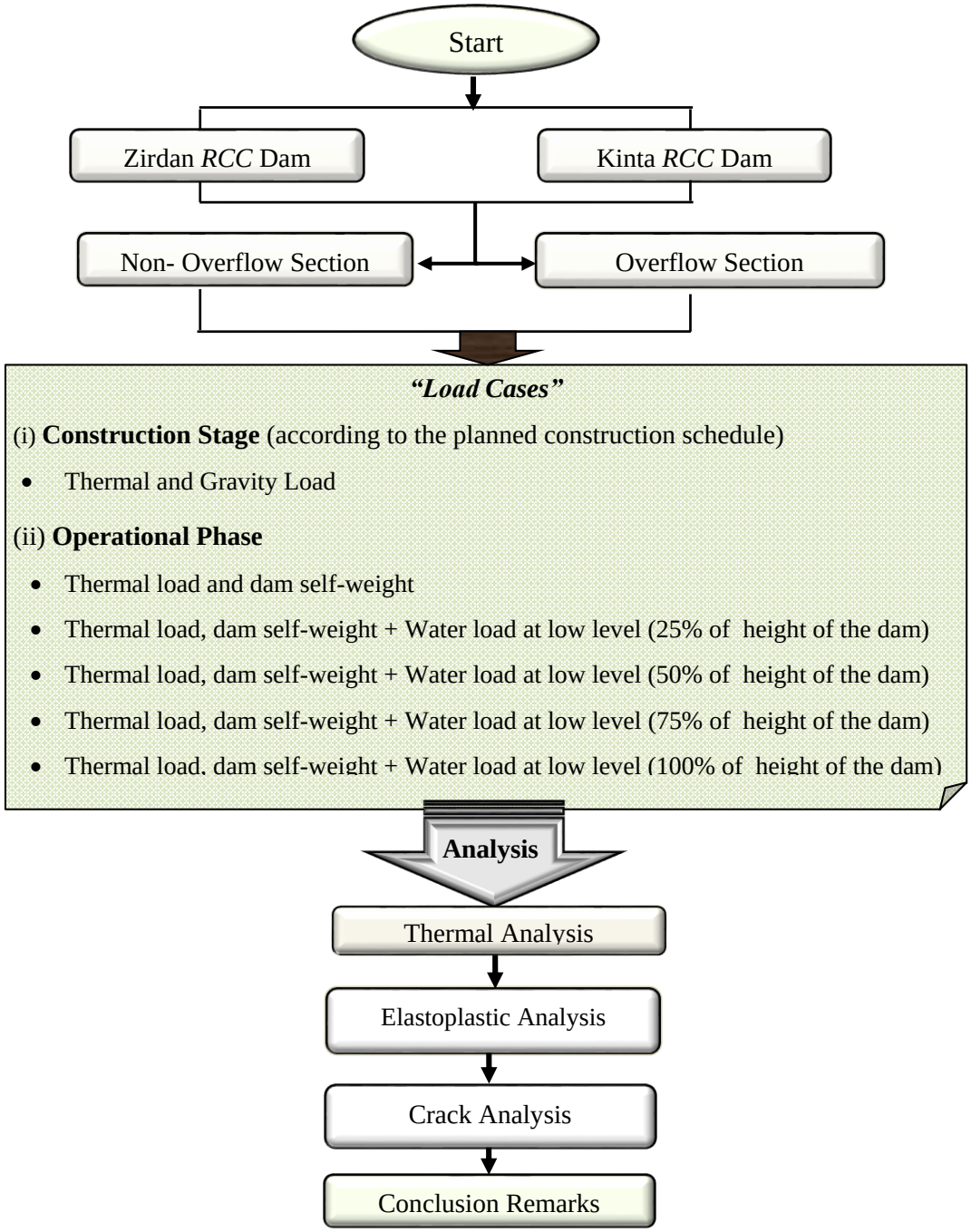

Figure 7.1 Flow Chart of the Study Implemented in the Present Chapter

7.2 Two– Dimensional Thermal- Stress Analysis of Kinta RCC Dam

7.2.1 Description of Kinta Dam

The detailed technical information of Kinta RCC dam which includes geometrical section, construction schedule and material properties are presented in Section 5.3.1. To study the structural response o Kinta RCC dam, two sections (overflow and non-overflow) have been selected along the length of the dam. These sections are shown in Figure 7.2.

The dam is modelled as a two-dimensional transient heat transfer model using a birth and death technique to simulate the real construction process of the dam according to the actual planned construction schedule (SUNGAI Kinta RCC dam 2002). The dam is divided into 26 lifts, each lift has a thickness of 3 m. Eight noded isoparametric element is used for discretization of dam body and foundation. Three finite element models have been prepared in the present study.

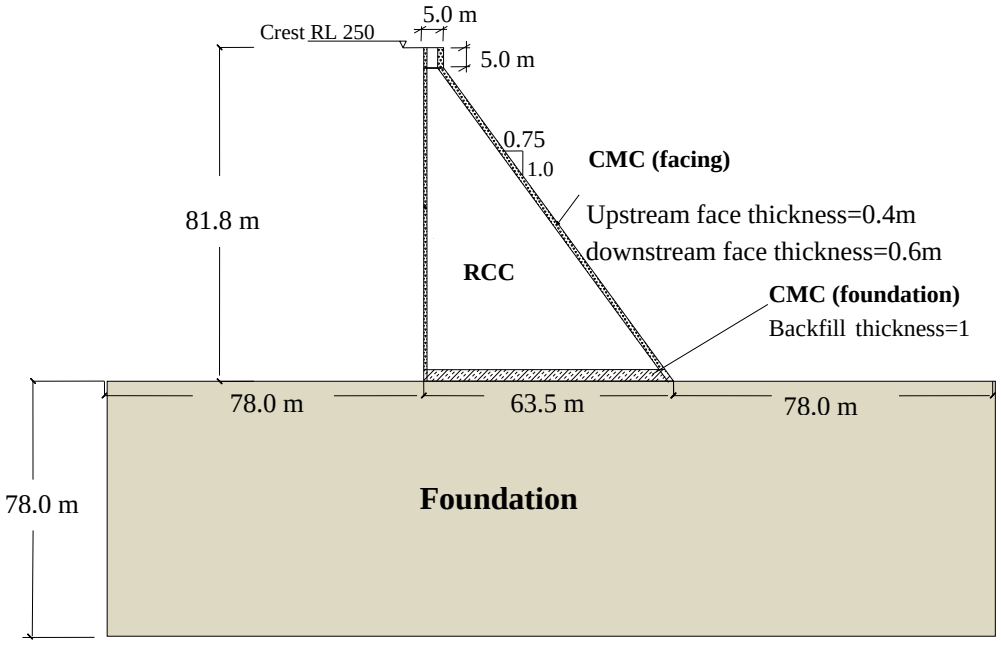

(a) Non- overflow Standard Section

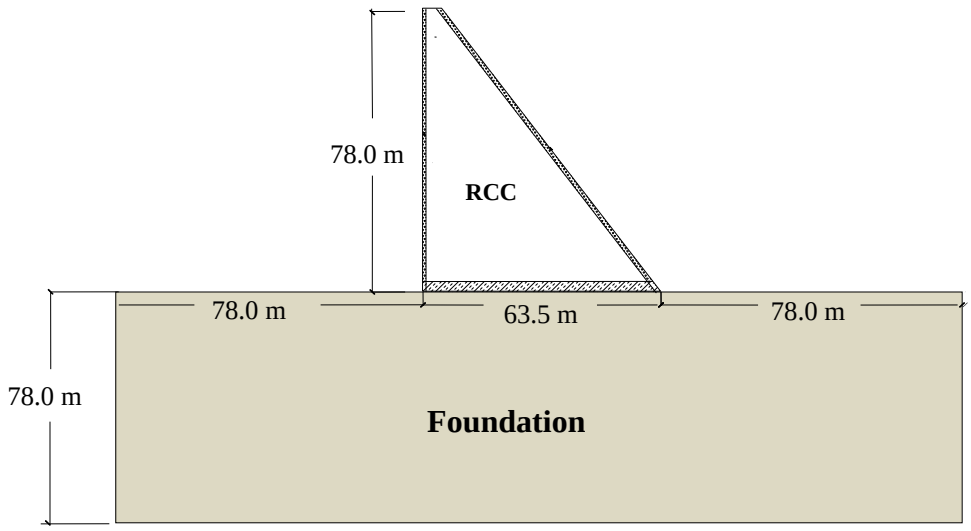

(b) Overflow Standard Section

Figure 7.2 Structural Geometry for Kinta RCC Dam

7.2.2 Two- Dimensional Finite Element Model

The two-dimensional finite element models of the two selected sections (Non-overflow and overflow sections) are shown in Figure 7.3. The finite element mesh of the dam body is generated according to the sequence of construction and also compatible with water impounding.

In addition, the water interaction is idealized using the modelling shown in Figure 7.4. The elements which model the water are assumed to be added in layers according to the reservoir filling schedule based on the procedures described in Section 4.2. The thickness of each water layer is kept equal to the corresponding opposite RCC lift in order to maintain the finite element continuities.

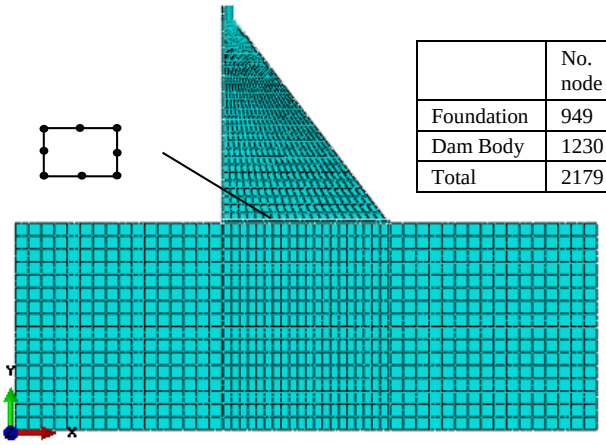

	No. node	No. element
Foundation	949	290
Dam Body	1230	390
Total	2179	680

(a) Non- overflow Standard Section

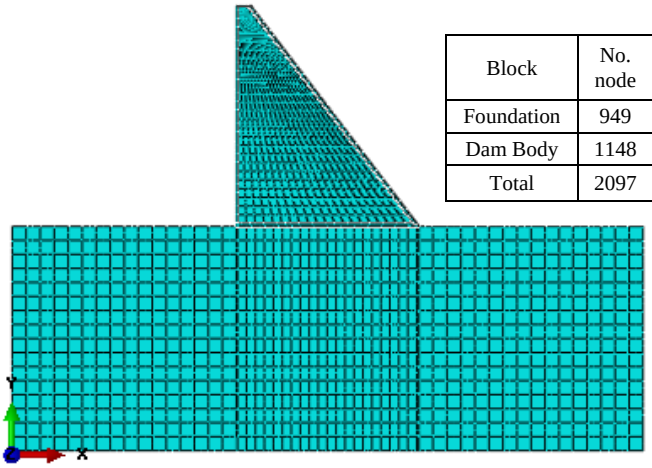

Block	No. node	No. element
Foundation	949	290
Dam Body	1148	364
Total	2097	654

(b) Overflow Standard Section

Figure 7.3 Finite Element Model- Mesh of the Kinta RCC Dam

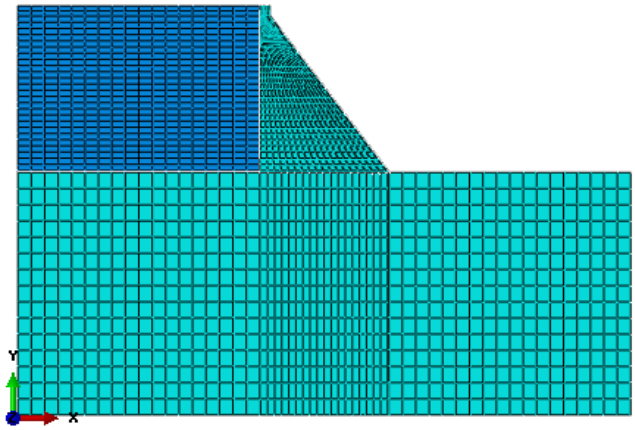

Figure 7.4 Finite Element Model - Mesh of the Dam Body, Foundation Block, and Reservoir (DFR) System

7.2.3 Temperature Distribution during the Construction

In this section, results from the thermal analysis performed on a numerical model of Kinta RCC Dam for the overflow and non- overflow sections are presented.

The plots of temperature distribution in the dam body for the different constructed lifts are shown in Figure 7.5. It is seen from these plots that, the maximum predicted temperature is 45^{o}C, and it was reached at the bottom of the dam after completion of the 10th stage as shown in Figure 7.5(a). This is due to the use of higher RCC placement temperatures combined with higher insulating property of this region due to its massive volume compared to the other locations. In addition, high temperature concentration

was observed at the top of the dam at the end of each lift as shown in Fig. 7.5(b) and (c) due to the hydration process being still high in this area compared with others in the dam body.

According to Neville (1983) the temperature difference between the interior and surface of the dam should not exceed 20ºC. The finite element results indicated that, boundary temperature is 32ºC, so the temperature inside the dam should not rise above 52ºC. Thus, the dam is considered safe against the surface gradient cracking.

Isothermal contour plot at the end of the dam construction for both sections (non-over flow and overflow) are shown in Figures 7.5 (d) and (e). The plots show that, a higher temperature zone is formed at the middle part of the dam body with maximum predicted temperature of 43ºC, which gradually decreases to reach approximately the air temperature at the boundaries.

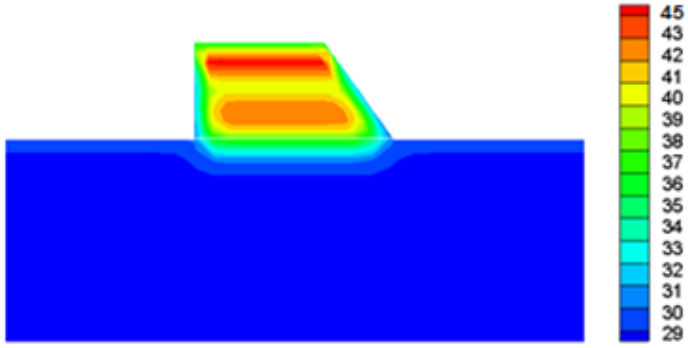

(a) Lift No.1

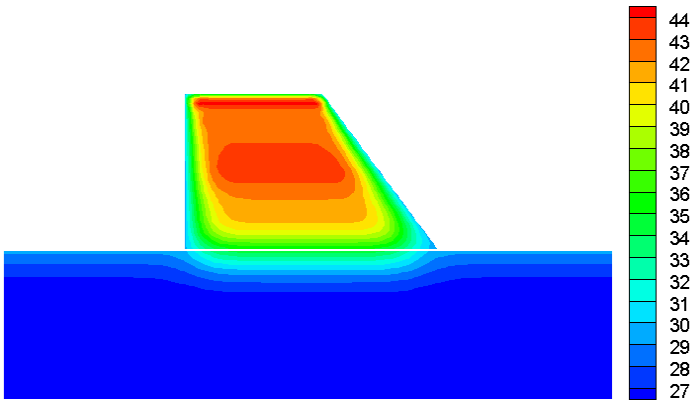

(b) Lift No.14

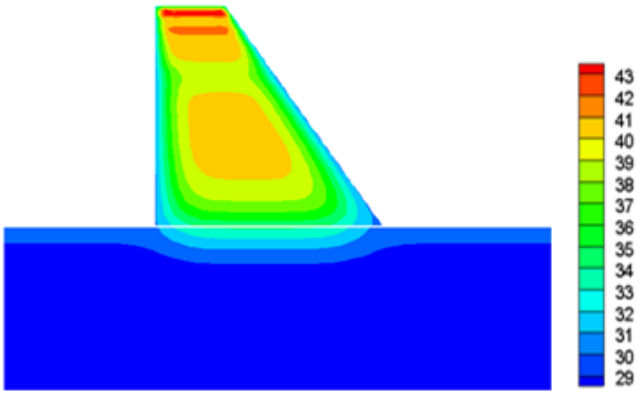

(c) Lift No.21

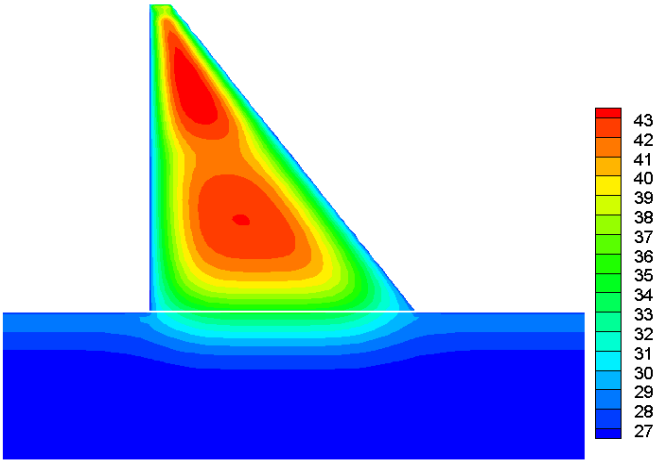

(d) End of Construction (Overflow Section)

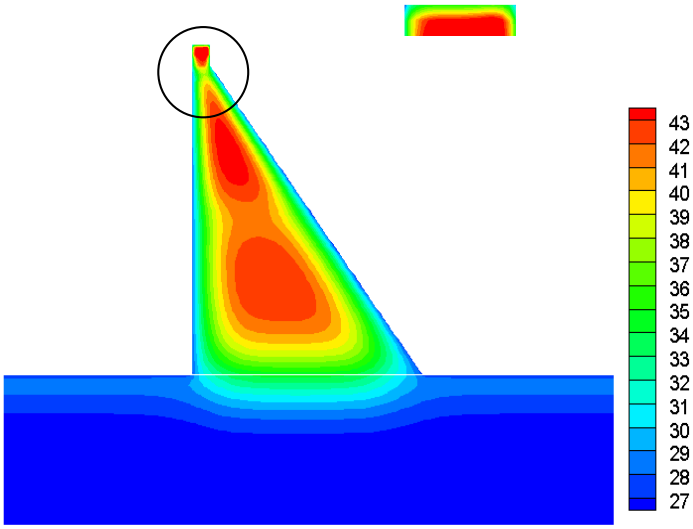

(e) End of Construction (Non-Overflow Section)

Figure 7.5 Temperature Distribution Contours (°C)

The variation of temperature with time for point (a), located at an elevation of 13.5 m from the base, is depicted in Figure 7.6. The plot demonstrates that the maximum temperature in the dam body was about 43ºC by 18th of October which occurred 10 days after the casting of the lift. This rise is due to the hydration of the cement at the early age. Then the temperature starts to drop and reaches 40ºC and remains nearly constant during the construction.

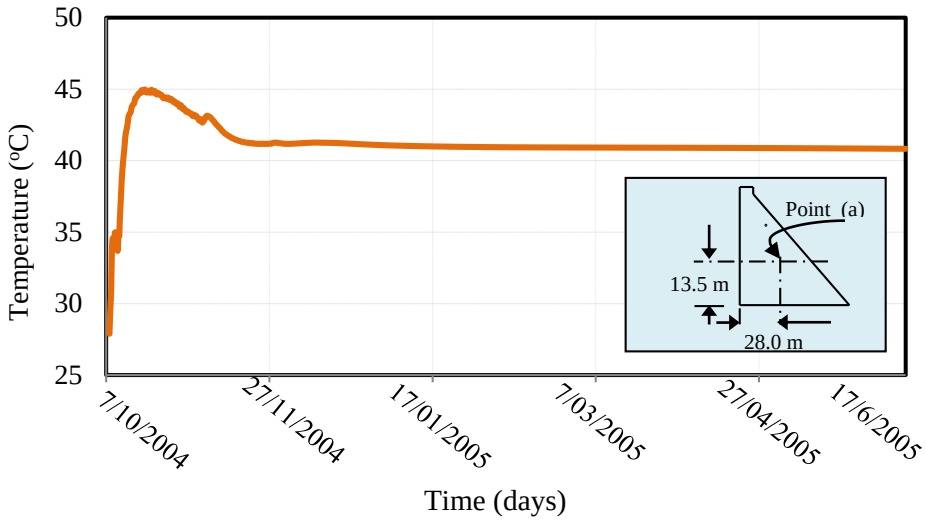

Figure 7.6 Predicted Temperature History at 13.5 m from the Base Measured at the Centre of the Dam (ºC)

7.2.4 Temperature Distribution during Water Impounding

The thermal analysis simulating the reservoir filling is performed using the schedule proposed for filling of Kinta dam reservoir as shown in Figure 7.7 (Crichton et al. 1999). An attempt has been made to draw the water interaction isothermal profiles for different levels of reservoir pounding and similar plots after one and three years as shown in Figure 7.8. The idealization of the reservoir mesh is set using the methodology described in Section 4.2. The maximum predicted temperature at the dam body centre is 43°C (at end of construction) after the reservoir is filled the temperature dropped to 41° C as shown in Figure 7.8. After one year, it dropped to 39° C and after three years to 37°C. The rate of heat dissipation at the upstream side is higher as compared to the downstream side; this may be due to the high insulating property of the dam reservoir resulting from its huge volume combined by the low conductivity of water.

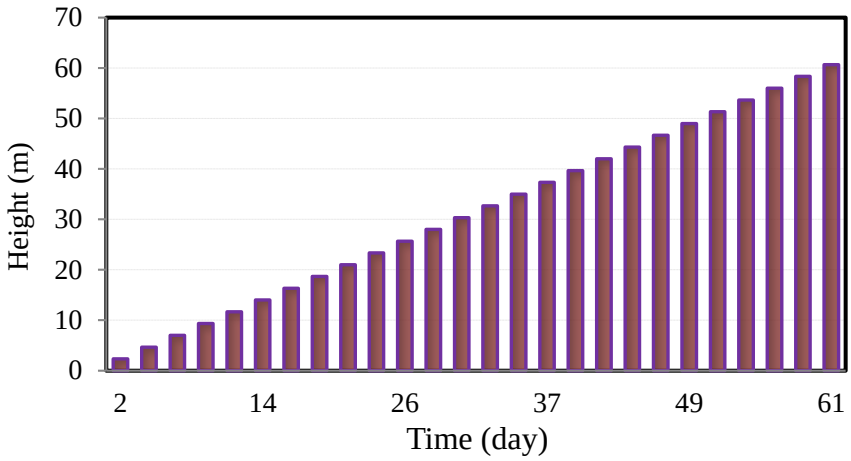

Figure 7.7 Filling Schedule of Kinta dam reservoir (Crichton et al. 1999)

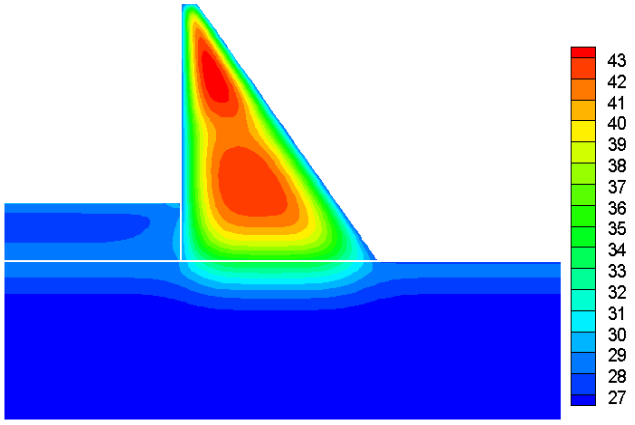

(a) After Filling of 25% of the Dam Reservoir

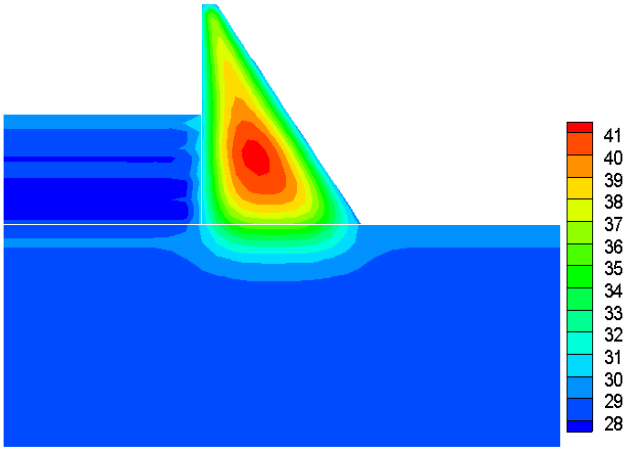

(b) After Filling of 50% of the Dam Reservoir

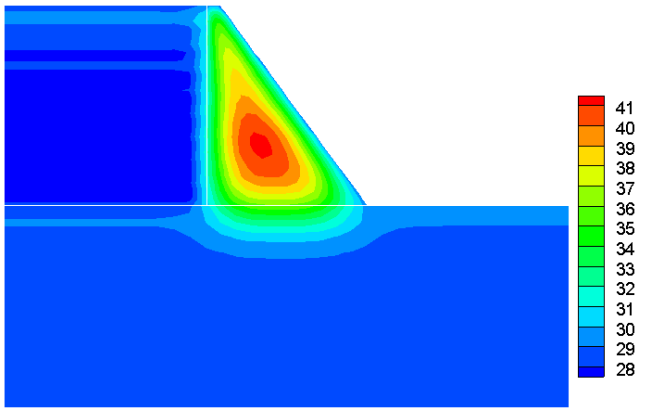

(c) After the Complete Filling of the Dam Reservoir

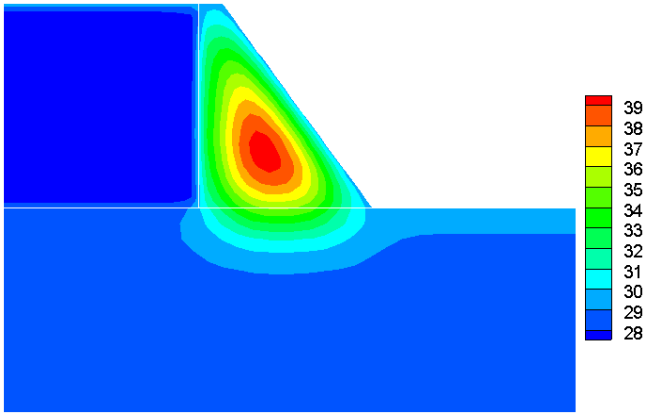

(d) After One Year of Reservoir Filling

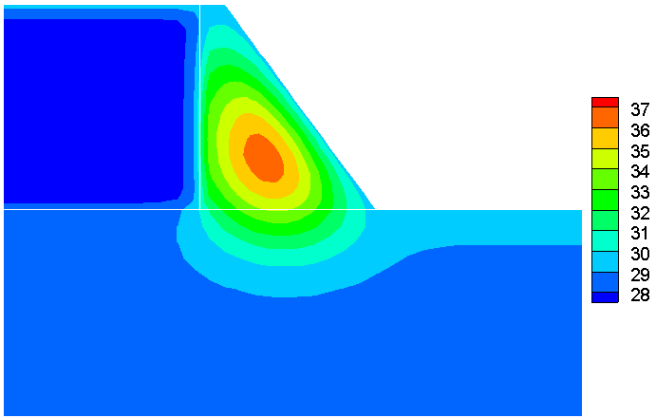

(e) After Three Years of Reservoir Filling

Figure 7.8 Water- Dam Body Interaction Thermal Responses (°C)

7.2.5 Temperature Effect on the Mechanical Properties

To execute the thermal stress analysis, the variation of the RCC mechanical properties with time and temperature should be taken into account. In this study, after the temperature field is computed, the methodology proposed in the Section 3.3.4 has been implemented to determine the variation of the elastic modulus with time considering the temperature effect.

In order to investigate the effect of temperature on the variation of the elastic modulus, Figure 7.9 has been included to show the temperature and the elastic modulus variation at the particular point (a) (Fig 7.6). It is obvious from the plot that, there is a significant difference between the two curves of the elastic modulus during the initial stage due to high temperature of hydration. Considering the temperature effect, the elastic modulus is increased by 45% in the first 10 days. However, the ultimate elastic modulus is not significantly affected. Consequently, the increases of the elastic modulus will accelerate the strength properties of the RCC materials (compressive and tensile strength).

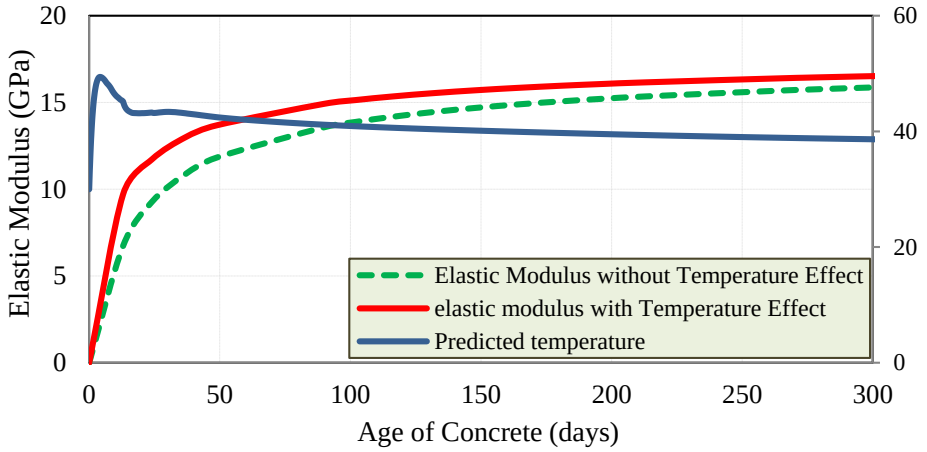

Figure 7.9 Temperature and the Variation of the Elastic Modulus at Point (a)

7.2.6 Stress Analysis

After thermal analysis has been performed, the structural analysis is conducted. The analysis is performed on a numerical model of Kinta RCC dam subjected to combined loading of thermal, gravity and hydrostatic loads.

An elasto-plastic model, including ageing and temperature effects, is adopted for the stress analysis to study the structural response during the construction and operational

phases of the RCC dam. The same time intervals for the heat transfer problem and the stress analysis was used in this study (Araujo and Awruch 1998).

The elasto-plastic interactive analysis of the entire system has been carried out by approximating the stress - strain relation of concrete as elasto-perfectly plastic. The concrete has been considered as yielding according to Mohr yield criterion which is widely used for concrete plasticity modelling (Asteris and Tzamtzis 2003; Yu et al. 2006).

In the framework of the present study, an initial analysis of the heat generation and dissipation through the dam was conducted. Later, structural analysis of the dam was carried out by converting the temperature changes into equivalent nodal forces in addition to dead weight of the dam and the hydrostatic force using the elastic matrix generated by the modified elastic modulus accounting for ageing and temperature effect (see Eq. 3.48) as presented in Section 3.3.4.

Based on the mathematical formulation described in Section 3.3.3, two parameters are needed for the Mohr-Coulomb criterion (*c* and *Ø*) as shown in Table 7.1. In order to illustrate the effect of time and temperature on the development of stresses within the dam body, the variation of maximum principal stresses have been shown for different sections of the dam body as indicated in Figure 7.10.

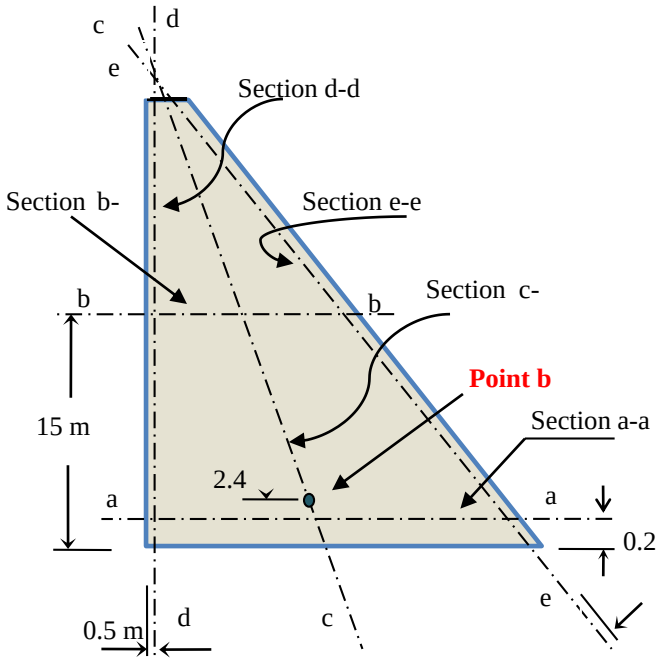

Figure 7.10 Diagram of the Dam

Table 7.1 Elasto-Plastic Material Properties (Abdulrazeg et al 2010)

Material	RCC	CMC	Rock
Cohesion *c* (MPa)	5.04	4.74	2.37
Friction Angle (deg.)	47.6	54.9	54.9

Figure 7.11 represents a comparison of the maximum principal evolution stresses for both cases of including and excluding temperature effects of interior Gaussian point (b) located along the centre line of the dam (section c-c). The results indicated that, the short-term stress evolution is increased. This is attributed to temperature influence on the elastic modulus as shown in Figure 7.9. Thus, when the temperature effects are considered, the maximum principal stresses increased from 0.44 MPa to 0.57 MPa, by 30%, after 100 days of casting. However, the long-term stress evolution will be reduced to 0.69 MPa, by 11 %, after three years. According to U.S Corps of engineers, the stress has not exceeded the limit at this point for the short term and the long term as well.

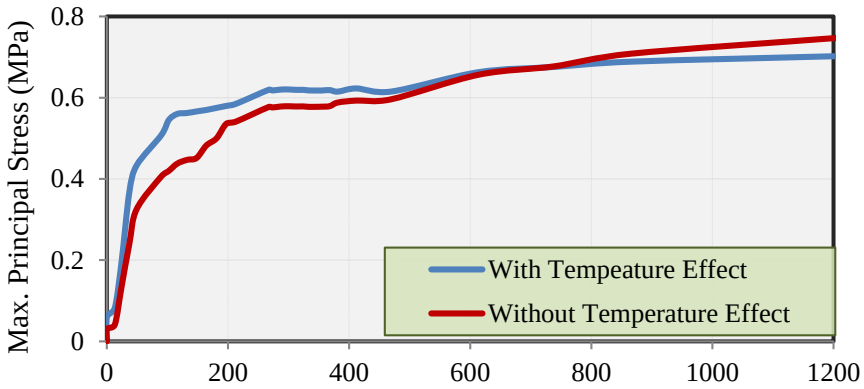

Figure 7.11 Max. Principal Stress History at 0.5 m from the Base Measured along Section c-c (MPa)

In this section, further study has been carried out to study the stress development and distribution in RCC dam based on the proposed elasto-plastic model (including time and temperature effects) described in Section 3.3. Results of the reference case study, simulating the real construction process and the first 3 years of the RCC dam's service life are discussed. This will provide an assessment of the dam design and the actual short - and long-term safety conditions of the construction and service life.

Figure 7.12 presents the principal stresses along the section (c-c) for different heights. The results indicate that the first peak tensile stress occurs shortly after placement of the RCC layers within the first 10 days after the casting of the lift. The tensile stress then increases and remains almost constant during the construction before the reduction because of the effect of the reservoir load on the upstream face.

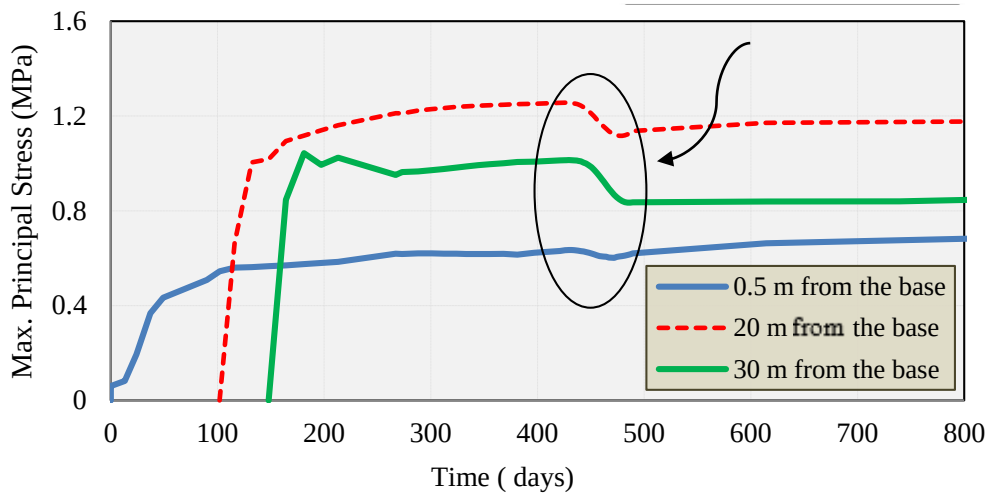

Figure 7.12 Maximum Principal Stresses at Centre of Dam (MPa)

Figure 7.13(a) shows the maximum principal stress path along section a-a (see Fig. 7.10) at the end of construction, at different reservoir levels and three years after the dam construction. The results indicate that the maximum tensile stress is located at the downstream side with the value of 3.85 MPa at the end of construction as shown in Table 7.2. According to ACI the allowable compressive strength is ranging from 6.9 MPa to over 27.6 MPa at the age of 1-year, and RCC mixtures are designed for a minimum strength of 13.8 MPa for durability reasons. The ratios of tensile strength to compressive strength for RCC mixtures have typically ranged from about 5 to 15 percent (ACI 207 1999). Thus, the tensile stress is exceeding the allowable tensile strength (0.69 to 2.07 MPa). Hence, this particular location needs special attention during the construction phase. However, this value is reduced due to the reservoir load, but at the same time, it will increase the tensile stress at the upstream side to 3.0 MPa. It could be concluded that, the upstream and the downstream regions at this level (toe and hill) are the regions of high tensile stress concentration, and special attention must be paid to these locations during the design and construction phases.

Moreover, further increase in the tensile stresses has been observed after three years of the dam construction. This is attributed to the cooling down of the dam body with time.

Table 7.2 Maximum Principal Stress Value along Section a-a (MPa)

	Upstream	Middle part	Downstream
End of construction	0.0	0.65	**3.85**
Reservoir level 25% of total height	-0.27	0.66	3.57
Reservoir level 50% of total height	-0.31	0.6	1.87
Reservoir level 75% of total height	0.23	0.6	1.78
Reservoir level 100% of total height	2.56	0.62	0.39
After three years of construction	**2.90**	0.73	0.78

The variation of the maximum principal stress along section (b-b) is presented in Figure 7.13(b) at the end of construction, reservoir filling and three years after the dam construction. The maximum tensile stress is observed at the downstream side at the end of construction (1.67 MPa), and at the upstream side is 0.71 MPa after the reservoir is filled. Generally, these stresses are not exceeding the allowable tensile strength given in the ACI standard of practice (ACI 207 1999).

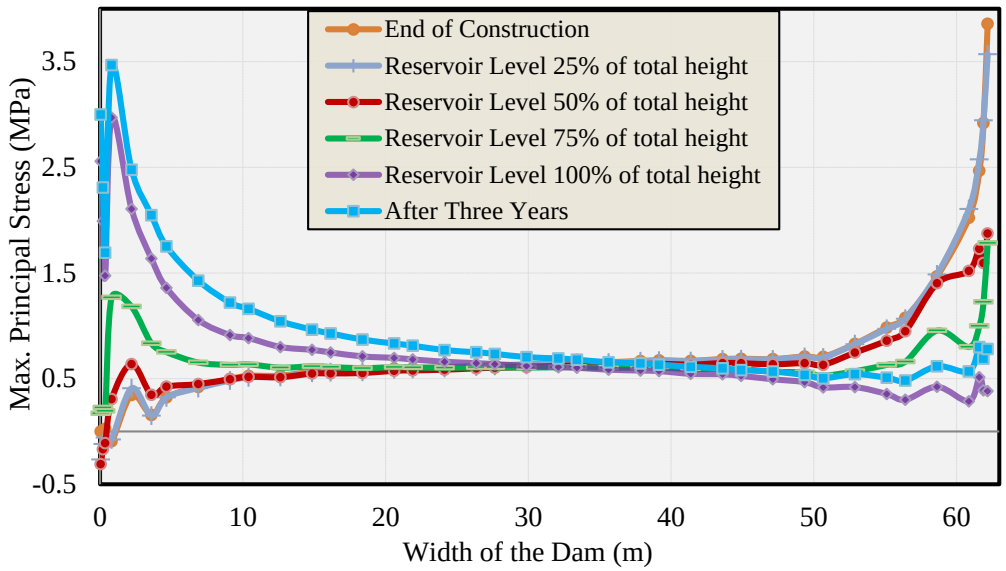

(a) The Maximum Principal Stress Path along Section (a-a) [*the Section is shown in Figure 7.10*]

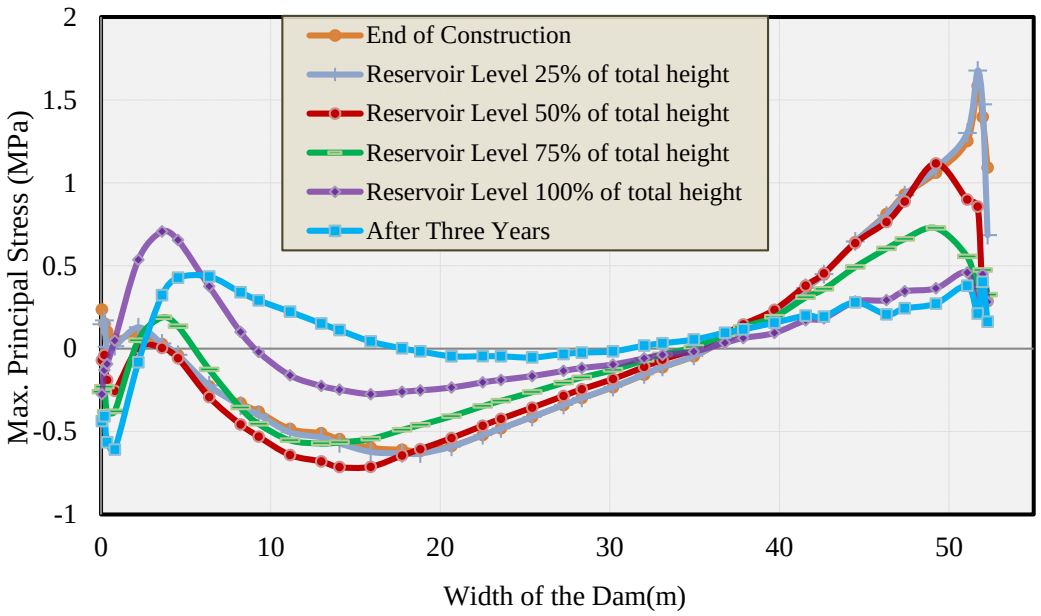

Maximum Principal Stress Path along Section (b-b) [*the Section is shown in Figure 7.10*]

Figure 7.13 The Maximum Principal Stress Variation (MPa)

In order to study the stress distribution along the dam's height, maximum principal stresses have been plotted for different sections of the dam body as indicated in Figure 7.10.

Figures 7.14 to 7.16 show the variation of the maximum principal stresses along different sections (c-c, d-d, and e-e) at different construction times and different reservoir levels. The maximum principal stress along section (c-c) is plotted in Figure 7.14. This plot indicates that, the maximum value of the tensile stress is reached at the end of construction (1.5 MPa), at the foundation, due to the contact of two dissimilar materials. However, the tensile stress has not exceeded the allowable tensile stress of concrete along the centre section (section c-c).

The maximum and minimum principal stresses are tabulated in Table 7.3. It can be seen that, there is marginal effect of the hydrostatic load comparing with horizontal sections.

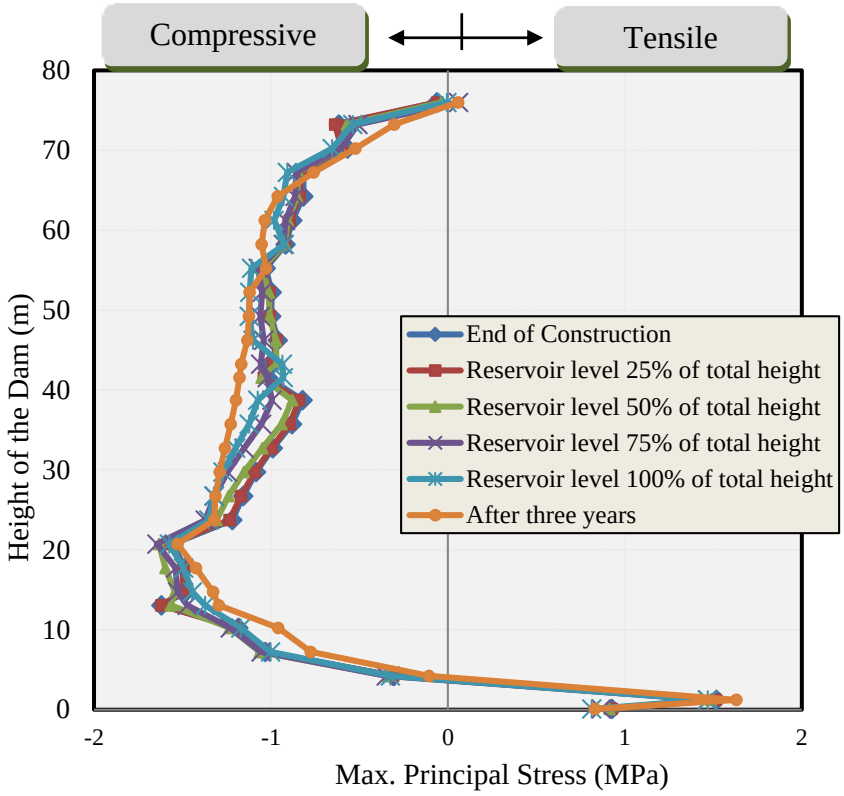

Figure 7.14 Variation of the Maximum Principle Stress along Section (c-c) [*the Section is shown in Figure 7.10*]

Table 7.3 The Principal Stress (MPa) Values along Section (c-c)

Height measured from the foundation	0.5 m		20.0 m		40.0 m		78.0 m	
	Max.	Min.	Max.	Min.	Max.	Min.	Max.	Min.
End of construction	**1.5**	-1.72	-1.5	-2.22	-1.02	-1.44	-0.06	-0.28
Reservoir level 0.25H	1.5	-1.74	-1.56	-2.24	-1.0	-1.5	-0.05	-0.3
Reservoir level 0.5H	1.48	-1.74	-1.63	-2.2	-1.0	-1.55	-0.05	-0.57
Reservoir level 0.75H	1.46	-1.8	-1.64	-2.3	-1.1	-1.6	-0.06	-0.62
Reservoir level H	1.46	-1.93	-1.57	-2.56	-0.93	-1.8	-0.06	-0.66
After 3 years	1.52	-1.92	-1.52	-2.4	-1.17	-1.88	-0.06	-0.7

Figures 7.15 and 7.16 represent the distribution of the maximum principal stress along sections (d-d) and (e-e), respectively at different construction time and reservoir filling levels. In addition, the maximum stress for different heights of the dam on both sides is shown in Table 7.4. It can be concluded that, the maximum stress is observed at

lower part of the downstream side (2.9 MPa). However, the hydrostatic pressure exerts high tensile stresses at the upstream and at the same time reduces the tensile stresses at the downstream. It can also be seen that, there is an increase in the tensile stress at the bottom of the dam at the upstream side. This is attributed to hydrostatic load.

Table 7.4 The Principal Stresses along Upstream and Downstream Sides

Height measured from the foundation	0.0		0.5H		H	
	U.S	D.S	U.S	D.S	U.S	D.S
End of construction	0.0	**2.9**	0.18	1.97	0.09	0.13
Reservoir level 0.25H	-0.11	2.94	0.25	2.08	0.01	0.06
Reservoir level 0.5H	-0.17	1.59	0.25	1.12	0.03	0.1
Reservoir level 0.75H	0.23	1.2	0.06	1.22	-0.04	0.09
Reservoir level H	1.99	0.4	-0.12	0.57	-0.02	0.03
After 3 years	2.3	0.5	-0.1	0.38	-0.04	0.05

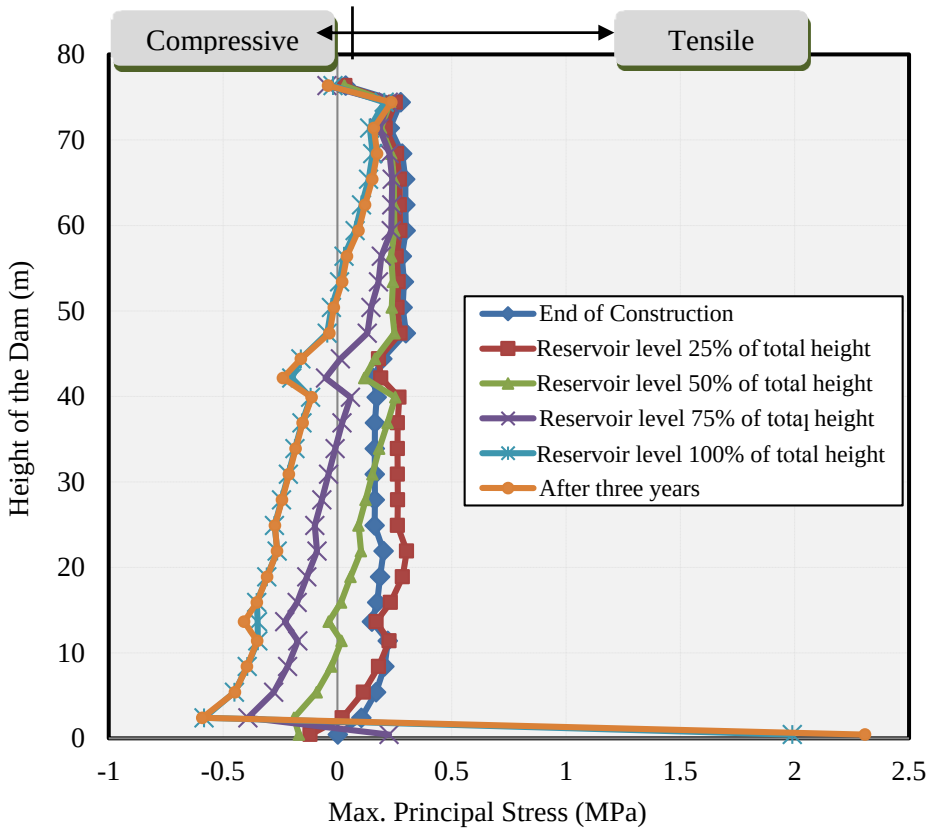

Figure 7.15 Variation of the Maximum Principal Stress along Section (d-d) [*the Section is shown in Figure 7.10*]

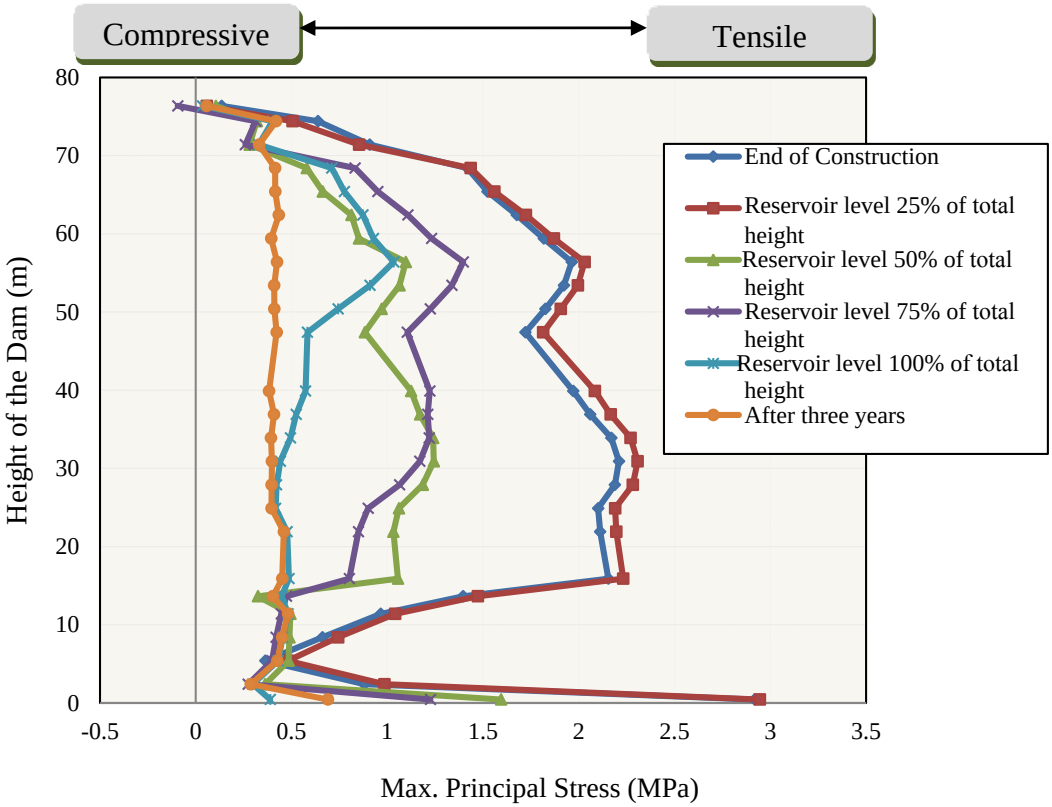

Figure 7.16 Variation of the Maximum Principal Stress along Section (e-e) [*the Section is shown in Figure 7.10*]

Figures 7.17(a) to 7.17(f) show the maximum principal stress contours in the dam body for different constructed lifts. The results indicate that, the tensile stress is developed at different levels of the dam body during the process of construction. In addition, high tensile stress zones are formed at the lower part of the dam with maximum value at the heel due to the external restraint caused by foundation, and at the upstream and downstream faces, because of the restraint against environmental thermal variations. Generally, it is observed that most of the dam body is under compressive stresses.

Figure 5.17(f) shows the contour plots for the evolution of the maximum principal stresses in the dam body 3 years after completion of the dam. It can be seen that, as the dam is cooling down, thermally induced tensile stresses progressively develop due to internal and external restraints.

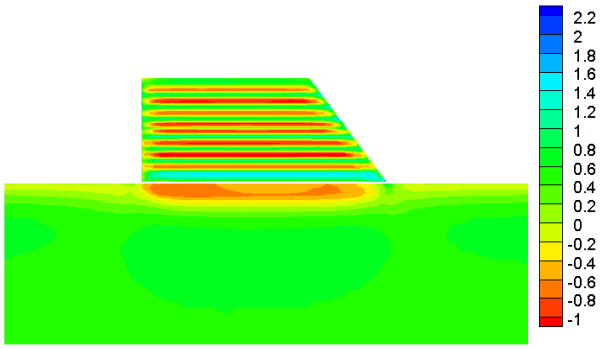

(a) Lift No.10

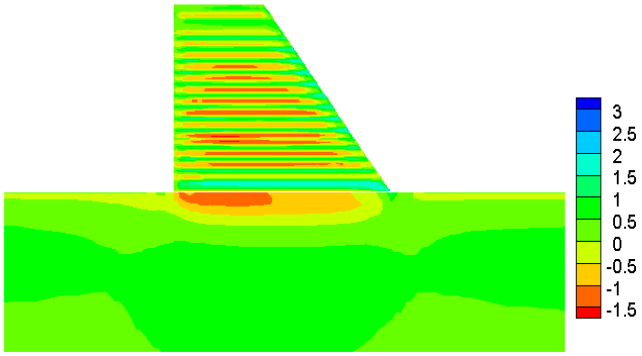

(b) Lift No.21

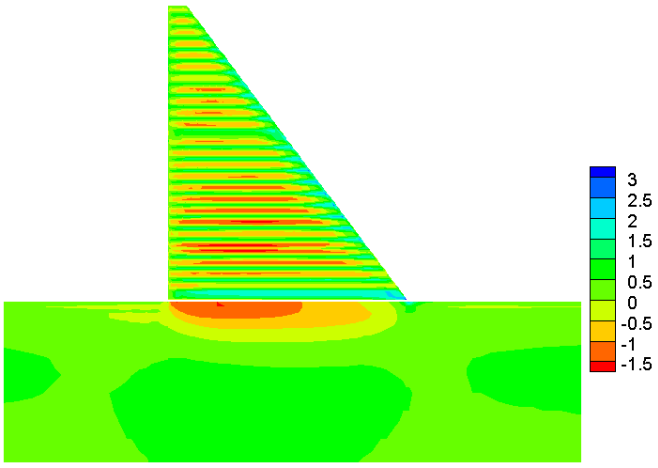

(c) End of construction (Overflow Section)

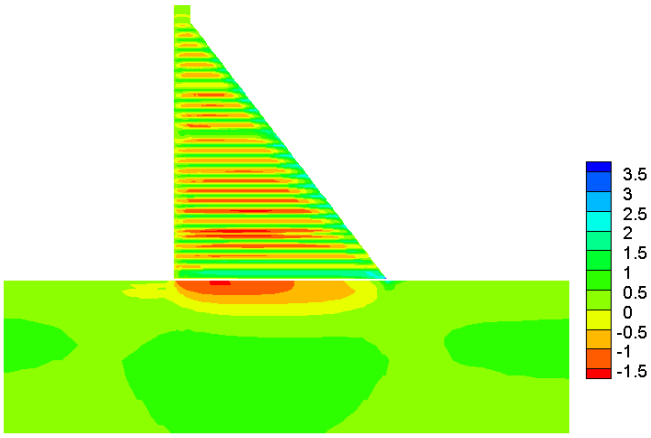

(d) End of construction (Non-overflow Section)

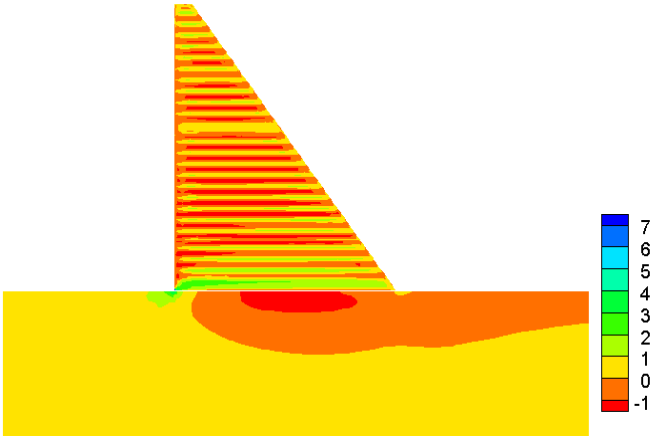

(e) After the filling of the reservoir

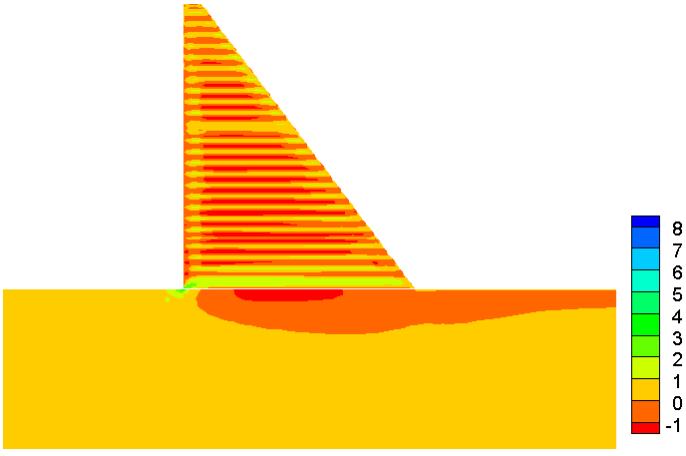

(f) Three years after dam construction

Figure 7.17 Maximum Principal Stress Distribution in Body of the Dam (MPa)

Figures 7.18(a) to 7.18(f) show the distribution of the minimum principal stresses (MPa) for different construction stages. High compressive stress zones are concentrate

at the centre of the dam, which gradually reduce toward the boundaries. In addition, a small region of high compressive stress has been observed at the lower part of the upstream, which will gradually move to the downstream as the reservoir is filled, due to the reservoir effect.

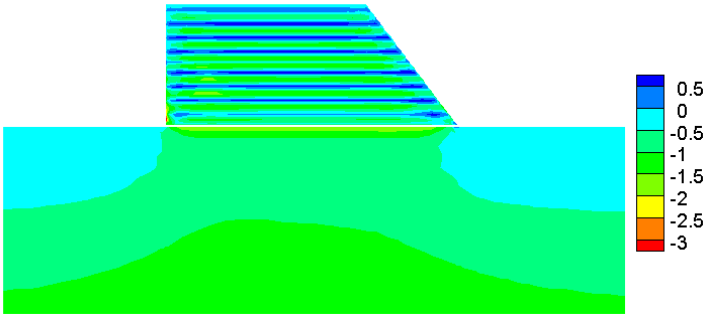

(a) Lift No.10

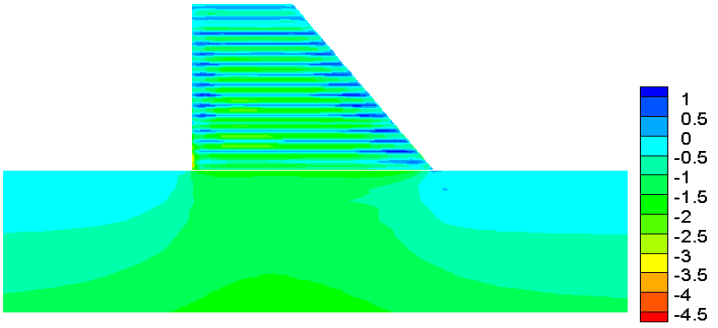

(b) Lift No.21

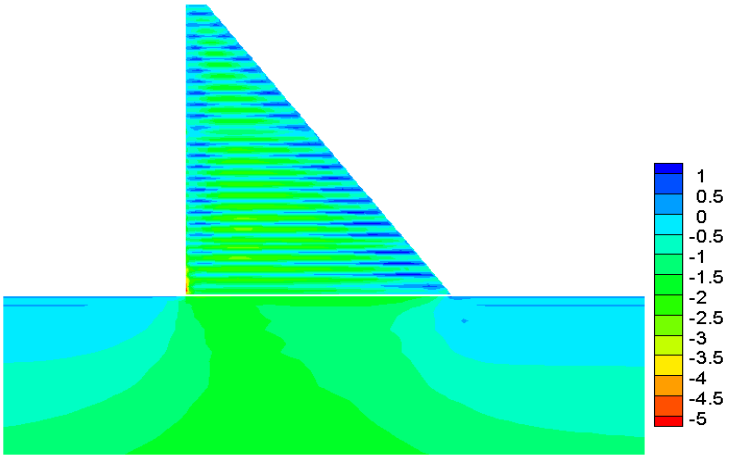

(c) End of construction (Overflow Section)

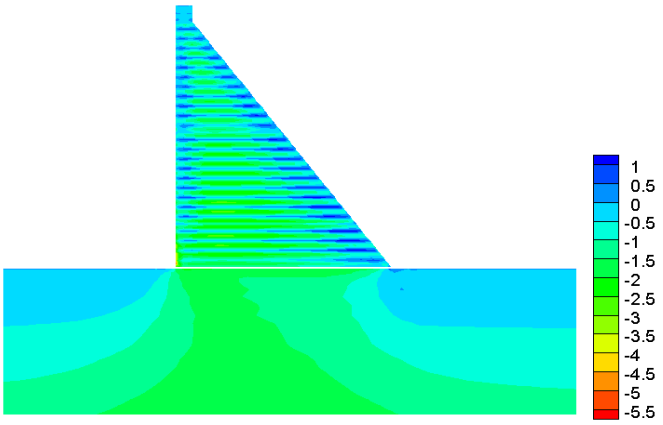

(d) End of construction (Non-overflow Section)

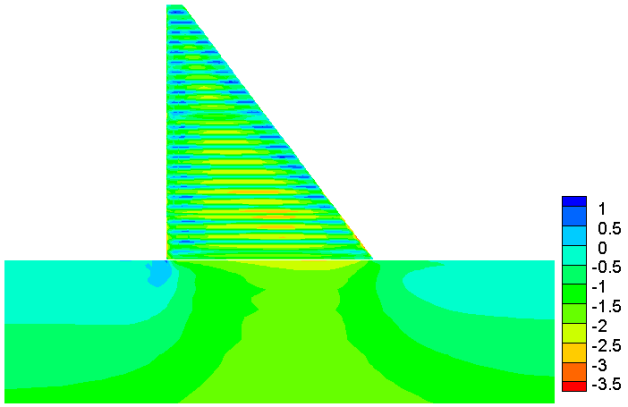

(e) After filling the reservoir

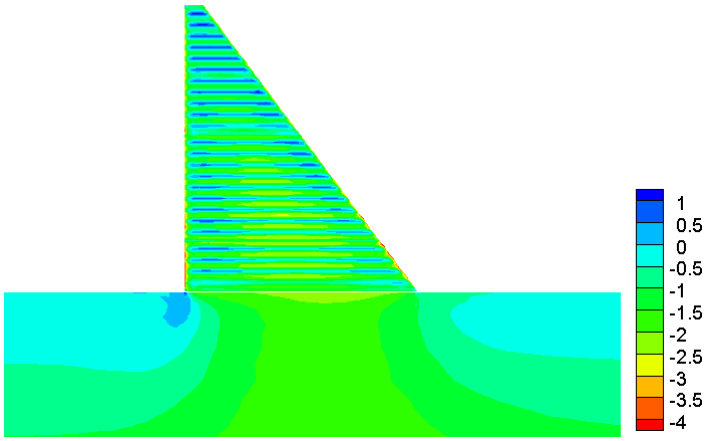

(f) Three years after dam construction

Figure 7.18 Minimum Principal Stress Distribution in Body of the Dam (MPa)

7.2.7 Two Dimensional Safety Evaluation of the Dam against Cracking

Simultaneously, during the stress analysis, the crack safety factor will be calculated at each Gaussian point and the safety of the dam against cracking is evaluated. Hence, all the properties of the materials are time and temperature dependent, especially elastic and strength properties, the variation of the crack factor with time and temperature are determined. Thus, this factor will be more realistic to represent the crack occurrence. If the safety coefficient of the cracking is greater than one, the element will be considered safe against cracks. However, if the coefficient is less than one, crack will develop in the dam body.

Figure 7.19 shows the variation of crack safety factor during the construction and operational phase of the dam at the elevation of 0.5 m from the base of the dam, due to the high stress concentration in this region. It is clear from the plot that, the dam is safe against cracking at upstream side during the construction stage; however, during the operational phase, the crack index drops below the allowable limit and this is attributed to the effect of the reservoir load at the upstream face. Conversely, for response at the downstream side, the crack factor drops below the allowable limit during the construction phase. This is clearly shown in Figure 7.13 where the upstream and the downstream are the regions of high tensile stress concentration. It can be concluded that, in the vicinity of both faces, the crack factors are below the allowable limit and do not meet the demands against crack development, thus cracks in the directions of upstream and downstream will inevitably develop.

An attempt is made to draw the crack safety domains at the end of construction and after the reservoir is filled. Figure 7.20 shows the contours of possible crack domains. It is clear from the plots that, at the end of construction the crack locations are at the lower part of the dam near the downstream side and the boundaries of the dam, which coincide with higher tensile stress zone (Fig.7.17-c). However, when the reservoir is filled, the cracks will appear at the upstream side due to the high hydrostatic pressure, which exerts high tensile stresses at the upstream and at the same time suppresses the tensile stresses at the downstream. Another crack location observed at the end of construction is at the upstream face at level of 0.6H as illustrated in Figure 7.20(a).

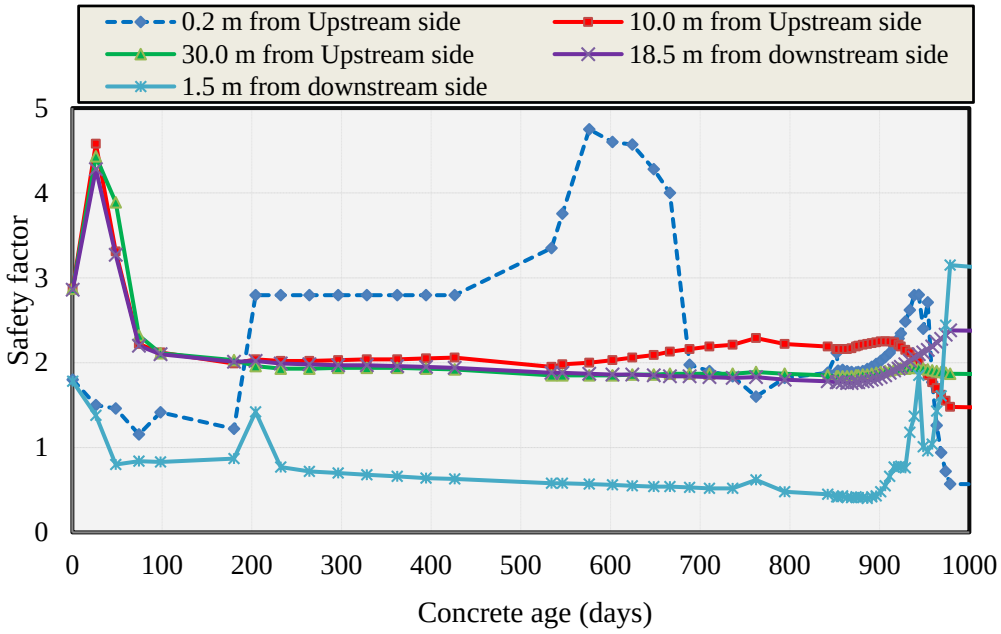

Figure 7.19 Crack Safety factor variation at level of 0.5 m

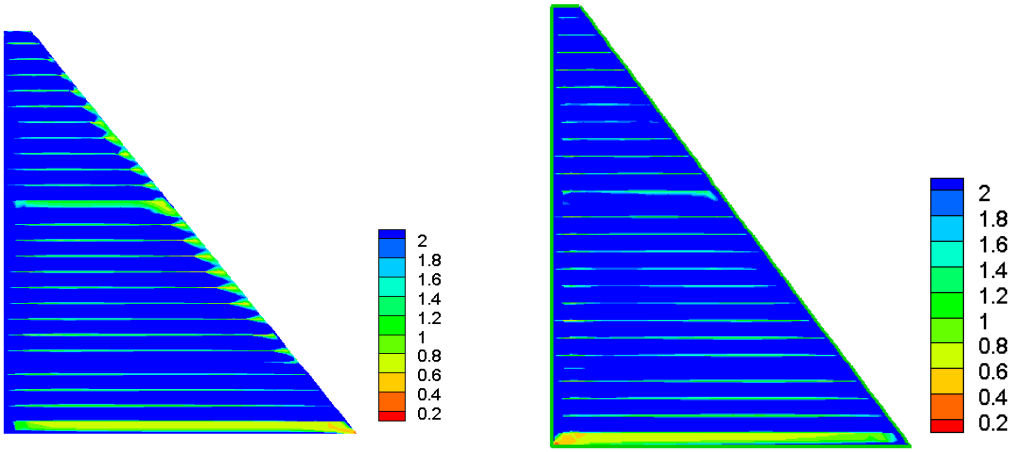

(a) At the End of Construction **(b) After the Reservoir is Filled**

Figure 7.20 Crack Contours of the Dam Body

7.3 Analysis Results and Discussion of Zirdan RCC Dam

In order to further confirm the applicability of the developed system, an attempt is made to analyse an actual RCC dam, the Zirdan dam built in a hot-dry region (Baluchistan of Iran). Many factors have been considered in this investigation, such as adiabatic temperature, placement schedule, galleries, climatic variation, and water interaction at the upstream face of the dam, taking into account the variation of temperature of the reservoir water with depth using the procedure described in Section 3.2.6.

7.3.1 Description of Case Study

Zirdan dam has been designed and constructed in South-East of Iran in a hot dry climate area (maximum temperature rises above 50^{o} C), over a seasonal temporary river with rushing floods. The maximum height of the dam is 64.5 m and the crest length is 350 m (Pazhouhab Consultant Engineers 1999). The dam structure is divided into 23 monoliths by full-length transverse contraction joints spaced typically at 15 m centres. Figure 7.21 shows the typical section of the dam and its main dimensions. The two galleries (one at the bottom and another one at the top) used for inspections are also shown in the Figure.

7.3.2 Material Properties and Site Conditions

The material properties for the RCC, the conventional mass concrete (CMC), and the rock foundation, are given in Table 7.5 (Pazhouhab Consultant Engineers 1999). These properties, which are the actual properties supplied by the consulting engineers, are used in the analysis as the input data. In addition, the average monthly air temperatures at the project site, shown in Figure 7.22, are used in the thermal analysis for the simulation of the heat transfer by the convection action.

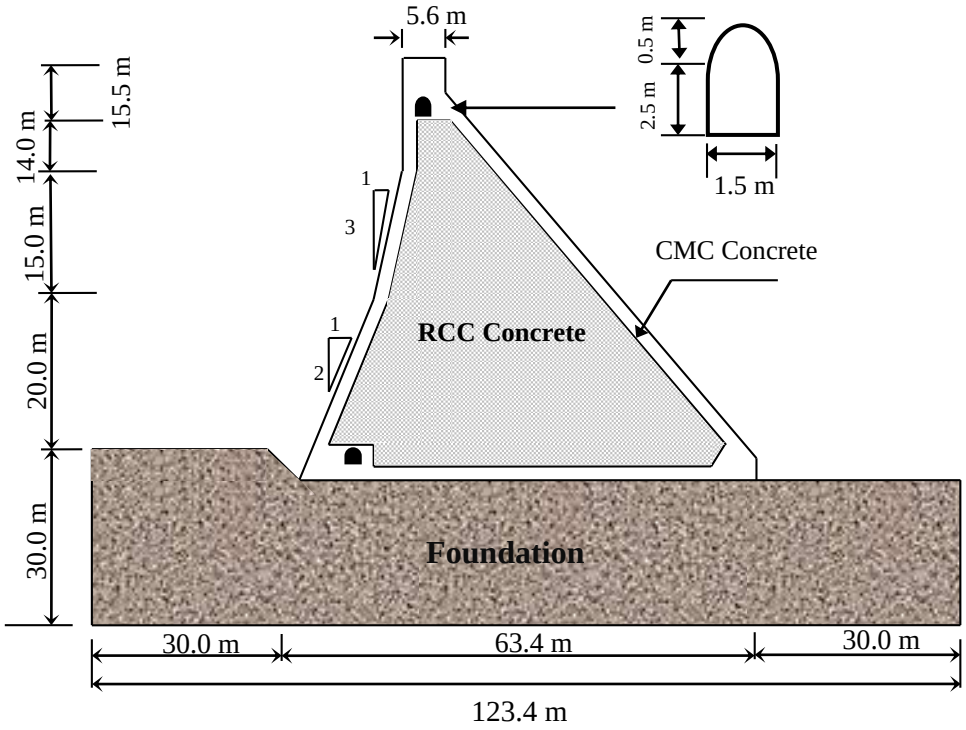

Figure 7.21 Structural Geometry for Zirdan RCC Dam (Technical report of Zirdan 1999)

Table 7.5 Thermal and Structural Properties of a Trial Segment (Pazhouhab Consultant Engineers 1999)

Parameter	unit	Symbol	RCC	CMC	Rock
Heat Conduction Coefficient	W/m °C	K	2.8	2.8	2.7
Heat Convection Coefficient	W/m^2 °C	h	15.25	15.25	15.25
Specific Heat	J/kg°C	c	1256	1256	1256
Density	kg /m^3	ρ	2400	2400	2710
Elasticity Modulus	GPa	E	1.67	2.25	0.6
Poisson's Ratio	-	ν	0.18	0.18	0.3

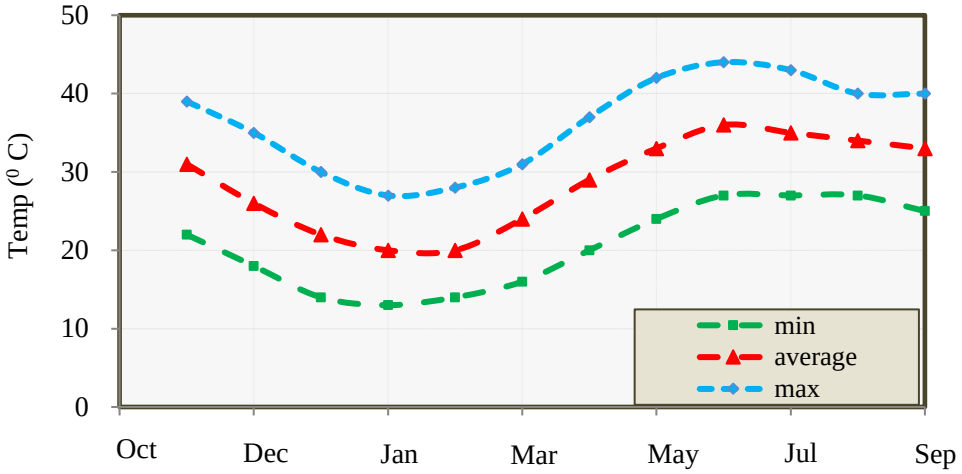

Figure 7.22 Monthly air Temperatures at Project Site

7.3.3 Finite Element Modelling of Zirdan RCC Dam

The dam is modelled as a two-dimensional transient heat transfer model using a birth and death procedure to simulate the real construction process of the dam according to the actual planned construction schedule (Pazhouhab Consultant Engineers 1999). The dam is divided into 21 lifts.

- **2- D Finite Element Model without Reservoir (Dam body/Foundation)**

The two-dimensional finite element models of the overflow and non-overflow sections along the dam width are shown in Figure 7.23. Eight noded isoparametric element is used for discretization of the dam body and foundation.

- **2- D Finite Element Model with Reservoir**

The finite element model is used to simulate the heat exchange between the impounding water and dam body at the upstream side as shown in Figure 7.24. The elements which model the water are assumed to be added in layers according to the reservoir filling schedule.

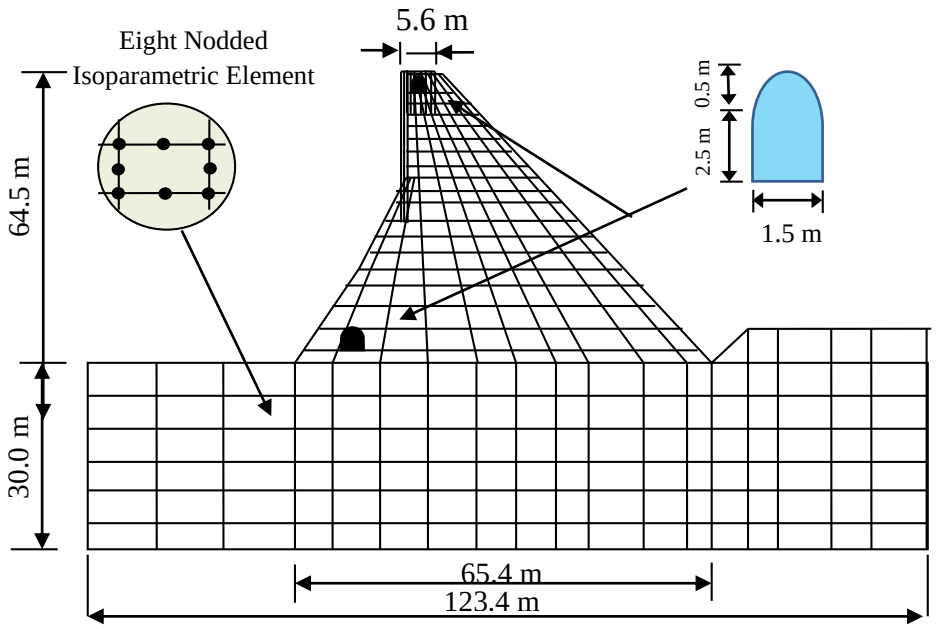

(a) Non-overflow Section

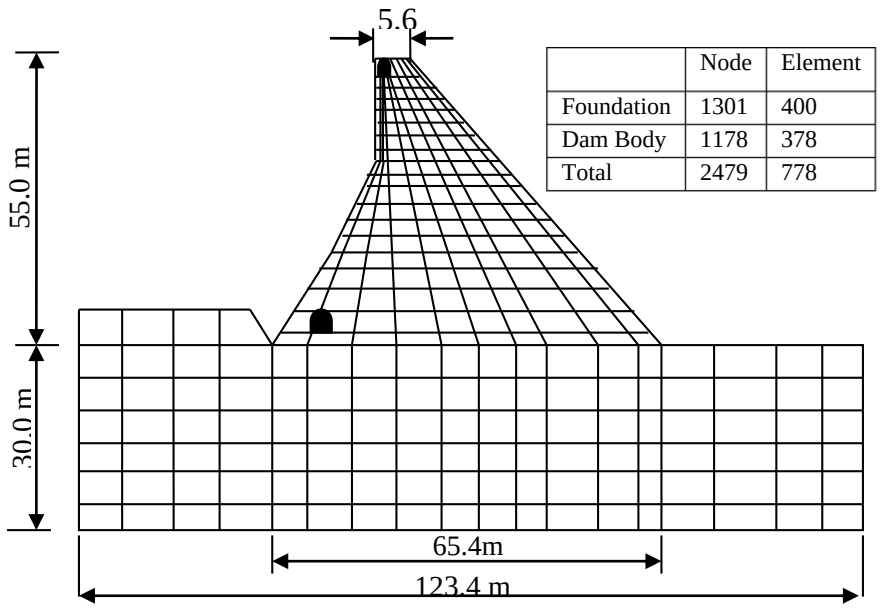

	Node	Element
Foundation	1301	400
Dam Body	1178	378
Total	2479	778

(b) Overflow Section

Figure 7.23 Two- dimensional Finite Element Model - Mesh of Zirdan Dam

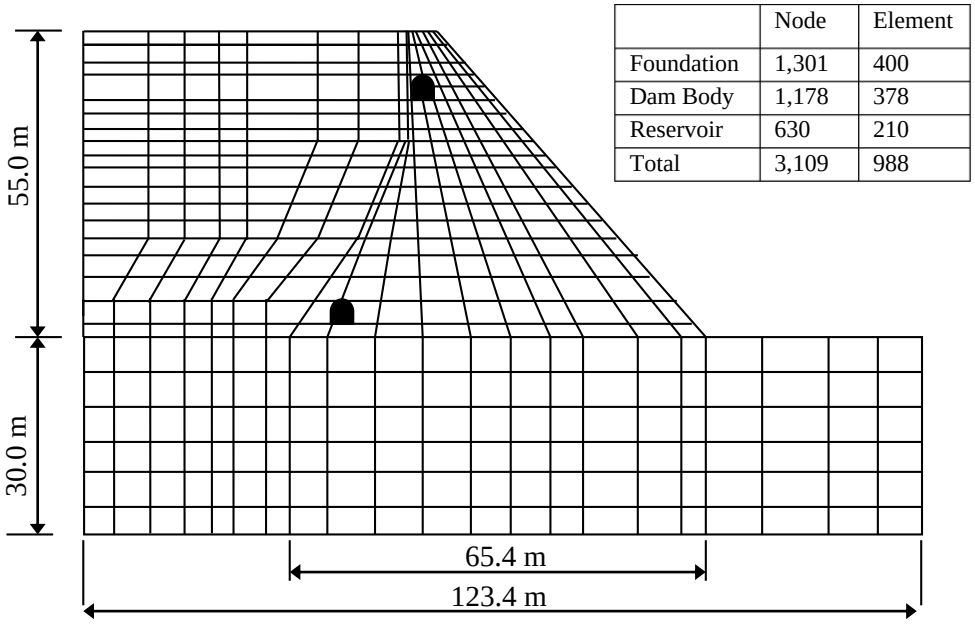

	Node	Element
Foundation	1,301	400
Dam Body	1,178	378
Reservoir	630	210
Total	3,109	988

Figure 7.24 Finite Element Mesh for Dam body, Foundation and Reservoir

7.3.4 Thermal- Stress Analysis Results and Discussion Considering the effect of the Gallery

- **Temperature Distribution during Construction**

Isothermal contour plots at the end of the dam construction for both overflow and non-overflow sections are shown in Figure 7.25. It is obvious from this plot that, the higher temperature zone is formed at the centre of the dam body with maximum predicted temperature of 44^{o} C, which gradually reduces to reach approximately the air temperature at the boundaries. Furthermore, a higher temperature zone with the value of about 49^{o} C, is formed at the top of the dam due to the high hydration exchange in this area compared to other parts of the dam body.

In addition, the isothermal contours reveal a clear picture of the gallery effect on the temperature development and distribution with the dam body. It can be noticed that, due to the presence of the two galleries, there is discontinuity in temperature distribution in the regions with a gallery and also the value of temperature is lower compared to other locations.

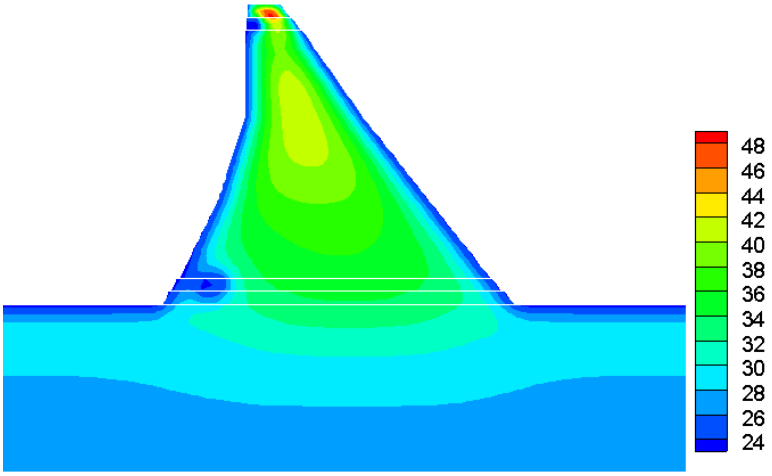

(a) Overflow Section

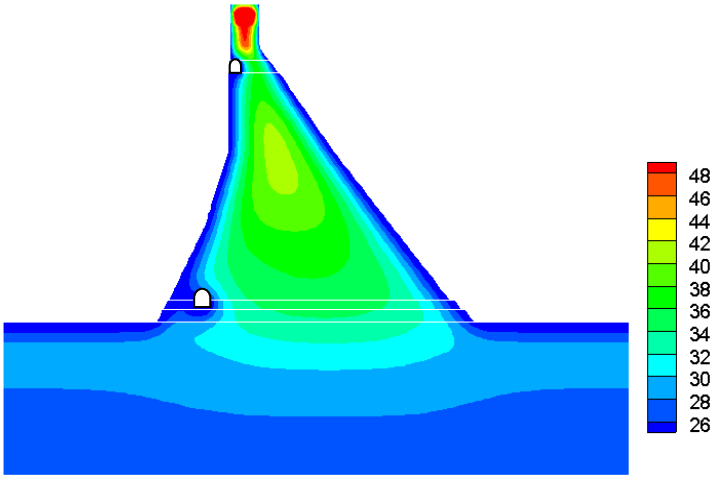

(b) Non-Overflow Section

Figure 7.25 Temperature Distribution after completion of Dam Construction

- **Temperature Distribution during Operational Phase**

It is necessary to predict the water temperature at various depths of the reservoir as a prescribed boundary condition for heat transfer equilibrium equation in concrete (Sheibany and Ghaemian 2006). In the context of finite element method, the formulations given in Section 3.2.6 have been used to simulate the initial temperature of the reservoir water. In addition, the methodology described in Section 4.2.2 was adopted to model the water impounding.

In order to examine the effect of heat exchange between dam body and impounding water, distribution of temperature at the end of reservoir filling is shown in Figure 7.26.

It is evident from Figure 7.25 (Temperature distribution at the end of construction) and Figure 7.26 (Temperature distribution after reservoir is filled) that, there is a reduction in the temperature of the dam body, at the upstream face of the dam due to direct contact with water. The plot also shows how the water temperature is reducing along the depth of water. The temperature of the core is reduced by 4^{o} C as well. The maximum predicted temperature at the dam body centre is 44 °C at end of construction whereas after the reservoir is filled the temperature dropps to 40^{o} C.

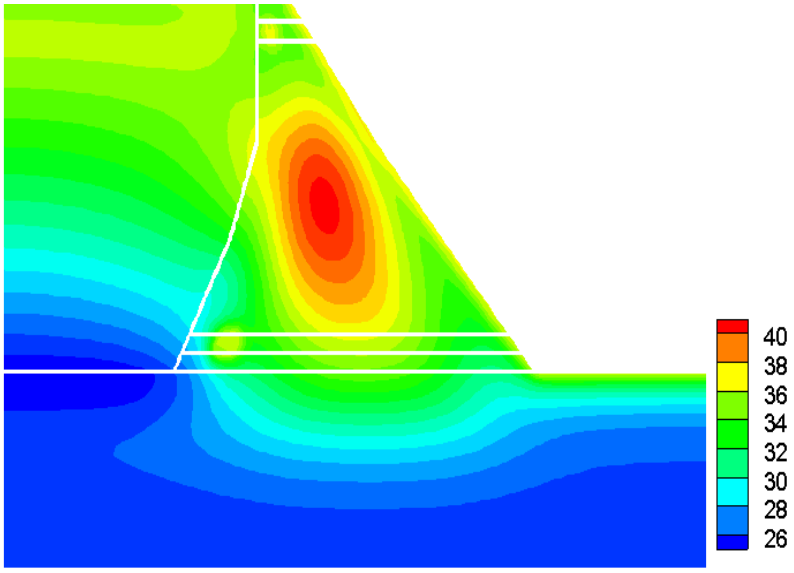

Figure 7.26 Water - Dam Body Interaction Thermal Response after Filling of the Dam

- **Stress Variation in the Dam Body**

The structural behaviour of the dam is presented in this Section via the stress development and distribution during both construction and operational phases. In order to study the stress distributions along the dam's height, maximum principal stresses have been plotted for different sections along the dam body as indicated in Figure 7.27. The Figure shows the variation of maximum principal stress along different sections, namely (a-a), (b-b), and (c-c) at the end of construction and different reservoir levels.

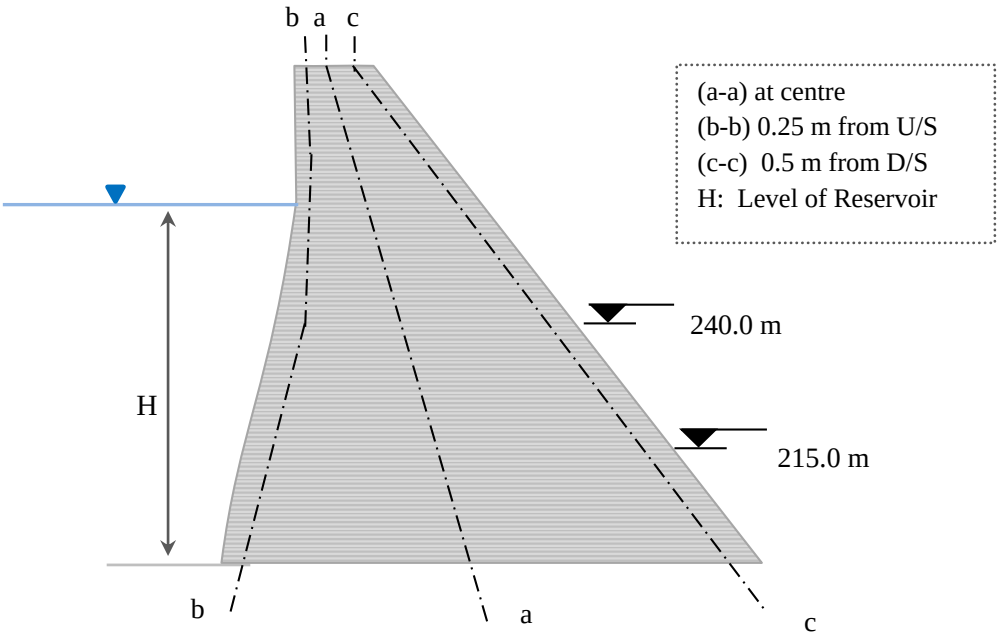

Figure 7.27 Diagram of the Dam

The maximum principal stress along section (a-a), is plotted in Figure 7.28(a). This plot shows that, the maximum value of the tensile stress is reached at the end of construction phase (1.4 MPa), at the lower part of the dam. However, the tensile stress has not exceeded the allowable tensile stress of concrete along the central section. Moreover, it is clear from the plot that, the first 0.2H is under tension and the rest of the height is under compression. It can be noticed that, the hydrostatic load does not have much effect on this section for the first 80% of the dam height. However, the hydrostatic load will increase the tensile stress significantly for the remaining 20% of the dam height and change it from 0.78 MPa (compressive) to 0.82 MPa (tensile) at the uppermost point of the dam.

Figures 7.28 (b) and (c) show the maximum principal stresses along the sections (b-b) and (c-c) (upstream and downstream). It is clear that, the tensile stresses are the highest close to both faces and reach values ranging between 3.12 MPa and 4.0 MPa, at the end of construction. This is due to high temperature gradient at the boundaries.

The plots also show that at the stream sides the tensile stresses are exceeding the allowable concrete stress and thus cracks in the directions of upstream and downstream will inevitably develop. However, the hydrostatic pressure reduces the tensile stresses at the downstream from 4.0 MPa to 1.6 MPa.

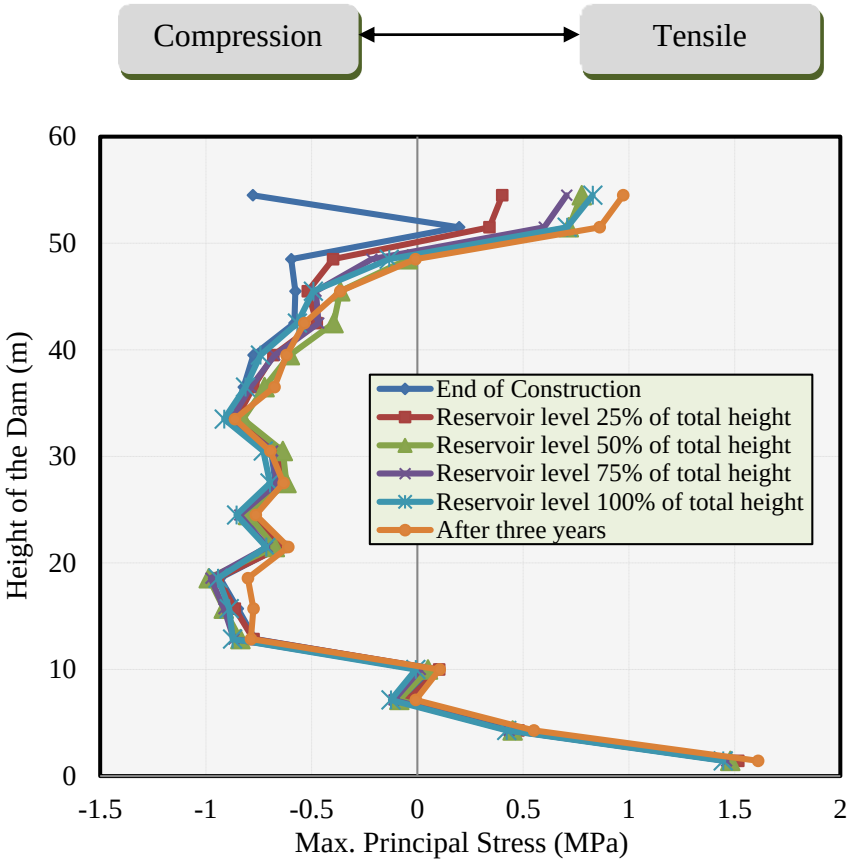

(a) Section a-a

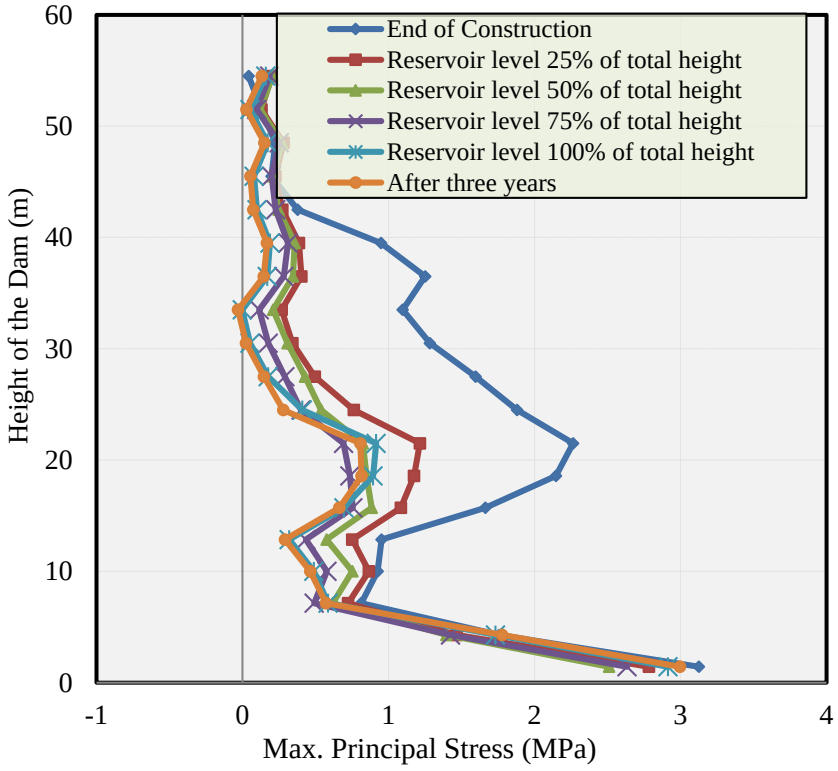

(b) Section b-b

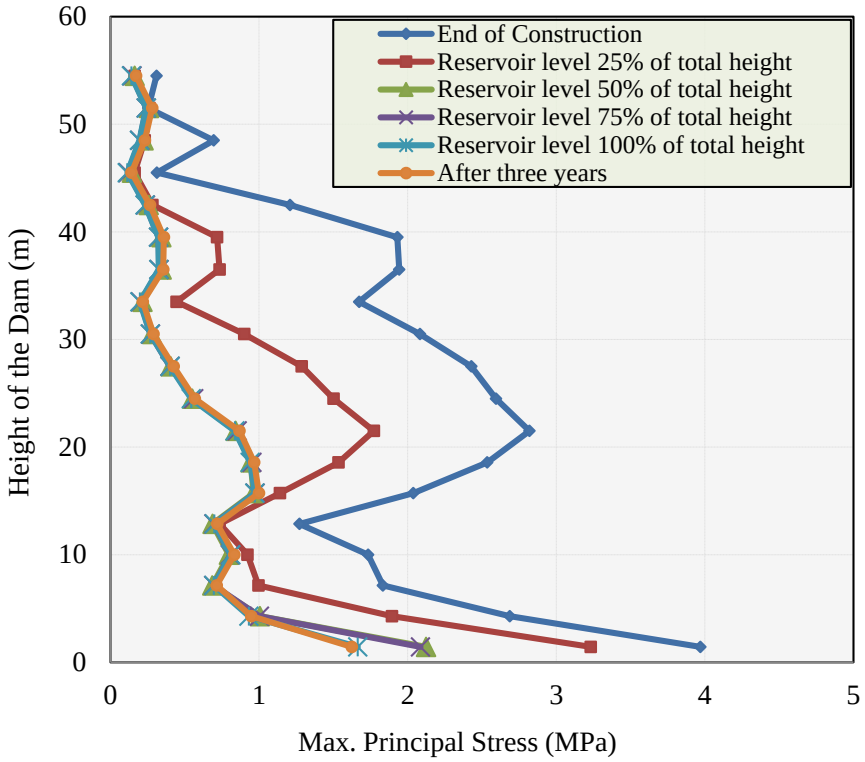

(c) Variation of Maximum Principal Stress along Section c-c

Figure 7.28 Variation of Maximum Principal Stress (MPa)

Figure 7.29 shows the variation of maximum principal stress across the block width (EL.215.0 m) at the end of construction and different reservoir levels. It is clear that, the tensile stresses are developed at the boundaries, with maximum value at the downstream face of 2.8 MPa at the end of construction. A maximum tensile stress value ranging between 2.2 MPa and 2.6 MPa develops in the vicinity of both faces

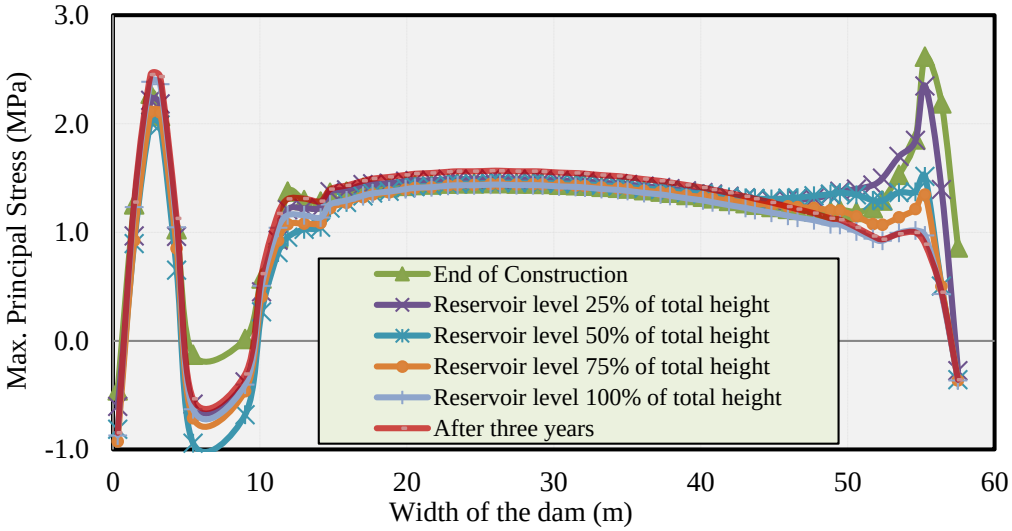

Figure 7.29 Variation of Maximum Principal Stress Path along the Dam Width (EL.215.0 m)

The distribution of the maximum principal stresses in the central part of the dam (block 13) around the gallery in January 2003 is shown in Figure 7.30. There are tensile stress concentrations in the upper part as well as the base of the gallery. However, the maximum tensile stresses in upper part of the gallery are not high enough to initiate cracks. The critical part is the base of the gallery, where the tensile stress is almost reaching the allowable tensile strength of concrete. Thus, special attention must be given to this region during the design and construction.

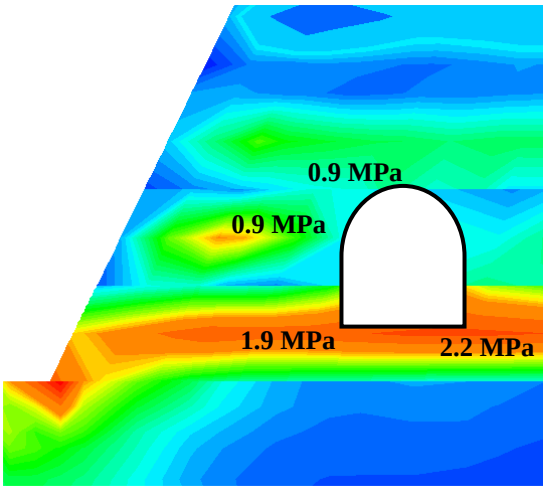

Figure 7.30 Stress concentrations around the Gallery (MPa)

7.3.5 Safety Evaluation of Zirdan RCC Dam against Cracking

In order to check the safety of the dam against cracking, an attempt is made to plot the crack safety factor at the second lift along the dam width at the end of construction, different reservoir levels and three years after the completion of dam construction.

Observing Figure 7.31, it is verified that, at the end of construction of the dam on the central region of the lifts, safety factor remains within the limit and the dam is safe against cracking; however, on the lateral parts (upstream and downstream faces), significant variations are observed and the crack index drops below the allowable limit (which is 1 in this case) due to high stress gradients. In addition, it is also observed that, the safety along this lift is improving after the reservoir is filled; especially at the downstream side, except for the upstream face that clearly shows the effects of gallery on forming the high tensile stress zones resulting in inevitable cracking.

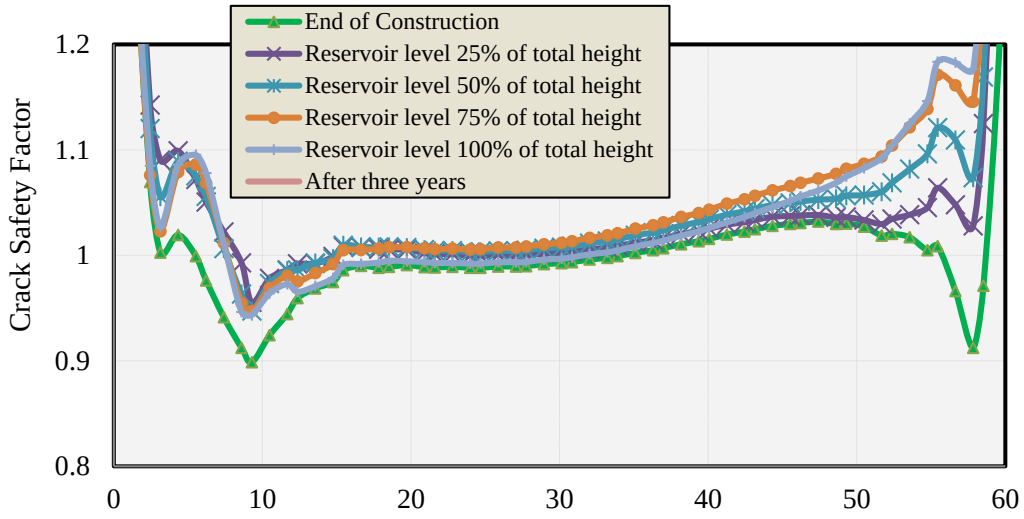

Figure 7.31 Safety Factors along the 2nd Lift

7.4 Discussion and Concluding Remarks

The capability of the developed system for thermal and structural analysis of gravity RCC dams has been demonstrated through analysing two real cases of RCC dams built in different environments during the construction process and after the first 3 years of service life of RCC dams. The first RCC gravity dam, namely, the Kinta RCC dam, is built in a tropical climate region in Malaysia and the second one is the Zirdan RCC dam built in a hot - dry climate region located in south part of Iran.

An elasto-plastic model is adopted to simulate the behaviour of RCC material. Ageing and temperature effects were considered in this approach by reformulating the experimental models of the RCC mechanical properties in a suitable normalized format so that it can incorporate the phenomenon of ageing and temperature effects. The same time intervals for the heat transfer problem and the stress analysis was used in this study (Araujo and Awruch 1998). Initially the thermal analysis was performed with time steps and the degree of equivalent hydration period was evaluated. Then, based on this, the elastic modulus was calculated. Simultaneously, during the stress analysis, the crack safety factor was calculated at each Gaussian point. Therefore, safety against cracking is guaranteed when the crack index is greater than 1.0 at the point under consideration.

According to the results of the analyses, the following could be concluded:

(i) The developed system is capable of simulating the thermal and structural response of RCC dams efficiently. This is clearly deduced from the reasonable temperature and stress distributions obtained from the two-dimensional analyses.

(ii) The capability of the developed system in incorporating the main features of the behaviour of concrete is shown for different conditions such as;

- The actual conditions of the site such as ambient temperature and wind speed.

- The evolution of the RCC mechanical properties with time and temperature, by reformulating the experimental models of the RCC mechanical properties in a suitable normalized format.

- Implementing appropriate boundary condition at the upstream side to simulate the temperature of the reservoir water variation with time and depth of the reservoir.

- The higher temperature zone was formed at the middle part of the dam body which gradually decreased to reach approximately the air temperature at the boundaries.

- The safety factor can give a good indication of the probability of crack occurring under stress states either in the short or the long term.

- The results have shown that, if the temperature effects are considered, the maximum principal stresses increase by 40% in the initial stage. This is because the temperature at the initial stage is high due to hydration. The temperature increase accelerates the initial elastic modulus of concrete which increased the stress during this stage.

- The maximum stresses develop mainly in the vicinity of both faces, where the temperature gradient is the highest. Thus, the upstream and the downstream regions are the most probable crack regions.

- An increase in the tensile stresses of about 11% to 20 % was observed after three years of dam completion. However, the locations and distribution shapes are mostly similar; this can be attributed to the cooling of the dam body with time.

CHAPTER 8

SEISMIC CRACKING ANALYSIS OF RCC GRAVITY DAMS UNDER THERMAL AND SEEPAGE EFFECTS

8.1 Introduction

Seismic safety evaluation of concrete dams under earthquake excitation is a complex problem and has been the subject of extensive research during the past decade. When such system is subjected to an earthquake, hydrodynamic pressures in excess of the hydrostatic pressures occur on the upstream face of the dam due to the vibration of the dam and impounding water. Consequently, the prediction of the dynamic response of the dam to earthquake loadings is a complicated problem and depends on several factors, such as interaction of the Dam with rock Foundation and Reservoir (DFR), and the computer modelling and the material properties used in the analysis. Therefore, appropriate methods of analysis and evaluation are required to accurately predict the overall stability of the dam during and at the end of the earthquake.

Large seismic events, in addition to the thermal and seepage effects, can cause the cracking and nonlinear behaviour and affect the stability of the hydraulic structures. Therefore, considering the importance of thermal and seepage loading on obtaining a reliable estimation of the final stress fields on structural behaviour of RCC dams, the seismic safety analysis of these structures should be considered including these loading combinations. Furthermore, the assumption of linear behaviour may not be appropriate in the analysis because tensile cracks will form and propagate in the concrete, affecting the fracture response of the concrete gravity dam.

Figure 8.1 illustrates a methodology for comprehensive seismic safety evaluation of existing concrete dams.

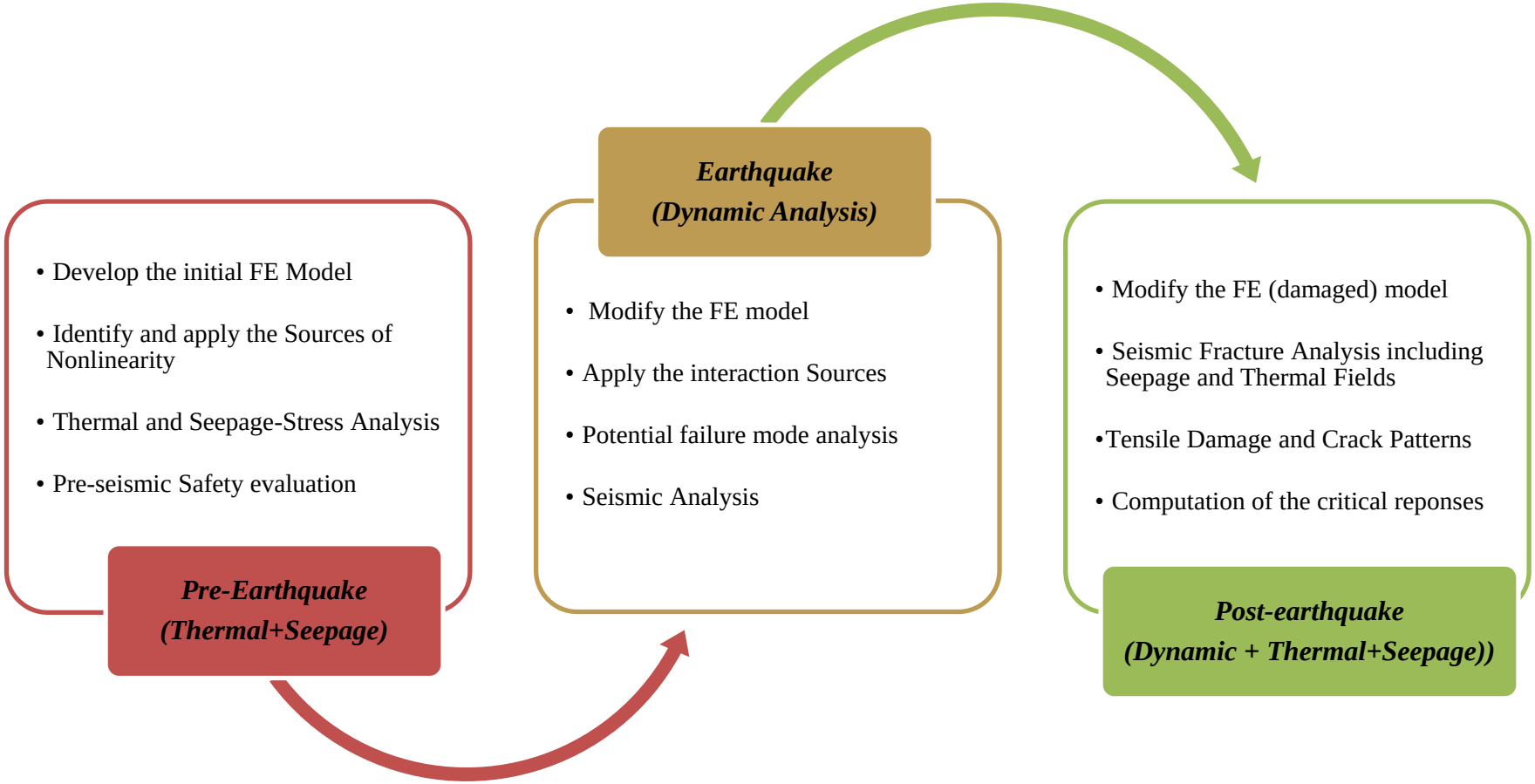

Figure 8.1 A Comprehensive Methodology for Deterministic Safety Evaluation of the Existing Concrete Dams

First, A finite element model is created and all the sources of nonlinearity (material, joints, geometry) are defined and then applied to the model. Coupled or uncoupled thermo-mechanical and hydro-mechanical analyses are implemented to determine the performance of the dam at the pre-earthquake condition. Pre-earthquake safety assessment of the concrete dams may be conducted for a relatively long period of time (based on the seismicity condition of the site). In such a case, safety evaluation analysis should include the ageing constitutive models. This step has been carried out in previous chapters by performing thermal and seepage analyses.

Second, a non-linear dynamic time history analysis of RCC dam is performed using the modified finite element code during strong earthquakes. The numerical modelling of concrete gravity dams involves material nonlinearities (the concrete in the body of the dam, the foundation material, and the water in the reservoir) and geometric nonlinearities (contact between the dam and the foundation, the dam and the reservoir, and the reservoir and the foundation).

Third, post-seismic analysis is performed at the end of earthquake taking into account the calibrated parameters obtained from the previous steps. Static stability analysis and seismic analysis are required to ensure the safety of the dam at this stage. Seismic safety evaluation of RCC dams including temperature and seepage fields during and at the end of earthquake i.e., second and third steps, are discussed in this Chapter.

Kinta Roller Compacted Concrete dam is selected as an application example to evaluate the response of the dam under seismic excitation. The analysis is performed on the deepest non-overflow section of Kinta dam. The structural response of the RCC dam subjected to the seismic excitation in terms of acceleration, displacement, stresses and cracking patterns accordance to failure mechanics are presented and discussed.

8.2 Seismic Analysis of Kinta RCC Dam including DFR Interaction

In this section, results from the seismic analysis performed on a numerical model of the Kinta RCC dam for both conditions of including and excluding inspection galleries are presented.

A system of openings is provided within the dam body to serve various purposes. The layout, size and shape of the openings are based on their requirements in a dam. Openings can develop a zone of tensile stresses, since concrete is not designed to take up any tension, it become necessary to reanalyse the dam section with openings. In this section, the effect of the existence of inspection galleries on evolution of tensile stresses and damage are studied.

8.2.1 General Characteristics

The detailed technical information of Kinta RCC dam including site geology, geometrical section and construction schedule are presented in Sections 5.3.1 and 7.2.1. The structural geometry of the non-overflow section (deepest section) and the location of the openings inside the dam body are illustrated in Figure 8.2 (Board of Engineers Malaysia (BEM), 2006).

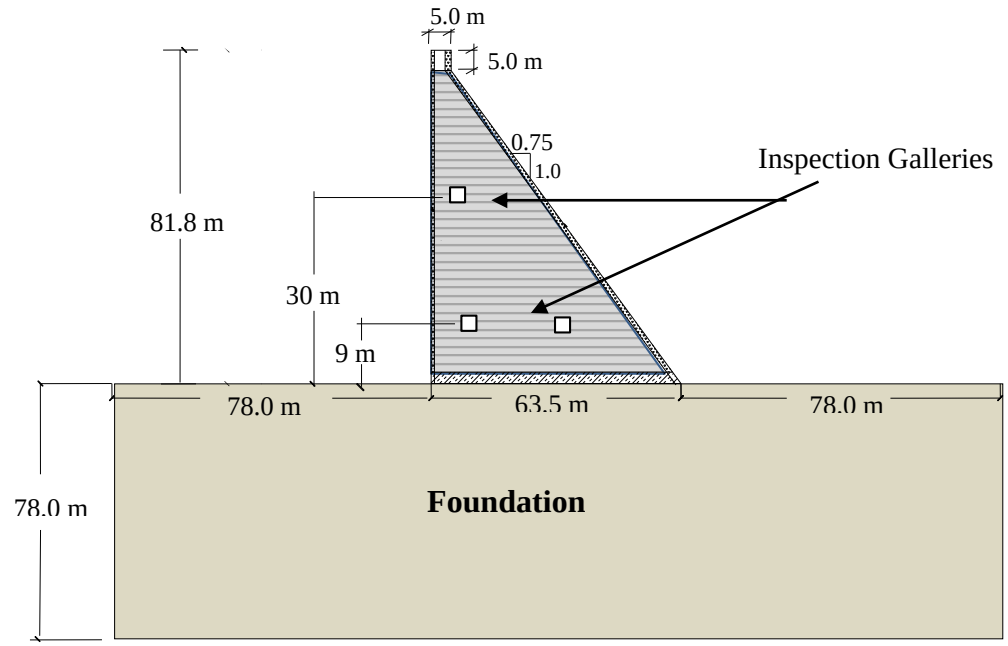

Figure 8.2 Structural Geometry for Kinta RCC Dam-Foundation System at the Deepest Section

8.2.2 Material Properties

The material parameters for the Rock foundation, RCC and CMC concrete which are used in the dynamic analysis are presented in Table 8.1. The properties are obtained from a technical report provided by GHD (2002). In addition, the tensile strength

values are considered as 10% of the compressive strength (US Army Corps of Engineers, 2000).

Table 8.1 Material Properties of the Kinta RCC Dam under Dynamic Condition

Material properties	Symbol	RCC	Foundation	CMC
Poisson's ratio	υ	0.2	0.2	0.2
Young modulus (GPa)	E	23	30	23
Mass density (kg/m^3)	ρ	2,325	2,650	2,325
Compressive strength (MPa)	f_c	20	18	20
Tensile strength (MPa)	f_t	2.5	2.25	2.5

Furthermore, the mechanical behaviour of the concrete material is modelled using the concrete damaged plasticity constitutive model. In obtaining some of these material properties, a number of assumptions are made. Of particular interest is the calibration of the concrete tensile behaviour.

To avoid unreasonable mesh-sensitive results due to the lack of reinforcement in the structure, the tensile post failure behaviour is given in terms of a fracture energy cracking criterion by specifying a stress-displacement curve instead of a stress-strain curve, as shown in Figure 8.3-a. Similarly, tensile damage is specified as a function of cracking displacement. This curve is shown in Figure 8.3-b.

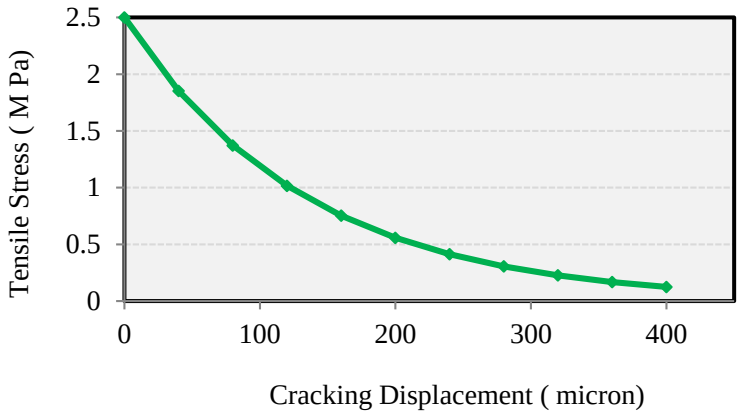

(**a) Tension Stiffening**

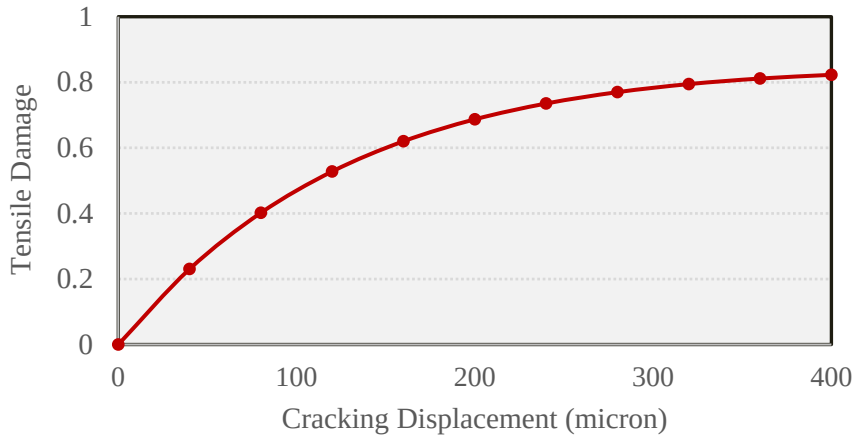

(b) Tension Damage

Figure 8.3 Tensile Properties of the Concrete

8.2.3 Finite Element Discretization

The 2-D finite element modelling of the Kinta dam is considered for the full reservoir and deepest block assuming plane stress behaviour. Figure 8.4 reveals the finite element mesh model of the dam body-foundation-reservoir (DFR) interaction including inspection galleries utilized in the analysis. In this case the dam body and foundation are modelled by CPS8R elements (8-noded bilinear plane stress quadrilateral, reduced integration, hourglass control). In addition, the reservoir water is modelled by AC2D8 elements (8-noded 2-D acoustic quadrilateral) using finite element software ABAQUS. The details of finite element mesh model excluding galleries are as described in Section 7.2.2.

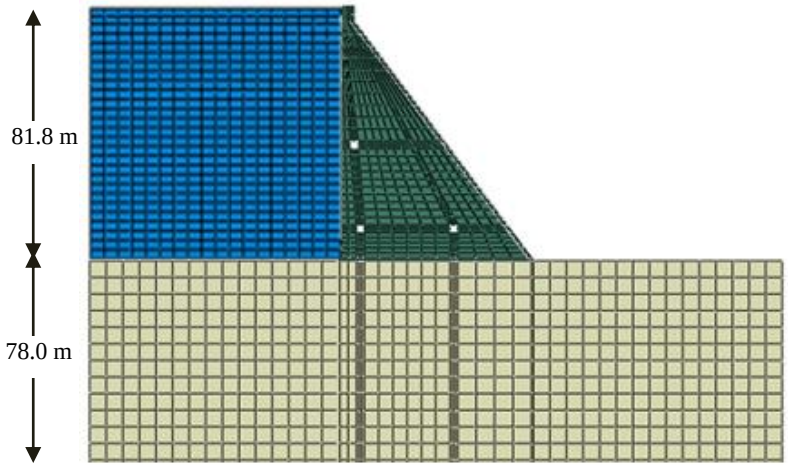

Figure 8.4 Finite Element Mesh Model of Kinta RCC Dam including Dam body-Foundation-Reservoir (DFR) Interaction

8.2.4 Loading Conditions

In the nonlinear dynamic analysis of RCC dams, both static and seismic loading are considered as follows;

- **Static Loading**

Prior to the dynamic simulation of the earthquake, the dam is subjected to gravity loading of the dam body and hydrostatic pressure on the upstream face of the dam as static loading conditions. These static forces acting on gravity dam are illustrated in Figure 8.5.

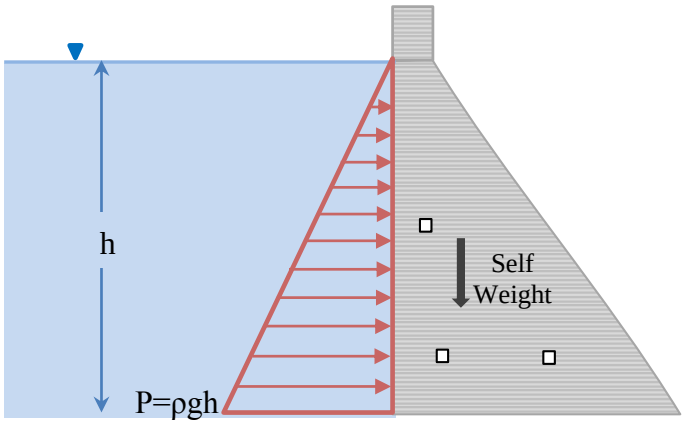

Figure 8.5 Static Loading on the RCC Dam, Considering Hydrostatic Pressure of Reservoir

- **Dynamic Loading**

Earthquake or seismic loads are the major dynamic loads (Major 1980, Schoeber 1981, Polyakov 1985, Wyatt 1989) being considered in the analysis and design of dams especially in earthquake prone areas. Both horizontal and vertical components of Koyna earthquake with peak ground acceleration (PGA) of 0.63g and 0.49g, respectively, are employed for the purpose of seismic analysis of Kinta dam. These records are given in Figure 5.33 in Chapter 5. As shown in these two graphs, duration of the motion is only 10 seconds. The peak ground acceleration for horizontal motion is at 3.13 seconds and for vertical acceleration is at 3.8 seconds, respectively.

In addition, during seismic excitation the motion of the dam causes a portion of the water in the reservoir to also move. Acceleration of this added mass of water produces pressures (hydrodynamic pressure) on the dam that must be taken into

account in dynamic analysis. This dam–reservoir dynamic interaction (hydrodynamic pressure), shown in Figure 8.6 resulting from the transverse component of ground motion can be modelled in a simple form of modelling reservoir using acoustic elements. The hydrodynamic pressures resulting from the vertical component of ground motion are assumed to be small and are neglected in all the simulations.

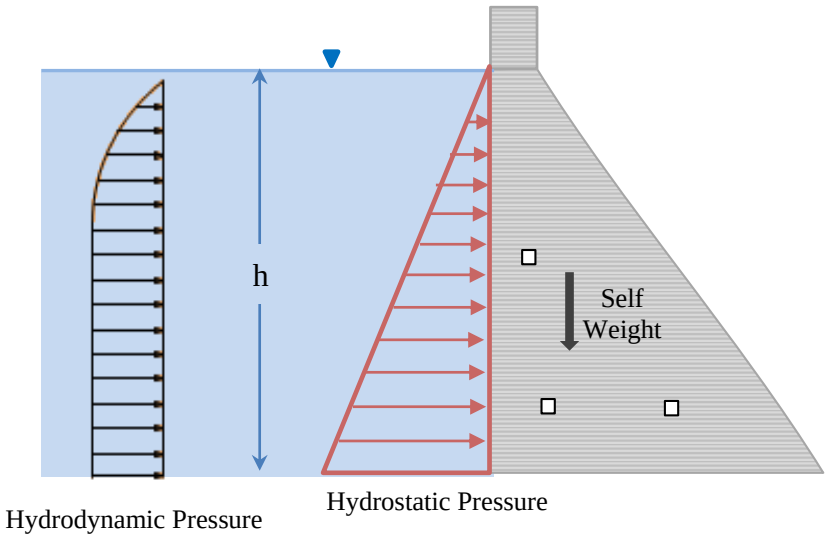

Figure 8.6 Dam-Reservoir Hydrodynamic Interaction

Furthermore, it is obvious that the damping ratio in the dynamic analysis problems, and particularly for RCC dams, is one of the important factors (Horii and Chen 2003). To get the real behaviour of dams under dynamic analysis, the damping of 5% of critical has been adopted similar to the previous research works (Mao, 1997; Horii, 2003). In this research the damping ratio was obtained for the whole RCC dam under free vibration condition. Due to this calculation the natural frequencies ω_1 and ω_2 with values of 9.571 and 51.238 rad/sec pertaining to first and secondmodes of vibration are calculated. This approach leads the values of $\alpha = 0.806$ and $\beta = 0.00164$ (Chopra, 2001) to be used when estimating damping by adopting Raileigh damping.

8.2.5 Analysis Results and Discussion

The nonlinear seismic fracture analysis of Kinta RCC Dam is carried out considering the effect of the dam-foundation- reservoir (DFR) interaction. Furthermore, the effects of galleries on the evolution of tensile stresses and damage are studied. The

response of the dam and its safety evaluation in terms of stresses, displacements and predicted crack patterns are presented and discussed as follows;

- **Stress Distribution**

To visualize the stress distribution in the dam body for the critical stress states Figures 8.7 and 8.8 display the maximum and minimum principal stress contours. Four different time steps are considered to compare the analysis results for both cases of including and excluding inspection galleries, respectively. It is clear from the plots that the distribution pattern of the stresses is approximately the same for both cases of with and without galleries situations; however, the values are different.

It is observed in part (a) of Figure 8.7 that at t = 1.5 sec, the crest of the dam vibrates in the downstream direction, showing that the heel of the dam is in tension. At this time, the maximum principal stress at the heel reaches 1.15 MPa considering the galleries and is 0.438 MPa neglecting the effect of openings, respectively.

In addition, on the upstream side of the neck of the dam, as the upper block of the dam oscillates towards the downstream side at times t =3 sec and t =4 sec, (parts (b) and (c) of Figure 8.7), the upstream face and the base of the dam near the heel is being stretched and maximum tensile stress concentration occurs in these regions. The increase of stress on the upstream face is perhaps associated with the sudden growth of transverse and vertical components of the ground accelerations which occurs within the time period of 3 to 4 Sec (Figure 5.33).

Furthermore, the plots clearly demonstrate that, the openings (inspection galleries) cause the maximum principal stresses to be slightly increased (by approximately 20%) and make the stress concentration around the galleries more obvious when compared to the stresses neglecting the openings.

The distribution of the maximum stresses at the end of the earthquake is shown in Figure 8.7(d), at time t=10 sec. Higher tensile stress zones are identified at the base of the dam’s body, top upstream and top downstream sides of the neck of the dam. However, due to openings, there is increase in stresses around the openings and in the dam.

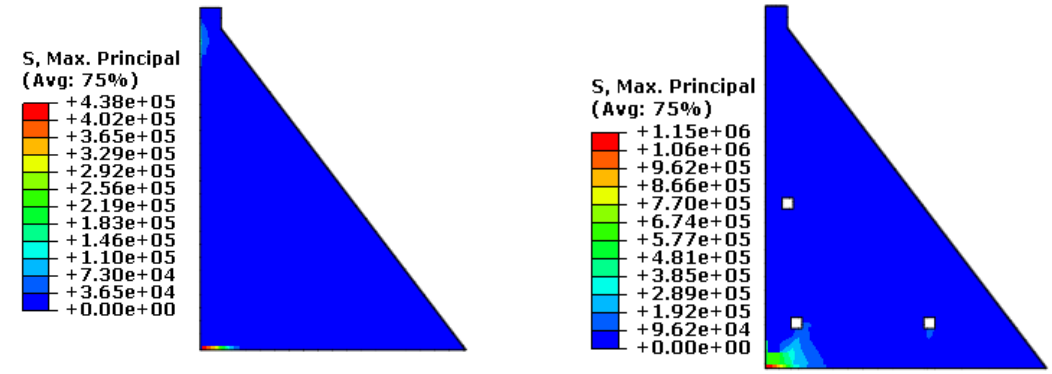

(a) Time= 1.5 Sec

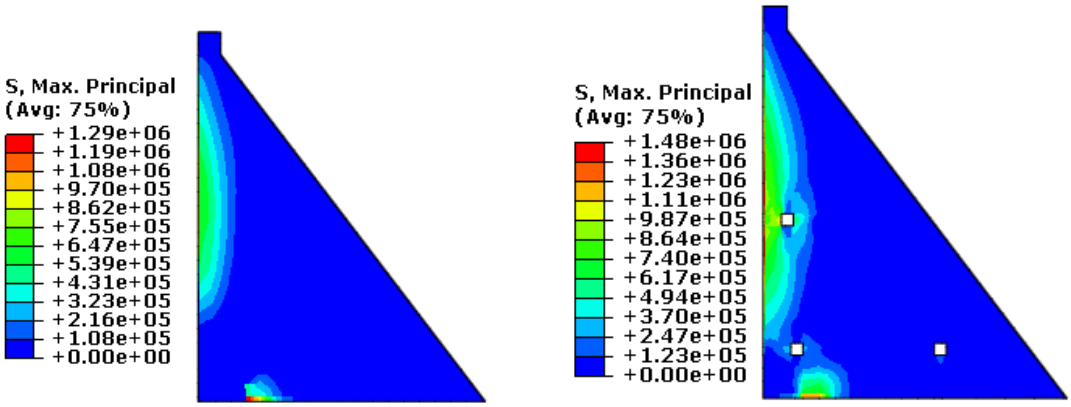

(b) Time= 3 Sec

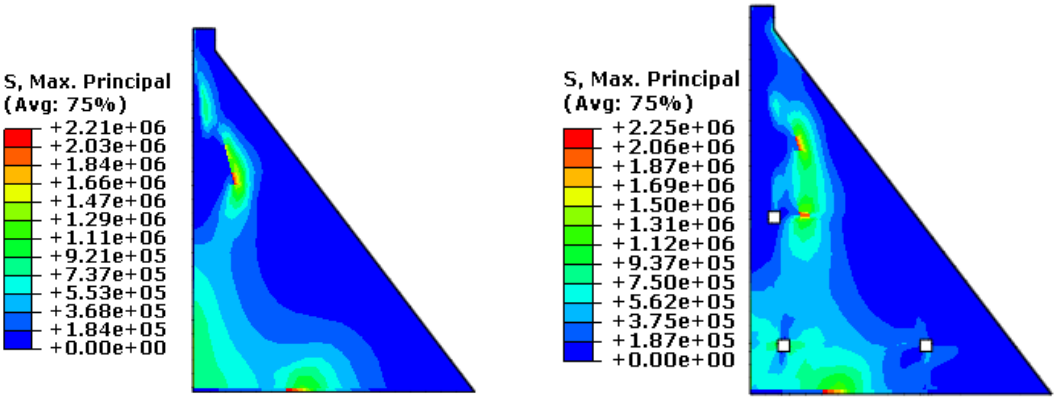

(c) Time= 4 Sec

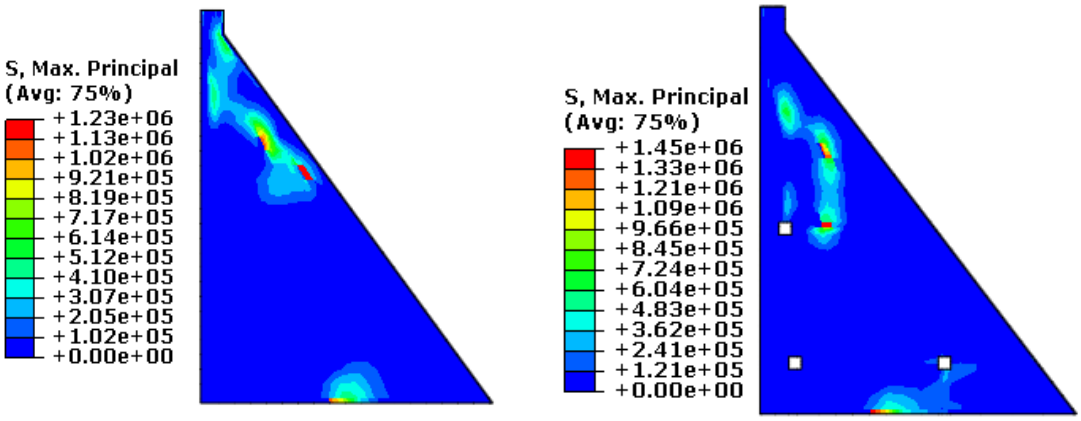

(d) Time= 10 Sec

Figure 8.7 Distribution of the Maximum Principal Stresses (Pa) in the Presence and Absence of Inspection Galleries

Figure 8.8 shows the distribution of the minimum principal stresses (Pa) at the end of earthquake. It is clear from the plots that, the upper block of the dam moves toward downstream which results in compression of the downstream side of the neck and toe of the dam. On the other hand, high compressive stress zones are concentrated at the downstream face and toe of the dam, which gradually reduces toward the crest of the dam. In addition, a small region of high compressive stress has been observed at the lower part of the upstream, especially at the toe.

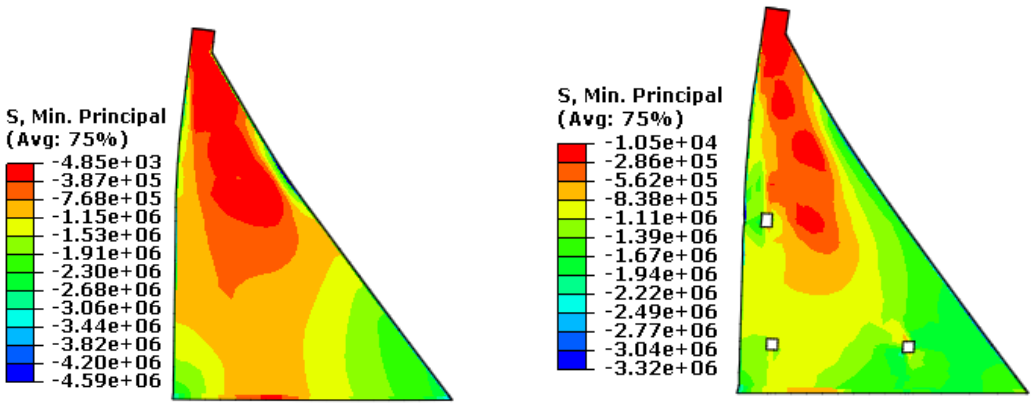

Figure 8.8 Minimum Principal Stress Distribution in Body of the Dam (Pa) at time t=10 sec

- **Displacements Variation**

An attempt has been made to plot the relative horizontal time history displacement of the dam body considering the DFR interaction. The displacements of the topmost (crest node) and lowest node of the dam body at upstream face are selected for the purpose of the analysis. These points are depicted in Figure 8.9.

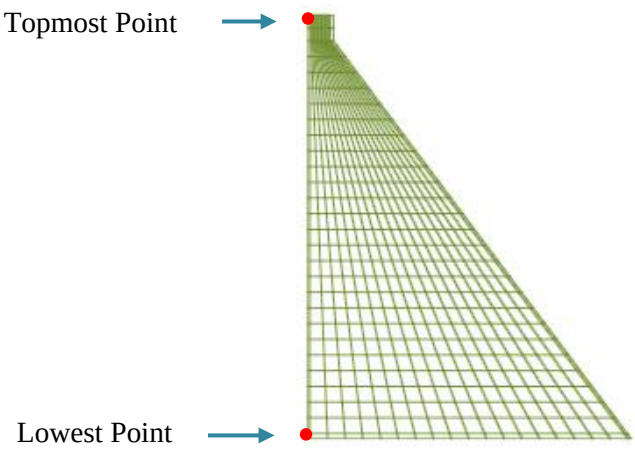

Figure 8.9 Location of Topmost and Lowest Point at the Upstream

Figure 8.10 illustrates the horizontal deformation of Kinta RCC dam at the end of earthquake, without and with gallery openings, respectively. It is clear from the plots that, the displacement of the dam increases with height for both conditions of including and excluding the gallery effects. However, the existence of openings decreases the settlement of the dam in contrast to neglecting the galleries as shown in Fig 8.10. The maximum displacement occurs in the dam crest with a value of 9.47 cm considering the opening effects. Whereas, excluding the effects of galleries increases the maximum value of deformation even further to 12.5 cm.

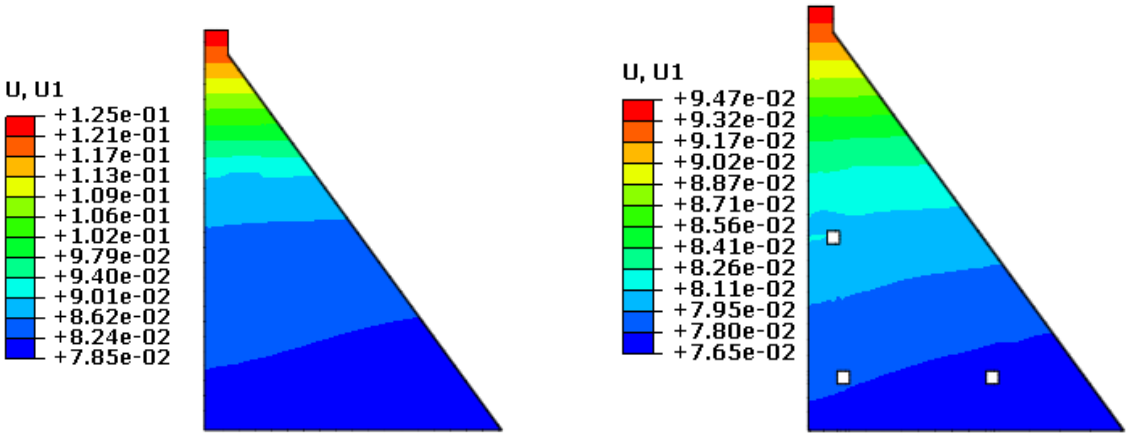

(a) Without Inspection gallery **(b) With Inspection gallery**

Figure 8.10 Horizontal Displacement Distribution (m)

Figure 8.11 shows the horizontal displacement at the left corner of the crest of the dam relative to the ground motion. The crest displacement (topmost point) remains

less than 30 mm during the first 3.5 seconds of the earthquake. However, after 3.5 seconds, the amplitude of the oscillations of the crest increases substantially.

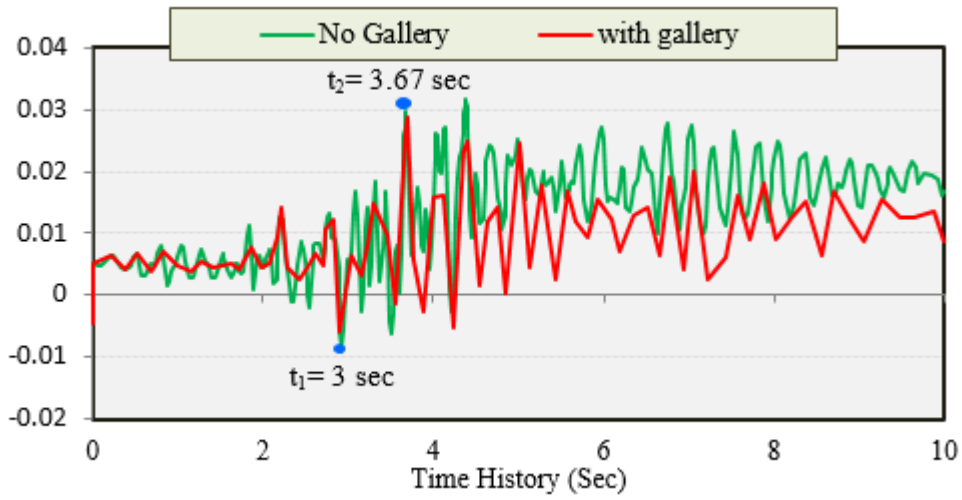

Figure 8.11 Horizontal Crest Displacement (relative to ground displacement)

- **Tensile Damage and Crack Patterns**

The nonlinear damage response of the dam, indicating the crack pattern, under seismic excitations is presented in this section. The concrete material remains elastic with no damage at the end of the second stage, ie, after the dam has been subjected to the gravity and hydrostatic pressure loads. Damage to the dam initiates during the seismic analysis in the third stage.

The evolution of damage in the concrete dam at different times during the earthquake is illustrated in Figure 8.12. Times t_1=3 sec and t_2=3.67 sec correspond to the first large excursions of the crest in the upstream and downstream directions respectively, as shown in Figure 8.11. Time t= 10 sec corresponds to the end of the earthquake.

At time t_1, damage has initiated at the base of the dam on the upstream face for both cases of including and excluding gallery effects. When the dam displaces toward the downstream direction at time t_2, the damage at the base leads to the formation of a localized crack-like band of damaged elements. This crack propagates into the dam along the dam–foundation boundary. At this time, some partial tensile damage is also observed on several elements along the upstream face leading to the formation of a horizontal crack that propagates toward the downstream crack. Moreover, it should

be noted that, by considering the effects of the opening, the cracking pattern is varied slightly and tensile damage is localized at the place of openings.

The distribution of tensile damage at the end of the earthquake is shown in Figure 8.12(c), at time t=10 sec. It can be seen that, the severe damage to the structure develops at this time.

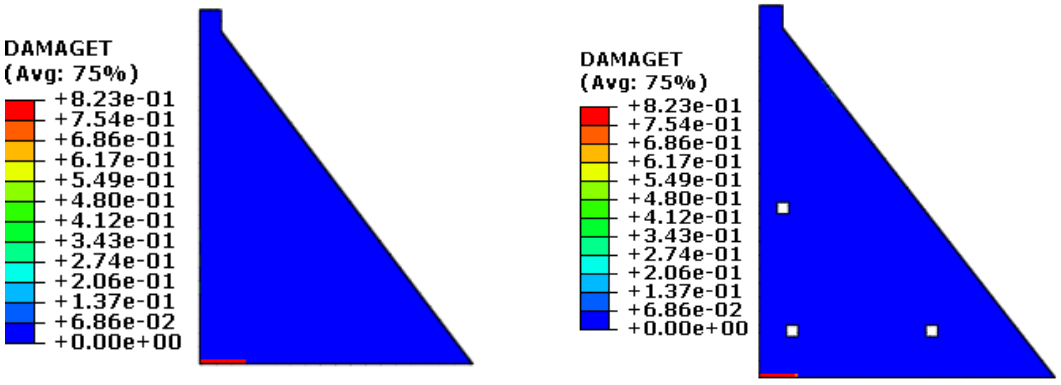

(a) t_1= 3 Sec

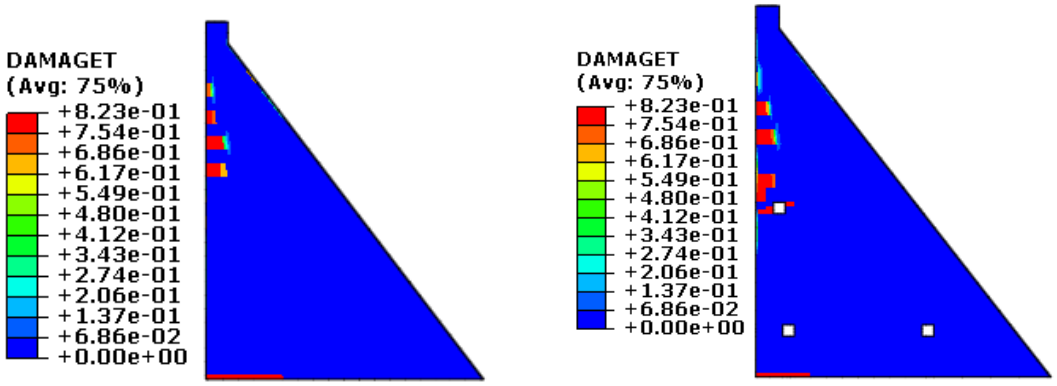

(b) t_2= 3.67 Sec

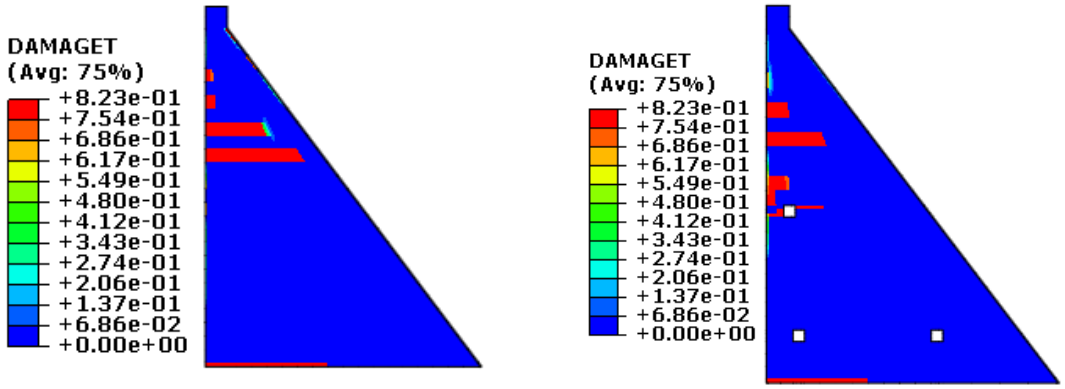

(c) t_3= 10 Sec

Figure 8.12 Evolution of Tensile Damage

Furthermore, failure mechanisms of some selected elements within the dam body (Figure 8.13) are plotted in Figure 8.14. In this case, heel elements are selected as these elements are the first elements to experience damage and cracking during the earthquake.

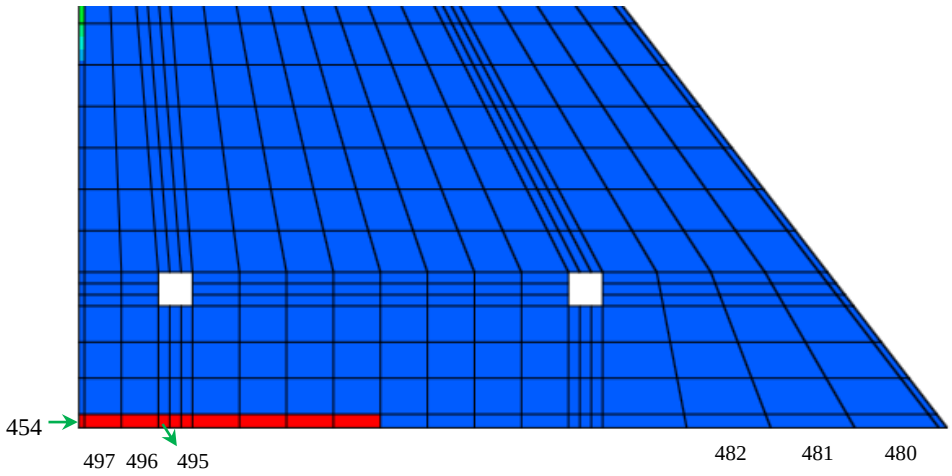

Figure 8.13 Selected Elements to Evaluate the Failure Mechanism of the Dam

It is noted that the time at which the cracks form at the dam heel (dam-foundation interface) is much earlier than when they appear at the upper part of the dam body. It appears that in the strong phase of the earthquake motion, i.e. after 2.5 sec, the formation of crack-like damage is visible in the heel region on the upstream side of the dam body. This can be attributed to the fact that the concrete-rock interface bond strength is likely to be lower than the parent concrete (Danay and Adeghe 1993).

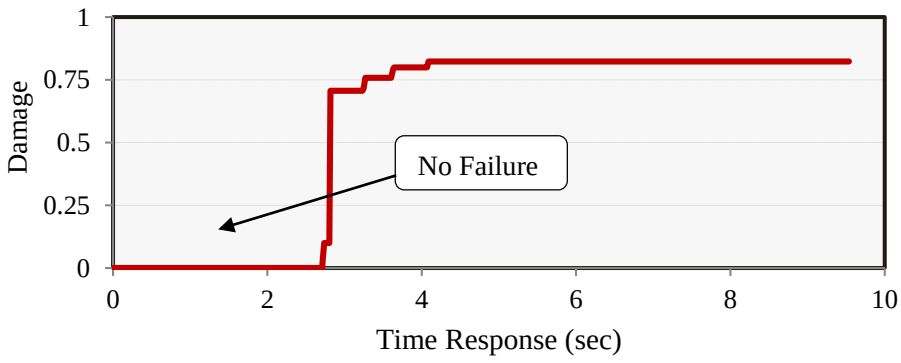

(a) Element No.454

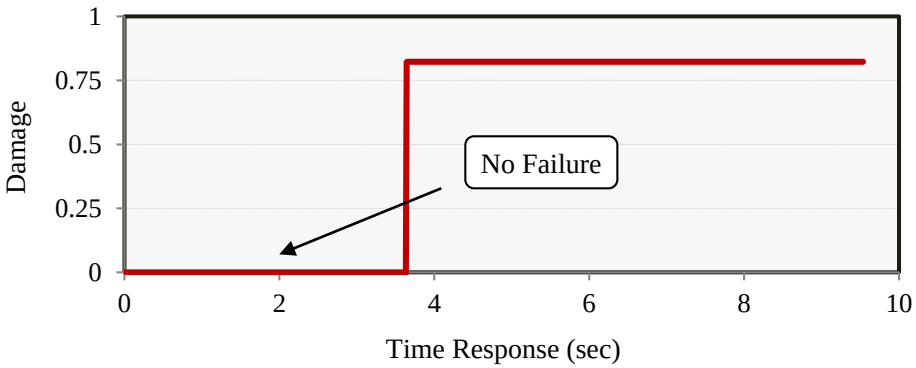

(b) Element No.497

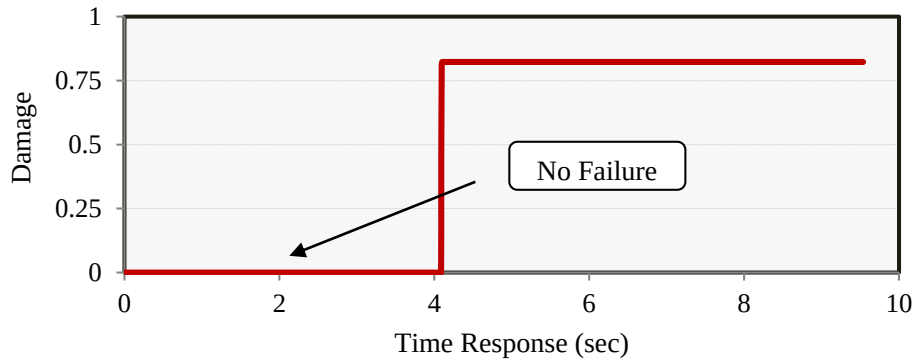

(c) Element No.496

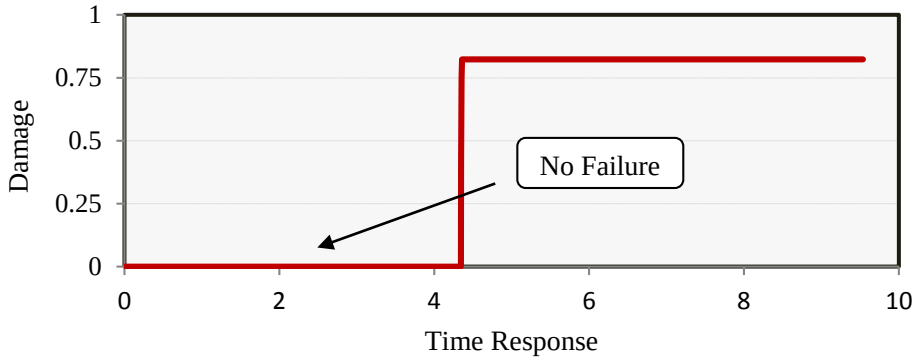

(d) Element No.495

Figure 8.14 Time History Response and Failure Mechanism of Selected Elements during Koyna Excitation

8.3 Seismic Fracture Analysis of RCC Dam Including Seepage-Thermal Effects

Seismic safety evaluation of Kinta RCC dam including Thermo-Hydro-Mechanical (THM) model during and at the end of earthquake is discussed in this section. The analysis is performed on the deepest non-overflow section of Kinta RCC dam.

The thermo-hydro-mechanical model is used for the simulation of combined thermal, seepage, and mechanical fields. Then in the sequential analysis, the combined thermal-seepage analysis is followed by the nonlinear time history seismic analysis. During the heat transfer and flow analysis, the stress distributions are recorded in the ABAQUS results file. This stress-time history is then used as input to the dynamic-stress analysis. The structural response of the RCC dam subjected to the seismic excitation including thermal and seepage fields in terms of acceleration, displacement, stresses and cracking patterns according to failure mechanics are presented and discussed.

8.3.1 Principal Stress Distributions

The maximum and minimum principal stress plots of the dam body are presented and compared in Figure 8.15 and Figure 8.16 respectively, with and without the effect of thermal-seepage fields. The maximum stress profiles (Figure 8.15-a to 8.15-d) are fairly similar, although the seismic stress response is slightly more severe in the presence of THM model. In addition, the minimum principal stress patterns (Figure 8.15-e) are also found to be similar for both cases of considering and neglecting temperature and seepage fields.

It is observed in part (a) of Figure 8.15 that the heel of the dam is in tension. Besides, at the same time (t=1.55 sec) the downstream face of the neck is being stretched and there is an increase in stresses by about 50% in this region taking into account the THM effects.

Furthermore, it is shown in Figure 8.15 (parts “b” and “c”) that the maximum stress response for excitations including seepage and temperature effects are larger than those excluding these affects. In general, at the upstream neck and heel of the dam, the maximum principal stresses have almost approached the concrete’s tensile

strength (2.07 MPa) for both cases of without and with THM model (Figure 8.15-c), which indicates that tensile damage is likely to take place in the vicinity of the upstream face of the neck and heel of the dam body.

At the upstream face of the dam neck at the time t=3 sec, although the maximum principal stress of the former case (1.29 MPa) is still smaller than the concrete's tensile strength (2.07 MPa), the maximum principal stresses for the latter case in the same regions along with downstream neck, are higher than the concrete's tensile strength, indicating that in this case tensile damage may also occur at the downstream face of the neck in addition to upstream neck and heel of the dam.

Finally at the end of earthquake at time t=10 sec, as shown in part (d) of Figure 8.15, the dam body vibrates in the upstream direction, resulting in an increase of the downstream tensile stress especially in the downstream neck and the toe of the dam. However, on the downstream side, the peak maximum principal stresses with and without THM model are 1.66 MPa and 1.23 MPa, respectively.

Figure 8.16 shows the distribution of the minimum principal stresses (Pa) at the end of earthquake for both conditions of considering and neglecting the thermos-hydro-mechanical effects. It is clear from the plots that, the downstream side of the base and toe of the dam are in compression. On the other hand, high compressive stress zones are concentrated at the downstream face and toe of the dam, which gradually reduces toward the crest of the dam.

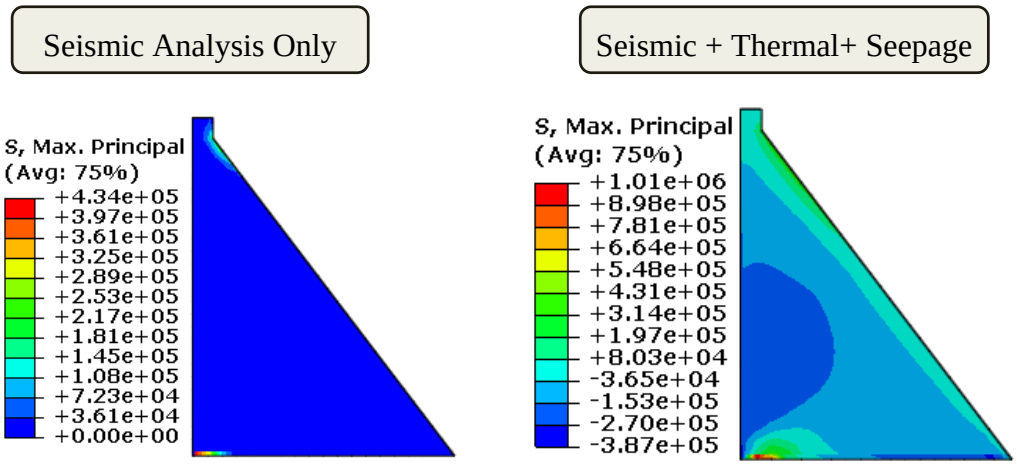

(a) Time = 1.55 sec

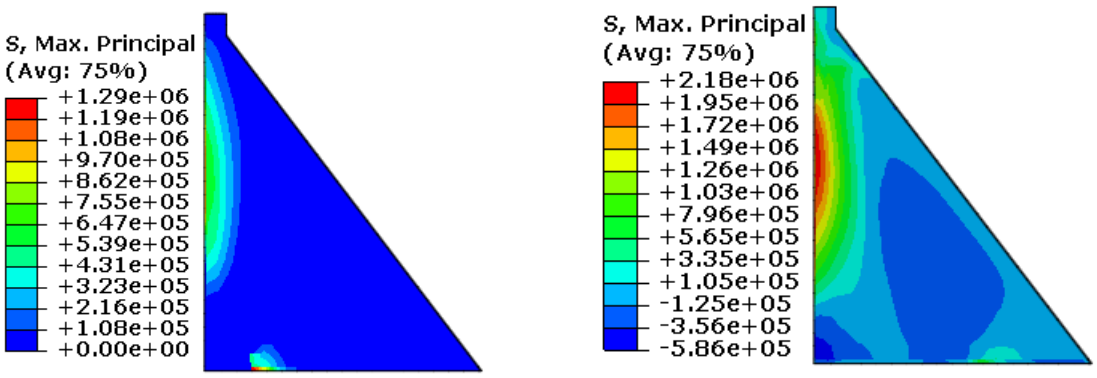

(b) Time = 3 sec

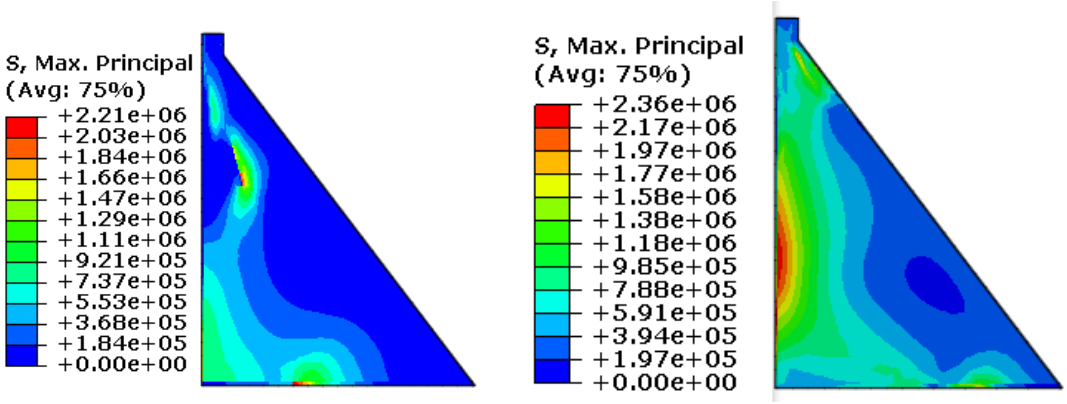

(c) Time = 4 sec

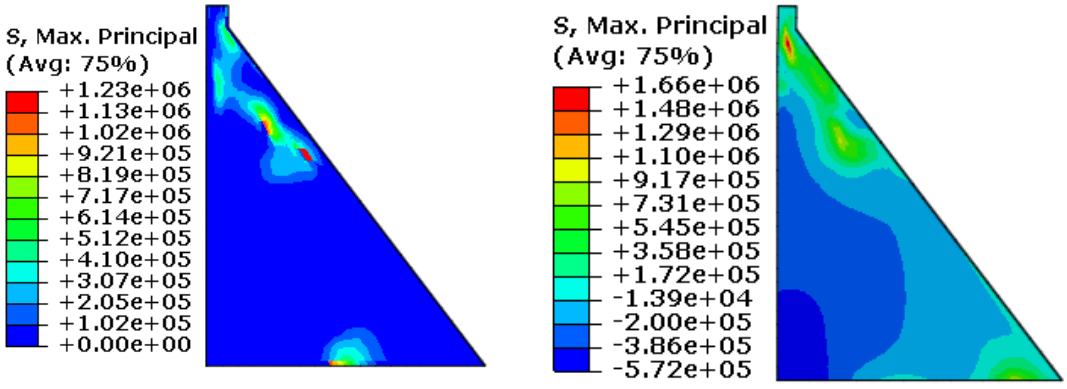

(d) Time = 10 sec

Figure 8.15 Comparison of Maximum Principal Stresses of the Dam Body with and without the Thermal-Seepage Effects (Pa)

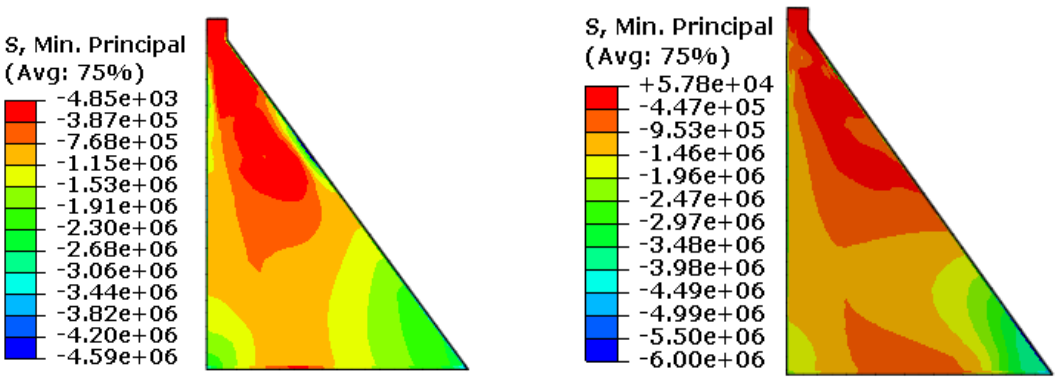

Figure 8.16 Minimum Principal Stresses of the Dam Body with and without the Thermal-Seepage Effects at the end of Earthquake (Pa)

8.3.2 Acceleration Variation

Figure 8.17 shows the distribution of the spatial acceleration of the dam body during and at the end of earthquake. It is observed that, the variation of acceleration in the lower region of the dam body is small while with increasing height of the dam, the acceleration tends to growth significantly specially in the case of considering the thermal and seepage effects.

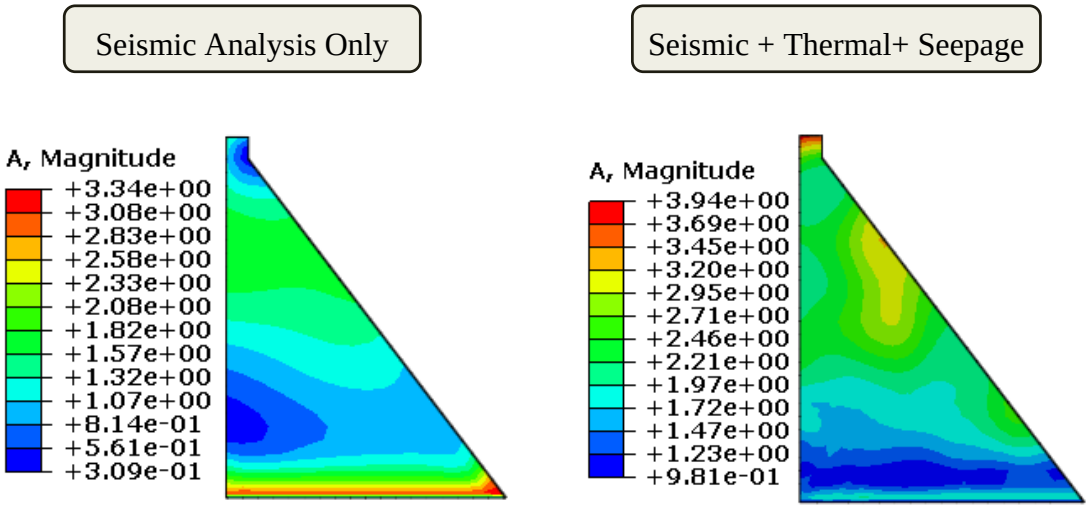

(a) Time = 1.55 sec

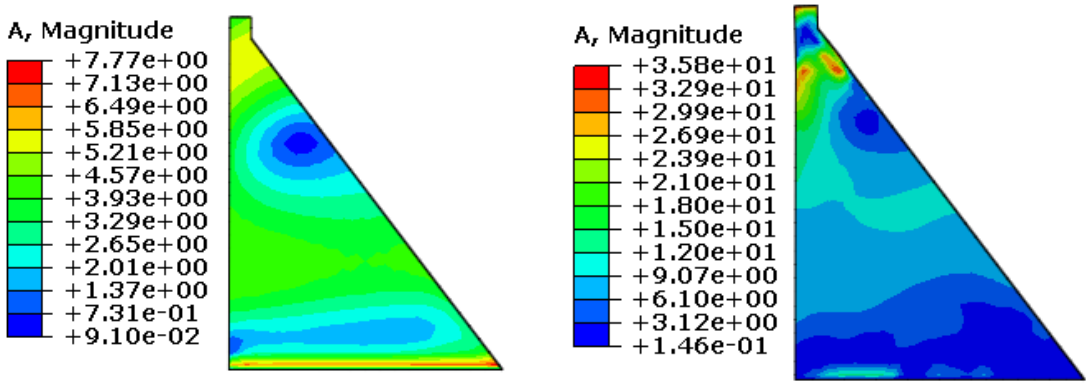

(b) Time = 3 sec

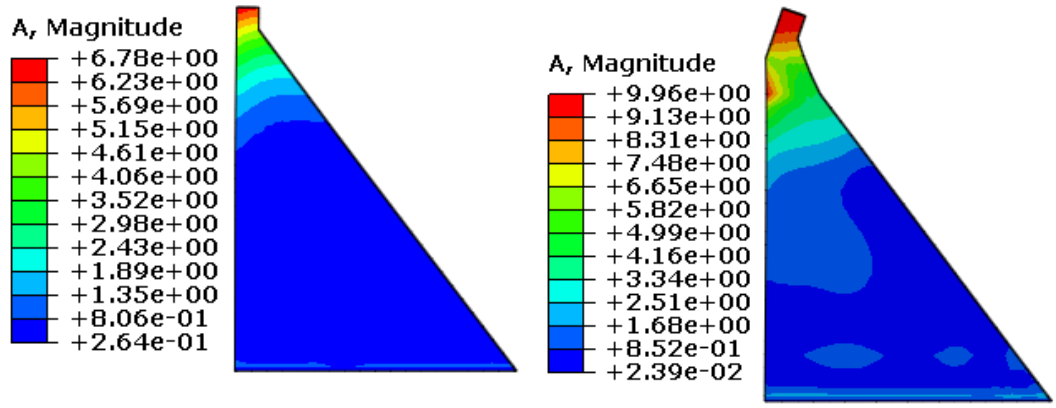

(c) Time = 10 sec

Figure 8.17 Peak Acceleration Distribution (m/s^2) of the Dam Body

The nonlinear relative acceleration response at the dam crest for excitations including the seepage and temperature effects and neglecting these affects is presented in Figure 8.18. It is found that in both conditions major large peak accelerations are experienced in the time range from approximately 2 sec to 7 sec.

In the first 3.5 sec, a clear trend of increasing acceleration response is observed for the two acceleration time histories. During the time interval between 3.5 sec and 5 sec, the nonlinear acceleration response in the presence of thermal and seepage actions substantially deviates from those of neglecting THM model, indicating that severe cracks have formed and propagated inside the dam. The damage caused by the cracks increases the vibration period of the system and renders the structure more flexible. After 5 sec and for the remainder of the time histories except for at about 7

sec, the response amplitude values are descending . The large accelerations in excess of 3 g will not cause any major issues except for sensitive and electronic equipment housed near the dam crest which are likely to suffer from such high acceleration levels.

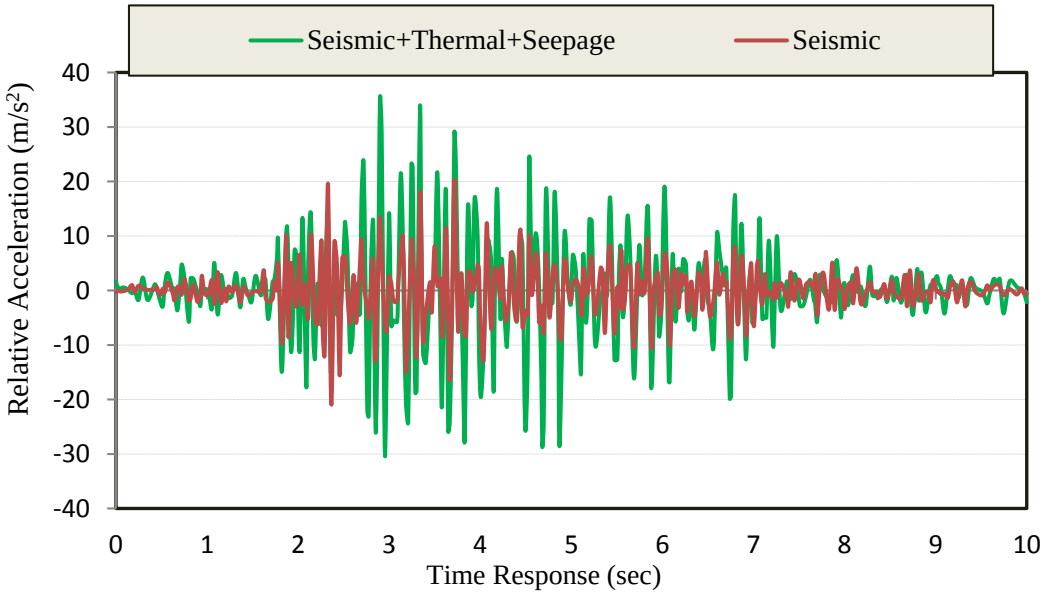

Figure 8.18 Relative Acceleration of the Crest Node at the Upstream Face of the RCC Dam

8.3.3 Displacements Variation

The total and horizontal displacement variations of Kinta RCC dam are shown in Figure 8.19 for both cases of seismic analyses including and excluding thermal-seepage effects. The former analysis indicates that considering the thermal and seepage loading increase the maximum horizontal and total displacements by approximately 50% in upstream and downstream directions at crest (Figures 8.19-b and 8.19-d). It clearly shows the effect of loading combinations on the deformation response of the dam. In addition, it is noted that in these contours, the deformation of the dam has been enlarged by a scale factor of 50.

The crest displacements on the upstream face of the dam relative to the ground are compared in Figure 8.20. The two displacement time histories are almost identical in pattern, although the response with THM model yields greater amplitudes than that without thermo-hydro-mechanical field. Therefore, it appears that combined loading tends toward a higher motion at the crest of the dam.

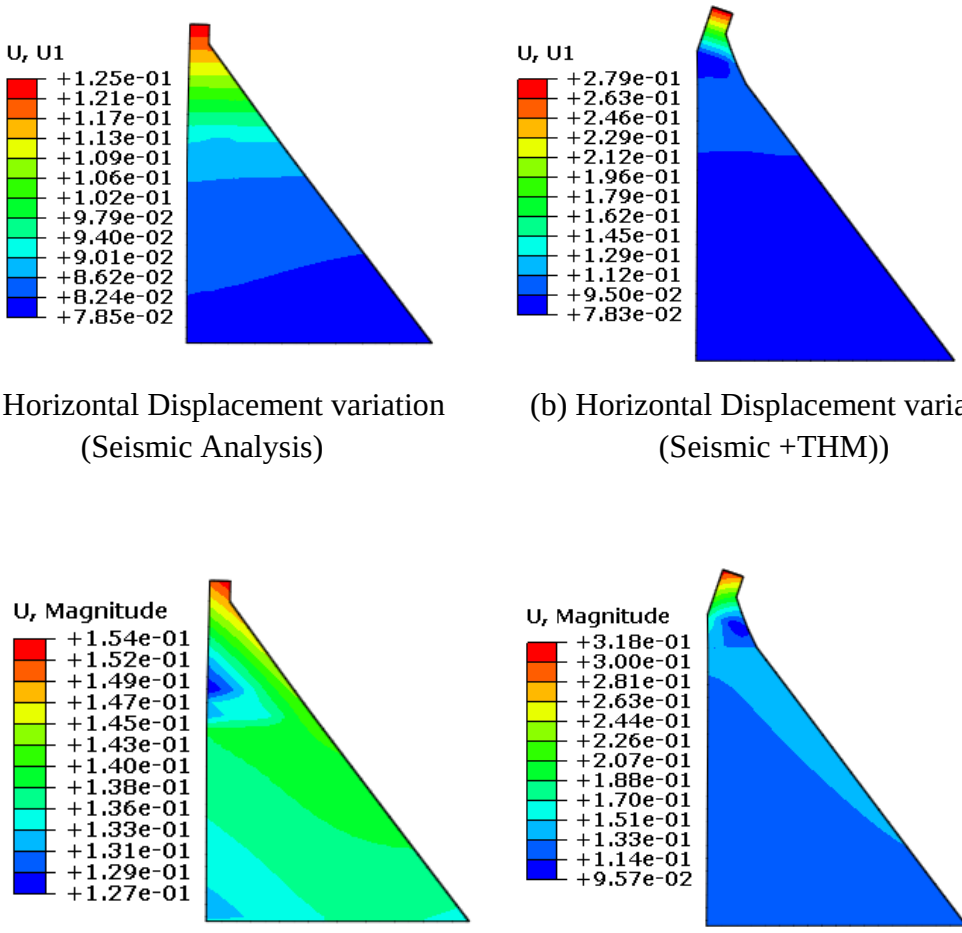

(a) Horizontal Displacement variation (Seismic Analysis)

(b) Horizontal Displacement variation (Seismic +THM))

(c) Total Displacement variation (Seismic Analysis)

(d) Total Displacement variation (Seismic +THM)

Figure 8.19 Displacement Distribution Contours (m)

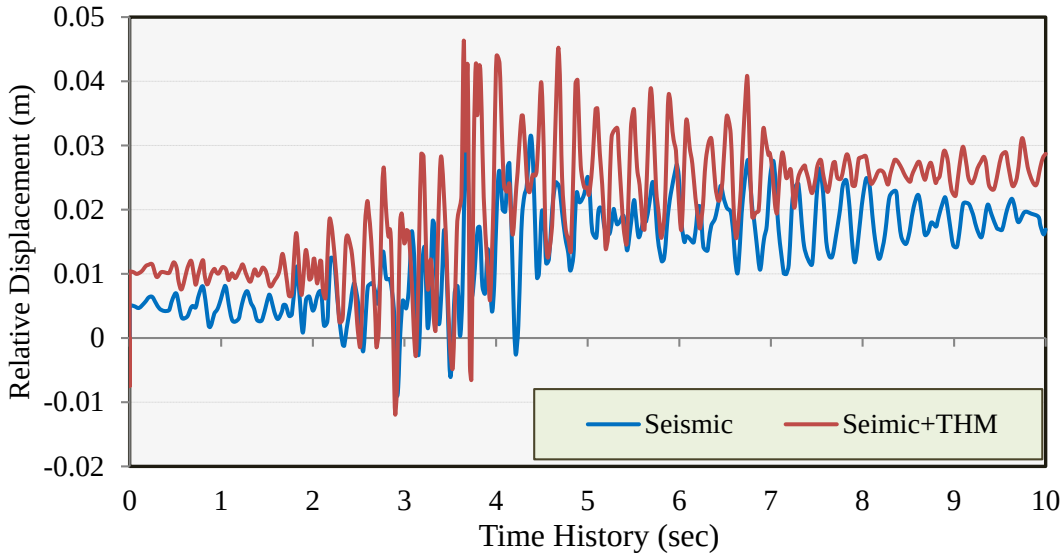

Figure 8.20 Comparison of Relative Displacement at Crest of the RCC Dam at Upstream Face

8.3.4 Tensile Damage and Crack Patterns

The nonlinear damage response of the dam pertaining to seismic excitations including seepage and thermal effects and excluding these effects are presented in Figure 8.21 at four selected time instants, which represent the evolution of the cracking process in the dam.

It is observed in part (a) of Figure 8.21 that, the damage in the dam body initiates at t=1.7 sec when the crest of the dam moves in the downstream direction while considering THM model. At this time, the formation of crack-like damage is visible in the heel of the dam body. However, there are no signs of crack formation at this time if only seismic loading is considered in the analysis.

During the next excursion at t = 3 sec (Figure 8.21-b), the downstream face of the dam neck is being stretched and the crack propagates inside the dam in the presence of thermal and seepage loading. While the crack starts forming in the heel of the dam body at this time in the absence of the THM model.

Finally in the remaining portion of ground excitation, form t=3.5 sec until the end of earthquake at t=10 sec, the crack penetrates deeper into the dam body for both loading conditions. Figure 8.21(d) illustrates the damage profiles of the dam at the end of the earthquake excitation at t=10 sec. The damage zones are found to take place in the slope transition region located on the downstream side of the dam and propagate towards the upstream face of the dam while taking into account the thermal-seepage fields indicating a more intense cracking behaviour. It is also noted that in the absence of thermo-hydro-mechanical loading, cracks are only observed on the upstream side around the neck of the dam.

It is then deduced from the comparison of the damage profiles between the two different loading combinations that excitations including THM model cause a more severe damage pattern than when neglecting it. Therefore, these loadings have to be taken into account while performing seismic analysis.

Seismic Analysis Only

Seismic + Thermal+ Seepage

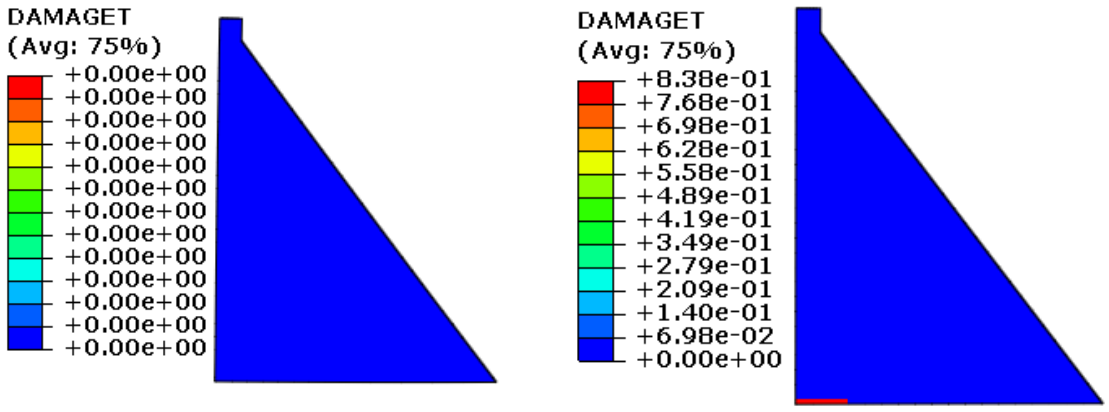

(a) Time = 1.7 sec

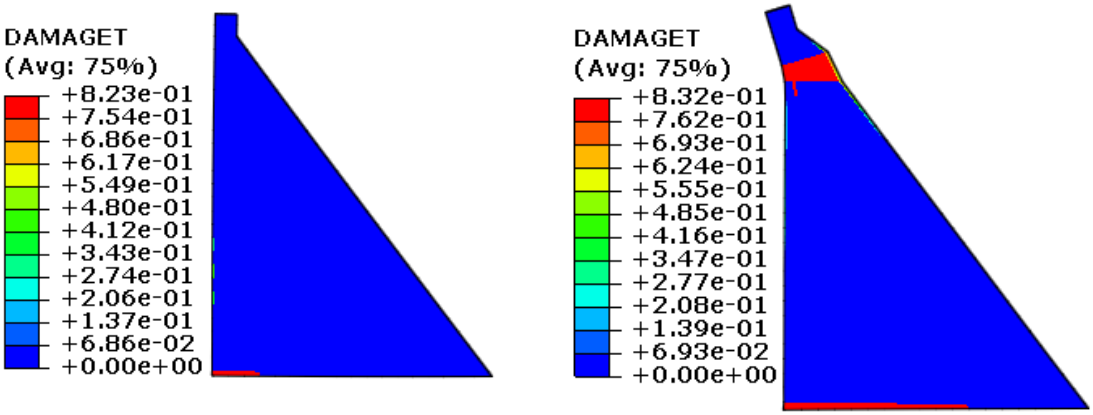

(b) Time = 3 sec

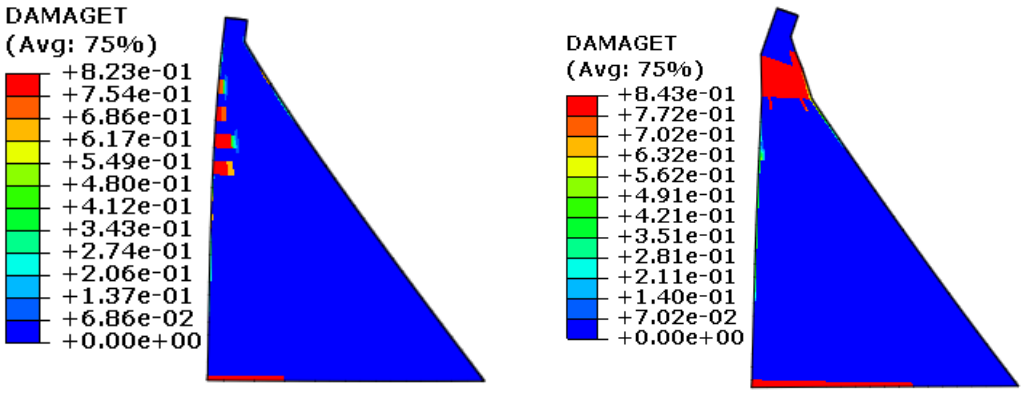

(c) Time = 3.67 sec

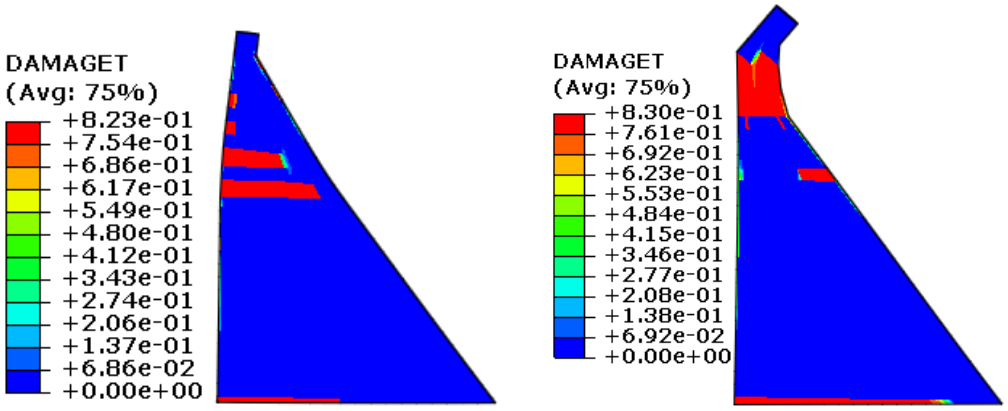

(d) Time = 10 sec

Figure 8.21 Evolution of the Tensile Damage and Cracking Process

Furthermore, failure mechanisms of heel elements within the dam body are plotted in Figure 8.22. It is noted that the time (t=1.7 sec) at which the cracks initiate at the dam heel (dam-foundation interface) is much earlier when considering the thermal-seepage effect in seismic analysis. This can be attributed to the fact that the concrete-rock interface bond strength is likely to be lower than the parent concrete.

In this case, heel elements are selected as these elements are the first elements to encounter the damage and cracking during the earthquake.

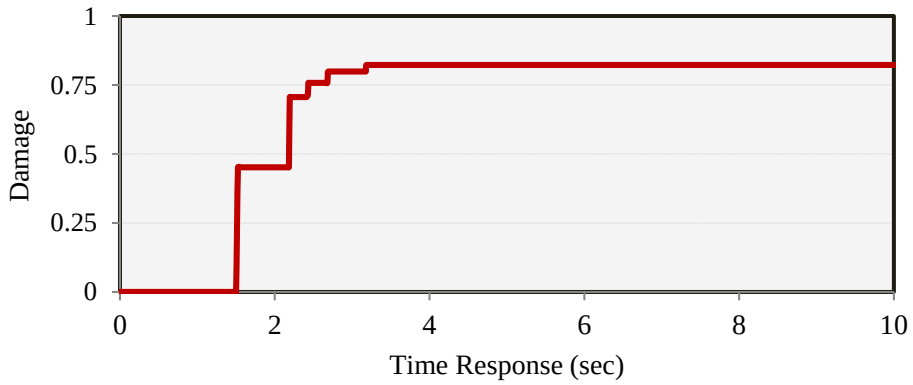

(a) Seismic Analysis Considering Thermal-Seepage Effects

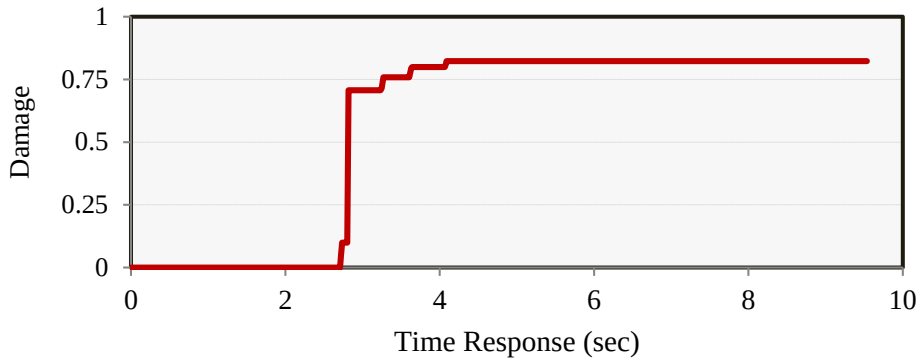

(b) Seismic Analysis Only

Figure 8.22 Time History Response and Failure Mechanism of Kinta RCC Dam

8.4 Conclusion

The nonlinear seismic fracture/safety analysis of the Kinta Roller-Compacted Concrete (RCC) gravity dam in Malaysia was carried out in this chapter. In addition, the importance of thermal and seepage loading on obtaining a reliable estimation of the final stress fields and structural behaviour of RCC dams was investigated by performing the seismic safety analysis of these structures including the thermo-hydro-mechanical (THM) loading combinations.

For this purpose, two-dimensional nonlinear time history dynamic finite element analysis was conducted to evaluate dam safety and the expected damage under simulated ground motion. The presented observations lead to the following remarks regarding the influence of critical loading condition along with earthquake ground motion on the response of the concrete gravity dams:

- The principal stress results clearly show that the responses of the stress considering the opening effects are higher than those when neglecting the galleries. The results also indicate that, at the heel and neck of the dam, while the minimum principal stresses still remain under the concrete's compressive initial yield strength, the maximum principal stresses have exceeded the tensile strength of the concrete, indicating that material yielding and tensile damage may have taken place in these vulnerable regions.

- It has been observed that openings in the dam induce higher stresses in the vicinity of them. In the present study, these openings have contributed up to 15%

to 17% increase in stresses. Moreover, the dynamic stresses are found to be more severe while considering the thermal-seepage loading in the analysis.

- The displacement of the dam is found to be increased with height for both conditions of including and excluding the gallery effects. However, the existence of openings decreases the settlement of the dam in contrast to when neglecting the galleries.

- Based on the failure mechanics results, the most critical regions to experience cracks are the heel region and upper middle zones of the upstream face. The cracks are launched from these regions and they are tended to the downstream face at the same level. It is noted that the time at which the cracks initiate at the dam heel is much earlier when considering the thermal-seepage effect in seismic analysis.

- The largest response quantities such as stresses, deformation and more severe tensile damage patterns are observed to occur in excitations including THM model.

CHAPTER 9

CONCLUSION AND FUTURE PERSPECTIVES

Chapter 9 summarizes the major conclusions and the broader impacts drawn from this study. Based on the results of this effort, recommendations for future research work are also made.

9.1 General Conclusions

This research aims to present a new comprehensive numerical procedure to evaluate the seismically induced cracking of RCC dams under the effects of thermal and seepage actions. In the context of finite element method, the system includes a combination of field problems (thermal and seepage fields), continuum mechanics (stress analysis), seismic hazard assessment and safety evaluation. The combination uses finite elements to introduce compatible units capable of analysing infrastructure, such as RCC dams, to evaluate and predict level of safety in terms of crack pattern development. The method, which is based on a principle of birth and death process, is capable of simulating and assessing the level of safety of the RCC dams during the construction and the operational phases.

The constitutive material model for concrete is based on the combination of damage mechanics and plasticity. It uses concepts of isotropic damaged elasticity in combination with isotropic tensile and compressive plasticity to represent the inelastic behaviour of concrete. The mathematical models for mechanical behaviour of material are given in the form of constitutive equations. The proposed constitutive models have been reformulated and presented in convenient forms for RCC materials. Ageing, temperature and confining pressure effects were taken into account and implemented in the proposed constitutive models. Appropriate boundary conditions were proposed for the water interaction at the upstream face of the dam, taking into account the variation of temperature of the reservoir water with depth.

The numerical modelling of concrete gravity dams involves material nonlinearities (the concrete in the body of the dam, the foundation material, and the water in the

reservoir) and geometric nonlinearities (contact between the dam and the foundation, the dam and the reservoir, and the reservoir and the foundation).

All the developments and analyses are performed using coded subprograms written in FORTRAN and developed in finite element program ABAQUS. Then, the validity of the proposed computational procedures and models has been confirmed by analysing and comparing the results obtained based on available experimental and analytical evidences. After the verification process, the material nonlinearity and proposed models are applied to analyse and evaluate the related dam safety against the cracking of an existing full-size dam. Finally, conclusions are drawn and recommendations are made based on the present research.

9.2 Specific Conclusions

The detailed conclusions drawn from this investigation are summarized in the following:

9.2.1 Field Problem (Seepage and Thermal Analysis)

- The developed and proposed system is capable of simulating the thermal, seepage and structural response of RCC dams efficiently. This is clearly deduced from the reasonable temperature, pore pressure and stress distributions obtained from the two-dimensional analysis.

- The coupling effect in seepage analysis makes the stress components increase in the RCC dam and the stress concentration near the dam heel more obvious. Therefore, the coupling effect should be taken into account in engineering design.

- If the modified seepage properties are considered in the hydro-mechanical analysis, the maximum stresses increase by about 15% and the stress concentration near the dam heel is more obvious.

- Results of thermal analysis clearly indicate that, the higher temperature zone is formed at the middle part of the dam body which gradually decreases to reach approximately the air temperature at the boundaries. This is due to the use of higher RCC placement temperatures combined with higher insulating property of this region due to its massive volume compared to the other locations.

- The significant thermal tensile stresses develop in the bottom part of the dam due to external restraint imposed by the foundation rock, and at the upstream and downstream faces, because of the restraint against environmental thermal variations.

- The maximum stresses develop mainly in the vicinity of both faces, where the temperature gradient is the highest. Thus, the upstream and the downstream regions are the most probable crack regions.

- In dam service life, an increase in the tensile stresses of 11% to 20 % was observed three years after the completion of the dam compared to construction phase. However, the locations and distribution patterns are mostly similar; this can be attributed to the cooling of the dam body with time.

- In addition, the isothermal contours reveal a clear picture of the gallery effect on the temperature development and distribution with the dam body. It can be noticed that, due to the presence of gallery, there is discontinuity in temperature distribution in the regions with gallery and also the value of temperature is lower compared to other locations.

- It has been observed that openings in the dam induce higher stresses in the vicinity of them in thermal analysis. In the present study, these openings have been responsible for 15% to 17% increase in stresses.

- Based on the failure mechanics results, the most critical regions to experience cracks are the heel region and upper middle zones of the upstream face. The cracks are launched from these regions and they are tended toward the downstream face at the same level.

- The safety factor can give a good indication of the probability of a crack occurring under stress states either in short or in the long term.

9.2.2 Seismic Fracture Analysis

- The numerical procedure developed in this study for the seismic response evaluation of RCC gravity dams under thermal and seepage actions provides a general framework for the analysis and design of these critical structures. The results of the evaluation indicate that different response patterns result when considering and neglecting THM model in seismic analysis, suggesting the significance of incorporating the thermal and seepage fields into the seismic assessment and design of concrete gravity dams.

- The principal stress results of seismic analysis clearly show that the responses reprented by the stress, considering the THM model, are slightly more severe than those neglecting this model. The results also indicate that, at the heel and neck of the dam, while the minimum principal stresses remain under the concrete's compressive initial yield strength, the maximum principal stresses have exceeded the tensile strength of the concrete for the ground motion chosen, indicating that material yielding and tensile damage may have occured in these vulnerable regions.

- It has been observed that openings in the dam induce higher stresses in the vicinity of them. In the present study, these openings have contributed between 15% to 17% to increase in stresses. Moreover, the dynamic stresses are found to be more severe while considering the thermal-seepage loading in the analysis.

- The displacement of the dam is found to be increased with height for both conditions of including and excluding the gallery effects. However, the existence of openings decreases the settlement of the dam in contrast to neglecting the galleries.

- Based on the failure mechanics results, the most critical regions to experience cracks are the heel region and upper middle zones of the upstream face. The cracks are launched from these regions and they are tended toward the downstream face at the same level.

- The largest response quantities such as stresses, deformation and tensile damage are observed to occur from approximately 3 sec to 5 sec after the commencement of the earthquake. This time period is also the strongest portion in the duration of the Koyna Earthquake record.

- Seismic safety evaluation of concrete dams relies heavily on the results of calibrated parameters obtained from thermo-hydro-mechanical analyses. Therefore, these loadings have to be taken into account while performing seismic analysis.

9.3 Recommendations for Further Research

Based on the results and the limitations of the present work, some recommendations for more research and further improvement of the numerical modelling of RCC dams are offered:

- Introducing the time dependent creep and shrinkage phenomenon in field problems.
- Considering the sediment effects on upstream face in seismic fracture analysis.
- Investigation on Arch RCC dam modelling and simulation details.
- Seismic safety evaluation of gravity dams under the effects of floodwater.
- Development of a theoretical model for transient water pressure variations along a tensile seismic concrete crack under hydro-mechanical water pressure-crack coupling.
- Conduct corresponding laboratory and/or field experiments if possible.

REFERENCE

ABAQUS, A & Manuals, EUs 2003, 'Version 6.3, Hibbitt, Karlsson & Sorensen', *Inc., USA*.

ABAQUS, V 2007, *6.7-1, Hibbitt, Karlsson & Sorensen*, Inc.

Abdo, F 2008, 'RCC Trends in Early 21st Century Medium-Size Dams', *Hydro Vision, HCI Publ.,(240)*, vol. 1.

Abdulrazeg, A, Noorzaei, J, Khanehzaei, P, Jaafar, M & Mohammed, T 2010, 'Effect of temperature and creep on roller compacted concrete dam during the construction stages', *Computer Modeling in Engineering and Sciences (CMES)*, vol. 68, no. 3, p. 239.

Agullo, L & Aguado, A 1995, 'Thermal behavior of concrete dams due to environmental actions', *Dam Engineering*, vol. 6, pp. 3-21.

Ahola, MP 1994, *Thermo-hydro-mechanical coupled modeling: Big-Ben Experiment, TC3: DECOVALEX-Phase III*, Center for Nuclear Waste Regulatory Analyses.

Akiyama, H 1985, *Earthquake-resistant limit-state design for buildings*, Univ of Tokyo Pr.

Akkose, M, Bayraktar, A & Dumanoglu, A 2008, 'Reservoir water level effects on nonlinear dynamic response of arch dams', *Journal of Fluids and Structures*, vol. 24, no. 3, pp. 418-35.

Akköse, M & Şimşek, E 2010, 'Non-linear seismic response of concrete gravity dams to near-fault ground motions including dam-water-sediment-foundation interaction', *Applied Mathematical Modelling*, vol. 34, no. 11, pp. 3685-700.

Akpinar, U, Aldemir, A & Binici, B 2011, 'Different analysis strategies for RCC dam design', in *5th international conference on Advanced Computational Engineering and Experimenting (ACE-X2011), Algarve, Portugal*.

Asteris, P & Tzamtzis, A 2003, 'Nonlinear seismic response analysis of realistic gravity dam-reservoir systems', *International Journal of Nonlinear Sciences and Numerical Simulation*, vol. 4, no. 4, pp. 329-38.

Ayothiraman, R, Maity D. and Kashung, G. 2006, 'Foundation-reservoir interaction in the seismic response of concrete gravity dam-a case study. ', in *Proceedings of 13th Symposium on Earthquake Engineering* Indian Institute of Technology Roorkee,, pp. 1147-58.

Ayotte, É, Massicotte, B, Houde, J & Gocevski, V 1997, 'Modeling the thermal stresses at early ages in a concrete monolith', *ACI Materials Journal*, vol. 94, no. 6, pp. 577-87.

Azmi, M & Paultre, P 2002, 'Three-dimensional analysis of concrete dams including contraction joint non-linearity', *Engineering Structures*, vol. 24, no. 6, pp. 757-71.

Bayagoob, KH 2007, 'Thermal And Structural Analyses Of Roller Compacted Concrete Dams', Universiti Putra Malaysia.

Bayagoob, KH, Noorzaei, J, Abdulrazeg, AA, Al-Karni, AA & Jaafar, MS 2010, 'Coupled thermal and structural analysis of roller compacted concrete arch dam by three-dimensional finite element method', *Structural engineering and mechanics*, vol. 36, no. 4, pp. 401-19.

Bazant, ZP, Cusatis, G & Cedolin, L 2004, 'Temperature effect on concrete creep modeled by microprestress-solidification theory', *Journal of engineering mechanics*, vol. 130, no. 6, pp. 691-9.

Berga, L, Buil, J, Bofill, E, De Cea, J, Perez, JG, Mañueco, G, Polimon, J, Soriano, A & Yagüe, J 2006, *Dams and Reservoirs, Societies and Environment in the 21st Century, Two Volume Set: Proceedings of the International Symposium on Dams in the Societies of the 21st Century, 22nd International Congress on Large Dams (ICOLD), Barcelona, Spain, 18 June 2006*, CRC Press.

Berga, L, Buil, J, Jofre, C & Chonggand, S 2003, 'Roller compacted concrete dams', in *Proceedings of the fourth International Symposium on Roller Compacted Concrete (RCC) dams, 17-18 november 2003*.

Bhattacharjee, S & Leger, P 1993, 'Seismic cracking and energy dissipation in concrete gravity dams', *Earthquake Engineering & Structural Dynamics*, vol. 22, no. 11, pp. 991-1007.

Bofang, Z 1997, 'Prediction of water temperature in deep reservoir', *Dam Engineering*, vol. 8, no. 1, pp. 13-25.

Bofang, Z 2013, *Thermal stresses and temperature control of mass concrete*, Butterworth-Heinemann.

Bougacha, S & Tassoulas, JL 1991, 'Effects of sedimentary material on the response of concrete gravity dams', *Earthquake Engineering & Structural Dynamics*, vol. 20, no. 9, pp. 849-58.

Buchanan, P, Nott, D, Egilat, B & Forbes, B 2012, 'The Use of 400mm RCC Lifts in The Enlarged Cotter Dam', in *The 6th International Symposium on Roller Compacted Comcrete (RCC) Dams, Zaragoza, Spain 2012*.

Burman, A, Reddy, B & Maity, D 2008, 'Seismic Analysis of Concrete Gravity Dams Considering Foundation Flexibility and Nonlinearity', *International Association for Computer Methods and Advances in Geomechanics (IACMAG)*.

Calayir, Y & Karaton, M 2005, 'Seismic fracture analysis of concrete gravity dams including dam–reservoir interaction', *Computers & structures*, vol. 83, no. 19, pp. 1595-606.

Cervera, M, Oliver, J & Manzoli, O 1996, 'A Rate-Dependent Isotropic Damage Model for the Seismic Analysis of Concrete Dams', *Earthquake Engineering & Structural Dynamics*, vol. 25, no. 9, pp. 987-1010.

Cervera, M, Oliver, J & Prato, T 2000, 'Simulation of construction of RCC dams. I: temperature and aging', *Journal of Structural Engineering*, vol. 126, no. 9, pp. 1053-61.

Chávez, JW & Fenves, GL 1995, 'Earthquake response of concrete gravity dams including base sliding', *Journal of Structural Engineering*, vol. 121, no. 5, pp. 865-75.

Chen, Y, Hu, R, Zhou, C, Li, D, Rong, G & Jiang, Q 2010, 'A new classification of seepage control mechanisms in geotechnical engineering', *Journal of Rock Mechanics and Geotechnical Engineering*, vol. 2, no. 3, pp. 209-22.

Chen, Y, Lu, L, Zhou, C & DAI, Y-h 2007, 'Application of the variational inequality approach of Signorini type to an engineering seepage problem', *Rock and Soil Mechanics S*, vol. 1, pp. 178-82.

Chong-Shi, G, Huai-Zhi, S & Hong, Z 2005, 'Study on coupling model of seepage-field and stress-field for rolled control concrete dam', *Applied Mathematics and Mechanics*, vol. 26, no. 3, pp. 355-63.

Chopra, AK 1978, 'Earthquake resistant design of concrete gravity dams', *Journal of the Structural Division*, vol. 104, no. 6, pp. 953-71.

Chopra, AK & Chakrabarti, P 1972, 'The earthquake experience at Koyna dam and stresses in concrete gravity dams', *Earthquake Engineering & Structural Dynamics*, vol. 1, no. 2, pp. 151-64.

Chopra, AK & Chakrabart 1973, 'The Koyna earthquake and the damage to Koyna dam', *Bulletin of the Seismological Society of America*, vol. 63, no. 2, pp. 381-97.

Chopra, AK & Zhang, L 1991, 'Earthquake-induced base sliding of concrete gravity dams', *Journal of Structural Engineering*, vol. 117, no. 12, pp. 3698-719.

Chuhan, Z, Guanglun, W, Shaomin, W & Yuexing, D 2002, 'Experimental tests of rolled compacted concrete and nonlinear fracture analysis of rolled compacted concrete dams', *Journal of materials in civil engineering*, vol. 14, no. 2, pp. 108-15.

Commission, FER 1999, 'Engineering guidelines for the evaluation of hydropower projects. Chapter 11-Arch Dams', *Washington DC*, vol. 20426, pp. 11-8.

Committee, A 1973, 'Effect of restraint, volume change, and reinforcement on cracking of massive concrete', *Journal of ACI*, pp. 445-70.

Committee, A, Institute, AC & Standardization, IOf 2008, 'Building code requirements for structural concrete (ACI 318-08) and commentary', in.

Conrad, M, Aufleger, M & Malkawi, AH 2003, 'Investigations on the modulus of elasticity of young RCC', *strain*, vol. 1, p. 4.0.

Craig, RF 2004, *Craig's soil mechanics*, CRC Press.

Crichton, AJ, Benzenati, I & Williams, T 2000, 'Kinta RCC Dam-Are over-Simplified Thermal-Structural Analyses Valid?', *Ancold Bulletin*, pp. 101-12.

Danay, A & Adeghe, L 1993, 'Seismic-induced slip of concrete gravity dams', *Journal of Structural Engineering*, vol. 119, no. 1, pp. 108-29.

de Araújo, J & Awruch, AM 1998, 'Cracking safety evaluation on gravity concrete dams during the construction phase', *Computers & structures*, vol. 66, no. 1, pp. 93-104.

DENG, X & WU, M 2009 'Research of Hybrid Analysis Model for Coupled Seepage and Stress in Rock Mass of Equivalent Continuum'.

Djehiche, A & Kotchev, K 2008, 'Control of seepage in earth dams with a vertical drain', *岩土工程學報*, vol. 30, no. 11, pp. 1657-60.

Domínguez, J, Gallego, R & Japón, BR 1997, 'Effects of porous sediments on seismic response of concrete gravity dams', *Journal of engineering mechanics*, vol. 123, no. 4, pp. 302-11.

Duffie, J & Beckman, W 2006, *Solar engineering ofthermal process*, Wiley, New York.

Dunlu, C, Zhongsheng, X & Songgui, W 1987, 'Seepage control of weakened rock foundation of Gezhouba—Erjiang sluice', *Journal of Hydrodynamics (Ser. A)*, vol. 2, no. 2, pp. 25-33.

Dunstan, M 2003, 'The state-of-the-art of RCC dams in 2003 an update of ICOLD Bulletin No. 125', *Roller Compacted Concrete Dams*, pp. 39-48.

Dunstan, MR 1992, 'A review of design criteria for high RCC dams', in *Roller Compacted Concrete III*, pp. 132-47.

Dursun, B & Gokcol, C 2011, 'The role of hydroelectric power and contribution of small hydropower plants for sustainable development in Turkey', *Renewable Energy*, vol. 36, no. 4, pp. 1227-35.

Feng-bo, W, Han-zhou, S & Chao-lei, C 2011, 'Primary study on permeability of concrete under confining pressure', *Yangtze River*, vol. 42, no. 24, pp. 58-60.

Fenves, G & Chopra, AK 1983, 'Effects of reservoir bottom absorption on earthquake response of concrete gravity dams', *Earthquake Engineering & Structural Dynamics*, vol. 11, no. 6, pp. 809-29.

Fenves, G & Chopra 1984, 'Earthquake analysis of concrete gravity dams including reservoir bottom absorption and dam-water-foundation rock interaction', *Earthquake Engineering & Structural Dynamics*, vol. 12, no. 5, pp. 663-80.

Ftima, MB & Léger, P 2006, 'Seismic stability of cracked concrete dams using rigid block models', *Computers & structures*, vol. 84, no. 28, pp. 1802-14.

Fujun, C, Guohua, F, Xiaogang, M & Zhinong, H 2012, 'Simulation analysis of crack cause of concrete overflow dam for Hadashan Hydro Project by 3-D FEM', *Systems Engineering Procedia*, vol. 3, pp. 48-54.

Ga, Z, Lianwei, Z, Jianmin, Z & Chunbo, J 2002, 'Seepage analysis for upstream cofferdam of Xiluodu hydropower station', *Journal of Hydroelectric Engineering*, vol. 3, pp. 54-61.

Gan, L, Shen, ZZ, Wang, R & Huang, QF 2014, 'Stress-Seepage Fully Coupling Model for High Arch Dam', in *Applied Mechanics and Materials*, vol. 513, pp. 4025-9.

Ghaemian, M & Ghobarah, A 1999, 'Nonlinear seismic response of concrete gravity dams with dam–reservoir interaction', *Engineering Structures*, vol. 21, no. 4, pp. 306-15.

Ghrib, F & Tinawi, R 1995, 'An application of damage mechanics for seismic analysis of concrete gravity dams', *Earthquake Engineering & Structural Dynamics*, vol. 24, no. 2, pp. 157-73.

Gogoi, I & Maity, D 2005, 'Seismic safety of aged concrete gravity dams considering fluid-structure interaction', *Journal of earthquake engineering*, vol. 9, no. 05, pp. 637-56.

Gu, C-s, Wei, B-w, Xu, Z-k & Liu, D-w 2013, 'Fluid-solid coupling model based on endochronic damage for roller compacted concrete dam', *Journal of Central South University*, vol. 20, pp. 3247-55.

Gu, C, Zhang, Z, Cai, X & Hou, Y 2011, 'Application of entropy-based fuzzy matter-element analysis in seepage monitoring of RCC dam', *Frontiers of Architecture and Civil Engineering in China*, vol. 5, no. 1, pp. 105-11.

Guanglun, W, Pekau, O, Chuhan, Z & Shaomin, W 2000, 'Seismic fracture analysis of concrete gravity dams based on nonlinear fracture mechanics', *Engineering Fracture Mechanics*, vol. 65, no. 1, pp. 67-87.

Gupta, HK 1992, *Reservoir induced earthquakes*, vol. 64, Elsevier.

Hansen, KD 1996, 'Roller compacted concrete: A civil engineering innovation', *Concrete International*, vol. 18, no. 3, pp. 49-53.

Harr, M 1962, 'Groundwater and Seepage, 315 pp', *McGraw-H tll, New York*.

Helwany, S 2007, *Applied soil mechanics with ABAQUS applications*, John Wiley & Sons.

Hibbit, K & Sorensen Inc, H 2002, 'ABAQUS Standard, Version 6.3-2', *HKS, Providence, RI*.

Hong, Y-W, Du, C-B & Jiang, S-Y 2010, 'Innovative design and construction of a high RCC gravity dam in high seismic intensity region', *Practice Periodical on Structural Design and Construction*, vol. 16, no. 2, pp. 67-72.

Horii, H & Chen, S-C 2003, 'Computational fracture analysis of concrete gravity dams by crack-embedded elements—toward an engineering evaluation of seismic safety', *Engineering Fracture Mechanics*, vol. 70, no. 7, pp. 1029-45.

Huang, J 2011, *Seismic Response Evaluation of Concrete Gravity Dams Subjected to Spatially Varying Earhquake Ground Motions*, vol. 72.

Husein Malkawi, AI, Aufleger, M & Al-Jammal, MR 2004, 'Temperature distribution in Al-Mujib roller compacted concrete (RCC) gravity dam', in *Geo Jordan 2004: Advances in Geotechnical Engineering with Emphasis on Dams, Highway Materials, and Soil Improvement*, pp. 35-48.

Husein Malkawi, AI, Mutasher, SA & Qiu, TJ 2003, 'Thermal-structural modeling and temperature control of roller compacted concrete gravity dam', *Journal of performance of constructed facilities*, vol. 17, no. 4, pp. 177-87.

Ihlenburg, F 2006, *Finite element analysis of acoustic scattering*, vol. 132, Springer Science & Business Media.

Incropera, FP & Dewitt, DP 2002, *Fundamentals of Mass and Heat Transfer*, Chapter.

Ishikawa, M 1991, 'Thermal stress analysis of a concrete dam', *Computers & structures*, vol. 40, no. 2, pp. 347-52.

Jaafar, MS, Bayagoob, KH, Noorzaei, J & Thanoon, WA 2007, 'Development of finite element computer code for thermal analysis of roller compacted concrete dams', *Advances in Engineering Software*, vol. 38, no. 11, pp. 886-95.

Japan Concrete Institute (JCI) 1986. *Standard specifications for design and construction of concrete structures,* Part 2 (construction). Tokyo.

Javanmardi, F, Léger, P & Tinawi, R 2005, 'Seismic structural stability of concrete gravity dams considering transient uplift pressures in cracks', *Engineering Structures*, vol. 27, no. 4, pp. 616-28.

Jiahai, X 1986, 'Seepage control of hydraulic structures on sand/gravel foundations', *Chinese Journal of Geotechnical Engineering*, vol. 8, no. 2, pp. 96-106.

Jiang, S-y & Du, C-b 2012, 'Seismic stability analysis of concrete gravity dams with penetrated cracks', *Water Science and Engineering*, vol. 5, no. 1, pp. 105-19.

Jiang, S, Du, C & Liu, Z 2009, 'Seismic safety evaluation of cracked concrete gravity dam', in *TCLEE 2009: Lifeline Earthquake Engineering in a Multihazard Environment*, pp. 1-9.

Junrui, C 2002, 'Analysis of coupled seepage and temperature fields in concrete dam', *Communications in numerical methods in engineering*, vol. 18, no. 6, pp. 399-409.

Junrui, C, Kanghong, L, Yanqing, W & Shouyi, L 2005, 'Coupled seepage and stress fields in roller compacted concrete dam', *Communications in numerical methods in engineering*, vol. 21, no. 1, pp. 13-21.

Junrui, C, Yanqing, W & Shouyi, L 2004, 'Analysis of coupled seepage and stress fields in rock mass around the Xiaowan arch dam', *Communications in numerical methods in engineering*, vol. 20, no. 8, pp. 607-17.

KRÜGER, D, Kavamura, E, Carvalho, N, Hecke, M, Machado, R & Lacerda, L 2003, 'Thermo-mechanical analysis of Roller Compacted Concrete Dams', *Roller Compacted Concrete Dams. Holanda*, pp. 625-32.

Küçükarslan, S 2004, 'Dynamic analysis of dam–reservoir-foundation interaction in time domain', *Computational Mechanics*, vol. 33, no. 4, pp. 274-81.

Kuzmanovic, V, Savic, L & Mladenovic, N 2013, 'Computation of thermal-stresses and contraction joint distance of RCC dams', *Journal of Thermal Stresses*, vol. 36, no. 2, pp. 112-34.

Lai, D & Liang, R 2008, 'Coupled creep and seepage model for hybrid media', *Journal of engineering mechanics*, vol. 134, no. 3, pp. 217-23.

Lanru, J & Xiating, F 2003, 'Numerical Modelling for Coupled Thermo-Hydro-Mechanical and Chemical Processes (Thmc) of Geological Media-International and Chinese Experiences', *岩石力学与工程学报*, vol. 22, no. 10, p. 1715.

Lee, J 1996, 'Theory and implementation of plastic-damage model for concrete structures under cyclic and dynamic loading', University of California, Berkeley.

Lee, J & Fenves, GL 1998a, 'Plastic-damage model for cyclic loading of concrete structures', *Journal of engineering mechanics*, vol. 124, no. 8, pp. 892-900.

—— 1998b, 'A plastic-damage concrete model for earthquake analysis of dams', *Earthquake Engineering & Structural Dynamics*, vol. 27, no. 9, pp. 937-56.

Léger, P & Javanmardi, F 2006, 'Structural stability of concrete gravity dams strengthened by rockfill buttressing: hydrostatic load', *Journal of geotechnical and geoenvironmental engineering*, vol. 132, no. 12, pp. 1592-9.

Leonard, M 2008, 'One hundred years of earthquake recording in Australia', *Bulletin of the Seismological Society of America*, vol. 98, no. 3, pp. 1458-70.

Lewis, RW & Schrefler, BA 1998, *The finite element method in the static and dynamic deformation and consolidation of porous media*, John Wiley.

Li, G & Desai, C 1983, 'Stress and seepage analysis of earth dams', *Journal of Geotechnical Engineering*, vol. 109, no. 7, pp. 946-60.

Lingfei, X & Li, Y 2008, 'Research on temperature control and anti-cracking simulation for xiaowan concrete high arch dam', in *Computer Science and Software Engineering, 2008 International Conference on*, vol. 5, pp. 1036-9.

Liu, X, Wang, S & Wang, E 2011, 'A study on the uplift mechanism of Tongjiezi dam using a coupled hydro-mechanical model', *Engineering Geology*, vol. 117, no. 1, pp. 134-50.

Long, Y, Zhang, C & Xu, Y 2009, 'Nonlinear seismic analyses of a high gravity dam with and without the presence of reinforcement', *Engineering Structures*, vol. 31, no. 10, pp. 2486-94.

Lopez, J, Castro, G., and Schrader, E 2003, 'RCC mix and thermal

behaviour of Miel I dam. In Roller Compacted Concrete Dams', in *Proceedings of the 4th International Symposium on RCC Dams*, Madrid, Spain, 17–19 November 2003, pp. pp. 789–98.

Lotfi, V & Espandar, R 2004, 'Seismic analysis of concrete arch dams by combined discrete crack and non-orthogonal smeared crack technique', *Engineering Structures*, vol. 26, no. 1, pp. 27-37.

Lubliner, J, Oliver, J, Oller, S & Onate, E 1989, 'A plastic-damage model for concrete', *International Journal of solids and structures*, vol. 25, no. 3, pp. 299-326.

Luna, R & Wu, Y 2000, 'Simulation of temperature and stress fields during RCC dam construction', *Journal of Construction Engineering and Management*, vol. 126, no. 5, pp. 381-8.

Lysmer, J 1969, 'Finite dynamic model for infinite media', in *Proc. of ASCE*, pp. 859-77.

Major, A 1980, *Dynamics in Civil Engineering: Analysis and Design (Revised and enlarged edition of Vibration Analysis and Design of Foundations for Machines and Turbines, 1962 ed.), Akadémiai Kiadó, Budapest and Collets Holdings Ltd*, London.

Mansouri, A, Neshaei, MAL & Aghajany, R 2011, 'Fracture analysis of concrete gravity dam under earthquake induced loads', *Journal of Applied Sciences and Environmental Management*, vol. 15, no. 2.

Mao, M & Taylor, C 1997, 'Non-linear seismic cracking analysis of medium-height concrete gravity dams', *Computers & structures*, vol. 64, no. 5, pp. 1197-204.

Mazloumi, A, Ghaemian, M & Noorzad, A 2012, 'Nonlinear seismic analysis of rcc dam considering orthotropic behavior of layers', in *International Symposium On Dams For a Changing World*.

Medina, F, Dominguez, J & Tassoulas, JL 1990, 'Response of dams to earthquakes including effects of sediments', *Journal of Structural Engineering*, vol. 116, no. 11, pp. 3108-21.

Mills-Bria, BL, Nuss, LK & Chopra, AK 2008, 'Current methodology at the Bureau of Reclamation for the nonlinear analyses of arch dams using explicit finite element techniques', in *The 14th World Conference on Earthquake Engineering October*, pp. 12-7.

Nehrin, A & Fujii, K 2001, 'Three Dimensional Finite Element Analysis Of a Roller Compacted Concrete (RCC) Dam Due to Variable Thermal Loads', *Journal of Civil engineering*, vol. CE29, pp. 65-86.

Neville, AM, Dilger, WH & Brooks, JJ 1983, *Creep of plain and structural concrete*, Construction press.

Noorzaei, J, Bayagoob, KH, Thanoon, WA & Jaafar, MS 2006, 'Thermal and stress analysis of Kinta RCC dam', *Engineering Structures*, vol. 28, no. 13, pp. 1795-802.

Oller, S, Onate, E, Oliver, J & Lubliner, J 1990, 'Finite element nonlinear analysis of concrete structures using a "plastic-damage model"', *Engineering Fracture Mechanics*, vol. 35, no. 1-3, pp. 219-31.

Ouria, A, Toufigh, M & Nakhai, A 2007, 'An investigation on the effect of the coupled and uncoupled formulation on transient seepage by the finite element method', *Am J Appl Sci*, vol. 4, no. 12, pp. 950-6.

Paggi, M, Ferro, G & Braga, F 2013, 'A multiscale approach for the seismic analysis of concrete gravity dams', *Computers & structures*, vol. 122, pp. 230-8.

Pazhuhab Consultant Engineers 1999. Technical Report of Zirdan Roller compacted concrete Dam. Iran.

Peck, RB & Terzaghi, K 1948, *Soil mechanics in engineering practice*.

Perumalswami, P & Kar, L 1973, 'Earthquake behavior of arch dams-reservoir systems', in *Fifth World Conference on Earthquake Engineering, Rome, Italy*.

Punmia, B & Jain, AK 2005, *Soil mechanics and foundations*, Firewall Media.

RCC, SKD 2002, *Study of Restrictions on RCC Temperature, Stage 2 Development of Ipoh Water Supply*, Technical report, GHD, SDN Bhd, Malaysia.

Rice, JD & Duncan, JM 2009, 'Deformation and cracking of seepage barriers in dams due to changes in the pore pressure regime', *Journal of geotechnical and geoenvironmental engineering*, vol. 136, no. 1, pp. 16-25.

Rizos, D & Karabalis, D 2000, 'Soil-fluid-structure interaction', *Wave Motion in Earthquake Engineering*.

Roland, WL, Perumal, N & Kankanhalli, N 2004, *Fundamentals of the finite element method for heat and fluid flow*, John Wiley and Sons Ltd. England.

Saetta, A, Scotta, R & Vitaliani, R 1995, 'Stress analysis of concrete structures subjected to variable thermal loads', *Journal of Structural Engineering*, vol. 121, no. 3, pp. 446-57.

Sarkar, R, Paul, D & Stempniewski, L 2007, 'Influence of reservoir and foundation on the nonlinear dynamic response of concrete gravity dams', *ISET Journal of Earthquake technology*, vol. 44, no. 2, pp. 377-89.

Sasaki, T, Uesaka, T & Nagayama, I 1998, 'A study on stress in concrete gravity dam using seismic data during Kobe Earthquake', *NIST special publication*, no. 931, pp. 130-43.

Schoeber, W 1981, 'Regarding the Load Bearing Behaviour of Large Dams, Die Wasserwirstchaft, Vol. 71, No. 4, April, 1981', *ICE Abstracts*, no. 81/1287 Part 8, p. 81.

Segerlind, LJ & Saunders, H 1987, *Applied finite element analysis*, American Society of Mechanical Engineers, 0739-3717.

Shahrbanouzadeh, M, Barania, GA & Shojaeec, S 2015, 'Analysis of flow through dam foundation by FEM and ANN models Case study: Shahid Abbaspour Dam', *Geomechanics and Engineering*, vol. 9, no. 4, pp. 465-81.

Shamsai, A, Dezfuli, EA, Zebardast, A & Vosoughifar, H 2010, 'A study of Seepage Under a Concrete Dam Using the Finite Volume Method', in *Fourteenth International Water Technology Conference, Cairo, Egypt*.

Sharan, S 1987, 'A non-reflecting boundary in fluid-structure interaction', *Computers & structures*, vol. 26, no. 5, pp. 841-6.

Sharma, R & Sharma, T 2008, *Irrigation engineering*, S. Chand.

Sheibany, F & Ghaemian, M 2006, 'Effects of environmental action on thermal stress analysis of Karaj concrete arch dam', *Journal of engineering mechanics*, vol. 132, no. 5, pp. 532-44.

Simulia, DS 2010, 'Abaqus analysis user's manual', *Dassault Systemes, Pawtucket, USA*.

Smoak, WG 1991, 'Crack repairs to upper Stillwater Dam', *Concrete International*, vol. 13, no. 2, pp. 33-6.

Su, H-Z, Wu, Z-r & Gu, C-S 2006, 'Mechanism of dam behavior assessment with fuzzy extension theory', *Yantu Lixue(Rock and Soil Mechanics)*, vol. 27, no. 11, pp. 1967-73.

Sugimura, Y, Miura, S & Konagai, K 2001, 'Damage to Shihkang dam inflicted by faulting in the September 1999 Chichi earthquake', in *Proc. workshop on seismic fault-induced failures, Tokyo, Japan*, pp. 143-54.

Sun, KM, Li, Z & Bagale, MR 2012, 'Research on the Concrete Dam Damage and Failure Rule under the Action of Fluid-Solid Coupling', in *Applied Mechanics and Materials*, vol. 226, pp. 1371-6.

Tatro, S & Schrader, E 1992, 'Thermal analysis for RCC—a practical approach', in *Roller compacted concrete III*, pp. 389-406.

Tekie, PB & Ellingwood, BR 2003, 'Seismic fragility assessment of concrete gravity dams', *Earthquake Engineering & Structural Dynamics*, vol. 32, no. 14, pp. 2221-40.

Terzaghi, K '1943, Theoretical Soil Mechanics, John Wiley & Sons, New York'.

Timoshenko, S & Goodier, J 1970, 'The ory of Elas tic ity', *McGraw-Hill, New York*.

Tsai, C-S & Lee, GC 1990, 'Method for transient analysis of three-dimensional dam-reservoir interactions', *Journal of engineering mechanics*, vol. 116, no. 10, pp. 2151-72.

U.S. Army Corps of Engineers 1995. *Gravity Dam Design*, Report EM 1110-2-2200, U.S. Army Corps of Engineers (USACE), USA.

U.S. Army Corps of Engineers 2006. *Roller Compacted Concrete*, Report EM 1110-2-2006, U.S. Army Corps of Engineers (USACE), USA.

U.S. Army Corps of Engineers 2003, *Engineering and Design Time-history Dynamic Analysis of Concrete Hydraulic Structures*. EM 1110-2-6051.

Walsh, J 2003, 'Effect of pore pressure and confining pressure on fracture permeability', in *International Journal of Rock Mechanics and Mining Sciences & Geomechanics Abstracts*, vol. 18, pp. 429-35.

Walsh, J & Grosenbaugh, M 1979, 'A new model for analyzing the effect of fractures on compressibility', *Journal of Geophysical Research: Solid Earth*, vol. 84, no. B7, pp. 3532-6.

Wang, F, Song, H & Cao, Z 2011, 'Primary study on permeability of concrete under confining pressure [J]', *Yangtze River*, vol. 24, p. 018.

Wieland, M, Brenner, R & Sommer, P 2003, 'Earthquake resiliency of large concrete dams: Damage, repair, and strengthening concepts', in *Proceedings of the 21st International Congress on Large Dams*.

Wilson, E 2000, *Static and dynamic analysis of structures Computers and Structures*, Inc.

Wilson, J, Lam, NT & Pham, L 2008, 'Development of the new Australian earthquake loading standard', *Earthquake Engineering in the low and moderate seismic regions of Southeast Asia and Australia*, vol. 8, pp. 25-30.

Wriggers, P 'Computational contact mechanics. 2002', *John Wiley&Sons*.

Wyatt, T 1989, 'Earthquake Effects, Loadings', *Civil Engineer's Reference Book, L. S Blake (Ed.), Fourth Edition, Butterworth, London*, p. 19.

Yu, H, Li, S, Liu, Y & Chen, C 2009, 'Evaluation and Rehabilitation of the Seepage Problems at the Fengman Dam', *EJGE*, vol. 14.

Yu, H, Li, S, Liu, Y & Chen, C 2011, 'Study on temperature distribution due to freezing and thawing at the Fengman concrete gravity dam', *Thermal Science*, vol. 15, no. 5, p. 27.

Yu, M-H 2006, *Generalized plasticity*, Springer Science & Business Media.

Zee, C-H, Zee, R & Zee, R 2011, 'Pore pressures in concrete dams', *Journal of geotechnical and geoenvironmental engineering*, vol. 137, no. 12, pp. 1254-64.

Zerva, A 2009, *Spatial variation of seismic ground motion. Modeling and engineering applications*, CRC Press, Taylor & Francis Group, Boca Raton, FL.

Zhang, S, Wang, G & Yu, X 2013, 'Seismic cracking analysis of concrete gravity dams with initial cracks using the extended finite element method', *Engineering Structures*, vol. 56, pp. 528-43.

Zhang, X-f, Li, S-y, Chen, Y-l & Chai, J-r 2009, 'The development and verification of relocating mesh method for the computation of temperature field of RCC dam', *Advances in Engineering Software*, vol. 40, no. 11, pp. 1119-23.

Zhiqi, HH, Z.; Jianping, H. ; Yirui, Z. 2007, 'Simulation analysis on thermal stress of Longtan RCC gravity dam,' in LG J.; Berga, Z.; Gaixin, C.; Cuiying, Z. (Eds.). (ed.), *New Progress on Roller Compacted Concrete Dams*, Guiyang, China, pp. 551–6.

Zhong, Z-H 1993, *Finite element procedures for contact-impact problems*, Oxford university press.

Zhongru, W 2003, 'Safety Monitoring Theory and Its Application of Hydraulic Structures.', *Beijing: Higher Education Press.*

Zhu, B 1997, 'Prediction of water temperature in deep reservoirs', *Dam Engineering*, vol. 8, pp. 13-26.

Zhu, Y, Semprich, S, Bauer, E, Yuan, C & Sun, D 2006, 'methods For Control Of Seepage In Rcc Dams With Watertight And Drainage Measures'.

APPENDIX A

Annotated Description of the DFLUX Subroutine

As discussed in Chapter 4 of the thesis, the DFLUX subroutine is available for modelling heat generation in concrete due to heat of hydration. A listing of this subroutine is provided with comments discussing various portions of the program. Comments which are for the purpose of this appendix only are placed in double quotations.

```
*** USER SUBROUTINE DFLUX ***
      SUBROUTINE DFLUX(FLUX,TEMP,KSTEP,KINC,TIME,NOEL,NPT,COORDS,
     and JLTYP)
      IMPLICIT REAL*8 (A-H,0-Z)
C**********************************************************************
C VERSION 2.0
C THE ADIABATIC CURVE IN THIS VERSION OF DFLUX IS BASED ON THE
C ORIGINAL CURVE USED FOR L&D26. UNITS IN THE T ARRAY ARE HOURS.
C UNITS IN THE HEAT ARRAY ARE BTU/(LB-IN**3)
C
CNQ IS THE NUMBER OF POINTS IN ARRAYS T & Q. ENTIME IS THE ENDTIME
C FOR DFLUX. STTIME GIVES THE START TIMES FOR ELEMENTS IN HOURS.
C THE DIMENSION OF STTIME MUST BE AS LARGE AS THE NUMBER OF ELEMENTS.
C YOU MUST CHANGE THE VALUES IN STTIME TO CONFORM TO YOUR PROBLEM.
C FOR INSTANCE, IF THE FIRST POUR IS MODELED USING 50 ELEMENTS,
C 50*0.0 WOULD START DFLUX AT TIME 0 FOR THE FIRST 50 ELEMENTS.
C
C**********************************************************************

"The array COORDS is simply for the coordinates, Q and T are for the arrays given
below and PROP is an array for the density and specific heat as given on the
DATA PROP card"

      DIMENSION COORDS(3),Q(20),T(20),PROP(2)

"STTIME is defined below."
      COMMON /ELDEF/ STTIME(736)
      DATAPROP/.08681,.21/
      DATA ENTIME/648.1/
```

```
      DATA NQ/20/
```

"Array T is the time associated with each heat flux given
in array Q"

```
      DATA T/.25,.5,.75,l., 1.25,1.5,1.75,2.,
     $ 2.5,3.,3.5,4.,6.,7.,8.,
     $ 9.,10.0,13.,15.,27./

      DATAQ/0.00716817,0.01285477,0.01651029,0.01342255,0.00867982,
     $ 0.00579574,.00414259,0.00369022,0.00264052,0.00238157,
     $ 0.00164695,0.00158670,0.00108267,0.00083101,0.00076965,
     $ 0.00067882,0.00051608,0.00057410,0.00043135,0.00023181/
```

"This indicates which elements are included into the model at which time. In this case, elements up through element 544 are included in the model at time 0.0. The next 96 elements are not included for 10 more days and the 96 elements after that are not included until 20 days later. This arrangement is good only for elements that are sequentially ordered in the placement schedule."

```
    DATA STTIME/544*0.,96*10.,96*20./
C
C**************
C    ENTIME = END OF RELATIVE HEAT GENERATION TIME + SMALL TOLERANCE
C
C    NQ = NO. OF HEAT GENERATION RATE POINTS
C
C    T = RELATIVE HEAT GENERATION TIME POINTS
C
C    Q = HEAT GENERATION POINT
C
C     STTIME = VECTOR CONTAINING PLACEMENT TIME FOR EACH ELEMENT
C
C      FLUX = HEAT GENERATION RATE RETURNED TO PROGRAM
C
C
C**************
```

"TREL is the relative time in the analysis for each lift."

```
      TREL = TIME - STTIME(NOEL)
      END = ENTIME
      IF( TREL.GT.0.0.AND.TREL.LT.END ) GO TO 10
      FLUX = 0.0
      RETURN
C
 10   CONTINUE
      FLUX = 0.0
      DO 20 1=1,NQ
      J = I
      TD = T(I)
      IF( TREL.LE.TD ) GO TO 30
 20   CONTINUE
C
      WRITE(6,35) KSTEP,KINC,TIME,NOEL
 35   FORMAT(/,' WARNING - PASSED THROUGH DFLUX WITHOUT ASSIGNING',
     & /,' FLUX. STEP=',I5,' INC=',I5,
     & /,' TIME =',F12.2,' ELEMENT =',15)
      RETURN
      "Flux value is converted from units of hours to units of days."
 30   FLUX=Q(J)*24.0
 C    WRITE(6,99) FLUX,TIME,TEMP,KSTEP,KINC,NOEL,NPT

 C99   FORMAT(3G15.6,4I8)
       RETURN
       END
```

APPENDIX B

Rayleigh Damping

Damping is simply defined as the process of energy dissipation in a vibrating system due to internal friction, material hysteresis effects, radiation to ground and other sources. In practical applications, in order to be able to define a suitable damping matrix for a multi-degree of freedom vibrating system, and for a homogeneous material, Rayleigh damping is commonly used. In Rayleigh damping, it is assumed that the damping matrix is proportional to both mass matrix [M] and stiffness matrix [K] and the linear combination of these two parameters in the form,:

$$[C] = \alpha[M] + \beta[K]$$

Where α , β are material-specific constants. For a given mode *i*, the damping ratio ξ_i , and the Rayleigh damping coefficients α and β have the following relationship:

$$\xi_i = \frac{\alpha}{2\omega_i} + \frac{\beta\omega_i}{2}$$

where ω_i represents the natural circular frequency of mode i. In Rayleigh damping, mass proportional damping part plays a more dominant role in the system response to low-frequency excitation, while, the stiffness proportional damping is more dominant for high frequency excitation. For the first two modal frequencies ω_1 and ω_2, the corresponding ξ_1 and ξ_2 can be obtained as:

$$\begin{cases} \xi_1 = \dfrac{\alpha}{2\omega_1} + \dfrac{\beta\omega_1}{2} \\ \xi_2 = \dfrac{\alpha}{2\omega_2} + \dfrac{\beta\omega_2}{2} \end{cases}$$

The above system of equations can be rearranged for α and β as follows:

$$\begin{cases} \alpha = \dfrac{2\omega_1\omega_2(\xi_1\omega_2 - \xi_2\omega_1)}{\omega_2{}^2 - \omega_1{}^2} \\ \beta = \dfrac{2(\xi_2\omega_2 - \xi_1\omega_1)}{\omega_2{}^2 - \omega_1{}^2} \end{cases}$$

When $\xi_1 = \xi_2 = \xi$

$$\begin{cases} \alpha = \dfrac{2\omega_1\omega_2\xi}{\omega_1 + \omega_2} \\ \beta = \dfrac{2\xi}{\omega_1 + \omega_2} \end{cases}$$

For hydraulic structures, seismic design specification: DL 5073-2000, gravity dam damping ratio can be selected in the range of 5% -10% of critical, In this thesis the more conservative 5% damping ration has been adopted, ie, $\xi = 0.05$. Based on calculated natural frequencies ω_1 and ω_2 with values of 9.571 and 51.238 rad/sec. α and β values can be obtained from the above two equations yielding $\alpha = 0.806$ and $\beta = 0.00164$.